

INFORMATION TO USERS

This manuscript has been reproduced from the microfilm master. UMI films the text directly from the original or copy submitted. Thus, some thesis and dissertation copies are in typewriter face, while others may be from any type of computer printer.

The quality of this reproduction is dependent upon the quality of the copy submitted. Broken or indistinct print, colored or poor quality illustrations and photographs, print bleedthrough, substandard margins, and improper alignment can adversely affect reproduction.

In the unlikely event that the author did not send UMI a complete manuscript and there are missing pages, these will be noted. Also, if unauthorized copyright material had to be removed, a note will indicate the deletion.

Oversize materials (e.g., maps, drawings, charts) are reproduced by sectioning the original, beginning at the upper left-hand corner and continuing from left to right in equal sections with small overlaps.

Photographs included in the original manuscript have been reproduced xerographically in this copy. Higher quality 6" x 9" black and white photographic prints are available for any photographs or illustrations appearing in this copy for an additional charge. Contact UMI directly to order.

ProQuest Information and Learning
300 North Zeeb Road, Ann Arbor, MI 48106-1346 USA
800-521-0600

UMI[®]

Optimal Tank Design and Directional Dynamic Analysis of Liquid Cargo Vehicles under Steering and Braking

Xiaodi Kang

A Thesis

in

The Department

of

Mechanical Engineering

Presented in Partial Fulfillment of the Requirements
for the Degree of Doctor of Philosophy at
Concordia University
Montreal, Quebec, Canada

March 2001

© Xiaodi Kang, 2001



National Library
of Canada

Acquisitions and
Bibliographic Services

395 Wellington Street
Ottawa ON K1A 0N4
Canada

Bibliothèque nationale
du Canada

Acquisitions et
services bibliographiques

395, rue Wellington
Ottawa ON K1A 0N4
Canada

Your file Votre référence

Our file Notre référence

The author has granted a non-exclusive licence allowing the National Library of Canada to reproduce, loan, distribute or sell copies of this thesis in microform, paper or electronic formats.

The author retains ownership of the copyright in this thesis. Neither the thesis nor substantial extracts from it may be printed or otherwise reproduced without the author's permission.

L'auteur a accordé une licence non exclusive permettant à la Bibliothèque nationale du Canada de reproduire, prêter, distribuer ou vendre des copies de cette thèse sous la forme de microfiche/film, de reproduction sur papier ou sur format électronique.

L'auteur conserve la propriété du droit d'auteur qui protège cette thèse. Ni la thèse ni des extraits substantiels de celle-ci ne doivent être imprimés ou autrement reproduits sans son autorisation.

0-612-59231-6

Canada

ABSTRACT

Optimal Tank Design and Directional Dynamic Analysis of Liquid Cargo Vehicles under Steering and Braking

Xiaodi Kang

Concordia University, 2001

The stability and dynamic response characteristics of partially-filled tank vehicles are adversely influenced by the movement of the liquid cargo within the tank. The directional dynamics and stability characteristics of partially-filled tank vehicles are analyzed and enhanced through formulation of an optimal tank configuration, and analytical models for analyses of vehicle responses to steady and transient steering maneuvers, and combined steering and braking inputs. A generic tank cross-section is initially proposed based upon an analysis of the currently used tank configurations. Three different constrained multi-variable optimization functions are formulated and solved to derive optimal tank cross-sections corresponding to various liquid fill conditions. The performance potentials of the optimal tank configurations are initially evaluated in terms of the load transfer properties and static rollover threshold acceleration limit of a partly-filled tractor-semitrailer tank vehicle through development and analyses of a static roll plane model. The influence of tank geometry on the directional response and dynamic roll stability characteristics is further investigated through development and analyses of a constant-speed three-dimensional model of the tank vehicle. The static and dynamic roll response characteristics of the vehicle equipped with two optimal tanks are compared with those of the vehicle with conventional tanks, under various directional maneuvers

and liquid fill conditions, to demonstrate the superior potential performance of the optimal tank designs.

A three-dimensional quasi-static model of the partially-filled generic tank is further developed to study instantaneous liquid load shift in both the roll and pitch planes under simultaneous applications of lateral and longitudinal accelerations. The tank model is integrated into a comprehensive variable-speed three-dimensional model of an articulated vehicle combination to investigate the impact of cargo shift on the dynamic response of partially-filled tank vehicles under braking-in-a-turn maneuvers. The dynamic characteristics of tank vehicles are compared with those of the equivalent rigid cargo vehicles to demonstrate the destabilizing effects of the liquid load shift. The dynamic responses of tank vehicles are further investigated in view of variations in vehicle maneuvers, fill volume, road condition, and tank cross-section. From the study, it is concluded that liquid cargo movement within a tank tends to reduce roll stability limits and yaw stability limits of the vehicle, when operating on a dry road and a wet/slippery road, respectively. The performance limits can be considerably enhanced through the use of the proposed optimal designs.

ACKNOWLEDGEMENTS

The author wishes to express his sincere appreciation to his thesis supervisors, Dr. S. Rakheja and Dr. I. Stiharu, for their guidance and efforts throughout the course of this investigation.

The author also wishes to acknowledge Quebec Government, Concordia University and CONCAVE Research Center for the financial support provided in the forms of FCAR Doctoral Scholarship, Graduate Fellowship, and Research Assistantship, respectively.

Thanks are due to the colleagues, faculty and staff of CONCAVE Research Center and of Mechanical Engineering Department, for their contributions to this study.

Finally, the author would like to express his special thanks to his parents, wife and other family members for their continuous encouragement and understanding.

TABLE OF CONTENTS

	Page
LIST OF FIGURES	x
LIST OF TABLES	xvi
NOMENCLATURE	xvii

CHAPTER 1

INTRODUCTION AND LITERATURE REVIEW	1
1.1 General	1
1.2 Review of the Literature	6
1.2.1 Directional Dynamics and Stability of Heavy Vehicles	6
1.2.2 Performance Measures Related to Directional Dynamics of Heavy Vehicles	25
1.2.3 Liquid Sloshing in Moving Containers	29
1.2.4 Dynamic Characteristics of Partially-Filled Tank Vehicles	37
1.2.5 Tank Design and Vehicle Stability	45
1.3 Objectives and Scope of the Dissertation	49
1.3.1 Objectives of the Investigation	50
1.3.2 Organization of the Dissertation	52

CHAPTER 2

A GENERIC TANK CROSS-SECTION AND SHAPE OPTIMIZATION	55
2.1 Introduction	55
2.2 Lateral Liquid Load Shift Analysis of Conventional Tanks	56
2.3 Formulation of a Generic Tank Cross-Section	61
2.3.1 Coordinates and Independent Parameters of the Generic Cross-Section	62
2.3.2 Characteristic Parameters of the Generic Cross-Section	65
2.4 Load Shift in a Partly-Filled Generic Tank (Roll Plane)	66
2.5 Determination of Optimal Tank Cross-Sections	73
2.5.1 Formulation of Optimization Functions	74

2.5.2 Constraints	77
2.5.3 Solution Method	77
2.6 Optimal Tank Cross-Sections corresponding to Various Fill Conditions	78
2.6.1 Optimal Cross-Sections for Specific Fill Volumes	78
2.6.2 Optimal Cross-Sections corresponding to Typical Fill Ranges	81
2.7 Summary	91

CHAPTER 3

STATIC ROLL STABILITY ANALYSIS OF VEHICLES WITH PARTLY-FILLED OPTIMAL TANKS	92
3.1 Introduction	92
3.2 Static Roll Plane Model of an Articulated Tank Vehicle	93
3.3 Equations of Static Roll Equilibrium	99
3.4 Load Shift in Partly-Filled Optimal Tanks	105
3.4.1 Load Shift Analysis of Optimal Tanks for Typical Fill Volumes	105
3.4.2 Load Shift Analysis of Optimal Tanks for Typical Fill Ranges	109
3.5 Rollover Threshold Limits of Partly-Filled Articulated Vehicles with Different Tanks	114
3.5.1 Optimal Cross-sections Obtained for Typical Fill Volumes	114
3.5.2 Optimal Tanks Obtained for Typical Fill Ranges	119
3.6 Influence of Optimal Tank Geometry on the Stress Distribution of the Tank Structure	126
3.7 Summary	127

CHAPTER 4

CONSTANT SPEED DIRECTIONAL DYNAMIC RESPONSE ANALYSES OF PARTLY-FILLED TANK VEHICLES	130
4.1 Introduction	130
4.2 Constant Speed Yaw/Roll Model of a Partly-Filled Articulated Tank Vehicle	132
4.2.1 Quasi-Static Model of a Partly-Filled Tank of Generic Cross-section	132
4.2.2 Constant Velocity Directional Dynamic Model of the Vehicle Combination	135
4.2.3 Equations of Motion of the Articulated Tank Vehicle	140

4.3 Directional Maneuvers and Performance Measures	144
4.4 Dynamic Response to Steering Inputs	147
4.4.1 Constant Load Partial Fill Conditions	148
4.4.2 Variable Load Partial Fill Conditions	171
4.5 Summary	175

CHAPTER 5

VARIABLE SPEED DYNAMIC MODEL OF A PARTLY-FILLED ARTICULATED TANK VEHICLE	177
5.1 Introduction	177
5.2 Three-Dimensional Model of a Partly-Filled Tank of General Cross-Section	178
5.2.1 Liquid Free Surface Equation	179
5.2.2 Patterns of Free Surface and Wetted Volume	182
5.2.3 Liquid Load Shift and Mass Moments of Inertia	189
5.3 Variable Speed Yaw/Roll Model of an Articulated Tank Vehicle	190
5.4 Equations of Motion	195
5.4.1 Coordinate Systems	195
5.4.2 Equations of Motion	197
5.4.3 Tire Forces	202
5.4.4 Suspension Forces	207
5.4.5 Constraint Forces and Moments	210
5.5 Method of Solution	211
5.6 Summary	212

CHAPTER 6

CARGO LOAD SHIFT AND ITS INFLUENCE ON DYNAMIC RESPONSE OF TANK VEHICLES UNDER BRAKING AND TURNING	214
6.1 Introduction	214
6.2 Liquid Load Shift under Braking and Steering Inputs	215
6.2.1 Cargo Load Shift within a Partly-Filled Tank of Circular Cross-section	216
6.2.2 Influence of Tank Cross-section on Cargo Load Shift	226
6.3 Vehicle Maneuvers and Performance Measures	234
6.3.1 Simulation Conditions	234

6.3.2 Performance Measures	237
6.4 Dynamic Response to Combined Braking and Turning Maneuvers: Cylindrical Tank Trailer	239
6.4.1 Dynamic Load Shift under Steering and Braking Inputs	240
6.4.2 Directional Response under Steering and Braking Inputs	244
6.4.3 Influence of Brake Treadle Pressure	248
6.4.4 Influence of Cargo Fill Volume	254
6.4.5 Influence of Road Conditions	256
6.5 Directional Response of Tank Vehicles with Optimal Tanks	262
6.6 Summary	267

CHAPTER 7

CONCLUSIONS AND RECOMMENDATIONS	270
7.1 Highlights of the Investigation	270
7.1.1 Formulation of a Generic Tank Cross-section and Shape Optimization	270
7.1.2 Analysis of Load Shift and Static Roll Stability of Vehicles with Partly-Filled Optimal Tanks	271
7.1.3 Directional and Roll Dynamic Response Analysis of Partly-Filled Tank Vehicles	272
7.1.4 Development of a Comprehensive Dynamic Model of Partly-Filled Tank Vehicles for Braking-in-a-turn Analysis	273
7.1.5 Analysis of Cargo Load Shift and its Influence on Dynamic Response of Tank Vehicles under Combined Braking and Steering	275
7.2 Conclusions	276
7.3 Recommendations for Future Work	281

REFERENCES	284
------------	-----

APPENDIX A

INFLUENCE OF TANK CROSS-SECTION ON TANK STRUCTURAL INTEGRITY	301
A.1 Finite Element Model of a Generic Tank and its Supports	301
A.2 Stress Distribution of Various Conventional and Optimal Tanks	308
A.3 Summary	322

LIST OF FIGURES

	Page
Figure 2.1 Commonly used tank cross-sections in liquid bulk transportation	57
Figure 2.2 Roll plane models of partly-filled circular and modified-oval tanks	59
Figure 2.3 Liquid load shifts in partly-filled conventional tanks	60
Figure 2.4 Schematics of a generic tank cross-section	62
Figure 2.5 Coordinate analysis of the generic tank cross-section	63
Figure 2.6 Roll plane model of a partially filled generic tank	67
Figure 2.7 The intercept of liquid free surface with tank periphery	69
Figure 2.8 Possible liquid free surface configurations	69
Figure 2.9 Comparison of optimal tank cross-sections derived on the basis of minimal overturning moment	80
Figure 2.10 Comparison of optimal tank cross-sections corresponding to different limiting values of Z_{cg0} ($\beta=0.5$ to 0.9)	81
Figure 2.11 Overturning moment arms and their mean values for different optimal cross-sections and fill volume ranging from 50% to 90%	83
Figure 2.12 Sum of overturning moment arms of different optimal cross-sections for two fill ranges	84
Figure 2.13 Comparison of optimal and conventional tank cross-sections	86
Figure 2.14 Comparison of optimal tank cross-sections corresponding to different limiting values of Z_{cg0} and unconstrained perimeter	86
Figure 2.15 Overturning moment arms and the average of arms due to load shift for fill volumes ranging from 50% to 90%	89
Figure 2.16 Sum of overturning moment arms as a function of Z_{cg0}	89
Figure 2.17 Comparison of symmetric optimal tank cross-section with those of the circular and modified-oval tanks	90
Figure 3.1 Three-composite-axle representation of a tractor semitrailer tank	95

vehicle

Figure 3.2	Roll plane model of the tank vehicle	95
Figure 3.3	Force-displacement characteristics of suspension springs of composite axles	98
Figure 3.4	Idealized representation of tractor frame compliance	98
Figure 3.5	Comparison of lateral deviations in c.g. coordinates of liquid cargo within optimal and currently used tanks	107
Figure 3.6	Comparison of vertical deviations in c.g. coordinates of liquid cargo within optimal and currently used tanks	108
Figure 3.7	Comparison of trajectories of liquid cargo c.g. within optimal and conventional tanks ($0 \leq a_y \leq 0.5$ g)	111
Figure 3.8	Comparison of trajectories of liquid cargo c.g. within the two sets of optimal tanks obtained with and without the perimeter constraint ($0 \leq a_y \leq 0.5$ g)	113
Figure 3.9	Rollover threshold acceleration limits of an articulated vehicle with various tanks as a function of fill volume (variable cargo load)	115
Figure 3.10	Comparison of rollover threshold acceleration limits of an articulated vehicle equipped with optimal and conventional tanks as a function of fill volume (constant cargo load)	117
Figure 3.11	Comparison of rollover threshold acceleration limits of a partly-filled articulated vehicle with optimal and conventional tanks (constant cargo load)	120
Figure 3.12	Rollover threshold acceleration limits of the vehicle with optimal tanks obtained with and without the perimeter constraint, and conventional tanks	123
Figure 3.13	Rollover threshold acceleration limits of the vehicle with conventional and optimal-oval tanks (variable cargo load)	125
Figure 3.14	Rollover threshold acceleration limits of the vehicle with conventional and optimal-oval tanks (constant cargo load)	125
Figure 4.1	Roll plane model of a partly-filled tank of generic cross-section	133
Figure 4.2	Roll plane representation of the partially-filled tank vehicle model	138
Figure 4.3	Pitch plane representation of the tank vehicle model and the attached	138

coordinate frames

Figure 4.4	Cornering force properties of a radial truck tire as a function of load and side-slip angle	139
Figure 4.5	Aligning moment property of a radial truck tire as a function of load and side-slip angle	139
Figure 4.6	Time history of steady ramp-step steer inputs and path coordinates of transient maneuvers	146
Figure 4.7	Influence of tank cross-section, fill volume and steer angle on the lateral load shift of liquid cargo within conventional and optimal tanks ($U=60$ km/h)	151
Figure 4.8	Influence of tank cross-section, fill volume and steer angle on the roll mass moment of inertia of liquid cargo within conventional and optimal tanks ($U=60$ km/h)	152
Figure 4.9	Influence of tank cross-section and fill volume on the directional response of the vehicle ($U=60$ km/h, $\delta_f=3$ degrees)	157
Figure 4.10	Influence of tank cross-section and fill volume on the lateral load transfer and path trajectory of the vehicle ($U=60$ km/h, $\delta_f=3$ degrees)	158
Figure 4.11	Directional response of the vehicle combination with different tanks to a steady steer input of 1 degree ($U=90$ km/h, $\beta=0.5$)	161
Figure 4.12	Directional response of the vehicle combination with different tanks to a steady steer input of 1 degree ($U=90$ km/h, $\beta=0.8$)	162
Figure 4.13	Articulation angle and path trajectory response of the vehicle combination with different tanks to a steady steer input of 1 degree ($U=90$ km/h)	163
Figure 4.14	Directional response of partly-filled tank vehicles to a path-change maneuver performed at 100 km/h ($\beta=0.5$)	165
Figure 4.15	Directional response of partly-filled tank vehicles to a path-change maneuver performed at 100 km/h ($\beta=0.8$)	166
Figure 4.16	Directional response of partly-filled tank vehicles to a evasive maneuver performed at 100 km/h ($\beta=0.5$)	167
Figure 4.17	Directional response of partly-filled tank vehicles to a evasive maneuver performed at 100 km/h ($\beta=0.8$)	168

Figure 4.18	Directional response of the vehicle with different tanks to a steady steer input of 3 degrees (variable cargo load, $\beta=0.5$)	173
Figure 4.19	Directional response of the vehicle with different tanks to a steady steer input of 3 degrees (variable cargo load, $\beta=0.8$)	174
Figure 5.1	Free surface of liquid cargo under application of longitudinal (F_{lx}) and lateral (F_{ly}) accelerations, and free body diagram of a liquid element	179
Figure 5.2	Liquid free surfaces under longitudinal and lateral accelerations	183
Figure 5.3	Patterns of liquid free surface in a partly-filled tank under simultaneous application of longitudinal and lateral accelerations	185
Figure 5.4	Roll plane representation of the partially-filled three-dimensional tank vehicle model	194
Figure 5.5	Pitch plane representation of the partially-filled three-dimensional tank vehicle model and attached coordinate systems	194
Figure 5.6	Tire lateral and longitudinal friction coefficients on a dry road	206
Figure 5.7	Suspension forces on a single axle	208
Figure 6.1	Variations in coordinates of liquid cargo c.g. as functions of longitudinal and lateral accelerations ($\beta=0.5$)	217
Figure 6.2	Variations in roll, pitch and yaw mass moments of inertia of liquid cargo as functions of longitudinal and lateral accelerations ($\beta=0.5$)	218
Figure 6.3	Variations in c.g. coordinates of liquid cargo under application of longitudinal and lateral acceleration fields	219
Figure 6.4	Variations in normalized mass moments of inertia of liquid cargo under application of longitudinal and lateral acceleration fields	220
Figure 6.5	Trajectories of liquid cargo c.g. in the roll, pitch and yaw planes under applications of a_{lx} and a_{ly} ($\beta=0.5$)	224
Figure 6.6	Trajectories of liquid cargo c.g. in the roll, pitch and yaw planes under applications of a_{lx} and a_{ly} ($\beta=0.8$)	225
Figure 6.7	Variations in c.g. coordinates of the liquid cargo as functions of longitudinal acceleration and tank cross-section ($a_{lx}=0.3 g$ and $\beta=0.5$)	230

Figure 6.8	Variations in c.g. coordinates of the liquid cargo as functions of longitudinal acceleration and tank cross-section ($a_{ly}=0.3\ g$ and $\beta=0.8$)	231
Figure 6.9	Trajectories of liquid cargo c.g. in the roll, pitch and yaw planes as functions of longitudinal acceleration and tank cross-section ($a_{ly}=0.3\ g$ and $\beta=0.5$)	232
Figure 6.10	Trajectories of liquid cargo c.g. in the roll, pitch and yaw planes as functions of longitudinal acceleration and tank cross-section ($a_{ly}=0.3\ g$ and $\beta=0.8$)	233
Figure 6.11	Steering and braking inputs	236
Figure 6.12	Dynamic load factor response of axle wheels under steering and braking input ($T_b=68.95\ \text{kPa}$)	241
Figure 6.13	Moments induced by variations in the coordinates of the cargo c.g. under steering and braking input ($T_b=68.95\ \text{kPa}$)	242
Figure 6.14	Directional response characteristics of the liquid and equivalent rigid cargo vehicles under steering and braking input ($T_b=68.95\ \text{kPa}$)	245
Figure 6.15	Wheel-slip responses under steering and braking input ($T_b=68.95\ \text{kPa}$)	246
Figure 6.16	Influence of brake treadle pressure on the moments induced by variations in the coordinates of the cargo c.g. ($\delta_f=0.5\ \text{degree}$)	250
Figure 6.17	Influence of brake treadle pressure on the DLF responses of axle wheels ($\delta_f=0.5\ \text{degree}$)	251
Figure 6.18	Influence of brake treadle pressure on the directional responses of the liquid and rigid cargo vehicles ($\delta_f=0.5\ \text{degree}$)	252
Figure 6.19	Influence of brake treadle pressure on the wheel-slip responses ($\delta_f=0.5\ \text{degree}$)	253
Figure 6.20	Directional response characteristics of the liquid and equivalent rigid cargo vehicles under steering and braking input ($\beta=0.8$, $T_b=68.95\ \text{kPa}$)	255
Figure 6.21	Moments induced by variation in the coordinates of the cargo c.g. under steering and braking input ($\delta_f=0.5\ \text{degree}$, road B)	258
Figure 6.22	Directional and roll response of the liquid and rigid cargo vehicles under steering and braking input ($\delta_f=0.5\ \text{degree}$, road B)	259

Figure 6.23	Wheel-slip response under steering and braking input ($\delta_f=0.5$ degree, road B)	260
Figure 6.24	Axle lateral force response under steering and braking input ($\delta_f=0.5$ degree, road B)	261
Figure 6.25	Dynamic load factor response of the vehicle with various tanks under steering and braking input ($\delta_f=0.8$ degree, $T_b=10$ psi, road A)	265
Figure 6.26	Directional and roll response of the vehicle with various tanks under steering and braking input ($\delta_f=0.8$ degree, $T_b=10$ psi, road A)	266
Figure A1	Schematic diagram of a generic tank and its supports	302
Figure A2	Geometric model of a generic tank and its supports	306
Figure A3	Quarter finite element model of the tank and its supports	307
Figure A4	Stress contour of the quarter circular tank	310
Figure A5	Stress distribution along longitudinal direction of the quarter circular tank	311
Figure A6	Stress contour of the quarter modified-oval tank	312
Figure A7	Stress distribution along longitudinal direction of the quarter modified-oval tank	313
Figure A8	Stress contour of the quarter OPT1 tank	314
Figure A9	Stress distribution along longitudinal direction of the quarter OPT1 tank	315
Figure A10	Stress contour of the quarter OPT2 tank	316
Figure A11	Stress distribution along longitudinal direction of the quarter OPT2 tank	317
Figure A12	Stress contour of the quarter Opt.5 tank	318
Figure A13	Stress distribution along longitudinal direction of the quarter Opt.5 tank	319

LIST OF TABLES

	Page
Table 2.1 Liquid free surface configurations and sets of integrals	72
Table 2.2 Geometric parameters of conventional and optimal cross-sections corresponding to different fill volumes	80
Table 2.3 Geometric parameters of optimal cross-sections corresponding to different limiting values of Z_{cg0} ($\beta=0.5$ to 0.9)	82
Table 2.4 Geometric parameters of optimal cross-sections corresponding to different Z_{cg0} (without perimeter constraint)	87
Table 3.1 Simulation parameters of the tank vehicle used in the analysis	104
Table 3.2 Comparison of load c.g. shift within tanks of various cross-sections ($a_y=0.4$ g and $\theta_{s3}=7$ degrees)	111
Table 3.3 Comparison of load c.g. shift within the two sets of optimal tanks	113
Table 3.4 Relative gains in rollover threshold limits of the vehicle with optimal tanks (OPT1 & OPT2): constant cargo load	120
Table 3.5 Relative gains in rollover threshold limits of the vehicle with optimal tanks (OPT1 _n and OPT2 _n): constant cargo load	123
Table 4.1 Description of symbols used in constant speed yaw/roll model	143
Table 4.2 Simulation parameters of a five-axle tank vehicle combination	148
Table 4.3 Lateral acceleration rearward amplifications of the vehicle with various tanks	170
Table 5.1 Domains of volume integration	187
Table 6.1 Simulation parameters of a five-axle tractor-tank-semitrailer combination	236

NOMENCLATURE

Symbol	Description
a_f :	acceleration vector of sprung mass f ($f=1, 2$)
a_{l2} :	acceleration vector of liquid cargo c.g.
a_{lx}, a_{ly}, a_{lz} :	longitudinal, lateral and vertical components of acceleration vector of liquid cargo c.g.
a_{uzi} :	vertical acceleration of unsprung mass i
a_{x2}, a_{y2}, a_{z2} :	longitudinal, lateral and vertical components of acceleration vector of trailer sprung mass
a_y :	lateral acceleration imposed on liquid cargo during steady turning
a_{y1} :	lateral acceleration at c.g. of tractor sprung mass
a_y^* :	rollover threshold acceleration limit
A_0 :	wetted tank cross-section area under static condition
A_c :	tank cross-section area
A_f :	estimated liquid volume per unit tank length
A_v :	matrix of vehicle parameter coefficients in static roll analysis
AT_{ij} :	aligning moment due to tire j on axle i
b_i :	half-track width of inner tires on axle i
B_t, C_t, D_t, E_t :	stiffness factor, shape factor, peak value and curvature factor in tire Magic Formula
B_{tr} :	brake torque coefficient
c_0 :	constant in three-dimensional liquid free surface equation
C_{ij} :	viscous damping coefficient
C_l :	instantaneous c.g. position of liquid cargo within a partly-filled tank

C_{t0} :	static c.g. position of liquid cargo within a partly-filled tank
CF_{ij} :	suspension Coulomb friction
d_i :	dual tire spacing of tires on axle i
D_{fi} :	matrix for coordinate transformation from i th unsprung mass system to f th sprung mass system
D_{sf} :	matrix for coordinate transformation from f th sprung mass system to the inertial system
DLF :	wheel dynamic load factor
DLF_l :	left wheel dynamic load factor
DLF_r :	right wheel dynamic load factor
f_c :	right-hand-side equation of a tank cross-section
f_i :	right-hand-side equation of arc i ($i=1, 2, \dots, 5$) of a generic tank cross-section
f_s :	liquid free surface equation
F_{gx}, F_{gy}, F_{gz} :	forces due to gravity of trailer sprung mass and liquid cargo
F_{lx}, F_{ly}, F_{lz} :	body forces per unit mass of liquid along tank body-fixed OX, OY and OZ directions
F_{ri} :	lateral force acting through the i th roll center
F_{tx} :	tire response variable in the Magic Formula
F_{xk} :	longitudinal force developed at the k th tire-road interface
F_{yi} :	lateral force developed by tires on axle i
F_{zr}, F_{zl} :	instantaneous vertical loads on right- and left-wheels of an axle
F_{zri}, F_{zli} :	instantaneous vertical loads on right- and left-wheels of axle i
FS_{il}, FS_{ir} :	forces developed by left and right suspension springs on axle i
FT_{ij} :	vertical force due to tire j on axle i
FY_{ij} :	lateral force developed at the j th tire road interface on axle i

g :	acceleration due to gravity
h :	fill height of liquid cargo in a tank
h_0 :	intercept of liquid free surface with Z-axis
H_1, H_2 :	overall width and height of a tank cross-section
H_{ri} :	height of the i th roll center from the ground plane
H_{ui} :	height of the i th unsprung weight center from the ground plane
i_n, j_n, k_n :	a right-hand orthogonal coordinate system fixed in space
i_{sf}, j_{sf}, k_{sf} :	body-fixed axis system on sprung mass f
i_{ui}, j_{ui}, k_{ui} :	body axis system fixed on unsprung mass i
$\bar{i}_{sf}, \bar{j}_{sf}, \bar{k}_{sf}$:	unit vectors describing body coordinate system fixed on sprung mass unit f
I_{xf}, I_{yf}, I_{zf} :	roll, pitch and yaw mass moments of inertia of sprung unit f
I_{xl}, I_{yl}, I_{zl} :	roll, pitch and yaw mass moments of inertia of liquid cargo about tank body-fixed axis system
$I_{xl2}, I_{yl2}, I_{zl2}$:	roll, pitch and yaw mass moments of inertia of liquid cargo with respect to tank trailer sprung mass system
I_{xui} :	roll mass moment of inertia of unsprung mass i
I_{zui} :	yaw mass moment of inertia of unsprung mass i
J_k :	effective mass moment of inertia of the k th wheel about its spin axis
K_c :	torsional compliance of tank-trailer structure
K_{ij} :	spring rate of the j th suspension spring ($j=1, 2$) on axle i
K_{tr} :	torsional compliance of tractor frame
$KOVT_{ij}$:	roll-resisting stiffness of tire j on axle i
KT_{ij} :	vertical stiffness of tire j on axle i
KY_{ij} :	lateral stiffness of tire j on axle i
L :	tank length

$L_M :$	effective overturning moment
$L_p :$	perimeter of a tank cross-section
$LTR :$	lateral load transfer ratio
$m_f :$	mass of sprung unit f
$m_l, m_{l2} :$	mass of liquid cargo
$m_{ui} :$	unsprung mass i
$M_{lx}, M_{ly}, M_{lz} :$	roll, pitch and yaw moments due to liquid cargo
$M_o :$	overturning moment due to liquid cargo
$M_{r1i} :$	roll moment due to torsional compliance of tractor frame
$M_{r2i} :$	roll moment due to shear force acting on tractor frame
$M_{r3i} :$	roll moment due to vertical load on fifth wheel
$M_{r4i} :$	roll moment due to torsional compliance of fifth wheel and trailer structure
$M_{rli} :$	roll moment due to liquid cargo
$N_1, N_2 :$	axle numbers on a sprung mass unit
$Opt.1-Opt.5 :$	optimal tanks obtained under five typical fill volumes (40%-70% and 100%)
$OPT1, OPT2 :$	optimal tanks obtained under two typical ranges of fill volumes (50% to 70% and 70% to 90%) with perimeter constraint
$OPT1_n, OPT2_n :$	optimal tanks obtained under two typical ranges of fill volumes (50% to 70% and 70% to 90%) without perimeter constraint
$OVT_{ij} :$	roll-resisting moment developed at the j th tire-road interface on axle i
$p_f, q_f, r_f :$	rotational velocities (roll, pitch and yaw rates) of sprung mass f
$p_{ui} :$	roll rate of unsprung mass i
$\dot{p}_f, \dot{q}_f, \dot{r}_f :$	angular accelerations of sprung mass f
$P :$	liquid pressure

P_b :	treadle pressure
P_{bk} :	effective line pressure in brake system k
Q :	domain of area integral
Q_v :	vector of vehicle parameter coefficients in static roll analysis
R :	radius of a circular arc
R_i :	radius of circular arc i of a tank cross-section ($i=1, 2, \dots, 5$)
R_{ti} :	effective radius of tires on axle i
R_{tk} :	effective rolling radius of k th wheel
RWA :	rearward amplification ratio
S	time in second
s_i :	half the suspension lateral spread of axle i
S_h, S_v :	horizontal and vertical shifts in tire Magic Formula
t :	time
T_{bk} :	braking torque about spin axis of the k th wheel
T_{bs} :	total brake torque due to all four brakes on a tandem set
T_d :	tandem axle spread
U_f, v_f, w_f :	translational (longitudinal, lateral and vertical) velocities of sprung mass f
$\dot{u}_f, \dot{v}_f, \dot{w}_f$:	translational accelerations of sprung mass f
U :	vehicle forward speed
U_{Mo} :	minimization function based upon overturning moment due to liquid cargo
U_Y :	minimization function based upon liquid lateral load shift
U_{YZ} :	minimization function based upon weighted sum of liquid load shift and c.g. height

$U_{\Sigma Mo}$:	minimization function based upon overturning moment due to liquid cargo for a range of fill volumes
$U_{\Sigma Y}$:	minimization function based upon liquid lateral load shift for a range of fill volumes
$U_{\Sigma Z}$:	minimization function based upon weighted sum of liquid load shift and c.g. height for a range of fill volumes
V :	domain of volume integration
V_0 :	initial fill volume of liquid within a tank
V_f :	estimated volume of liquid within a tank
W_2 :	weight of tank trailer structure
W_5 :	fifth wheel load
W_f :	sprung weight supported by front axle due to tractor alone
W_{fr} :	vertical shear force acting through tractor frame
W_l :	weight of liquid cargo in a tank
W_r :	sprung weight supported by rear axle due to tractor alone
W_{si} :	sprung weight supported by axle i
W_t :	weight of tank semitrailer structure
W_{ui} :	unsprung weight i
W_{β} :	weighting factor corresponding to fill volume ratio β
x_t :	tire service variable in the Magic Formula
X_b, X_{b2} :	longitudinal distance between origin of tank body axis system and c.g. of tank trailer sprung mass
X_l, Y_l, Z_l :	instantaneous longitudinal, lateral and vertical c.g. coordinates of liquid cargo in terms of tank body-fixed system
X_{l2}, Y_{l2}, Z_{l2} :	instantaneous c.g. coordinates of liquid cargo in terms of tank trailer sprung mass system
X_{ui} :	longitudinal location of axle i from c.g. of the sprung mass to which the axle is attached

$y, z :$	lateral and vertical coordinates of a point on periphery of a tank cross-section
$y_i :$	lateral displacement of tires on the outside of the turn on axle i
$Y_{ci}, Z_{ci} :$	coordinates of center of arc i of a tank cross-section
$Y_i, Z_i :$	coordinates of arc intersection points of a tank cross-section
$Y_{max} :$	maximum value of Y -coordinate of entire periphery of a tank cross-section
$Y_{l0}, Z_{l0} :$	static c.g. coordinates of liquid cargo in terms of tank body-fixed system
$Y_A, Z_A :$	coordinates of left-hand-side intersection point (A) of liquid free surface with the tank cross-section
$Y_B, Z_B :$	coordinates of right-hand-side intersection point (B) of liquid free surface with the tank cross-section
$Z_{ji} :$	vertical distance between fifth wheel and c.g. of the i th sprung weight
$Z_b, Z_{b2} :$	vertical distance between tank base and c.g. of tank trailer sprung mass
$Z_{cg} :$	tank cross-section c.g. height
$Z_{cg0} :$	upper limit of tank cross-section c.g. height
$Z_{fi} :$	vertical height of tractor frame with respect to c.g. of the i th sprung weight
$Z_{ri} :$	vertical distance between the i th roll center and c.g. of the sprung mass
$Z_{ui} :$	vertical distance between c.g. of unsprung mass and roll center on axle i
$Z_{AC}, Z_{BD} :$	equations of lines AC and BD in terms of X -coordinate
$Z_{AF}, Z_{BH} :$	equations of curves AF and BH in terms of X -coordinate
$\Delta :$	symbol put in front of a variable to represent variation of the variable
$\Delta X :$	variation in vehicle response vector
$\Delta X_l, \Delta Y_l, \Delta Z_l :$	variations in c.g. coordinates of liquid cargo
$\Delta Y_{l\beta} :$	lateral deviation of cargo c.g. under a steady lateral acceleration and specified fill ratio β

α :	gradient of liquid free surface in the pitch plane
α_i :	angle of circular arc i of a generic tank cross-section ($i=1, 2, \dots, 5$)
α_{ui} :	pitch angle of unsprung mass i
β :	liquid fill volume ratio
β_l, β_u :	lower and upper limits of fill volume ratio
χ :	vector of design variables
δ_f :	front wheel steer angle
δ_{ij} :	suspension spring deflection
ε :	liquid volume error per unit tank length
γ :	articulation angle
$\gamma_1, \gamma_2, \gamma_3$:	weighting factors for liquid load shift and c.g. height (ΔY_l , ΔZ_l and Z_{cg}) in tank optimization solution
φ :	gradient of liquid free surface in the roll plane
μ :	road adhesion coefficient
$\theta_{sf}, \alpha_{sf}, \varphi_{sf}$:	roll, pitch and yaw angles of sprung mass f
θ_{si} :	roll angle of sprung weight supported by axle i
θ_{ui} :	roll angle of unsprung weight i
ρ :	mass density of liquid cargo
ω_k :	angular velocity of k th wheel about its spin axis

CHAPTER 1

INTRODUCTION AND LITERATURE REVIEW

1. 1 GENERAL

Heavy vehicles with their high center of gravity (c.g.), and excessive weights and dimensions are known to exhibit lower directional stability and controllability limits than the other road vehicles, such as passenger cars and light trucks. Such vehicles thus pose relatively higher risks to highway safety. A review of heavy vehicle accidents in the U.S. and Canada revealed that heavy trucks were involved in 28% of single vehicle accidents, as compared with 19% for passenger vehicles [1]. Highway accidents involving heavy vehicles may cause significant amount of property damage and human fatalities [2]. Most heavy vehicle accidents result from maneuver induced instabilities, such as roll instability and yaw instability. Rollover is the most dangerous mode of instability, which may develop during cornering, lane change, or braking-in-a-turn maneuvers. Particularly, the rollover immunity levels of heavy commercial vehicles are known to be so low that a moderately severe maneuver can cause significant destabilizing forces and moments leading to vehicle rollover. It has been estimated that about 14% of trucks involved in fatal accidents rolled over and nearly 60% of truck driver fatalities occurred in rollover events [2].

A roll instability occurs whenever the overturning moment, generated by the centrifugal forces, exceeds the net stabilizing moment. For articulated vehicles, roll instabilities are initiated at the trailer's axles due to excessive load transfer with only

minimal changes in the dynamic response of the tractor. When the normal load acting on the trailer's tires approaches zero, the tires lose contact with the ground indicating the onset of a potential rollover. The yaw instability, caused by braking and steering maneuvers coupled with lock-up of axle wheels, may be classified into three different types: (i) jackknifing or extensive tractor yaw motion, which may occur when the tractor's rear axle wheels experience lock-up; (ii) trailer swing or trailer yaw motion, which may occur when the trailer's axle wheels experience lock-up; and (iii) snaking or trailer lateral oscillation, which is inherent and may be easily excited by rapid steering inputs or external perturbations at high speeds [3, 4]. The last type of instability, also termed as the flutter mode oscillation, is characterized by periodic yaw motion of the trailer about its equilibrium position, while the jackknifing and trailer swing represent a sudden and violent loss of control, and are usually followed by a rollover. Furthermore, heavy vehicles may experience loss of directional control, also termed as plow-out, which may occur when the tractor's front axle wheels experience lock-up [5]. As a consequence of the amplified directional motion of the rearmost trailer, the vehicle combination becomes more susceptible to rollover.

Tank vehicles are extensively used for transportation of liquid cargoes, which frequently involve hazardous materials, such as flammable, toxic, corrosive and other chemical products. According to HMIR (Hazardous Material Incident Report) [6, 7], most hazardous materials are carried in bulk and 79% of them are transported by tank vehicles, of which most are tractor semitrailer combinations. Tank vehicles, employed in general purpose chemical transportation, are often partially-filled due to regulations governing the maximum axle loads and variations in the weight density of various liquid

products, while those employed in fuel transportation encounter partial fill conditions during their delivery routes. In addition to the heavy vehicle design characteristics, partially-filled tank vehicles pose additional safety problems due to the unique interactions between the vehicle and the moving cargo inside the partially-filled tank. The cargo movement, referred to as sloshing within the tank, coupled with the dynamics of the heavy vehicle, increases significantly with increase in vehicle weights and dimensions. The forces and moments arising from a directional maneuver may yield considerable dynamic load shifts in the roll and pitch planes due to the sloshing of the load within the partially-filled tank, resulting in significant reduction in the longitudinal and lateral stability limits, and high local pressures and stresses/deformations, which may cause structural failure [8-10]. The variety of factors to be considered for safe transportation of bulk liquids includes adequate loading and unloading procedures, structural integrity of the tank to withstand stresses due to liquid surge, containability in the event of an accident, and enhanced stability and controllability limits of the vehicle [11]. The potential safety hazards posed by partially-filled tank vehicles are directly related to their directional dynamics and stability limits as well as structural integrity of the tank. The handling and stability characteristics of tank vehicles are thus dependent on factors other than the normal trucking practices, such as tank geometry, high and variable center of gravity (c.g.) location, liquid fill level, lateral and longitudinal load shifts during turning, braking and lane change type of highway maneuvers, as well as liquid-structure interactions.

With the increase in the volume of motor vehicles carrying dangerous liquids, accidents involving such vehicles have gained increased attention due to the associated

unreasonable risks to health, safety, and property in commerce. This necessitates critical examination of the accident experiences in order to ratify the problem and avert the potential hazards. Various studies on accident analyses have indicated that tank vehicles are involved in single vehicle highway accidents at a higher rate than the rigid cargo vehicles [12-15]. The analysis of the road accidents involving single tank vehicles on Canadian roads showed that most of the accidents occurred while performing a cornering or lane change maneuver, where the liquid sloshing was considered as a major factor contributing to the vehicle accidents [11-13]. An investigation by Rohm and Haas Company [15] revealed that vehicle rollover was the primary cause of spillage of dangerous liquids, and in many cases the accidents resulted in secondary fires and/or explosions, human fatalities, economic loss and environmental damage. It has been further reported that majority of the cases of cargo spillage are attributed to the puncture of tank shell, which mostly occurs in accidents involving rollover and crash [15, 16]. Although the existing accident data are often incomplete and even contradictory, the reported data invariably emphasize the importance of tank vehicle operational safety against maneuver-induced instability, attributed to cargo sloshing and other related factors.

In view of the consistent increase in the volume of motor vehicles carrying dangerous liquids and relatively higher risks associated with accidents involving such vehicles [15-20], it is essential to explore alternate design and operational measures to enhance their maneuver stability and structural integrity, and to ensure that cargo tank vehicles possess safety performance characteristics that are either comparable to or better than those of the other highway vehicles. While the directional response and stability

characteristics of various conventional heavy vehicles carrying rigid cargoes have been extensively investigated in the past, only a few attempts have been made towards analysis and enhancement of vehicle stability and controllability under the influence of cargo movement. The studies on safety performance of partially-filled tank vehicles have been primarily limited to either the roll plane or the pitch plane analysis, and lack a complete integration of vehicle dynamics with a three-dimensional cargo slosh analysis as well as effective design recommendations to enhance the vehicle safety characteristics.

The primary objective of this dissertation research is thus formulated to contribute towards enhancement of highway transportation safety through systematic analysis of the directional response and stability characteristics of tank vehicles, as well as formulation of new design concepts and recommendations. This dissertation research involves the study of road tank design through formulation and optimization of a generic tank configuration, effects of optimal tank geometry on the stability characteristics of tank vehicles through development and analyses of static roll plane and dynamic yaw/roll vehicle models, evaluations of tank vehicle dynamic behavior under typical braking in turning maneuvers through development and analyses of a three-dimensional tank vehicle model with variable speed, and structural integrity of different tank designs. A review of the literature on directional dynamics and stability characteristics of heavy vehicles, performance measures related to directional dynamics of heavy vehicles, liquid sloshing in moving containers, and road tank designs is presented in the following section to formulate the scope of this dissertation research.

1.2 REVIEW OF THE LITERATURE

Research on safety performance of tank vehicles encompasses studies on directional dynamics and stability of conventional heavy vehicles, liquid sloshing dynamics in moving containers, and liquid-vehicle interactions. Various reported studies on these aspects are therefore reviewed to build a knowledge base on design and analysis methodologies, and to develop the scope of the dissertation research. The published works relevant to various aspects of this investigation are reviewed and grouped under different subjects in the following subsections to derive appropriate methodologies and the scope of the dissertation research in a systematic manner.

1.2.1 Directional Dynamics and Stability of Heavy Vehicles

Due to increased concerns towards highway safety, the directional dynamics and stability characteristics of various configurations of heavy vehicles have been extensively investigated during the past three decades. These studies have evolved into a series of safety performance measures, and weight and dimensional regulations. A large number of analytical vehicle models of varying complexities have been developed for dynamic analyses of heavy vehicles under various operating conditions [3-5, 21-49]. The degrees of freedom associated with the models vary considerably, depending upon the number of axles and units of the vehicle combinations, the analysis objectives and simplifying assumptions. Simple models have been used to assess the performance of vehicle systems or subsystems in the linear range, under constrained directional motions, while more comprehensive models are employed to derive the vehicle response with appropriate consideration of highly complex and nonlinear force generating subsystems, such as tires, suspensions, articulation mechanisms and brake system.

The studies on heavy vehicle dynamics and stability have been thoroughly reviewed in many published articles [3, 5, 22, 23, 29, 31, 33, 34, 43, 49]. A review of research efforts starting from early works in 1937 on the dynamic performance of articulated highway vehicles was published in 1971 by Dugoff and Murphy [23]. Of the cited references, about one third related to directional response (lateral and yaw) of the vehicles to steering inputs and external disturbances, including steady-state turning, directional stability analyses, aerodynamic effects on dynamic stability, simulation of nonlinear effects and experimental investigations. The others pertained to theoretical analysis and experimental works on braking performance as well as directional response to combined steering and braking inputs. It was concluded that the most significant contributions to the advancement of knowledge in the dynamics of articulated vehicles could be made through more accurate characterization of tire mechanics, validation of predictive models of vehicle performance and the use of these models to assess the potential for loss of control over a wide range of vehicle parameters and operating conditions. In 1982, Vlk [29] conducted a more detailed review on the lateral dynamics of commercial vehicle combinations based upon nearly 250 published studies dealing with directional performance, roll dynamics, braking performance as well as combined steering and braking characteristics of tractor-semi-trailers, truck-trailers and multi-articulated vehicles. It was concluded that the dynamic behavior of articulated vehicles has not been addressed to sufficient details. Nalecz and Genin [5] presented a review of the dynamic stability of heavy articulated vehicles in 1984 on the analytical and experimental investigations into undesirable response characteristics of heavy commercial vehicles, including loss of control during braking, directional instability

during cornering, roll instability and amplified directional motions. The most recent review of studies on static stability of articulated commercial vehicles emphasizes on the results attained from analyses of 'Highway Trains', the vehicle combinations with multiple articulation points and multiple axles [33].

1.2.1.1 Directional dynamic analyses

The earlier studies on analyses of heavy vehicles were primarily based upon yaw plane dynamics of straight trucks and articulated vehicle combinations to study their lateral stability performance. The yaw and lateral directional dynamic response characteristics of various heavy vehicle combinations have thus been extensively investigated through development and analyses of various linear and nonlinear yaw plane models. While majority of the reported yaw-plane models assume linear-cornering characteristics of the tires, some studies have incorporated nonlinear cornering properties of tires based upon regression functions and Magic Formula.

Jindra [50-52] was one of the first to derive a complete set of linear differential equations for analyzing the yaw plane motions of articulated vehicles, and investigated the problems of directional stability and control of tractor-semitrailer, tractor-trailer and tractor-double-trailer combinations traveling at a constant forward speed in a steady turn. The vehicles were treated as linear dynamic systems, and the generalized coordinates were considered as the lateral and yaw motions of the tractor, and the yaw displacement of the trailers relative to the tractor. The roll degree-of-freedom (DOF) of the tractor and trailer bodies together with bounce and pitch were neglected in the analyses, while the changes in the vertical loads of the tires were incorporated through an approximation function. The cornering properties of the tires were assumed to be linear functions of the

sideslip angles, while the studies were restricted to small oscillations. The analyses were performed to investigate two basic problems of vehicle handling: (i) control of the vehicle combination to follow a desired circular path, associated with the steady-state solutions; and (ii) the dynamic stability against external disturbances, derived from the solution of the characteristic equations. The influence of various design parameters, such as position of c.g., fifth wheel location, trailer length, loading condition, yaw moment of inertia, and tire characteristics, on steering characteristics and dynamic directional stability of the vehicles were studied by analyzing the characteristic equations. It was concluded that the amplitude of yaw oscillations of the trailer increases with an increase in the yaw moment of inertia of the trailer body, and an increase in drawbar length and trailer wheelbase results in reduced yaw oscillations. The strong influence of forward speed on the directional stability of the vehicle combinations was also emphasized. These models clearly predicted the periodic yaw response of the trailer about its equilibrium, but did not yield information about aperiodic trailer swing and jackknifing due to lack of a bounded and nonlinear tire model.

Ellis [53] developed a non-linear yaw plane model of an articulated vehicle, similar to that developed by Jindra [50–52], while it incorporated the dynamics due to unsteady forward vehicle speed and large angles between the tractor and semitrailer. The nonlinear tire properties were characterized as a polynomial function and the characteristic equation was used to study the stability of the vehicle. It was shown that the position of the fifth wheel and the location of trailer load are significant factors in the design and operation of the tractor semitrailer vehicle, and that friction at the fifth wheel causes a considerable variation in handling characteristics, particularly on roundabouts.

Schmid [54] investigated the lateral stability of an articulated vehicle by examining the roots of the governing characteristic equation derived for a linearized mathematical model with three-DOF, including lateral and yaw motions of the tractor and the trailer yaw motion. The equations of motion were derived upon incorporating the influence of braking and acceleration, and the conditions of instability were derived from the characteristic equation. Using the yaw plane model, Schmid found that an aperiodic deviation from the desired direction of travel (aperiodic instability) is influenced by the position of the resultant tire side force of the hauling vehicle with respect to the common c.g. of the actual mass of the hauling vehicle and the trailer mass component horizontally supported at the pin of the hauling vehicle. The study concluded that the resultant tire side force should be applied behind the common c.g. in order to ensure the yaw stability of the truck-trailer combination. The vehicle combination tends to deviate from its desired path above a certain traveling speed, when this condition is not fulfilled. Pacejka [55] used a linearized yaw plane model of an articulated vehicle to study its handling characteristics during steady-state turning. Nalecz and Genin [5] concluded that heavy vehicles, in general, begin to show unstable behavior as the lateral acceleration approaches 0.3 to 0.4 g, depending upon the tire-road interactions. Vlk [56] examined the yaw stability of articulated freight vehicles through analysis of a linear yaw plane model. From the steady and transient turning analyses, it was concluded that a tractor-semitrailer vehicle preserves yaw stability at speeds exceeding 70 km/h, while a tractor-trailer combination becomes oscillatory unstable at speeds beyond 60 km/h.

Mikulcik [57] was the first to make extensive study of the cornering and braking behavior of tractor-semitrailer combinations in the nonlinear region of operation. A more

general mathematical model was developed to study the directional response of a three-axle tractor-semitrailer subject to large steer inputs. Subject to the constraints posed by the fifth wheel, the model incorporated the yaw, pitch and roll, longitudinal, vertical and lateral motions of both the tractor and trailer units. The analyses were performed to study the nonlinear jackknifing behavior, and it was shown that the conclusions derived from the linear theory could be completely different from those derived from a nonlinear theory. Jackknifing is directly dependent upon nonlinearities in the vehicle system, which may become evident under certain conditions of operation. This, however, is entirely ignored when the equations are linearized about the vehicle's equilibrium. The study also showed the possibility of jackknifing even in the absence of braking under limit steering conditions. The nonlinear system model was further used to evaluate the effects of different braking procedures and stabilizing elements at the fifth wheel on the stability and control of the vehicle. Mikulcik's model was later extended and generalized for more complex studies [58-61]. Mikulcik [62] also developed a set of algebraic equations to determine the stability boundaries of a car-trailer system. A general criterion governing both the oscillatory and aperiodic stability was derived using the Routh criterion. The graphical representation showed a stable region bounded by limits of oscillatory and aperiodic instabilities.

A comprehensive linear yaw plane model was developed to investigate the lateral and yaw response of tractor-trailer combinations comprising multiple units with multiple axles by Mallikarjunarao and Fancher [64] based on the work of Jindra et al. [50-52]. The cornering forces and aligning moments generated at the tire-road interface were assumed linear functions of the side-slip angle of the tire and the longitudinal slip introduced by

the dual tire sets. Each unit of the articulated vehicle was assumed as a rigid body, and the unsprung masses were assumed to be rigidly attached to their respective sprung masses. The characteristic equations for the linear yaw plane model were developed, and the natural modes of oscillation and the directional stability limits of the vehicle were evaluated using eigenvalue analysis. Directional response characteristics of the Michigan double tanker were also investigated via computer simulation, and compared with those of other freight vehicles to demonstrate the performance potential of a modified hitch. The study concluded that the lateral acceleration response of the pup-trailer of a Michigan double tanker is significantly larger, when compared with that attained by the tractor during an obstacle-avoidance maneuver performed at highway speeds. This rearward amplification of lateral acceleration response was considerably reduced by increasing the rigidity of the pin-~~hook~~ connection. This yaw plane model has been extensively used for directional analyses of various heavy vehicles [65-69].

A comprehensive nonlinear yaw plane model of an articulated vehicle incorporating the kinematics and dynamics of externally mounted articulation dampers and nonlinear cornering characteristics of tires was developed by Vallurupalli and Rakheja et al. [70, 71] to study the influence of articulation dampers on the yaw and lateral response of the vehicle. A kinematic analysis of the dampers, mounted externally to the articulation mechanism of the articulated vehicle, was performed to derive the lateral damping forces and yaw damping moments acting on the sprung masses. The cornering forces and aligning moments of the radial tires were characterized by a nonlinear function in normal load, sideslip angle and pneumatic trail. The equations of motion of the vehicle were solved for high speed lane-change and evasive maneuvers,

and it was concluded that additional articulation damping significantly reduces the cornering demand on the tires, and thus improves the lateral and yaw stability limits of the vehicle combination.

1.2.1.2 Roll dynamics analyses of heavy vehicles

The yaw plane models can provide effective assessment of rearward amplification, dynamic off-tracking, as well as yaw and lateral stability limits of heavy vehicle combinations. Such models offer considerable advantages in which relatively fewer number of parameters are required to evaluate the directional performance of the vehicle with reasonably good accuracy. The major limitation of the models is their inability to evaluate the roll stability limits of the vehicles, since the contributions due to roll and pitch motions as well as suspension dynamics can not be evaluated. Various reported studies on highway accidents have clearly established rollover as a common mode of failure for heavy vehicles [72-77]. The rollover property of a vehicle is strongly related to its static rollover threshold, defined as the maximum level of lateral acceleration that the vehicle can withstand without overturning under a steady-turning maneuver [78]. The roll properties of heavy vehicles have been investigated through development of single and multi-axle roll plane models of varying complexities. These models, in general, incorporate either linear or nonlinear vertical and roll stiffness characteristics of suspensions, lateral stiffness properties of tires, and torsional compliance of the vehicle structure and the articulation mechanisms. While majority of the roll plane models have been developed to analyze the static rollover threshold under steady turning maneuvers [78-85], the dynamic roll characteristics of the vehicle under transient directional maneuvers have been addressed in few studies [86-94].

The role of tire-road interactions in the roll stability of heavy vehicles was investigated by Shapley [79] through development of a roll plane model, which incorporated the influence of pneumatic tires by treating them as lateral springs. All the displacements and rotations were assumed to be small in developing the model. It was indicated that the roll instability of a vehicle could arise from two sources, one related to the high c.g. location and the other due to the tire and suspension characteristics. Isermann[80] developed a roll plane model of an articulated vehicle to investigate the sensitivity of the rollover threshold to variations in design and loading conditions. The suspension characteristics, torsional properties of the tractor frame and the fifth wheel, and the nonlinearities arising from the lateral load transfer during a directional maneuver were incorporated in the model. Considerable simplifications with regard to roll behavior were made in the modeling, such as assumption of small angular displacements and negligible transient dynamic forces. Miller and Barter [81] developed a model, following the work of Isermann [80], to compute the rollover threshold limits of articulated vehicles, while neglecting the contribution due to all dynamic forces. Lumped dual tires and linear tire properties were used in the modeling. It was assumed that rollover occurs when the sum of the forces acting on the trailer c.g. falls outside of the trailer's outside wheels.

A sophisticated static roll model (SRM) of the articulated vehicle was developed by Mallikarjunarao et al. [78] to estimate the rollover threshold of articulated vehicles during steady turning maneuvers. For multi-axle tractor-semitrailer combinations, the axles with similar suspension properties were grouped together such that all axles on the vehicle were represented by a set of three composite axles: a tractor front axle, an

equivalent tractor rear axle and an equivalent semitrailer axle. The tractor body was modeled as two sprung weights coupled through torsional stiffness of the tractor frame. The sprung weight of the semitrailer was coupled to the tractor rear weight by the torsional stiffness of the fifth wheel and semitrailer structure. Tires were modeled as linear springs, while the non-linear properties of suspension springs were included in the model. The static equilibrium equations of the vehicle in the roll plane were solved iteratively for small increments in roll angle of the semitrailer sprung mass. The static roll model was further validated using the results attained from tilt table test.

An extensive parametric sensitivity analysis of the model was carried out by El-Gindy [82], where the vehicle design parameters were classified into three groups based upon their influence on the rollover threshold. The first group included the set of parameters that have no effect on the roll response, while the second group of parameters represented those that must be considered in the model. The last group represented the most important required input parameters, which need to be measured accurately. Rakheja and Piche [85] investigated the static rollover thresholds of tractor semitrailers with different vehicle combinations using the static roll model developed in [78]. Computer simulations were performed to quantify the dependency of compliance factor and thus the rollover threshold on various design and operational parameters. A compliance factor with a typical value of 0.72 was introduced to reflect the influence of the compliance of suspension springs and tires on the rollover threshold of the vehicle combinations.

The tripped and maneuver-induced dynamic roll stability characteristics of heavy vehicles have also been investigated in a few reported studies [86-94]. Heavy vehicles, in

general, exhibit maneuver-induced roll instability due to their low rollover limits. The maneuver-induced roll dynamics and stability characteristics of heavy vehicles have thus been investigated in different experimental and analytical studies. Gillespie and Verma [90] developed a single-composite axle roll plane model to analyze the dynamic roll response of articulated vehicles. In this model, all the axles on the vehicle were lumped together and represented by a single composite axle. The study resulted in an overestimate of the rollover thresholds due to single lumped-axle representation. The rollover dynamics of commercial vehicles has been further studied using a nonlinear roll plane model by Verma and Gillespie [91]. Large displacements and rotations were accounted for in the analytical model so that it could be used for the study of roll dynamics well beyond the limits of wheel lift-off. The model was used to illustrate some of the dynamic phenomena associated with vehicle rollover, especially the interactive coupling between the roll and the vertical modes of motion. Accuracy of the model was demonstrated by comparing the analytical results with the experimental data. It was shown that rollover of a vehicle could occur at lateral acceleration levels lower than its static acceleration limit or rollover threshold due to roll resonance of the vehicle. It was concluded that the limiting dynamic acceleration is dependent on the vehicle's suspension characteristics, especially the backlash in the suspension, and that the elimination of the suspension backlash could improve the roll rigidity of vehicles. Finally, it was suggested that the rollover limit for a vehicle should be judged by the vehicle's resonant response and the potential for the roll resonant frequency to be excited in normal maneuvers. Das [92] investigated maneuver-induced rollover threshold of commercial vehicles using this model. While computer simulations were carried out

based on the available low speed experimental data, curve-fitting techniques were applied to extrapolate for the threshold values of lateral acceleration and forward velocity. Relative rollover conditions and dynamic rollover threshold of heavy vehicles were analyzed by Liu et al. [93, 94] to establish an array of potential dynamic rollover indicators towards development of an early warning device. A relative roll instability indicator defined as Roll Safety Factor (RSF) was proposed and shown to be a highly reliable indicator regardless of vehicle configurations and operating conditions. The correlation of various potential rollover indicators with the RSF was then investigated for a five-axle tractor semitrailer combination. The study showed that the trailer lateral acceleration and axle roll angles are closely correlated with the RSF.

1.2.1.3 Three-dimensional yaw and roll plane analyses

The yaw and roll plane models due to their simple nature have been extensively used to study the uncoupled yaw and roll dynamic response of heavy vehicles. In view of the strong coupling between these two motions, a number of three-dimensional vehicle models with varying complexities have also been developed. The National Swedish Road and Traffic Research Institute [95, 96] developed a test procedure for control of the dynamic stability of heavy vehicle combinations and proposed criteria that should be met for approval. A nonlinear yaw/roll model, including four-DOF (longitudinal, lateral, roll and yaw) motions for the leading vehicle unit and two-DOF (roll and yaw) for each of the rear units, was developed to analyze the lateral and roll stability characteristics in terms of two accident-risk related criteria: (i) overturning risk factor value, calculated from the relative wheel loads; and (ii) rearward risk factor amplification, defined as the ratio of the maximum risk factor of a rear unit to that of the leading unit. The model was further

enhanced to permit analysis of steerable axles and to simulate heavy vehicle combinations with up to three articulation points and up to nine axles, subject to driving or braking forces, lateral load transfer, etc. Several full-scale field tests were performed to validate the simulation program, and to develop test methods to assess the directional performance of heavy vehicles. The results indicated that the rearmost unit of an articulated vehicle possesses the highest risk factor. Finally, suggestions regarding suitable vehicle design parameters, such as number of articulations, steered axle location, tire data, geometric configuration, load condition and roll stiffness were also made. The assumption of small roll angles limited the use of this model for simulation of rollovers. Ellis [97] developed a model of an articulated vehicle with six-DOF, including tractor forward speed, lateral velocity, yaw velocity and roll angle together with the trailer articulation and roll motions. The analysis incorporated various important flexibilities of the combination and employed the fifth wheel to transmit moments between the tractor and trailer, while the moment in roll direction was neglected.

A comprehensive three-dimensional directional dynamic model of commercial vehicle combinations, referred to as Yaw/Roll model, was developed to study the roll dynamic behavior of single and multiple articulated vehicles engaged in constant speed maneuvers, which may approach rollover condition [98-100]. The equations of motion of the vehicle were formulated by treating each of the sprung masses as a rigid body with motions along five-DOF, including lateral, vertical, yaw, roll and pitch motions, while each axle was treated as a beam axle with roll and bounce-DOF. The model further incorporated the nonlinear force-deflection and hysteresis of the suspension springs, and nonlinear cornering force and aligning torque characteristics of the tires, while the

suspension roll center was assumed to be located at a fixed distance from the sprung mass c.g. The pitch angles of sprung masses and the relative roll angles between the sprung and unsprung masses were assumed to be small, such that the small angle assumption could hold. Further, the principal axes of inertia of the sprung and unsprung masses were assumed to coincide with their respective body fixed coordinate systems. The steering maneuvers could be performed either in an open-loop manner by defining the time history of the front-wheel steer angles, or in a closed-loop manner by describing the path coordinates, where the steer angle is generated using the path coordinates in conjunction with a simplified driver model. The simulation program could analyze vehicle combinations involving up to four units and eleven axles, and thus resulted in a maximum of 52-DOF. The vehicle model permitted the dynamic analysis of vehicles with up to five steerable axles, in addition to the front axle, where the steering may be generated through self-steering or kinematic-controlled steering mechanisms. The simulation model is particularly versatile in representation of multiple-axle configurations and different types of hitch mechanisms between the vehicle units, which enables the analyses of A-, B- and C-train combinations.

The Yaw/Roll model has been extensively used to evaluate roll, yaw and lateral directional response characteristics of various vehicle combinations with different articulation mechanisms [101-104]. Using this model, Ervin et al. [101] investigated the influence of size and weight variables on the dynamic stability and control characteristics of heavy trucks and trailer combinations. It was clearly established that directional performance characteristics of these vehicles are quite sensitive to variations in vehicle parameters. The Yaw/Roll model was also used to study the dynamics and stability

characteristics of Canadian log-hauling trucks [102-104]. While the Yaw/Roll model has been extensively used to assess the directional dynamics of various heavy vehicle combinations under constant forward speed, the model is considered to be quite complex due to its large number of DOF and requirement of large number of geometrical, inertial, suspension and tire parameters. In addition, the Yaw/Roll model does not adequately evaluate the rollover property of vehicles that exhibit yaw divergence at lateral acceleration levels lower than the rollover limit.

1.2.1.4 Directional response under braking and turning

Majority of the studies on directional dynamics have been performed under either steering or braking inputs [105-112]. The variations in speed and tire properties under simultaneous braking and steering result in considerable complexities in analysis. The simple linear formulations are no longer sufficient for valid investigations on braking-in-a-turn, especially in the upper range of lateral acceleration and braking deceleration/driving acceleration values. The combination of variable speed maneuvers, together with cornering is one of the most commonly encountered highway maneuvers, which has been associated with most vehicle accidents. During variable speed maneuvers, the load transfer in the longitudinal direction due to acceleration or deceleration can lead to wheel lock-up, resulting in possible yaw instability and loss of directional control of the vehicle.

Leucht [113] developed a three-axle tractor-semitrailer model, which is frequently referred to as TBS (total braking and steering) model, to investigate the behavior of the vehicle subjected to various braking applications in a turn. The vehicle forces were modeled in the plan view (top view) with four-DOF, including longitudinal, lateral and

yaw motions of the tractor, and yaw motion of the semitrailer. The basic assumptions made are similar to those described for linear yaw plane models. Two major differences, however, should be noted: (i) the lateral tire forces were expressed as nonlinear functions of slip-angle and vertical load; (ii) the dynamic load transfer effects (due to pitch and roll contributions) in both the longitudinal and lateral directions were taken into account in a quasi-static manner in determining the normal load on each tire. The model also allowed for the effect of frictional moment at the fifth wheel coupling, and was used to study the influence of design parameters and operating conditions on the directional behavior of the vehicle. The influence of loading conditions, brake-torque distribution and load-sensitive brake-torque control on the directional response of the vehicle during braking was investigated to identify the operating conditions and design parameters, which promote jackknifing. The variations in loading conditions were identified among the major causes of undesirable directional response under normal operation with a fixed brake-torque distribution.

Murphy et al. [114] carried out a series of tests to study the directional behavior of various heavy vehicles during braking. The investigation was aimed at improving the braking performance through advanced braking systems. Singh [115] used a nonlinear model, assuming negligible bounce, pitch, and roll motions, to investigate the directional performance of a four-axle truck trailer combination during braking and turning maneuvers. It was shown that the center of mass of the truck should be closer to the front axle than to the rear axle of the truck in order to reduce the jackknifing tendency. The distance from the center of mass of the truck to the front hitch should be large, and a full trailer should have a long drawbar to reduce the magnitude of trailer swing. The influence

of various anti-lock brake system (ABS) designs on the directional behavior of heavy vehicles has also been investigated in many studies [116-118].

The research efforts, in recent years, have been directed towards development of increasingly sophisticated computer simulation models to handle complex tire characteristics [119-127]. Since the directional dynamics of vehicle combinations is strongly related to the forces and moments generated at the tire-road interface, nonlinear tire models have been used in the lateral stability analyses of heavy vehicles subject to braking and steering maneuvers. The directional dynamics of heavy vehicles under simultaneous applications of braking and steering have been further investigated through development of variable speed three-dimensional yaw/roll models. The Phase IV model [119] represents the most comprehensive vehicle dynamics model developed in the 1980's for analysis of yaw, roll and lateral stability of heavy vehicles subject to braking and steering maneuvers. The model integrates the properties of braking and anti-lock brake system, nonlinear cornering properties of tires under simultaneous braking and steering maneuvers using lookup tables, nonlinear force-deflection properties of suspension springs, properties of the articulation mechanism and driving/braking torque. The directional analysis can be performed using either open-loop directional maneuver, where the time histories of the front wheel steer angles are specified, or closed-loop driver path-follower maneuver, where the coordinates of the path are specified. The braking input is defined by the brake application pressure versus time. The vehicle model is developed to analyze different vehicle combinations comprising up to three units and ten axles, such as trucks, tractor-semitrailer combinations, doubles, and triple combinations, with a maximum of 71 DOF.

The Phase IV model is considered to be quite complex and it requires extensive vehicle data. The simulation model has been used to assess various vehicle performance measures including handling, static and dynamic roll stability, lateral dynamics, yaw oscillations and braking performance. Recently, the Phase IV model has been incorporated into a Human-Vehicle-Environment (HVE) simulation platform [121], resulting in Engineering Dynamics Vehicle Dynamic Simulator (EDVDS) [122]. The most significant modeling difference is the removal of the small angle assumption, allowing study of complete vehicle rollover. The EDVAD also employs the surface profile to allow the vehicle tires to follow a 3-D terrain profile of arbitrary complexity. The extended semi-empirical tire model permits the study of severe handling maneuvers wherein tire slip-angles approach and exceed 90 degrees. EDVDS further incorporates a drivetrain model, permitting its use in tractive effort and gradability studies. User interface was substantially improved by replacing Phase IV's batch processing interface with the HVE simulation environment. The TruckSim software [125, 126] developed by Sayers and Riley has also received wide acceptance for simulating and analyzing the dynamic braking and handling behavior of trucks, buses, and tractor-trailer combinations. The attraction of this program arises in part from its foundation of truck modeling methods developed at the University of Michigan Transportation Research Institute (UMTRI), and the use of an advanced graphical user interface to make the software both easy to understand and user-friendly. The interface also provides convenient means to evaluate vehicle performance by means of animations, and time history plots of engineering variables of interest. The control inputs include powertrain parameters,

braking and steering. The powertrain input may be a constant power input, a constant speed, or a time history of the speed.

Yang et al. [128] developed a nonlinear yaw plane model with limited roll DOF of a tractor- semitrailer vehicle to study its braking and steering response. The vehicle combination was modeled as a six-DOF dynamic system, including four-DOF for the tractor (longitudinal, lateral, yaw and roll motions) and two-DOF for the trailer (articulation and roll angles). The prediction abilities of the proposed model were examined by comparing its directional response with those derived from the well-known Yaw/Roll model and the reported measured data. It was concluded that the c.g. heights of the tractor and trailer units are the most significant factors, while the parameters describing the horizontal distances between tractor front axle and its c.g., and between trailer axle and its c.g. are relatively less significant. The tire properties and the fifth wheel yaw damping, in general, strongly affect the dynamic response of the trailer and the tractor, respectively. The roll stiffness of the fifth wheel mostly influences the lateral acceleration of the trailer, the yaw rate and roll angle response of the tractor.

The above reported studies, however, did not consider the effects of cargo movement on the overall dynamics of the vehicle system. The cargo is generally assumed to be rigidly attached to the trailer beds and thus the cargo interactions with the dynamics of the vehicles are neglected.

While many studies have described the development of various computer simulation models to analyze the directional dynamics and stability characteristics of various heavy vehicle combinations, there exist relatively few published studies on comparison of these models. El-Gindy and Wong [129] conducted a comparative study of

various computer simulation models developed for directional and stability analysis of heavy vehicles, including the linear yaw plane, the TBS, the Yaw/Roll and the Phase IV models [63, 98, 113, 119]. The transient steering response characteristics of a tractor-semitrailer in a lane-change maneuver, analyzed using the four simulation programs, were observed to be qualitatively similar. A comparison of the simulation results with the measured data further revealed that the more sophisticated Phase IV model does not necessarily yield more accurate transient response than the simpler linear yaw plane model.

1.2.2 Performance Measures Related to Directional Dynamics of Heavy Vehicles

Although the directional dynamics and stability characteristics of heavy vehicle combinations have been extensively reported in the literature, most of the studies did not directly address the most important safety related concerns of the regulators and operators. Majority of the studies reported analytical methods and influence of various design and operating parameters on the directional response behavior of specific vehicle configurations, while the analyses were frequently conducted under different steering inputs, operating speeds and braking inputs. The studies thus did not permit relative highway safety performance evaluations of different vehicle configurations due to lack of standardized and controlled inputs, and performance measures. The dynamic performance of the vehicle combination is often assessed in terms of lateral acceleration, yaw rate and roll angle response of the vehicle units, which may be related to yaw and roll instabilities [71, 72, 128-130]. A few studies have evaluated the dynamic characteristics of the vehicle combination in terms of safety-related performance

measures, such as load transfer ratio, rearward amplification and effective lateral acceleration [94-97].

In light of the extensive variations in commercial vehicle configurations, tire and suspension designs, and operating limits, a need to develop well defined performance measures has been identified to establish the relative dynamic stability and safety performance measures of heavy vehicles under representative steering inputs. A series of performance measures related to roll, yaw and lateral dynamics of heavy vehicle combinations, have evolved in recent years [95, 96, 101]. The first set of performance measures was developed for the Canadian Vehicle Weights and Dimensions Study by Road and Transport Association of Canada (RTAC) [101]. The performance measures, primarily derived from the Yaw/Roll and Phase IV simulation programs have been used to assess the impact of relaxed weights and dimensions regulations in Canada [98, 119]. These measures attempted to address the safety concerns related to directional stability, control, off-tracking and braking performance of heavy vehicles. Although not formally adopted by RTAC, this set of measures continues to be referred to as 'RTAC measures'. They were used to provide the scientific and technical basis for regulatory changes introduced in most Canadian provinces following the Weights and Dimensions Study. These regulations were designed to encourage the use of preferred vehicle combinations, which were judged superior to other configurations from safety performance point of view. Winkler and Bogard [131] developed simple predictors of the performance measures for A-trains by applying regression techniques to determine the relationships between the measures of interest and vehicle design parameters. The study examined different performance measures, including rearward amplification, yaw damping

coefficient and those defined by RTAC (high-speed transient offtracking, static rollover threshold, dynamic load transfer ratio, low-speed transient offtracking and high-speed steady-state offtracking).

EI-Gindy and Woodrooffe [132] evaluated the influence of variations in various design parameters on the selected dynamic performance of B-train doubles, namely, friction demand, dynamic load transfer ratio, offtracking and handling. The study involved parameters that could be potentially regulated, such as wheel base, tandem axle spread, and fifth wheel location. A “three-point” handling performance measure was also suggested for assessing the vehicle design parameters. Winkler et al. [134] described two regulatory scenarios pertaining to the basic resistance to rollover and the obstacle avoidance maneuvering capability of longer and heavier commercial vehicles. The primary goals of the scenarios were to provide reasonable assurance that all vehicles would have a static rollover threshold exceeding 0.35g and exhibit rearward amplification less than or equal to 2.0. Aurell and Winkler [135] described the test procedures proposed by the International Standards Organization (ISO/SC9/T22) for evaluating dynamic performance of heavy vehicles. The proposed stability criterion involved two basic performance regimes, namely the forced and the free response of articulated vehicles, which are evaluated in terms of rearward amplification, dynamic off-tracking, yaw damping, mode shape and zero damping speed (the speed at which the damping of free oscillatory movements of the vehicle combination approaches zero).

EI-Gindy [136] reviewed the existing performance measures for commercial vehicles and summarized the methods for their evaluation. The study further proposed the

pass/fail criteria based upon recommended target values for different measures, which are summarized below:

- (1) Handling performance measures to assess the handling quality of the vehicle;
- (2) Static rollover threshold (SRT) to assess the rollover limits of heavy vehicles under steady turns;
- (3) Dynamic rollover stability in terms of load transfer ratio (LTR) and rearward amplification (RA) to assess the dynamic roll stability limits under transient maneuvers;
- (4) Yaw damping ratio (YDR) to assess the rate of decay of yaw oscillations of the trailer;
- (5) Friction demand of the drive-axle tires to assess the low and high-speed jackknifing potentials of vehicle combinations;
- (6) Lateral friction utilization (LFU) to assess the low and high-speed lateral slippage potentials;
- (7) Low and high-speed steady-state and transient offtrackings to assess the maneuverability over tight intersections and safety risks on highways;
- (8) Braking performance to assess the braking efficiency, stopping distance, response time and jackknifing potentials of vehicle combinations.

McFarlane et al. [137] attempted to derive correlations among eight different performance measures, including static roll stability (SRS), rearward amplification (RA), load transfer ratio (LTR), high-speed transient off-tracking, high-speed friction utilization, high-speed steady-state off-tracking, low-speed off-tracking and low-speed friction utilization. The study established highest correlation between: (i) LTR and SRS; (ii) RA/SRS and LTR; (iii) high-speed transient off-tracking and SRS; and (iv) high-speed steady-state off-tracking and SRS. It was concluded that SRS is the single most important performance measure, since it features in all the correlations.

1.2.3 Liquid Sloshing in Moving Containers

The sloshing of liquids and resulting fluid-structure interactions have been identified as important issues in the area of transportation engineering and many other fields since 1950's. These include the movement of liquid fuels within automobile tanks; movement of liquid products and chemicals in tank trucks, railroad cars and oceangoing vessels; fuel tanks of airplanes and space-crafts; liquid motions in containers of offshore structures, etc. Sloshing of liquid in a partially-filled container subjected to external excitations from the retaining structure may cause coupled dynamic interactions between the liquid and structure. The coupled problem associated with interactions of the sloshing liquid with the moving vehicle has been recognized as an important issue related to directional stability of various vehicles [138]. The dynamic interactions can adversely affect the dynamics and stability of the vehicles as well as the structural integrity of the retaining structures. The vehicle and the retaining structure may be subjected to excessive forces and moments, when fundamental slosh frequency lies in the vicinity of the natural frequency of the vehicle structure or the control frequency.

Liquid sloshing has been investigated in connection with stability of satellites since the start of the space age in the early 1950's. Cooper [139] and Abramson [140] conducted comprehensive reviews on the topic of liquid sloshing problems. These preliminary works presented some important analytical solutions, and conducted experiments to examine the validity of some of the theoretical models. The monograph edited by Abramson [140] gives the most thorough survey of the earlier literature, including more than 500 citations published prior to 1966, specially related to behavior of fluids in oil tanks of aircraft and space vehicles. Since the 1960's, a great number of

investigations on liquid sloshing have been carried out in different fields of applications: space vehicles, cargo ships, large ground storage tanks and canals, etc. A variety of theories and approaches to analyze fluid sloshing have been developed for different tank configurations and input excitations. Some of these studies, which are relevant to the sloshing of cargoes in tank trucks are briefly summarized below.

1.2.3.1 Hydrodynamic models and solution methods

The field related to liquid motion in moving containers includes a great number of analytical, numerical and experimental studies focusing on different aspects of this problem. The first aspect includes physics of sloshing covering such subjects as flow patterns in containers and development of sloshing models. The second aspect concerns with governing equations and solution methods. One of the most general approaches used to simulate liquid motions involves the use of Navier-Stokes and continuity equations in conjunction with appropriate boundary conditions. These formulations, however, are nonlinear and quite complex, when applied to moving vehicles. The nonlinear effects are mostly associated with the free surface due to fluid motion, fluid-tank interface due to the tank geometry, and fluid viscous damping and couplings of different sloshing modes. The variations in the free surface coordinates with time leads to additional difficulties in the analysis of differential equations. The fluid slosh analysis in majority of the reported studies have thus been performed with considerable simplifications, namely inviscid fluid and irrotational flows, thereby permitting the use of potential flow theory [139-141].

Majority of the existing theories on fluid sloshing are based on the assumptions of inviscid incompressible fluid, where a velocity potential exists, and small amplitudes of fluid motion compared with container dimensions, often the depth of the fluid. The fluid

slosh model is thus described by a linear second order Laplace equation with appropriate boundary conditions, which can be solved analytically by employing the classical method of separation of variables. The complexities associated with the free-surface equation are overcome either by neglecting the nonlinear terms assuming relatively small wave height and fluid velocities or by linearization [142, 143]. Both the linear and linearized sloshing theories yield reasonable agreement with the experimental data for small amplitude liquid motion [139-143]. One of the early works was performed by Budiansky [142] in 1960 to estimate the natural frequencies, mode shapes and forces exerted on the walls of partially-filled circular canals and spherical tanks due to lateral excitation resulting in small amplitude liquid oscillations. Budiansky solved the sloshing problems based on potential fluid theory and analyzed the forces and moments acting on the circular canal surfaces. The linear or linearized slosh analyses, however, may yield certain errors when sloshing occurs with large amplitudes.

The early studies on nonlinear slosh analyses were based upon more exact free surface boundary conditions [144-146]. Abramson performed a series of experimental and analytical studies on forced response of liquids in cylindrical and spherical tanks with separating walls. Experimental data were used to examine the validity of the mathematical models and to understand the effect of geometrical and physical variables on the free surface oscillation. Majority of the reported studies, both theoretical and experimental, however, investigated the liquid motions under harmonic disturbances, while the sloshing analyses under arbitrary excitations were reported in relatively few studies.

In the past few decades, many numerical algorithms have also been developed to study the sloshing behavior of liquids in stationary and moving containers using finite difference, finite element, and boundary element methods [147-164]. While the boundary element methods are mostly based on potential flow theory, the finite-element and finite-difference based methods are based upon the solutions of Navier-Stokes equations for viscous fluids. The numerical methods employ different algorithms to achieve solutions of the Navier-Stokes equations, such as MAC (Marker and Cell Method)-type methods, developed by Welch [147] and Hirt et al. [148]. The SOLA-SURF and SOLA-VOF techniques, frequently referred to as Navier-Stokes codes [143], have also been used to study liquid motions involving complex liquid free surfaces with relatively large amplitudes of waves, and considerable impacts on the tank ceiling and walls [149-164].

Solaas [165] conducted a literature review of various solution methods and their properties for solving liquid slosh problems. Different analytical procedures, numerical techniques and model tests were assessed based on their performance in solving sloshing problems with various fluid properties (potential flow or viscous flow), tank motion characteristics, degrees of freedom, and liquid fill levels. The suitability and effectiveness of a commercial program FLOW-3D developed by Flow Science Inc., which solves Navier-Stokes equations by use of a finite-difference based code [148], was also evaluated. It was concluded that nonlinear analytical methods to the liquid governing equations are feasible only for very few simple cases of liquid motions, and that the available numerical methods and algorithms mostly deal with two-dimensional problems. The specific numerical procedure for a sloshing problem depends largely on the particular tank geometry, liquid depths and physical characteristics, excitation amplitudes

and frequencies, and must be formulated based on each specific problem. In addition, certain approximations in the solution procedures have to be made to make the mathematical problem tractable. There exists, however, no generally accepted computational procedure that could work robustly and accurately with nonlinear sloshing problems characterized by the presence of time-varying free surfaces, especially in cases of three-dimensional and coupled liquid-container interaction problems.

More recently, Ortiz [166] presented a review on various solution procedures for fluid motion involving a free surface, and concluded that majority of past works on liquid sloshing are based upon prescribed motion of the liquid retaining structure, where the motions of the liquid and container are uncoupled, and that there is very little published information on true fluid-structure interaction problems including full nonlinear sloshing effects, where the true interaction is defined as interaction in which both the motion of the container and the motion of the fluid are found in a closed-form numerical procedure. Ortiz and Barhorst [166, 167] developed a closed-form methodology for modeling coupled fluid-structure interaction problems. The main objective of the investigation was to find a path for rigorously solving a coupled problem involving a structure and a fluid with nonlinear sloshing. Three steps are involved in coupling the motions of the fluid and the structure: (i) finding the equations of motion for the structure as functions of the liquid pressure field; (ii) building a field equation for the pressure in the liquid domain as function of the accelerations of the moving frame attached to the container; and (iii) coupling these two sets of equations, which is accomplished by building a boundary-value problem for the instantaneous interaction pressure. The motion of the structure was not prescribed but found as part of the solution procedure. The fluid motion was modeled

as incompressible viscous flow using Navier-Stokes equations and potential flow using Laplace equations, respectively. A multi-body flexible system with a two-dimensional container carrying a fluid was considered and three examples were given, including a simple vehicle model, which represented the vehicle as a two-DOF mass-spring-damper system on a given rough road (vertical and longitudinal dynamics).

1.2.3.2 Equivalent mechanical modeling approaches

An alternate approach based on mechanical analogy has been proposed to estimate liquid slosh characteristics by a simple equivalent mechanical model [140, 141, 168-170]. An equivalent mechanical model is an assemblage of spring-mass-damper or pendulum system arranged in such a manner as to represent the dynamic behavior of liquid oscillation within its container. Dynamic equivalence is taken to mean the equivalence of force and moment resultants, frequencies of oscillation, and mass and inertial properties.

Two reasons necessitate the use of an equivalent mechanical model to represent the sloshing behavior of a contained liquid. Firstly, since the problem of forced damped liquid oscillations is actually nonlinear in nature, an exact solution is practically impossible. However, through the use of an equivalent mechanical model, the nonlinear nature of forced damped liquid oscillations can be approximated by equivalent linear damping in the form of dashpots, thereby making it possible to obtain finite results near the resonant frequencies of the liquid. This is not possible in the linear or linearized fluid analysis, where the liquid is assumed inviscid. Secondly, the overall problem of vehicle dynamics and stability is greatly simplified in that the equations of motion of the vehicle system are not so complex. The monographs edited by Abramson [140] and Roberts et al.

[141] list a number of equivalent mechanical models and analysis procedures for various tank shapes and motion characteristics. For example, Dodge [169] developed an equivalent mechanical model, comprising a simple spring-mass-damper system, to investigate the dynamic liquid sloshing within the fuel tanks of a spacecraft, and established the fundamental sloshing frequencies, mode shapes and forced response characteristics, for typical tank configurations used in space vehicles. More recently, Abzug [171] analyzed the influence of coupled dynamic interaction between the liquid slosh within fuel tanks and an airplane's normal modes of motion on the stability and control of the airplane. A mass-spring damper model was used to simulate the two-dimensional motion of the sloshing fuel.

The simplicity of the analogy equation allows the effect of liquid sloshing to be easily integrated with the equations of vehicle motion for further analysis. However, the complications associated with definition of pendulum or spring-mass elements including their configuration, number, stiffness, and damping coefficients require experimental investigations which, in principle, must be conducted for each specific problem. Too much in this matter depends on the researcher's experience and intuition since a good guess should be made prior to mathematical analysis and validation of the equivalent system. Thus, this method either involves experimental definition of the parameters of the equivalent mechanical model or can be carried out by use of an appropriate sloshing theory. However, in the latter case, the approach loses its attractiveness since the linear analytical solutions are already available, and the equivalent model based upon the linear theory, will exhibit all the limitations inherent with the theory, while nonlinear solutions

are generally extremely difficult to obtain, especially in cases of coupled fluid-structural interaction problems, as indicated earlier.

1.2.3.3 Modeling and analyses relevant to tank vehicles

Although the numerical techniques have been successfully employed for analyses of fluid motions in fixed containers of simple cross-sections, the analyses for moving road containers have not been addressed. This may be attributed to complexities arising from relatively complex geometry of road containers, nature of excitations and coupling modes, and coupled fluid-vehicle interactions [8]. The handling and stability analyses of road tankers involve forces and moments arising from tire-road interactions, braking, steering, and combined braking and steering. Strandberg [8] reported a review of analytical and experimental studies pertaining to liquid motions in vehicles, including natural frequencies of liquid slosh in partially-filled containers and slosh forces in different containers. The study further investigated the lateral stability of road tanks through scale model tests and computer simulation techniques. The lateral sloshing force developed in a scale model tank was measured under lateral displacement excitations generated by a hydraulic-servo drive. This measured force was integrated into a simplified vehicle model, which was analyzed to study the lateral stability of the vehicle. The proposed methodology, however, would pose more complexities when full scale tank is considered under representative excitations.

Steady-state and quasi-static roll plane sloshing models were developed based upon hydrostatic theory and used to study the destabilizing effects of shifting cargo on the roll stability of tank vehicles by Rakheja et al. [172] and Ranganathan et al. [173]. These models assumed negligible contributions due to fluid viscosity and slosh dynamic

forces, while the fundamental slosh frequency is assumed to be considerably higher than the highest steering frequency. Although the quasi-static models do not predict the slosh forces due to free surface oscillations, the computed mean values of the vehicle motion revealed reasonably good agreement with the experimental results [192, 193].

Popov et al. [174-177] developed a comprehensive nonlinear liquid slosh model represented by a two-dimensional incompressible Navier-Stokes and continuity equations together with appropriate boundary conditions along the rigid walls and the free surface. Analytical formulations were presented for steady-state and transient analyses of liquid motion within rectangular and circular cross-section containers subject to a uniform acceleration. The differential equations were solved numerically in an Eulerian mesh using the finite difference methodology [147]. The validity of the dynamic slosh model was also presented through laboratory tests performed on a scale model container. The study investigated the influence of various input parameters on the main loading factors, such as the liquid forces, overturning moments, heights of the free surface, and the damped frequencies of liquid vibrations. The authors recommended further studies on different tank shapes and three-dimensional analyses of coupled liquid motions in the lateral and longitudinal directions, under vehicle motions caused by simultaneous braking and steering.

1.2.4 Dynamic Characteristics of Partially-Filled Tank Vehicles

Dynamic analysis of partially tank vehicles has been addressed in only a few studies due to the complexities associated with modeling of fluid dynamic behavior inside the moving tanks and fluid-vehicle interactions. Slibar and Troger [178] studied the dynamics of an articulated tank vehicle using an equivalent single-DOF mechanical

oscillator to simulate the liquid slosh force in the roll plane. The motion of the liquid cargo in the roll plane was represented by two lumped masses coupled through a linear spring and a viscous damper. The two-DOF fluid slosh model was coupled with a six-DOF vehicle model, including the lateral, yaw and roll motions of the tractor, relative yaw motion of the dolly, and yaw and roll motions of the trailer body. The study presented the steady-state frequency response characteristics of the yaw and roll deflections of the vehicle, and concluded that partial-fill condition yields a resonant response that is considerably larger than that observed in rigid freight vehicles. Strandberg [8] developed a simplified model to investigate the influence of liquid sloshing behavior on the skidding and overturning tendencies of tank vehicles, upon neglecting the roll and yaw motions. The investigation was based on measured liquid sloshing forces in a laterally oscillated scale model tank having dynamic similarity with a real tank. The fundamental slosh frequencies of liquid motions within the partially-filled tank were determined using a scale model. The study also presented the influence of variations in directional maneuvers, tank configurations, and anti-sloshing devices on the behavior of tank vehicles. The study suggested to reduce the number of articulations and a piston arrangement to eliminate fluid slosh effects in partially-filled cylindrical tanks. The Highway Safety Research Institute at University of Michigan conducted analyses as well as full-scale testing of tank vehicles and concluded that these vehicles exhibit poor directional stability and low levels of rollover immunity during dynamic maneuvers executed at highway speeds [64, 179, 180]. The study also recommended an in-depth investigation into the possibility of designing tankers that maximize the safety for such

vehicles. However, the relative motions of liquid cargo with respect to the tank were neglected in the analyses.

Culley et al. [181] undertook a survey of trucking companies on safety and stability problems related to shifting cargoes, including accident involvement, typical equipment as well as loading and hauling procedures, and investigated the effects of dynamic cargo shifting on the lateral/roll stability and braking performance of articulated trucks through full-scale tests. The study identified severe problems for two cases, sloshing of liquid cargo and swinging of hanging meat. Vehicle configurations consisting of tractor with baseline van, and unbaffled, baffled and compartmentalized tank trailers, including low-density (MC-306) and high-density (MC-312) cargo tankers, were considered. The test maneuvers included braking, cornering, lane change, and cornering with braking on both dry and wet road surfaces. The study concluded that the vehicles carrying shifting cargoes reveal reduced stability limits compared with the baseline rigid cargo vehicle, and that the lateral stability was significantly influenced by the c.g. location of the loaded trailer. Further tests on larger cross sections of vehicles and a wider variety of loading conditions were suggested for thorough analysis of the nature of the problems caused by shifting cargoes. Bohn et al. [182] analyzed the stability of partially-filled tank vehicles through computer simulations. The equations of motion for sloshing fluid within an elliptical tank were derived using Lagrange's equation assuming small amplitudes of sloshing wave (three-dimensional linear sloshing model). The effects of sloshing liquid cargo on the limiting performance characteristics of articulated trucks were evaluated by integrating the liquid slosh model with a three-dimensional vehicle simulation model (TDVS) developed by Illinois Institute of Technology Research

Institute. Both vehicle configurations and maneuvers were modeled to correspond with the full-scale experiments reported by Culley et al. [181]. The slosh model, however, was not adequately verified due to lack of experimental data. The inadequate consideration of braking in the TDVS model also did not permit the braking performance analyses. In addition, the simulation results did not correlate well with those derived from the experimental study due to differences in operating conditions. It was concluded that the simulation model was extremely sensitive to rollover, and the sloshing dynamics augmented TDVS simulation was considered as qualitative and inconclusive.

Khandelwal and Nigam [183] developed an equivalent mechanical model of liquid in a rectangular container to simulate the dynamics of a vehicle carrying liquid cargo over a railway track with constant acceleration. The mechanical model comprised a fixed mass and a pendulum corresponding to the fundamental mode of the fluid motion, while only bounce and pitch degrees of freedom were included for the vehicle with rigid tires. Mallikarjunarao [184] investigated the impact of changes in tank vehicle design on the safety risks and economic aspects of transporting gasoline in Michigan. A static roll-plane model was developed for calculating the steady-turning rollover threshold of the tank vehicle, and a yaw/roll model was developed to study the directional and roll dynamics of articulated vehicles engaged in steering maneuvers approaching rollover condition. The influence of specific changes in vehicle design, such as tank cross-section, suspension properties, track width, etc., on the safety properties of the tank vehicle was evaluated. In addition, data on gasoline tanker accidents in Michigan were analyzed and rollover accidents were identified as the principal cause of gasoline leakage and fires.

However, the effects of liquid load shift were not considered in the investigation, as the tank was assumed to be either completely filled or empty.

A systematic investigation into influence of liquid sloshing motion within partially-filled tanks on directional dynamics and stability characteristics of tank vehicles was carried out by researchers at Concave Research Center [11, 172, 173, 187-188]. A steady-state fluid slosh model in the roll plane was developed and integrated with the roll plane model of an articulated vehicle to evaluate the rollover threshold acceleration limits of partially-filled tank vehicles [172]. A quasi-static fluid slosh model was developed and integrated with a three-dimensional vehicle model to investigate the dynamic behavior of the tank vehicle subject to constant steer, and lane change and evasive maneuvers [173]. The rollover threshold limits, directional response and stability characteristics of the partially-filled tank vehicle were then compared with those of the equivalent rigid cargo vehicles to demonstrate the adverse influence of liquid load shift. Parametric sensitivity analyses were conducted to study the influence of tank vehicle configuration, liquid fill level, steering inputs, and vehicle speed on the directional response and stability characteristics of the tank vehicle combinations [189-191]. The results showed that partially-filled tank vehicles as well as the equivalent rigid cargo vehicles exhibit stable behavior during lane change maneuvers at typical highway speeds. However, the excessive load shift encountered during an evasive maneuver could lead to wheel lift-off and possible rollover in case of liquid tank vehicles.

Field tests were performed using a truck with a small-size sprayer tank to validate the analytical model [192, 193]. The study concluded that the results obtained from the vehicle model, incorporating quasi-static fluid slosh analyses, correlated well with mean

values derived from the field measured data for different fill levels, vehicle speeds, and typical steering maneuvers. Motion of the liquid free surface and the corresponding lateral load transfer, attained via computer simulation, were further compared with those established from the field measured data to conclude that a quasi-static analytical model could accurately predict the fluid slosh loads.

A comprehensive dynamic model of a tractor tank semitrailer was further developed by integrating a two-dimensional finite-difference based non-linear dynamic fluid sloshing model [187] to the three-dimensional vehicle dynamics model [173]. The dynamic slosh forces and moments obtained from the dynamic liquid model were coupled with the vehicle dynamics model to study the directional response characteristics of the tank vehicle. The dynamic characteristics of the partially-filled tank vehicle employing the dynamic slosh model were compared with those employing the quasi-static vehicle model [173], for steady as well as transient directional maneuvers. Simulation results revealed that during a constant steer maneuver, the dynamic fluid slosh loads introduce oscillatory directional response about the steady-state value calculated from the quasi-static vehicle model. The directional response characteristics obtained using the quasi-static and dynamic fluid slosh models during transient steer inputs showed good correlation. Based upon the studies, it was concluded that a quasi-static model could predict the directional response characteristics of tank vehicles quite close to those evaluated using the comprehensive fluid slosh model during various typical highway maneuvers.

Simplified approaches for estimating the rollover threshold limits of partially-filled tank vehicles were also explored using moment equilibrium in the roll plane [194,

195]. These studies established that **tank** geometry is an important factor that influences the lateral load shift and thus the directional response and stability characteristics of partially-filled tank vehicles. The studies, however, were performed only for conventional tank shapes, which are observed to have certain limitations related to their geometry from vehicle stability point of view. In addition, these studies considered the load transfer caused by fluid sloshing in the roll plane alone, and the vehicle motion was limited to constant speed steering maneuvers.

The influence of fundamental slosh frequency and dynamic slosh forces on the dynamics of a tank vehicle was investigated by Ranganathan et al. [196] through an equivalent mechanical system model based upon the pendulum analogy, proposed by Abramson [140]. A simple pendulum model representing the fundamental frequency of the fluid oscillation was developed and its parameters were identified as function of the fill level and fluid dynamics. The fluid model was then integrated with a 3-dimensional model of the vehicle to compute the directional response characteristics of the tank vehicle with constant forward speed.

Rakheja and Wang [197] analyzed the braking process of partially-filled and compartmented tank vehicles, and the influence of partition location on the braking performance of the vehicle system. A pitch-plane kineto-static model of partially-filled circular and ellipsoidal tanks was developed and integrated to the braking model of tank vehicles to study the effects of longitudinal fluid slosh on the braking performance. Longitudinal load transfer, stopping distance, braking time and time lag between front and rear axle wheel lockup were obtained, and parametric studies were performed to derive optimal sizes of compartments. Pitch plane tank vehicle models were further

developed by integrating a steady-state liquid model and a mechanical analogy model of a partially-filled circular tank, respectively, to a pitch plane model of a five-axle tractor semitrailer to predict the straight line constant deceleration braking behavior of the tank vehicle in terms of dynamic normal load factor [198, 199].

Ibrahim et al. [200] investigated the ride behavior of trucks carrying two spherical fluid containers. A mathematical model of a medium weight truck with bounce and longitudinal DOF was formulated, which incorporated physical and dynamic characteristics of the fluid cargoes. The fluid cargoes in the tanks were simulated as nonlinear pendulums with specific damping coefficients. The partial filling ratio and liquid cargo viscosity were shown to play major roles in the vehicle ride behavior. Bogomaz et al. [201] proposed a three-dimensional mechanical pendulum analogy based on potential flow theory for liquid cargo mobility simulation. The liquid motions included longitudinal, lateral and yaw DOF. Hydrodynamic parameters of the mechanical system were determined using the solution of a three-dimensional boundary-value problem of the liquid cargo in the tank. The validity of the mathematical models was demonstrated through comparison of the analytical results with the test data. It was observed that the hydrodynamic parameters essentially relied upon the fill level. The study further analyzed the dynamics of a railway tank car in the pitch plane incorporating a single-degree of freedom pendulum analogy model. Aquaro et al. [202] presented a approach for determining the rollover threshold of a tank truck using finite element analysis methods, incorporating the nonlinear behavior of suspension spring and tank flexibility. The study used simple mechanical pendulums to represent the fluid slosh effects in an elliptical tank, beam elements to characterize the torsional and bending

stiffness of the tank structure, and spring-damper elements to simulate the suspension system.

In a recent study, Salem et al. [203] conducted a literature review on the work done related to the rollover stability of partially-filled tank vehicles, including fluid-structure interaction, yaw and roll stability of heavy vehicles, and fluid-vehicle dynamic interaction. It was concluded that although a number of studies have been conducted on topics related to partially-filled heavy-duty vehicle rollover stability, no model exists so far that can predict the rollover of a partially-filled tanker with general configuration (such as number of units, shape of the tank, etc.). Furthermore, tank trucks undergoing combined braking and turning maneuvers need further investigation since the only model [182] tackling this kind of maneuvers did not reveal consistent experimental and analytical results, especially for elliptically-shaped tanks.

1.2.5 Tank Design and Vehicle Stability

The design standards and safety regulations for vehicles carrying dangerous goods have been outlined by the CSA (Canadian Standards Association) B338-1982 [204] in Canada and Title 49 of CFR (Code of Federal Regulations) [205] in the U.S. These standards apply to cargo tanks used for highway transportation of dangerous goods via road mode and portable tanks used for transportation of dangerous goods through other modes. These standards describe basic requirements for design, construction, testing, inspection, re-testing, qualification and maintenance, and identification aspects of such tanks. Highway tanks are designated with specifications MC 306, MC 307, MC 312/331, etc. The modified-oval cross-section (MC 306) tanks, made of aluminum, are designed for only 20.7 kPa (3 psi), which are primarily used to haul petroleum products. The

circular cross-section (MC 307 and MC 312) tanks, made of stainless steel, are often designed for 241 kPa (35 psi) and are generally used to haul chemicals, flammable and corrosive liquids. MC 331 tanks are used to haul compressed gases such as anhydrous ammonia and propane at high pressures. Some of the general design and construction requirements applicable to these cargo tanks are described below:

- **Construction Practices:** The general construction practices for cleanbore and compartmented tanks are listed in section 173 of the U.S. DOT (Department of Transportation) code.
- **Materials:** All sheet and plate materials required for shell, heads, bulkheads and baffles are designated by ASME Boiler and Pressure Vessel's Code [205]. Additional material requirements, however, apply to those parts that are exempted from the above code.
- **Structural Integrity:** the maximum calculated design stress at any point of the tank may not exceed the lesser of the maximum allowable stress value prescribed in Section 8 of the ASME code, or 25 percent of the tensile strength of the material used. Additional structural integrity is necessary for cases where applicable, such as change in dynamic loading, internal pressure and temperature gradient.

The standards also address the design requirements for joints, manholes, openings, piping, valves and fittings, supports, circumferential reinforcements and accident damage protections. The standards, however, do not address the adverse influence of liquid sloshing forces in partially-filled tanks on the stability and handling of tank vehicles. The tanks, in general, are designed based on their structural integrity rather than on vehicle system stability considerations.

In view of the adverse influence of liquid sloshing on tank vehicle stability and safety performance, various attempts have been made to explore different tank designs in order to reduce liquid sloshing. Thus far, the only effective and accepted means of reducing the slosh loads are separating walls or baffles, both of which are implemented along the lateral cross-section of the tank [8-10, 140, 141, 170]. The combined effect of separating walls is to reduce the amplitude of free surface oscillations and consequently the slosh loads, and to augment natural frequencies of oscillations as compared with those of fluids in uncompartmented containers. However, the influence of separating walls has not been studied enough, and the design concepts of compartmented and baffled tanks do not have a solid theoretical basis. The slosh damping effects are mostly determined by experimental and semi-empirical methods [140, 141, 170]. The number, location and sizes of separating walls and baffles, as well as the size of baffle orifices are often chosen intuitively, and their effect on slosh loads have been addressed in very few studies.

Strandberg [8] investigated the influence of separating walls and baffles on the lateral stability of road tankers through scale model experiments. It was shown that the compartment width is an important parameters in conventional tanks and it was recommended that the compartment width must not exceed 0.6 m for a peak lateral acceleration of 0.4 g in order to ensure safe operation of the vehicle under cornering or lane change maneuvers. Wang and Rakheja [206] studied the influence of location of partitions on the braking performance of a partially-filled tank truck, and illustrated a methodology to determine the optimal compartment sizes to minimize the magnitude of longitudinal load transfer. The results clearly demonstrated that equal length

compartments yield minimal longitudinal load transfer under straight-line braking, irrespective of the liquid fill level, for both 2- and 3-compartment tank trucks.

While the addition of baffles tends to effectively resist the liquid sloshing along the longitudinal axis of the tank, their influence on the lateral liquid sloshing is insignificant. The experimental results, obtained by Strandberg [8], showed significant benefits of longitudinally placed separating walls in reducing the lateral slosh loads. In a recent study, Ibrahim [207] developed anti-slosh dampers to reduce the lateral motion of liquid cargo within partially-filled cylindrical tanks. The dampers consisted of partitions, containing rectangular slots and holes of different sizes, fitted vertically and passing through the longitudinal axis of the tank. A small-scale experimental model of a cylindrical tank subject to lateral excitations was designed to measure the viscous damping and damped natural frequency of liquid loads. The measured loading parameters were then applied to the full size tank using similarity analysis. The results showed significant reduction in lateral shift of the liquid cargo. The longitudinal partitions, however, are considered infeasible due to the additional weight and cost.

Roll stability analyses of partially-filled tank vehicles have further indicated that magnitude of lateral liquid sloshing under various vehicle maneuvers is strongly affected by the tank geometry, specifically the cross-section [8, 189]. The circular cross-sectional tanks, employed in general purpose transportation of liquid products, yield high center of mass location, but considerably less load transfer under a steady turning lateral acceleration field, especially under lower fill volumes. The modified-oval tanks used in transportation of fuel oils, on the other hand, yield lower c.g. height and relatively larger load transfer, when compared with that observed for circular tanks. Under high fill

volumes, the modified oval tanks exhibit higher roll stability limit than that of the circular tanks. This is mostly attributed to lower c.g. height associated with the modified oval geometry. Previous investigations on roll stability limits of partly-filled tank trucks have thus established that a circular cross-sectional tank may be preferred for low fill volumes, while a modified oval geometry may be desirable for high fill volumes [8, 189]. This implies that the roll stability limits of partly-filled tank vehicles over a wide range of fill volumes may be enhanced through selection of appropriate tank geometry, such that an adequate compromise between the c.g. height and liquid load shift can be attained. Mallikarjunarao [184] proposed a semi-rectangular tank profile to achieve lower c.g. height by varying the top and side radii as well as the blend radii of the conventional modified oval tank (MC306 Al) profile. Richardson [208] proposed a low profile modified rectangular tank to achieve lower c.g. height. Klingenberg et al. [209] presented a new concept tank truck configuration to enhance the roll stability of the vehicle by lowering the tank body height and increasing the cross-section width. The effects of liquid load shift, however, were ignored in these investigations. Popov et al. [210, 211] investigated the optimal shapes of rectangular and elliptic road containers by minimizing the overturning moment caused by the liquid load. The studies were limited to rectangular and elliptic cross-sectional tanks while the shapes were optimized based on a single design parameter.

1.3 OBJECTIVES AND SCOPE OF THE DISSERTATION

From the review of reported investigations on the subject of dynamics of heavy vehicles, in general, and tank vehicles in particular, it is apparent that the directional dynamics and stability characteristics of various configurations of commercial vehicles

have been extensively investigated. The contributions due to cargo movement and cargo-vehicle interactions, however, have been either neglected or considered under limited maneuvers. Majority of the reported studies on dynamics of tank vehicles have considered the movement of liquid cargo in the roll plane alone under constant speed steering maneuvers. Few studies have also investigated the fluid motion in the pitch plane alone under straight line braking. The fluid slosh analyses in these studies are mostly based upon either steady-state motion of inviscid fluid or equivalent mechanical models. Although majority of the studies have concluded on significant effects of tank geometry, specifically the cross-section, only limited efforts have been made to derive optimal tank cross-sections to minimize the magnitude of load shift within partly-filled tanks. The reported studies on roll stability and straight-line braking performance have thus been performed for conventional tank geometry, including circular and modified-oval cross-section tanks. Further studies to derive optimal tank cross-sections based upon a more general shape are thus desirable. Moreover, liquid load transfer, and its influence on vehicle handling and stability characteristics under combined steering and braking maneuvers have not been addressed. The objectives of this dissertation research are thus formulated to address two important issues related to tank vehicle stability. These include the identification of an optimal tank geometry and directional performance analyses under combined steering and braking inputs.

1.3.1 Objectives of the Investigation

The overall objective of this dissertation research is to contribute towards enhancement of highway transportation safety associated with relatively low stability limits of partially-filled tank vehicles through development of systematically analytical

methodologies and tank designs. The study involves development and analyses of fluid slosh, tank and vehicle models, and optimization-based design methodologies to enhance safety performance of tank vehicles. The specific objectives of the dissertation research are summarized below:

- a) Propose a generic tank geometry to describe the cross-sections of currently used tanks in transportation of fuel oils and bulk liquids.
- b) Formulate and solve constrained optimization problems involving roll moments caused by movement of the liquid cargo load within the partially-filled generic tank to derive optimal tank geometry as a function of the fill volume.
- c) Evaluate performance characteristics of optimal tanks in terms of liquid cargo load shift in the roll plane, and analyze the influence of tank geometry on the stress distribution of the tank structure.
- d) Analyze static roll performance characteristics of the vehicle with various tank designs as functions of fill volume through development and analyses of a static roll plane model of an articulated vehicle equipped with a partially-filled generic tank, and identify optimal tank geometry for different partial-fill conditions.
- e) Carry out directional response and stability analyses of the vehicle equipped with conventional and optimal tanks under various steering maneuvers performed at constant forward speed and fill conditions through development and analyses of a nonlinear analytical model of the tank vehicle combination.
- f) Develop a three-dimensional quasi-static model of a partially-filled generic tank to compute simultaneous liquid load shift in both the roll and pitch planes under various longitudinal and lateral acceleration excitations.

- g) Develop a comprehensive variable speed three-dimensional model of a partially-filled articulated tank vehicle, incorporating nonlinear lateral and longitudinal force properties of tires and their interactions with the road surface.
- h) Analyze dynamic response and stability characteristics of articulated vehicles with partially-filled tanks of various cross-sections subject to combined steering and braking maneuvers.

1.3.2 Organization of the Dissertation

In Chapter 2, a generic tank geometry is proposed based upon geometry analysis of currently used tank cross-sections. Different multi-variable optimization functions are further formulated to derive optimal tank cross-sections corresponding to various liquid fill conditions, subject to constraints imposed on the total capacity, overall width and height, and perimeter.

The performance characteristics of optimal tank configurations are evaluated in terms of liquid load transfer and static rollover threshold acceleration limit of a partially-filled articulated tank vehicle in Chapter 3. A static roll plane model of the partially-filled tank vehicle is formulated by integrating the steady-state roll plane model of the partially-filled generic tank with that of the vehicle. The load shift and roll performance characteristics of the vehicle with the optimal cross-sections are then compared with those of the vehicle with currently used tank cross-sections for various liquid fill conditions. The results are discussed to highlight the potential performance benefits of the proposed optimal geometry. Stress analysis is further carried out to evaluate the influence of the proposed optimal tank cross-sections on the stress distribution of the tank structure.

In Chapter 4, the influence of tank geometry on the directional response and dynamic roll stability characteristics of a partially-filled articulated tank vehicle is investigated through development and analyses of a constant speed three-dimensional model of the tank vehicle. The dynamic response characteristics of the vehicle with two optimal tanks are compared with those of the vehicle equipped with conventional tanks, under various directional maneuvers and liquid fill conditions, to demonstrate the potential performance benefits of the optimal tank designs.

A comprehensive three-dimensional model of a partially-filled articulated tank vehicle with variable speed is developed in Chapter 5 to study its dynamic response under simultaneous steering and braking operations. A three-dimensional quasi-static model of a partially-filled generic tank is developed to study instantaneous liquid load shift in both the roll and pitch planes (including longitudinal, lateral and vertical directions) under simultaneous applications of lateral and longitudinal accelerations. The tank model is then integrated into a comprehensive three-dimensional model of the articulated vehicle combination with variable forward speed to investigate the influence of liquid load shift on the dynamic performance of the partially-filled tank vehicle under combined cornering and braking maneuvers.

In Chapter 6, the yaw/roll tank vehicle model incorporating variable forward speed, developed in Chapter 5, is employed to simulate and analyze the cargo load shift in the roll and pitch planes and its impact on the dynamic response and stability characteristics of the partially-filled articulated tank vehicle combination under braking-in-a-turn maneuvers. The performance of the vehicle with a partially-filled conventional tank of circular cross-section is then compared with that of a corresponding equivalent

rigid cargo vehicle to demonstrate the destabilizing effects of liquid load shift. Parametric sensitivity analysis is further carried out to examine the influence of vehicle maneuvers, liquid load fill volume, tire-road friction property, and tank cross-section on the directional characteristics and braking behavior of the vehicle combination.

The highlights of the dissertation research, major conclusions drawn and recommendations for future work are finally presented in Chapter 7.

CHAPTER 2

A GENERIC TANK CROSS-SECTION AND SHAPE OPTIMIZATION

2.1 INTRODUCTION

The roll stability of partially-filled tank vehicles is strongly influenced by both the c.g. height of the tank trailer and magnitude of liquid load transfer in a complex manner. Circular cross-sectional tanks (MC 307 and MC 312), employed in transportation of general-purpose liquid products, yield high c.g. location, but relatively less load transfer under partial fill condition and application of a lateral acceleration field. Modified-oval cross-sectional tanks (MC 306), used in delivery of fuel oils, yield relatively lower c.g. height, but considerably larger lateral load transfer under a lateral acceleration disturbance, when compared with that encountered in partially-filled circular tanks of nearly identical cross-section area, especially under low fill volumes. A circular cross-section tank is thus considered to provide relatively higher roll stability under low fill volumes, while a modified-oval geometry yields better roll stability under high fill volumes [189, 190]. Alternate tank cross-sections have been proposed in the past to achieve low c.g. height, while the influence of tank geometry on the resulting liquid load transfer under partial fill conditions has not been addressed [184, 208, 209].

In view of the limitations associated with the conventional tank cross-sections, a generic tank geometry is formulated in this Chapter to describe various commonly used tank shapes. Optimal tank cross-sections are realized to achieve both low c.g. height and minimal lateral load transfer for varying fill volumes. Three constrained multivariable minimization functions are formulated on the basis of overturning moment caused by moving cargo load under partial fill conditions, lateral load shift with prescribed cross-

section c.g. height, and weighted sum of c.g. height and shifts in c.g. coordinates of liquid cargo. The minimization problems are solved to derive optimal cross-section parameters corresponding to typical fill volumes and ranges of fill volumes.

2.2 LATERAL LIQUID LOAD SHIFT ANALYSIS OF CONVENTIONAL TANKS

Movement of liquid cargo within a partly-filled tank is strongly dependent upon its cross-section, fill volume and severity of the vehicle maneuver. Tanks with circular, elliptic, modified-oval and modified-square cross-sections, shown in Figure 2.1, are mostly commonly used for bulk transportation of chemicals, fuel oils, etc. Among these, the circular and modified oval tanks are by far the most popular tank cross-sections used for transportation of general-purpose liquid products and fuel oils, respectively. These cross-sections exhibit symmetry about the vertical and horizontal axes, and their geometry can be described by a number of parameters, ranging from 1 to 5. A circular cross-section can be described by its radius (R) alone, while the elliptic cross-section is defined by its major and minor diameters (H_1 and H_2). A modified-square tank is defined by three parameters: width (H_1), height (H_2) and blend radius (R). A total of five independent parameters are required to describe the modified-oval cross-section. These include radii of the top/bottom (R_1) and side (R_3) surfaces, blend radii (R_2), overall height (H_2) and overall width (H_1).

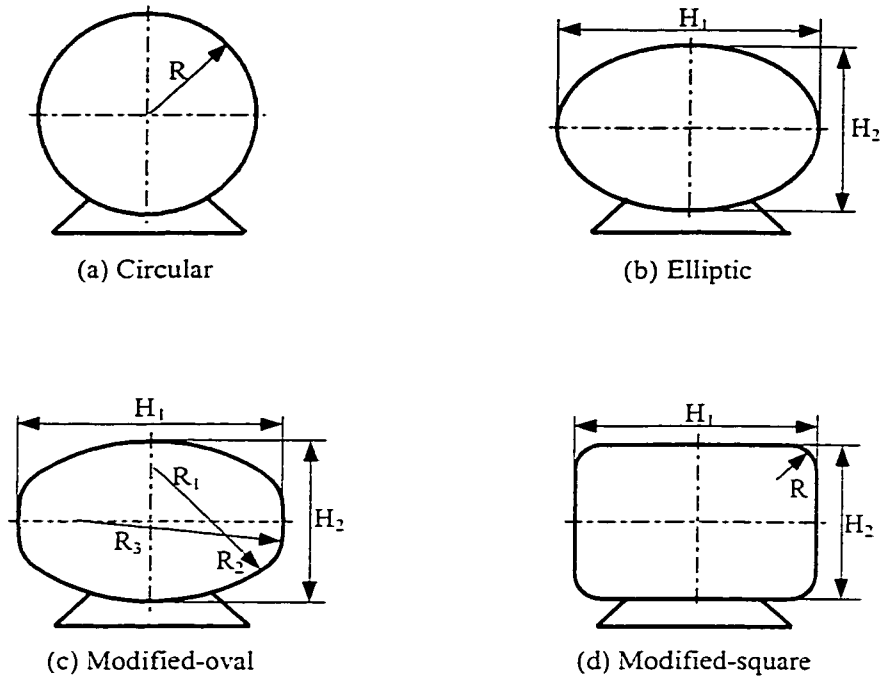


Figure 2.1: Commonly used tank cross-sections in liquid bulk transportation.

The center of gravity (c.g.) of the liquid bulk within a partly-filled tank experiences lateral and vertical shifts under vehicle roll and lateral acceleration encountered in a turning maneuver. The shift in the c.g. coordinates yields a destabilizing roll moment, which contributes to relatively lower roll stability limits of such vehicles. The magnitude of lateral load transfer of liquid cargo within a partly-filled tank depends upon tank cross-section, fill volume and severity of the steering maneuver. In view of vehicle roll stability, each tank cross-section offers certain advantages and limitations related to its geometry. While wider tank cross-sections, such as modified oval and modified square, yield lower c.g. heights, they cause larger movement of the mass center under partial fill conditions. A cross-section with relatively lower width, such as circular, yields higher c.g. height but lower c.g. shift along the lateral and vertical axes under application of a lateral acceleration field.

The shift in lateral and vertical coordinates of c.g. of the liquid bulk in a partly-filled tank subject to constant lateral acceleration field and sprung mass roll angle encountered during a turning maneuvers can be conveniently derived from a quasi-static analysis of the liquid free surface, assuming inviscid fluid and negligible contributions due to fundamental slosh frequency [172]. For low speeds, under steady state conditions, the entire liquid cargo within partly-filled tanks is assumed to translate as a bulk, as shown in Figure 2.2 for the conventional circular and modified-oval tanks. In the figure, a_y is the lateral acceleration in g units, imposed on the liquid due to tank acceleration, and θ_{s3} is the tank roll angle, while W_l represents the weight of liquid cargo and Z_{l0} denotes c.g. height of liquid cargo in the absence of roll angle ($\theta_{s3}=0$) and lateral acceleration ($a_y=0$). The c.g. of liquid bulk within each partly-filled tank experiences a shift from its static position, C_{l0} , to C_l , under application of tank roll and vehicle lateral acceleration.

The gradient of the liquid free surface can be determined from the pressure variations along the lateral (j_s) and vertical (k_s) axes of the tank. The total pressure variations, dP , at the free surface must vanish:

$$dP = \frac{\partial P}{\partial j_s} dj_s + \frac{\partial P}{\partial k_s} dk_s = 0 \quad (2.1)$$

where

$$\begin{aligned} \frac{\partial P}{\partial j_s} &= a_y \cos \theta_{s3} + \sin \theta_{s3} ; \quad \text{and} \\ \frac{\partial P}{\partial k_s} &= -a_y \sin \theta_{s3} + \cos \theta_{s3} \end{aligned} \quad (2.2)$$

Assuming small angles of the tank roll and inclination of the liquid free surface, the gradient of the free surface due to tank roll and lateral acceleration is expressed as [172]:

$$\varphi = \frac{a_y + \theta_{s3}}{1 - a_y \theta_{s3}} \quad (2.3)$$

where the tank roll angle, θ_{s3} , is expressed in radians.

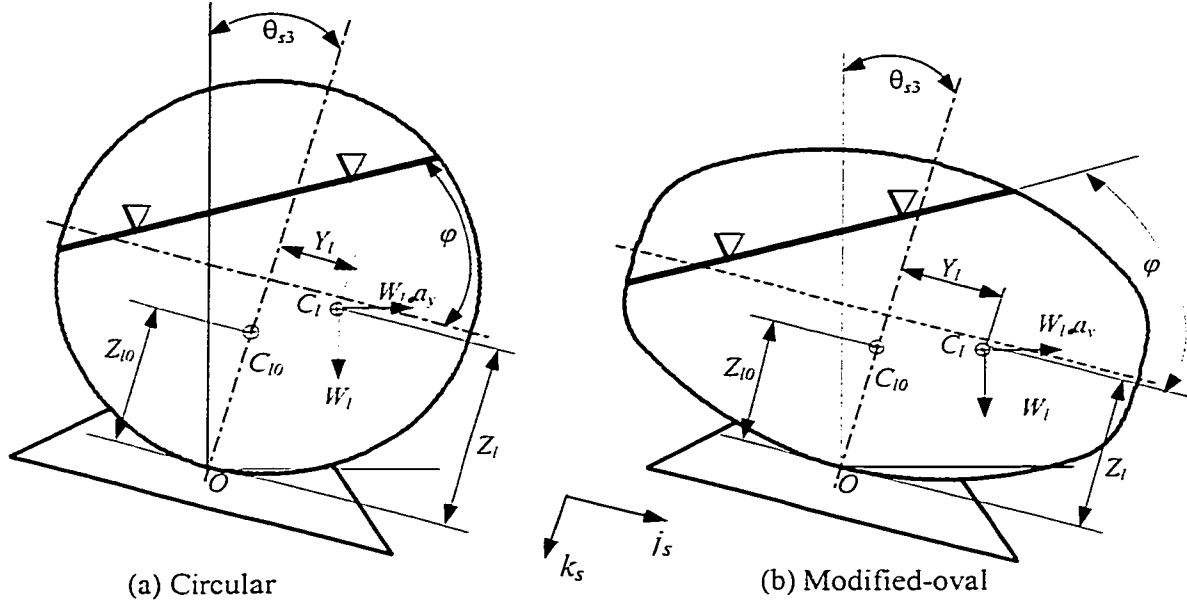
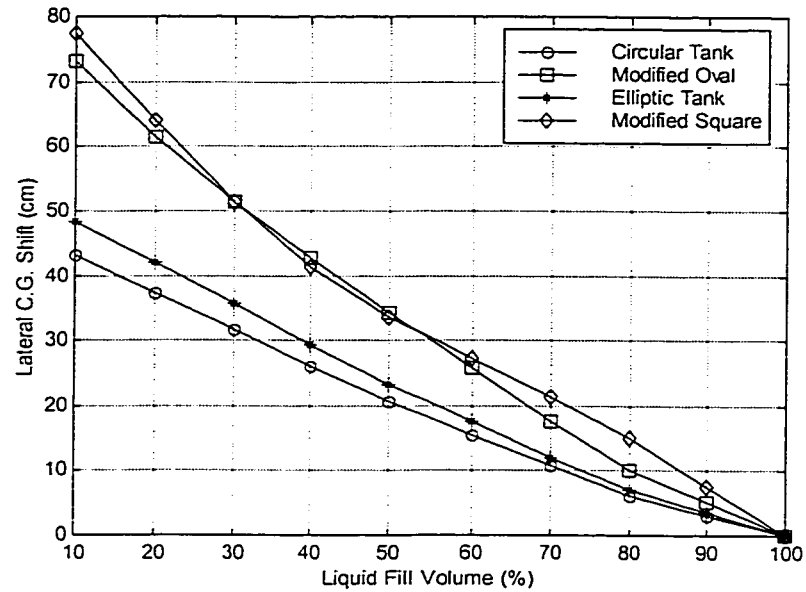


Figure 2.2: Roll plane models of partly-filled circular and modified-oval tanks.

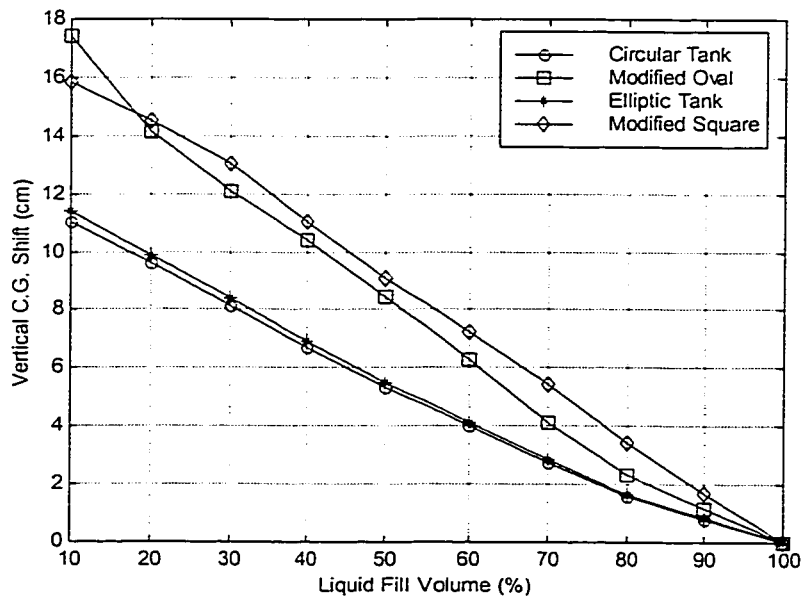
The instantaneous coordinates of the cargo c.g. are then derived from the tank geometry and the free surface gradient. Figure 2.3 illustrates the shift in the lateral and vertical c.g. coordinates of different tank cross-sections as functions of the fill volume, while geometric parameters are chosen to yield nearly identical cross-sectional area for all the shapes. The shifts or deviations in the c.g. coordinates are computed with reference to the c.g. coordinates $(0, Z_{b0})$ under static conditions ($a_y = \theta_{s3} = 0$). The results clearly show that wider tanks, such as the modified-oval and modified-square tanks, yield considerably larger shift in vertical and lateral coordinates of cargo c.g. for entire range of fill volumes.

For nearly identical volume/unit length of the tank, the circular ($R=2.03/2$ m) and elliptic ($H_1=2.10$ m, $H_2=2.00$ m) tanks yield c.g. height of 1.015 m and 1.00 m,

respectively. The modified-oval cross-section ($R_1=1.78$ m, $R_2=1.39$ m, $R_3=1.78$ m, $H_1=2.44$ m, $H_2=1.65$ m) yields considerably lower c.g. height of 0.825 m. The modified-square cross-section ($H_1=2.26$ m and $H_2=1.50$ m and $R=0.39$ m) yields the lowest c.g. height of 0.75 m.



(a)



(b)

Figure 2.3: Liquid load shifts in partly-filled conventional tanks.

2.3 FORMULATION OF A GENERIC TANK CROSS-SECTION

The cargo c.g. height and magnitude of load c.g. shift directly relate to the magnitude of destabilizing overturning moment and thus the roll stability of a partly-filled tank vehicle. From Figure 2.3, it is apparent that wider cross-section tanks yield considerably lower c.g. height but significantly larger load shift. The cross-sections with lesser width, on the other hand, yield less load shift but excessively higher c.g. location. The roll stability of a vehicle may be enhanced by reducing both the overall c.g. height and magnitude of lateral c.g. shift under steady turning maneuvers. It is thus desirable to minimize the magnitude of load shift through selection of alternate cross-sections. A tank cross-section with larger number of independent parameters, required to describe its geometry, can provide increased flexibility to achieve desired volume with relatively lower c.g. height. A cross-section symmetric about the vertical centerline, with wider bottom and narrower top, could yield both the lower height of the center of mass of liquid bulk and less load shift for a range of fill volumes. A generic tank shape, shown in Figure 2.4, is thus formulated for further analyses and to realize an optimal cross-section that can provide lower c.g. height and less magnitude of lateral load shift.

The proposed periphery of the generic tank can be observed as a combination of eight circular arcs symmetric about the vertical axis. This cross-section is considered to be sufficiently general to describe many possible tank shapes. A circular cross-section may be realized upon selecting equal radii for all the eight arcs. The periphery approaches to that of a modified-oval tank, when $R_1=R_5$, $R_2=R_4$, and the corresponding circular arc angles are equal ($\alpha_1=\alpha_5$, $\alpha_2=\alpha_4$). A modified-square shape may be realized by selecting large values for R_1 , R_3 and R_5 , while an elliptic shape can be achieved through

selection of appropriate arc angles and radii. By placing the origin 'O' of the tank body fixed axis system, YZO , at middle of the lowest arc (arc 1), as shown in Figure 2.4, the equation for each circular arc can be expressed as:

$$(y-Y_{ci})^2 + (z-Z_{ci})^2 = R_i^2 \quad (i=1, 2, \dots, 8) \quad (2.4)$$

where Y_{ci} and Z_{ci} are coordinates of center of arc i of radius R_i . The angles corresponding to arcs 1-5 are represented by $\alpha_1, \alpha_2, \alpha_3, \alpha_4$ and α_5 , respectively, as shown in the figure. The left-hand side arcs 6, 7 and 8 are symmetric to the right-hand side arcs 4, 3 and 2 about Z -axis, respectively.

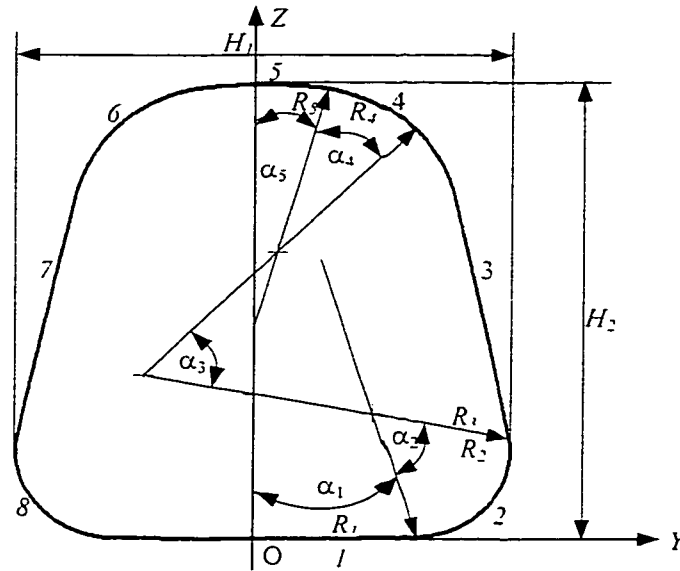


Figure 2.4: Schematics of a generic tank cross-section.

2.3.1 Coordinates and Independent Parameters of the Generic Cross-section

A particular tank periphery is realized to achieve a specific cross-section area or desired volume. The tank cross-section is derived from coordinates of the intersection points between two adjacent circular arcs, which can be obtained through simultaneous solution of equations for arc i and $i+1$. The solution yields maximum and minimum

values of vertical coordinates of arcs i and $i+1$, and the corresponding lateral coordinates. As an alternative, coordinates of the intersection points can be directly determined from geometric analysis by considering that two adjacent arcs possess identical slope at the intersection point. The resulting formulation can further yield the minimum number of independent variables required to uniquely define the tank cross-section. The coordinates of different intersection points of the circular arcs, $(Y_i, Z_i; i=0, 2, \dots, 5)$, shown in Figure 2.5, are derived as follows:

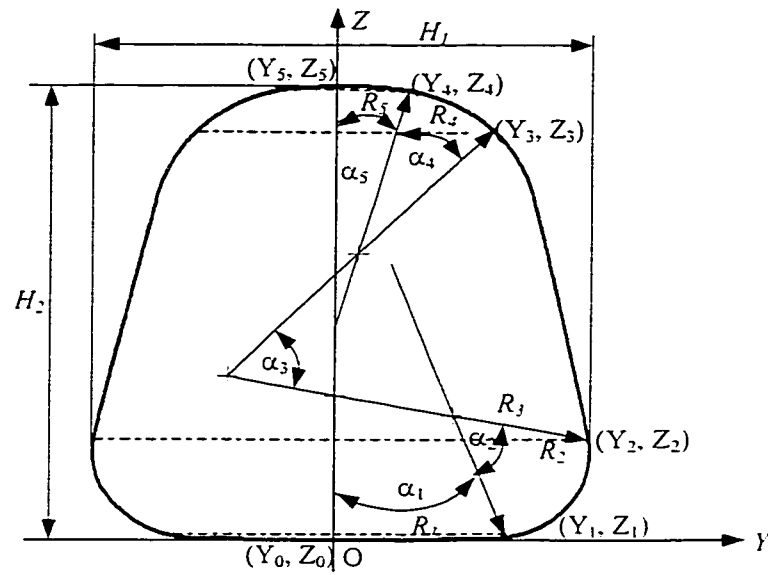


Figure 2.5: Coordinate analysis of the generic tank cross-section.

$$Y_0 = 0; \quad Z_0 = 0$$

$$Y_1 = R_1 \sin \alpha_1; \quad Z_1 = R_1(1 - \cos \alpha_1)$$

$$Y_2 = Y_1 + L_{12} \cos(\alpha_1 + \alpha_2 / 2); \quad Z_2 = Z_1 + L_{12} \sin(\alpha_1 + \alpha_2 / 2)$$

$$Y_4 = R_5 \sin \alpha_5; \quad Z_4 = H_2 - R_5(1 - \cos \alpha_5)$$

$$Y_3 = Y_4 + L_{34} \cos(\alpha_5 + \alpha_4 / 2); \quad Z_3 = Z_4 - L_{34} \sin(\alpha_5 + \alpha_4 / 2)$$

$$Y_5 = 0; \quad Z_5 = H_1 \tag{2.5}$$

where $L_{12} = 2R_2 \sin(\alpha_2/2)$ and $L_{34} = 2R_4 \sin(\alpha_4/2)$. The coordinates of centers of arcs (Y_{ci}, Z_{ci}) are derived in a similar manner, and expressed as:

$$\begin{aligned}
Y_{c1} &= 0; & Z_{c1} &= R_1 \\
Y_{c2} &= Y_2 - R_2 \sin(\alpha_1 + \alpha_2); & Z_{c2} &= Z_2 + R_2 \cos(\alpha_1 + \alpha_2) \\
Y_{c3} &= Y_2 - R_3 \sin(\alpha_1 + \alpha_2); & Z_{c3} &= Z_2 + R_3 \cos(\alpha_1 + \alpha_2) \\
Y_{c4} &= Y_3 - R_4 \sin(\alpha_4 + \alpha_5); & Z_{c4} &= Z_3 - R_4 \cos(\alpha_4 + \alpha_5) \\
Y_{c5} &= 0; & Z_{c5} &= H_2 - R_5
\end{aligned} \tag{2.6}$$

The coordinates of center of arc 3 can also be expressed by the following geometric relationships:

$$Y_{c3} = Y_3 - R_3 \sin(\alpha_4 + \alpha_5); \text{ and } Z_{c3} = Z_3 - R_3 \cos(\alpha_4 + \alpha_5) \tag{2.7}$$

The simultaneous solution of equations (2.6) and (2.7) for Y_{c3} and Z_{c3} yields the following:

$$\begin{aligned}
R_3 &= \frac{(Z_3 - Z_2)}{\cos(\alpha_1 + \alpha_2) + \cos(\alpha_4 + \alpha_5)}; \text{ and} \\
Y_2 - Y_3 &= \frac{(Z_3 - Z_2)[\sin(\alpha_1 + \alpha_2) - \sin(\alpha_4 + \alpha_5)]}{\cos(\alpha_1 + \alpha_2) + \cos(\alpha_4 + \alpha_5)}
\end{aligned} \tag{2.8}$$

In addition, a relationship among different arc angles can be derived as:

$$\alpha_1 + \alpha_2 + \alpha_3 + \alpha_4 + \alpha_5 = \pi \tag{2.9}$$

The above equations suggest that the cross-section of the generic tank can be defined by eleven variables and three equality constraints described in Equations (2.7) through (2.9). These constraint equations can be eliminated by considering R_3 and α_3 as dependent variables (intermediate design variables). The tank cross-section can thus be uniquely defined by eight variables. The cross-sectional area, however, when constrained

to achieve a desired volume capacity, reduces the number of independent design parameters to seven, which include R_1 , α_1 , R_2 , R_3 , R_4 , R_5 and α_5 .

2.3.2 Characteristic Parameters of the Generic Cross-section

The overall width (H_1), overall height (H_2), perimeter (L_p), cross-section area (A_c) and cross-section c.g. height (Z_{cg}) are considered as the characteristic parameters, since they directly relate to weights and dimensional regulations, transportation efficiency and cost, and stability characteristics and safety performance of tank vehicles. The overall tank width must be constrained by the maximum allowable width ($H_1 \leq 2.44$ m) and is related to maximum value of the Y -coordinate of the entire periphery (Y_{max}). Unlike the currently used symmetric tank cross-sections, the proposed generic geometry may yield Y_{max} within the lower half of the cross-section, most likely within arcs 2 or 3. A general methodology is thus formulated to seek the maximum lateral coordinate of the periphery and thus the maximum width, and the associated arc, such that:

$$H_1 = 2 Y_{max} = 2 * \max \{ y = Y_{ci} + R_i \} \quad (i = 1, 2, \dots, 5) \quad \text{Subject to } Z_{i-1} \leq z < Z_i \quad (2.10)$$

where y and z represent the lateral and vertical coordinates of a point on the circular arc, respectively.

The overall height of the tank is obtained from radius and vertical coordinate of arc 5, such that $H_2 = Z_{c5} + R_5$. The perimeter (L_p) of the tank can be derived from:

$$L_p = 2 \sum_{i=1}^5 R_i \alpha_i \quad (2.11)$$

The cross-sectional area (A_c) and c.g. height (Z_{cg}) of the tank can be further derived from the following area and area moment integrals:

$$A_c = 2 \sum_{i=1}^5 \int_{Z_{i-1}}^{Z_i} f_i(z) dz; \text{ and } Z_{cg} = \frac{2}{A_c} \sum_{i=1}^5 \int_{Z_{i-1}}^{Z_i} f_i(z) z dz \quad (2.12)$$

where Z_i and Z_{i-1} represent the maximum and minimum vertical coordinates of arc i , as described in Equation (2.5), and $f_i(z)$ denotes its right-hand-side equation in terms of vertical coordinate z , derived as:

$$f_i(z) = Y_{ci} + \sqrt{R_i^2 - (z - Z_{ci})^2} \quad (i=1, 2, \dots, 5) \quad (2.13)$$

2.4 LOAD SHIFT IN A PARTLY-FILLED GENERIC TANK (ROLL PLANE)

The roll plane model of the partly-filled tank of generic cross-section is illustrated in Figure 2.6. For the proposed generic tank, mounted on the trailer frame, W_l and W_t represent the weights of liquid cargo and empty tank trailer structure, respectively; Z_b is the vertical distance from tank base (origin of the tank-fixed coordinate system) to c.g. of the empty tank trailer. Assuming small angles, inviscid fluid and negligible contribution due to fundamental slosh frequency, the entire fluid bulk is considered to move as a rigid body under steady-state conditions. The gradient of the liquid free surface can be determined from Equation (2.3).

The instantaneous coordinates of liquid bulk c.g. under application of a_y and θ_{s3} , denoted by $C_l(Y_l, Z_l)$, are then derived from equation of the liquid free surface and tank geometry. The equation of the inclined free surface of the liquid bulk due to tank roll and vehicle lateral acceleration encountered during steady state turning can be expressed in terms of its gradient and lateral coordinate, as:

$$z = y \tan \varphi + h_0 \quad (2.14)$$

where h_0 is intercept of the liquid free surface with Z -axis in the tank-fixed coordinate system.

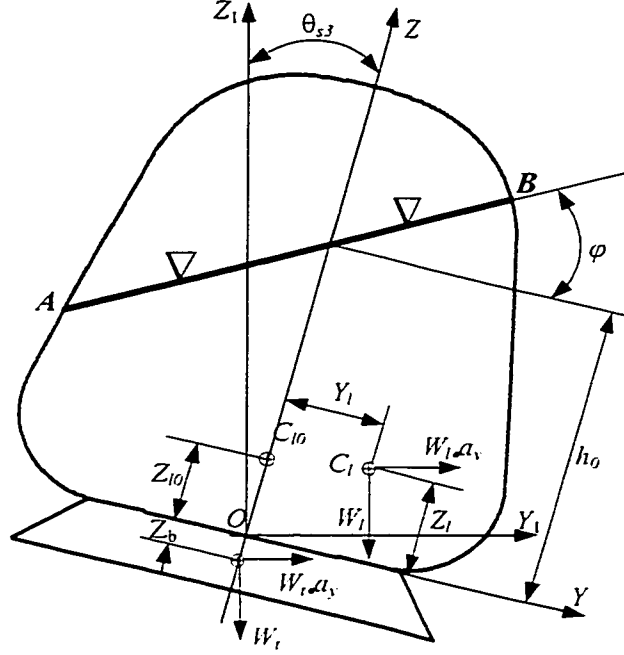


Figure 2.6: Roll plane model of a partially-filled generic tank.

The intercept is determined using an iterative procedure based upon the assumption that liquid volume per unit length remains constant, while neglecting pitch motion of the tank. For a given initial fill height h , the algorithm identifies two arcs on the left- and right-sides of the central Z -axis, which are intersected by the liquid free surface by comparing the initial liquid height h with the minimum and maximum heights (Z -coordinates) of each arc describing the tank cross-section. Considering the symmetry about Z -axis and that liquid free surface under static condition ($\alpha_j = \theta_{sj} = 0$) intersects arc i on the right-hand side, such that $Z_{i-1} \leq h < Z_i$, the corresponding liquid volume per unit length in the tank can be computed from the area integral:

$$A_0 = 2 \left[\sum_{j=1}^{i-1} \int_{Z_{j-1}}^{Z_j} f_j(z) dz + \int_{Z_{i-1}}^h f_i(z) dz \right] \quad (2.15)$$

where $f_i(z)$ and $f_j(z)$ represent the right-hand-side equations of arcs i and j , respectively, as described in Equation (2.13).

The coordinates of c.g. of the liquid bulk within the tank, under static condition ($a_y = \theta_{s3} = 0$), are then derived from:

$$Y_{10} = 0; \text{ and } Z_{10} = \frac{2}{A_0} \left[\sum_{j=1}^{i-1} \int_{Z_{j-1}}^{Z_j} f_j(z) z dz + \int_{Z_{i-1}}^h f_i(z) z dz \right] \quad (2.16)$$

For the inclined free surface realized under application of lateral acceleration and tank roll angle, the algorithm identifies two arcs intersected by the liquid free surface in a similar manner. The coordinates of the intersection points are computed by simultaneous solution of Equations (2.4) and (2.14), while the initial value of intercept h_0 is assumed to be equal to h . Assuming that liquid free surface intersects the left-hand side of the tank periphery at point $A(Y_A, Z_A)$, and right-hand side at point $B(Y_B, Z_B)$, as shown in Figure 2.7, the liquid volume per unit length can be computed from area integral:

$$A_f = \iint_Q dy dz \quad (2.17)$$

where Q defines the domain of area integral. For the proposed generic tank cross-section, many possible domains of integration exist depending upon free surface gradient and fill volume.

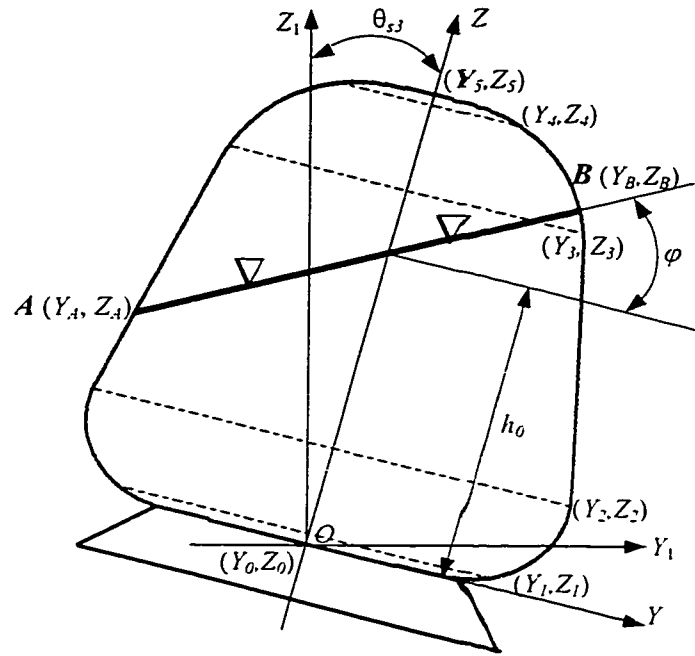


Figure 2.7: The intercept of liquid free surface with tank periphery.

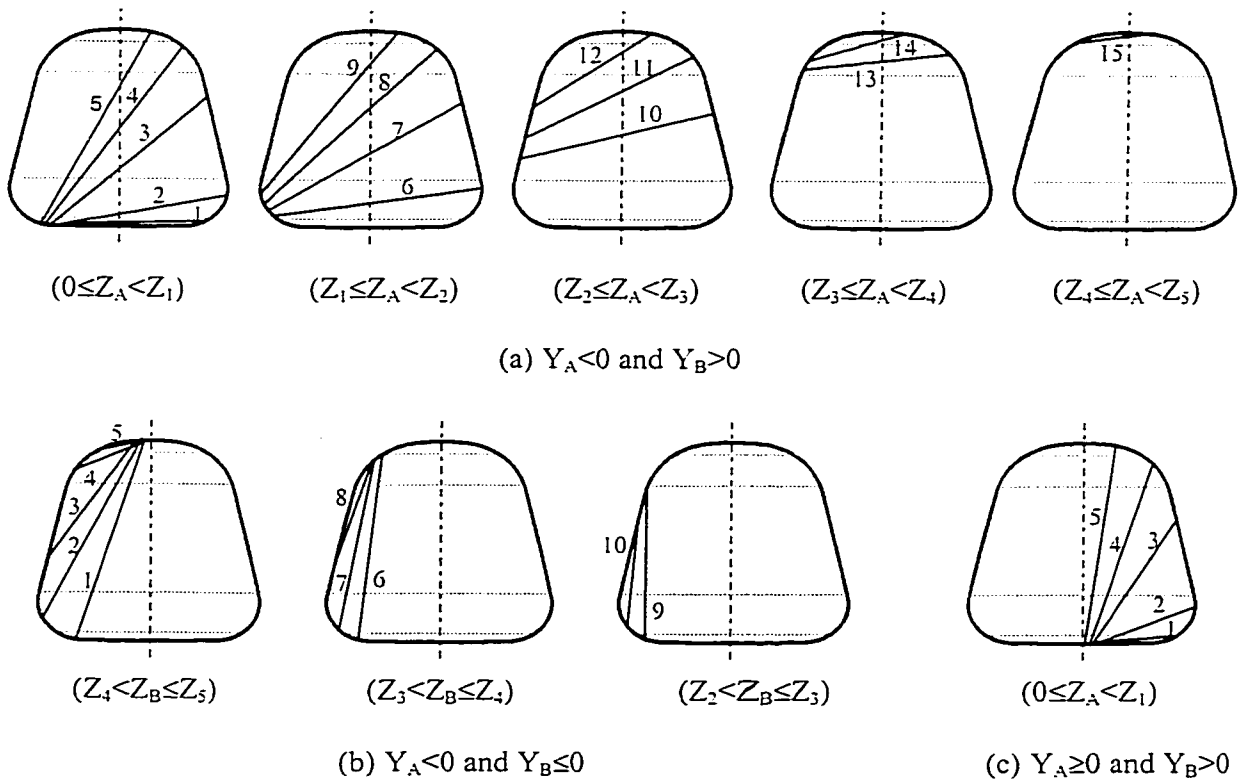


Figure 2.8: Possible liquid free surface configurations.

Under low to medium levels of roll angle and lateral acceleration, the intersection points A and B are expected to lie on the left- and right-sides of the centerline, respectively, such that $Y_A < 0$ and $Y_B > 0$. A total of fifteen possible intersection coordinates may exist, as shown in Figure 2.8 (a). For $0 \leq Z_A < Z_1$, five different intersection configurations (1-5) may exist depending on the position of point B . For $Z_1 \leq Z_A < Z_2$, $Z_2 \leq Z_A < Z_3$ and $Z_3 \leq Z_A < Z_4$, there exist four (6-9), three (10-12) and two (13-14) possible configurations, respectively. There exists only one configuration (15) when $Z_4 \leq Z_A < Z_5$.

Under high levels of roll angle and lateral acceleration, the free surface of the liquid may entirely lie within the same half of the tank, as shown in Figures 2.8 (b) and 2.8 (c). High fill volume coupled with large free surface gradient causes the free surface to locate itself entirely on the left-hand of the Z -axis ($Y_A < 0$ and $Y_B \leq 0$). In this case, variable number of possible configurations of the free surface, generally 1-11, may exist, depending on the particular tank geometry, fill volume, and free surface gradient, as shown in Figure 2.8 (b). The low fill volume coupled with large free surface gradient can cause free surface to locate itself entirely on the right-hand side of the Z -axis ($Y_A \geq 0$ and $Y_B > 0$). Although a large number of configurations are possible, the configurations 1-6 shown in Figure 2.8 (c) are considered to represent most general cases. It should be noted that only the configurations that correspond to $Y_A \leq Y_B$ and $Z_A \leq Z_B$ are physically possible (for left turning of the tank vehicle). The limits of area integral derived for different free surface intersections are summarized in Table 2.1.

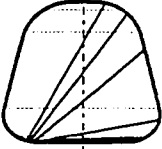
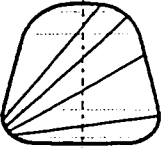
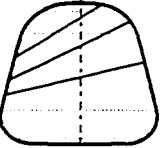
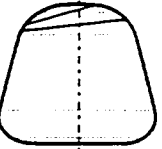
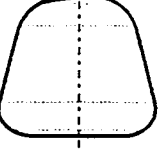
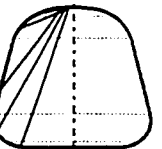
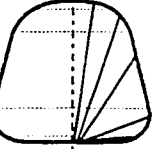
Equation (2.17) is solved using the respective domain of integration, illustrated in Figure 2.8 and listed in Table 2.1, to compute the liquid volume per unit length A_f . The estimated volume is then compared with that attained under static condition (A_0) to derive

the corresponding volume error per unit tank length, $\varepsilon = |A_f - A_0|$. The iterative process is repeated, for an adjusted value of the intercept h_0 , until the prescribed convergence is achieved.

The corresponding load shift due to liquid motion can be computed from the instantaneous location of the center of mass, (Y_l, Z_l) , evaluated from the following area moment integrals:

$$Y_l = \frac{1}{A_f} \iint_{\mathcal{Q}} y dy dz ; \text{ and } Z_l = \frac{1}{A_f} \iint_{\mathcal{Q}} z dy dz \quad (2.18)$$

Table 2.1: Liquid free surface configurations and sets of integrals.

Free surface configurations and limiting values of coordinates of points A and B			Integral limits
Y_A and Y_B	Z_A	Z_B	
$Y_A < 0$ and $Y_B > 0$ 	$0 \leq Z_A < Z_1$	$0 \leq Z_B < Z_1$ ($n^*=1$) $Z_1 \leq Z_B < Z_2$ ($n=2$) $Z_2 \leq Z_B < Z_3$ ($n=3$) $Z_3 \leq Z_B < Z_4$ ($n=4$) $Z_4 \leq Z_B < Z_5$ ($n=5$)	$2 \int_0^{Z_1} \int_0^{f_1} + \sum_{k=1}^n \int_{Z_{k-1}^*}^{Z_k^*} \int_{f_{k-1}}^{f_k}$ $Z_0^* = Z_A, Z_k^* = Z_k$ ($k=1, \dots, n-1$), $Z_n^* = Z_B$
	$Z_1 \leq Z_A < Z_2$	$Z_1 \leq Z_B < Z_2$ ($n=2$) $Z_2 \leq Z_B < Z_3$ ($n=3$) $Z_3 \leq Z_B < Z_4$ ($n=4$) $Z_4 \leq Z_B < Z_5$ ($n=5$)	$2 \left(\int_0^{Z_1} \int_0^{f_1} + \int_{Z_1}^{Z_2} \int_0^{f_2} \right) + \sum_{k=2}^n \int_{Z_{k-1}^*}^{Z_k^*} \int_{f_{k-1}}^{f_k}$ $Z_1^* = Z_A, Z_k^* = Z_k$ ($k=2, \dots, n-1$), $Z_n^* = Z_B$
	$Z_2 \leq Z_A < Z_3$	$Z_2 \leq Z_B < Z_3$ ($n=3$) $Z_3 \leq Z_B < Z_4$ ($n=4$) $Z_4 \leq Z_B < Z_5$ ($n=5$)	$2 \left(\int_0^{Z_1} \int_0^{f_1} + \int_{Z_1}^{Z_2} \int_0^{f_2} + \int_{Z_2}^{Z_3} \int_0^{f_3} \right) + \sum_{k=3}^n \int_{Z_{k-1}^*}^{Z_k^*} \int_{f_{k-1}}^{f_k}$ $Z_2^* = Z_A, Z_k^* = Z_k$ ($k=3, \dots, n-1$), $Z_n^* = Z_B$
	$Z_3 \leq Z_A < Z_4$	$Z_3 \leq Z_B < Z_4$ ($n=4$) $Z_4 \leq Z_B < Z_5$ ($n=5$)	$2 \left(\int_0^{Z_1} \int_0^{f_1} + \int_{Z_1}^{Z_2} \int_0^{f_2} + \int_{Z_2}^{Z_3} \int_0^{f_3} + \int_{Z_3}^{Z_4} \int_0^{f_4} \right) + \sum_{k=4}^n \int_{Z_{k-1}^*}^{Z_k^*} \int_{f_{k-1}}^{f_k}$ $Z_3^* = Z_A, Z_k^* = Z_k$ ($k=4, \dots, n-1$), $Z_n^* = Z_B$
	$Z_4 \leq Z_A < Z_5$	$Z_4 \leq Z_B < Z_5$ ($n=5$)	$2 \left(\int_0^{Z_1} \int_0^{f_1} + \int_{Z_1}^{Z_2} \int_0^{f_2} + \int_{Z_2}^{Z_3} \int_0^{f_3} + \int_{Z_3}^{Z_4} \int_0^{f_4} + \int_{Z_4}^{Z_5} \int_0^{f_5} \right) + \int_{Z_5}^{Z_n^*} \int_{f_5}^{f_n}$
$Y_A < 0$ and $Y_B \leq 0$ 	$0 \leq Z_A < Z_1$ ($m^{**}=1$) $Z_1 \leq Z_A < Z_2$ ($m=2$) $Z_2 \leq Z_A < Z_3$ ($m=3$) $Z_3 \leq Z_A < Z_4$ ($m=4$) $Z_4 \leq Z_A < Z_5$ ($m=5$)	$Z_4 \leq Z_B < Z_5$ ($n=5$)	$2 \sum_{i=1}^5 \int_{Z_{i-1}^*}^{Z_i^*} \int_{f_{i-1}}^{f_i} - \sum_{k=m}^n \int_{Z_{k-1}^*}^{Z_k^*} \int_{f_{k-1}}^{f_k}$ $Z_{m-1}^* = Z_A, Z_k^* = Z_k$ ($k=m, \dots, n-1$), $Z_n^* = Z_B$
$Y_A \geq 0$ and $Y_B > 0$ 	$0 \leq Z_A < Z_1$ ($m=1$)	$0 \leq Z_B < Z_1$ ($n=1$) $Z_1 \leq Z_B < Z_2$ ($n=2$) $Z_2 \leq Z_B < Z_3$ ($n=3$) $Z_3 \leq Z_B < Z_4$ ($n=4$) $Z_4 \leq Z_B < Z_5$ ($n=5$)	$\sum_{k=m}^n \int_{Z_{k-1}^*}^{Z_k^*} \int_{f_{k-1}}^{f_k}$ $Z_{m-1}^* = Z_A, Z_k^* = Z_k$ ($k=m, \dots, n-1$), $Z_n^* = Z_B$

Notes:

- (1) * n = the No. of arc intersecting the free surface at right-hand side of the Z-axis ($n=1, 2, \dots, 5$);
- (2) ** m = the No. of arc intersecting the free surface at left-hand side of the Z-axis ($m=1, 2, \dots, 5$);
- (3) f_i and f_k represent the right-hand-side equations of arcs i and k , respectively, as described in Equation (2.13), while f_s is the equation of the liquid free surface in terms of vertical coordinate z , derived from Equation (2.14) as:

$$f_s(z) = \frac{z - h_0}{\tan \varphi} \quad (2.19)$$

2.5 DETERMINATION OF OPTIMAL TANK CROSS-SECTIONS

The roll stability of a partly-filled tank vehicle is directly related to static c.g. height of the sprung weight and lateral load shift determined mostly from the shift in lateral coordinate of the liquid load c.g. under a lateral acceleration field. Both the c.g. height and shift in c.g. coordinates due to the movement of the liquid cargo are further affected by cross-section of the tank and fill volume. The roll stability of a partly-filled tank vehicle can be enhanced by minimizing the overall c.g. height of the liquid cargo, and magnitudes of lateral and vertical shifts in c.g. coordinates encountered during a steady-turning maneuver. As described earlier, circular cross-section tanks yield lower degree of load transfer but high c.g. of the cargo. The modified-oval and square cross-section tanks yield lower c.g. height but considerable load shift under a lateral acceleration field. An optimal tank cross-section is thus explored to minimize both the cross-section c.g. height (cargo c.g. height under 100% fill condition), and magnitudes of deviations in lateral and vertical coordinates of the cargo c.g. (ΔY_l , ΔZ_l) under application of tank roll and lateral acceleration.

2.5.1 Formulation of Optimization Functions

Three different optimization functions are formulated to determine optimal geometric parameters of the generic tank cross-section illustrated in Figure 2.4.

The conventional tanks are known to exhibit most significant lateral load shift (ΔY_l) and thus the overturning moment about the sprung mass roll center under a lateral acceleration field, specifically under low fill volumes [189]. The first optimization function, $U_Y(\chi)$, is thus formulated based upon the lateral load shift alone corresponding to a particular liquid fill volume ratio, β , defined as the ratio of the wetted cross-sectional area to the total cross-sectional area (A_f/A_c). The cross-sectional c.g. height is constrained to a prescribed value and the contribution due to shift in vertical coordinate of the c.g. is considered negligible, such that:

$$U_Y(\chi) = \Delta Y_{l\beta} ; \text{ and } Z_{cg} \leq Z_{cg0} \quad (2.20)$$

where Z_{cg0} is the specified upper limit of the cross-section c.g. height. $\Delta Y_{l\beta}$ is lateral deviation of the cargo c.g. under a steady lateral acceleration and specified fill ratio β . In the shape optimization function, χ represents the vector of design variables. As described in Section (2.3.1), a generic tank geometry can be uniquely described by eight independent variables. Considering the equality constraint imposed by desired volume per unit length or cross-sectional area, the design vector for the tank geometry is given by $\chi = \{R_1, \alpha_1, R_2, R_3, R_4, R_5, \alpha_5\}^T$, where T designates the transpose.

To ensure minimal lateral load shift over a range of fill volumes, a composite lateral load shift measure is formulated as:

$$U_{\Sigma Y}(\chi) = \sum_{\beta} W_{\beta} \Delta Y_{l\beta} ; (\beta_l \leq \beta \leq \beta_u) \text{ and } Z_{cg} \leq Z_{cg0} \quad (2.21)$$

where β_l and β_u are the lower and upper limits of fill volume ratios considered for the optimal solution, while W_β is a weighting factor corresponding to fill volume β . Z_{cg0} is a specified tank cross-section c.g. height. Based on this composite objective function, tanks with different cross-sections can be achieved by selecting different values for Z_{cg0} . A very low tank cross-section can be obtained by constraining Z_{cg0} to a value considerably smaller than the c.g. height of the conventional modified-oval tank. A narrow tank cross-section, on the other hand, can be achieved by letting Z_{cg0} to approach a relatively larger value. The solution of optimization problem described in Equations (2.20) and (2.21) can yield optimal designs to minimize the lateral load shift. The contributions due to c.g. height and shift in vertical coordinate of the cargo c.g. are neglected.

A second optimization problem is thus formulated based upon weighted sum of primary contributing factors at a particular fill volume, $(\Delta Y_l, \Delta Z_l, Z_{cg})$, such that:

$$U_{yz}(\chi) = (\gamma_1 \Delta Y_l^* + \gamma_2 \Delta Z_l^* + \gamma_3 Z_{cg}^*)_\beta \quad (2.22)$$

Similar to Equation (2.19), the optimization function can be formulated for a range of fill volumes in order to derive a generally applicable optimal design, such that:

$$U_{yz}(X) = \sum_{\beta} W_{\beta} \{ \gamma_1 \Delta Y_l^* + \gamma_2 \Delta Z_l^* + \gamma_3 Z_{cg}^* \}_{\beta} \quad (\beta_l \leq \beta \leq \beta_u) \quad (2.23)$$

where $\Delta Y_l^* = \Delta Y_l / \Delta Y_{lmax}$, $\Delta Z_l^* = \Delta Z_l / \Delta Z_{lmax}$, and $Z_{cg}^* = Z_{cg} / Z_{cgmax}$, corresponding to a fill volume β , and γ_1 , γ_2 and γ_3 are weighting factors for the three contributing factors, ΔY_l , ΔZ_l and Z_{cg} . ΔY_{lmax} and ΔZ_{lmax} are the maximum values of lateral and vertical shifts of liquid c.g., considered to be equal to those obtained for a modified-oval cross-section of identical cross-section area. Z_{cgmax} is the maximum value of the c.g. height, which is considered to be that of a circular cross-section tank of identical area. The weighting

factors, γ_1 , γ_2 and γ_3 , are selected on the basis of relative contributions of the three contributing factors, ΔY_l , ΔZ_l and Z_{cg} .

Based upon the objective functions, described in Equations (2.22) and (2.23), optimal tanks with different cross-sections can be obtained by setting various combinations of values to γ_1 , γ_2 and γ_3 . While a higher value of γ_3 can lead to optimal design with low c.g. height, larger values of γ_1 and γ_2 will yield to a relatively narrow tank cross-section. It should be noted that a unit increase in ΔY_l causes an increase in overturning moment equal to W_l , while a unit increase in ΔZ_l causes the moment to increase by $W_l a_y$. This suggests that the values of γ_1 and γ_2 should be selected to be larger than that of γ_3 .

Alternatively, the roll stability of a partially-filled tank vehicle may be enhanced by directly minimizing the overturning moment due to motion of the liquid cargo about the c.g. of the tank-trailer structure, as shown in Figure 2.6. The third optimization problem is thus formulated to minimize the overturning moment caused by the moving liquid cargo, which is mostly a function of primary contributing factors incorporated in the optimization problem of Equation (2.22), namely the c.g. height, and shift in the lateral and vertical coordinates of the cargo c.g. The optimization function corresponding to a given fill volume is formulated as:

$$U_{M_o}(\chi) = M_o \quad (2.24)$$

where M_o is the overturning moment due to the liquid cargo about the c.g. of the tank-trailer structure. This overturning moment can be derived from the forces shown in Figure 2.6.

$$M_o = W_l [(Z_b + Z_l) \cos \theta_{s3} - Y_l \sin \theta_{s3}] A_v + W_l [(Z_b + Z_l) \sin \theta_{s3} + Y_l \cos \theta_{s3}] \quad (2.25)$$

The above optimization function over a range of fill volumes may be expressed as:

$$U_{\Sigma M_o}(\chi) = \sum_{\beta} W_{\beta} M_{o\beta} (\beta_l \leq \beta \leq \beta_h) \quad (2.26)$$

2.5.2 Constraints

The three optimization functions, presented in Equations (2.20) through (2.26), are solved in conjunction with a number of limit constraints to ensure a feasible design, which include:

- a) An equality constraint is imposed to ensure that the cross-section area of the tank is equal to that of a modified-oval tank (MC 306), such that $A_c = 3.2586 \text{ m}^2$.
- b) The overall tank height is limited to the diameter of the circular tank (MC 307), such that $H_2 \leq 2.03 \text{ m}$.
- c) The overall tank width is limited to that of the MC 306 tank, such that $H_1 \leq 2.44 \text{ m}$.
- d) The arc radii, R_i , are selected to be either equal to or larger than a certain threshold value to endure structural integrity of the tank. The minimum value for the blend radii is limited to that of the conventional MC 306 tanks, such that $R_i \geq 0.39 \text{ m}$ ($i=1, 2, \dots, 5$).

2.5.3 Solution Method

The three constrained multi-variable optimization functions, described in Equations (2.20) through (2.26), are solved using sequential quadratic programming method to determine optimal tank geometry for different liquid fill volumes and volume ranges, under typical values of lateral acceleration ($a_j = 0.3$ to 0.4 g) and roll angle ($\theta_{s3} = 7$ - to 9 degrees). The solutions are obtained for different limiting values of cross-sectional c.g. height (Z_{cgo}) in the case of Equations (2.20) and (2.21), and different weighting factor

combinations (γ_1 , γ_2 and γ_3) in the case of Equations (2.22) and (2.23), while Equations (2.24) and (2.25) are solved directly. Equal weighting factor (W_β) is selected for each specific fill volume in the case of solutions for fill ranges.

Each optimization problem is firstly solved for different starting values of the design vector and the results are analyzed to identify global optimum and to examine the validity of the optimal solutions. The solutions invariably converged to nearly similar cross-sectional parameters, irrespective of the selected starting vector. Although the solutions of different optimization problems corresponding to different fill volumes and fill ranges resulted in different geometric parameters of the optimal cross-sections, the resulting shapes are quite comparable. The solutions converged towards relatively high radii for arcs 1 and 3 (7), and considerably lower blend radii (arcs 2, 4, 6 and 8), resulting in a nearly conical shape, irrespective of the optimization function employed. For identical reference values of lateral acceleration and tank roll angle, and liquid fill volume or fill range, the three formulations, however, result in similar solutions for the tank shapes, specifically for H_1 and H_2 , when an appropriate combination of weighting factors (γ_1 , γ_2 and γ_3) and Z_{cg0} values is selected.

2.6 OPTIMAL TANK CROSS-SECTIONS CORRESPONDING TO VARIOUS FILL CONDITIONS

2.6.1 Optimal Cross-sections for Specific Fill Volumes

The constrained optimization problems are initially solved to derive optimal tank geometry for fill volumes ranging from 40% to 70% with an increment of 10%, and 100%, respectively. Figure 2.9 illustrates five optimal tank cross-sections obtained corresponding to the five different fill volumes derived from the optimal solution based

on the overturning moment, Equation (2.24). Table 2.2 summarizes the design parameters together with the cross-sectional c.g. height and perimeter. The table also presents a comparison of optimal design parameters with those of the conventional tanks.

An examination of the optimal tank geometry corresponding to different fill volumes can provide considerable insight into the contributions due to liquid load shift and c.g. height. The optimal solution, corresponding to 50% fill volume (Opt.2), converges to moderately narrow top, relatively high c.g. and considerably lower width to reduce the lateral load shift, as shown in Figure 2.9 and Table 2.2. The 60% and 70% fill volumes yield tank geometry (Opt.3 and Opt.4) with lower c.g. height, wider bottom and narrower top. Low fill volume (40%) (Opt.1) results in nearly rectangular cross-section with higher overall c.g. height and relatively wider top. The optimization corresponding to 100% fill volume yields tank design (Opt.5) with the lowest c.g. height, due to the absence of liquid slosh. It should be noted that all the optimal configurations yield identical total cross-sectional area.

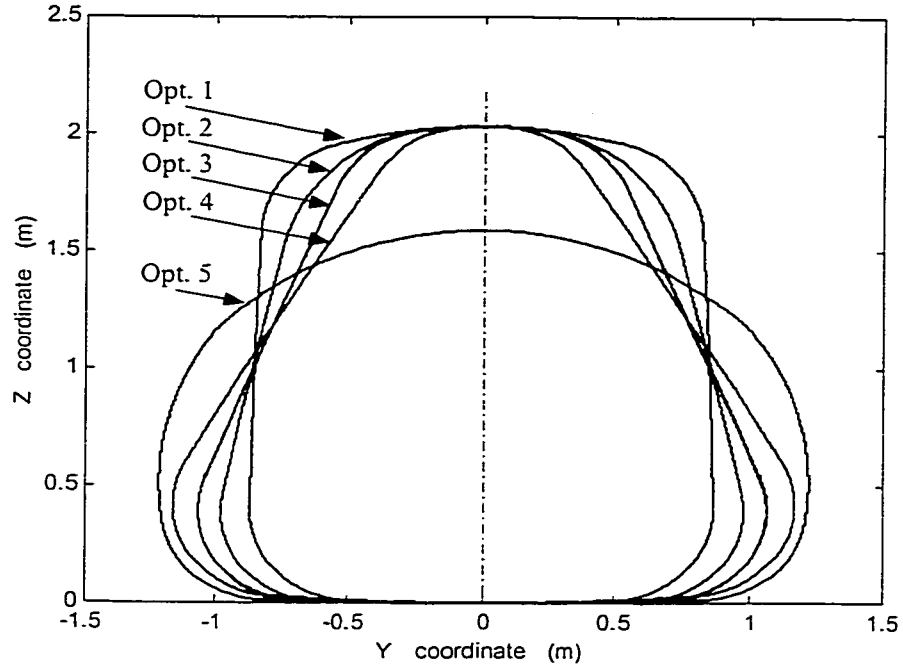


Figure 2.9: Comparison of optimal tank cross-sections derived on the basis of minimal overturning moment.

Table 2.2: Geometric parameters of conventional and optimal cross-sections corresponding to different fill volumes (All dimensions are in m).

Optimal Configuration	Reference Fill Volume (%)	Design Parameters							c.g. Height	Perimeter
		H_1	H_2	R_1	R_2	R_3	R_4	R_5	Z_{cg}	L_p
Opt. 1	40	1.74	2.03	9.98	0.39	35.00	0.39	2.05	0.99	6.66
Opt. 2	50	1.96	2.03	25.00	0.39	50.00	0.63	1.84	0.92	6.69
Opt. 3	60	2.13	2.03	25.00	0.39	50.00	0.39	1.64	0.88	6.82
Opt. 4	70	2.30	2.03	25.00	0.39	50.00	0.39	1.65	0.84	6.90
Opt.5	100	2.44	1.59	25.00	0.39	14.53	0.44	1.41	0.72	6.94
Modified-oval	-	2.44	1.65	1.78	0.39	1.78	0.39	1.78	0.83	6.63
Circular	-	2.03	2.03	1.02	1.02	1.02	1.02	1.02	1.02	6.38

2.6.2 Optimal Cross-Sections Corresponding to Typical Fill Ranges

The cargo tanks, specifically those employed in general-purpose transportation of liquid products, encounter varying fill levels due to variations in weight density of the products. The optimal cross-sections are thus explored for most probable variations in fill volume. The optimization function, described in Equations (2.21), is solved for fill volumes ranging from 50% to 90%, subjected to an additional constraint imposed on its perimeter. The tank perimeter is limited to a maximum value equal to that of a MC 306 tank (6.63 m) in order to limit the weight of the tank. Figure 2.10 illustrates six candidate optimal tank cross-sections realized upon minimizing the lateral load shift. The solutions are realized with equal weighting for different fill volumes and six different limiting values of Z_{cg0} ranging from 0.76 m to 0.96 m. The resulting geometric parameters together with those of conventional tanks are summarized in Table 2.4.

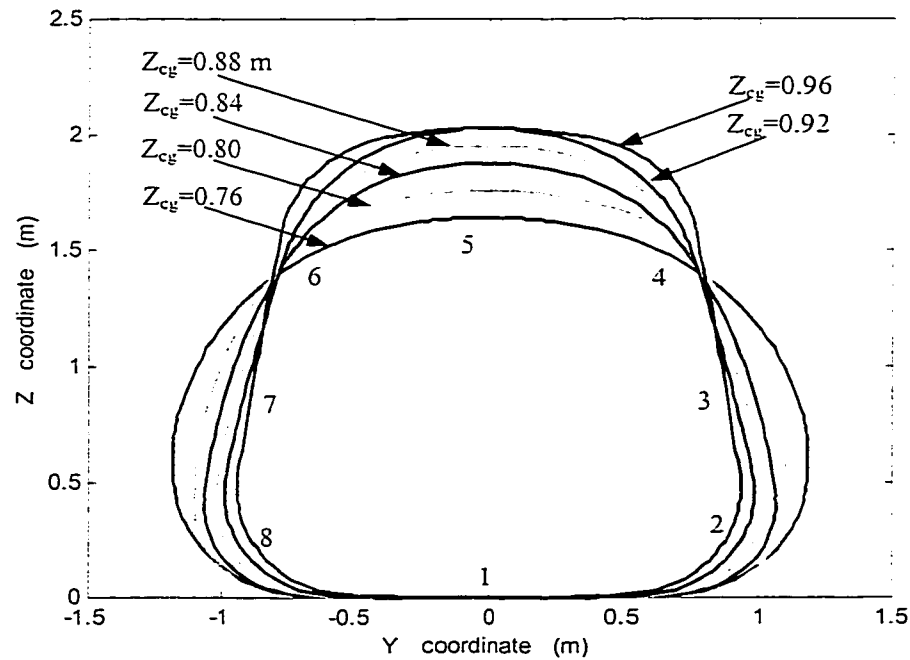


Figure 2.10: Comparison of optimal tank cross-sections corresponding to different limiting values of Z_{cg0} ($\beta=0.5$ to 0.9).

Table 2.3: Geometric parameters of optimal cross-sections corresponding to different limiting values of Z_{cg0} ($\beta=0.5$ to 0.9).

Prescribed c.g. Height (m)	Design Parameters (m)							Perimeter (m)
Z_{cg0}	H_1	H_2	R_1	R_2	R_3	R_4	R_5	L_p
0.76	2.38	1.64	15.55	0.52	0.94	1.10	1.89	6.63
0.80	2.22	1.76	23.66	0.39	1.72	0.48	1.47	6.63
0.84	2.14	1.88	24.96	0.39	2.60	0.80	1.70	6.63
0.88	2.05	1.95	25.00	0.41	4.22	0.72	1.80	6.63
0.92	1.98	2.03	24.97	0.45	10.50	0.72	1.66	6.63
0.96	1.88	2.03	24.84	0.46	33.50	0.50	1.84	6.63
Modified-oval	2.44	1.65	1.78	0.39	1.78	0.39	1.78	6.63
Circular	2.03	2.03	1.02	1.02	1.02	1.02	1.02	6.38

The results show that a relaxed value of Z_{cg0} yields an increase in tank height (H_2) and decrease in tank width (H_1). A further examination of the optimal tank geometry corresponding to different limiting values of Z_{cg0} provides additional insight into relative contributions due to c.g. height and liquid load shift. The solutions corresponding to medium to high values of Z_{cg0} (0.84-0.88 m and 0.92-0.96 m) converge to low overall width and moderately narrow top in order to reduce the magnitude of liquid load shift. Lower limiting values of Z_{cg0} (0.76-0.80 m) yield tank geometry with considerably larger width and lower height to achieve lower c.g. height. The perimeters of all the optimal cross-sections invariably approach the limiting value.

The load shift properties of the candidate optimal tank cross-sections, illustrated in Figure 2.10 and Table 2.3, are further evaluated under varying fill volumes in terms of overturning moment of the cargo about origin of the tank-body coordinate system. The total overturning moment is computed from:

$$M_o = W_l [(Y_l \cos \theta_{s3} - a_y Y_l \sin \theta_{s3}) + (Z_l \sin \theta_{s3} + a_y Z_l \cos \theta_{s3})] \quad (2.27)$$

The effective overturning moment arm is also evaluated upon normalizing the moment M_o with respect to the cargo load, such that $L_M = M_o / W_l$. Figure 2.11 illustrates the overturning moment arm, L_M , computed for different optimal cross-sections as a function of fill volume, ranging from 50% to 90%. From the results, it is apparent that low c.g. height optimal tanks yield low overturning moment under high fill volumes. The optimal cross-sections with higher c.g. height could be considered desirable for relatively lower fill volume. The results suggest that a single cross-section can not satisfy the minimal load shift requirements under wide variations in fill volumes. Figure 2.11 further illustrates the mean moment arm of each optimal cross-section, computed over the volume fill range of 50% to 90%.

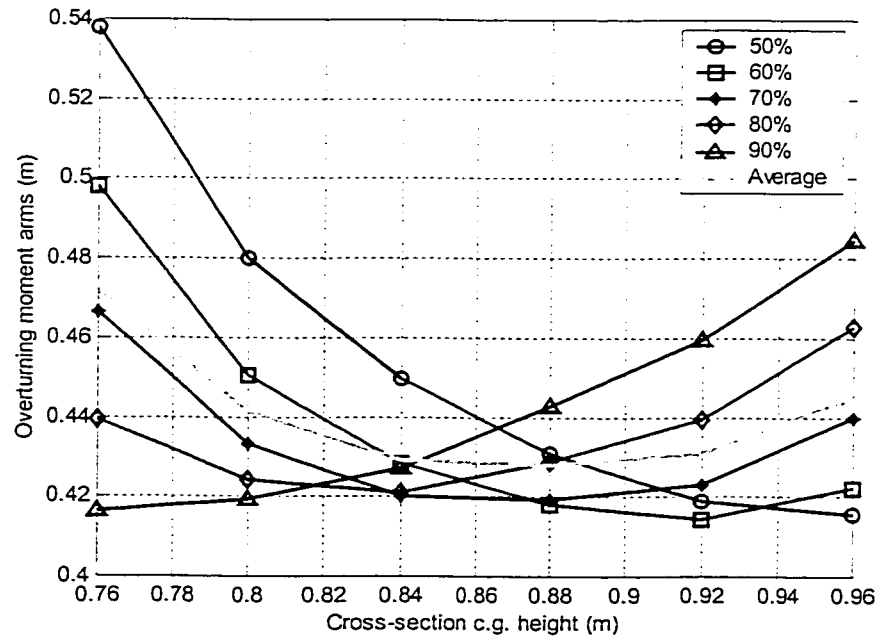


Figure 2.11: Overturning moment arms and their mean values for different optimal cross-sections and fill volume ranging from 50% to 90%.

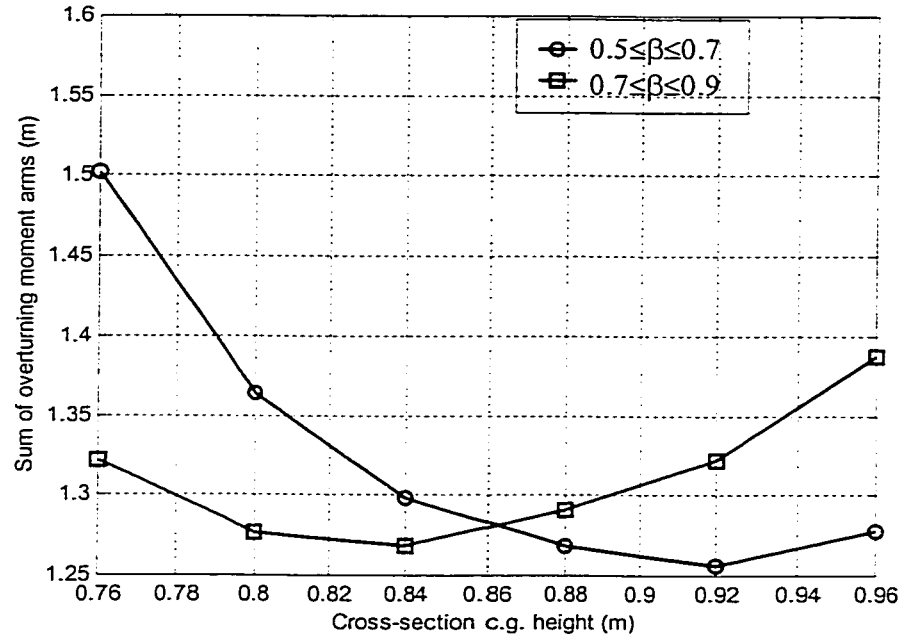


Figure 2.12: Sum of overturning moment arms of different optimal cross-sections for two fill ranges.

A further analysis of the overturning moment arms suggests two evident minima, corresponding to two ranges of fill volumes: 50% to 70% and 70% to 90%. A summation of moment arms corresponding to these two fill ranges, illustrated in Figure 2.12, reveals that the optimal cross-section with high c.g. ($Z_{cg0}=0.92$ m) can be considered optimal for fill volume ranging from 50% to 70%. The relatively lower width of this cross-section yields lower lateral load shift under low to medium fill volumes, while the contributions due to high c.g. (Z_{cg0}) remain small due to low fill volume. The optimal cross-section with lower c.g. height ($Z_{cg0}=0.84$ m), on the other hand, yields lower magnitude of overturning moment for relatively higher fill volumes, ranging from 70% to 90%. Although the optimal design with cross-section c.g. height of 0.88 m appears to yield the lowest sum of overturning moment arms in the entire fill volume range (50% to 90%), as shown in Figure 2.11, it does not yield the minimum when two different fill ranges are

considered. These results further suggest that the overturning moment is predominantly affected by lateral load shift under low to medium fill volumes, and by the c.g. height under medium to high fill volumes. Two different optimal cross-sections are thus proposed and referred to as '*OPT1*' and '*OPT2*', respectively, corresponding to $Z_{cg0}=0.92$ m and $Z_{cg0}=0.84$ m, to achieve minimal overturning moments under two different ranges of fill volumes (50% to 70% and 70% to 90%). Figure 2.13 presents a comparison of the two optimal cross-sections with those of the conventional circular and modified-oval tanks.

It should be noted that the optimal solutions are strongly influenced by the limit constraint imposed on the perimeter. The effect of the perimeter constraint could be investigated through study of optimal solutions attained upon eliminating it. Figure 2.14 illustrates the six optimal tank cross-sections obtained in the absence of the perimeter constraint corresponding to different limiting values of Z_{cg0} ranging from 0.76 m to 0.96 m. Table 2.4 summarizes the geometric parameters of the optimal cross-sections and their perimeters.

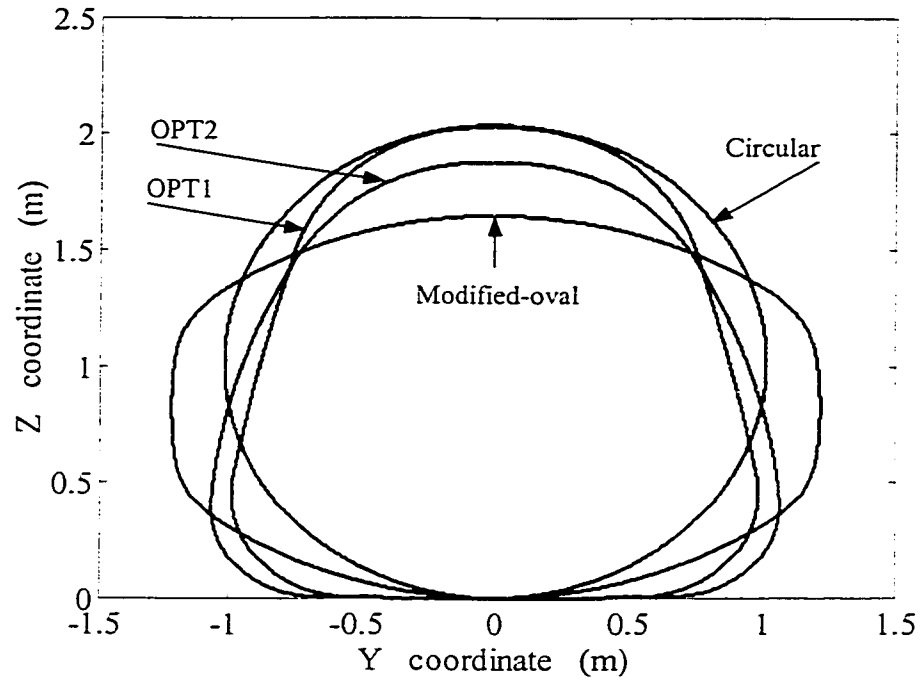


Figure 2.13: Comparison of optimal and conventional tank cross-sections.

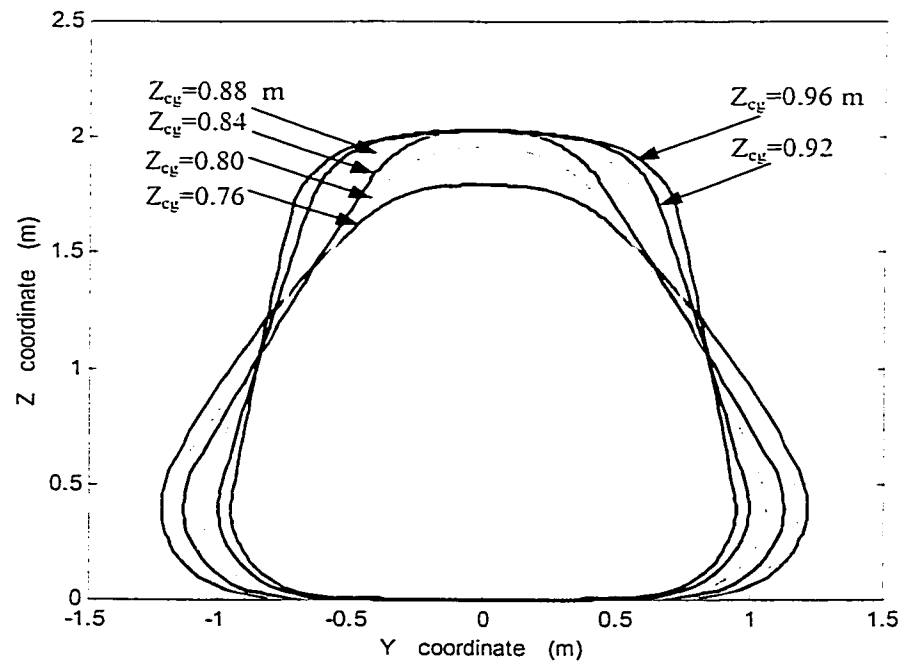


Figure 2.14: Comparison of optimal tank cross-sections corresponding to different limiting values of Z_{cg0} and unconstrained perimeter.

Table 2.4: Geometric parameters of optimal cross-sections corresponding to different Z_{cg0} (without perimeter constraint).

Prescribed c.g. Height (m)	Design Parameters (m)							Perimeter (m)
Z_{cg0}	H_1	H_2	R_1	R_2	R_3	R_4	R_5	L_p
0.76	2.44	1.80	23.46	0.39	3.65	0.50	1.50	6.82
0.80	2.37	1.96	24.85	0.39	33.5	0.50	1.80	6.91
0.84	2.26	2.03	25.00	0.39	33.5	0.42	1.65	6.90
0.88	2.13	2.02	24.36	0.39	33.50	0.39	1.84	6.81
0.92	2.00	2.03	24.89	0.39	33.50	0.39	2.05	6.75
0.96	1.90	2.03	24.90	0.39	33.50	0.39	1.84	6.71
Modified-oval	2.44	1.65	1.78	0.39	1.78	0.39	1.78	6.63
Circular	2.03	2.03	1.02	1.02	1.02	1.02	1.02	6.38

Compared with the optimal cross-sections obtained with constrained perimeter, the solution for a given Z_{cg0} converges to larger radii for arcs 1 and 3(7), and lower radii for arcs 2 (8) and 4 (6). The resulting cross-sections thus yield increased height and width and the shape approaches a conical cross-section with narrow top and wide bottom. The cross-section perimeter increases with increase in Z_{cg0} in the 0.76 m to 0.80 m range and decreases with increase in Z_{cg0} in the 0.80 m to 0.96 m range. A comparison of Figures 2.10 and 2.14 reveals that limiting the perimeter results in relatively round shapes, with considerably smaller values of H_1 and H_2 , and larger blend radii, especially for low values of Z_{cg0} . The perimeters of the optimal cross-sections derived in the absence of the perimeter constraint are approximately 1.2% to 4.2% higher than that of a modified-oval cross-section.

Figure 2.15 illustrates the overturning moment arm L_M , computed for six optimal cross-sections listed in Table 2.4, as a function of the fill volume. The figure also

illustrates mean moment arm for each fill volume. The sums of overturning moments of each cross-section corresponding to two range of fill volumes, 50% to 70% and 70% to 90%, are illustrated in Figure 2.16. The results show that the optimal cross-section with c.g. height of 0.84 m yields the lowest value of mean moment arm in the entire fill volume range (50% to 90%). The summation of overturning moment arms suggests that optimal cross-sections with c.g. heights of 0.88 m and 0.80 m can be considered to yield the lowest overturning moment for low to medium fill volumes (50% to 70%) and medium to high fill volumes (70% to 90%), respectively. Similar to the optimal solutions attained with constrained perimeter, two optimal cross-sections are identified and referred to as ' $OPT1_n$ ' and ' $OPT2_n$ ', corresponding to $Z_{cg0}=0.88$ m and $Z_{cg0}=0.80$ m, respectively. Compared with the values of Z_{cg0} attained for optimal configurations subject to constrained perimeter, the Z_{cg0} values of optimal cross-sections in the present case shift towards lower values. This shift demonstrates the effect of perimeter constraint in reducing the optimal tank cross-section c.g. height.

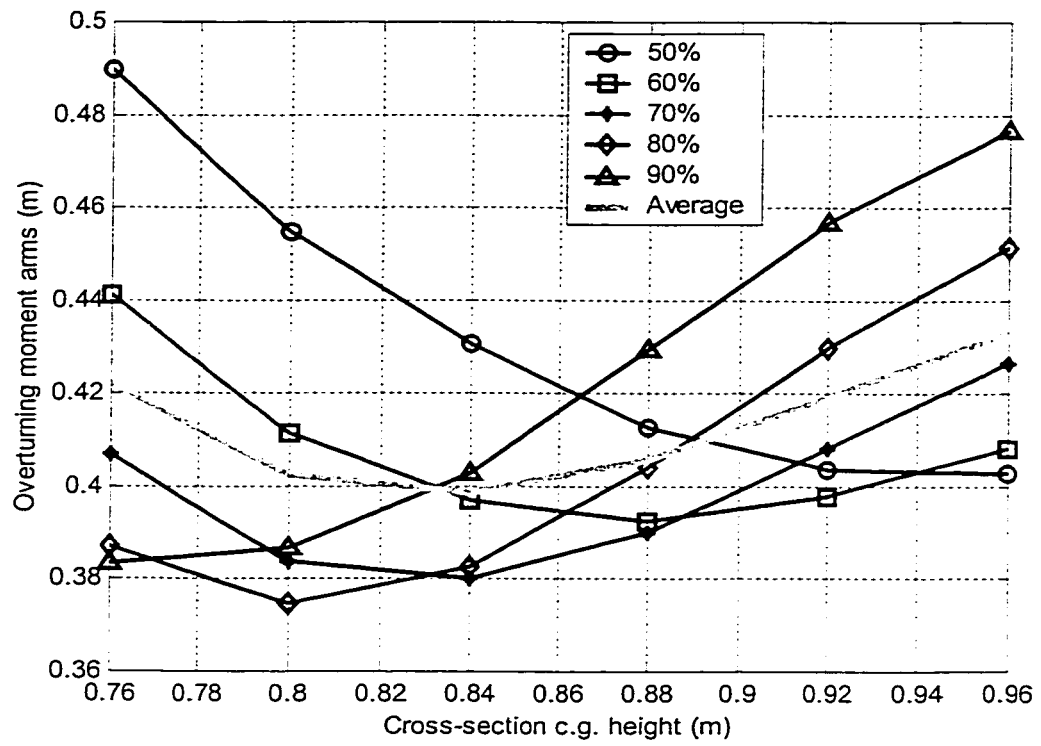


Figure 2.15: Overturning moment arms and the average of arms due to load shift for fill volumes ranging from 50% to 90%.

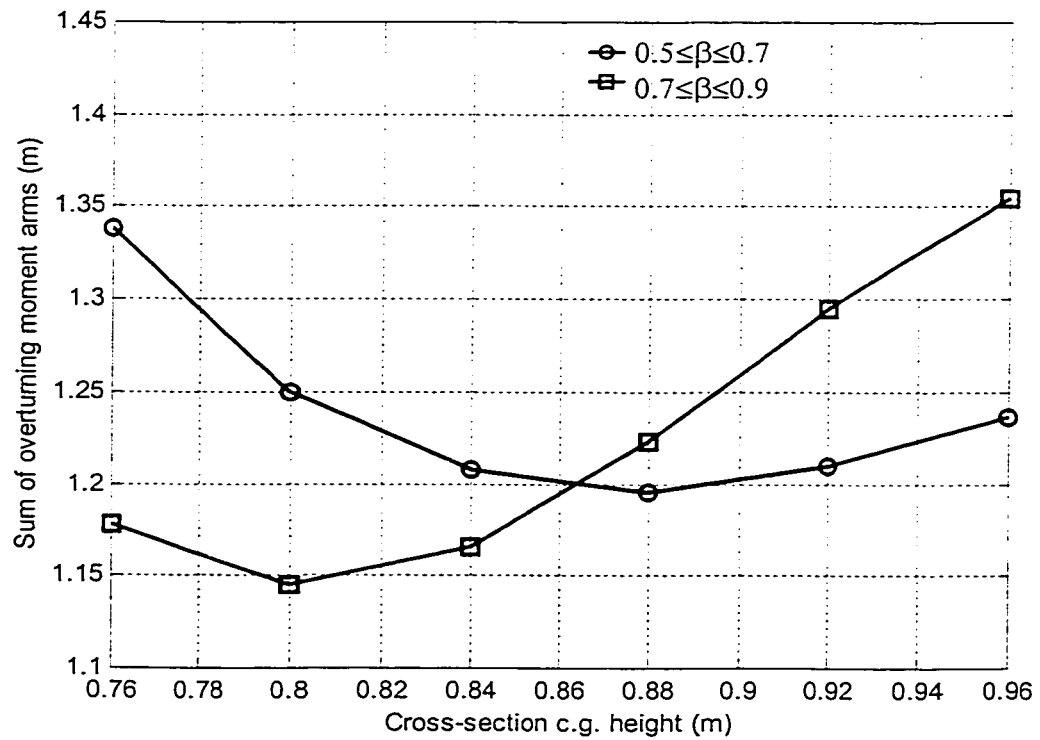


Figure 2.16: Sum of overturning moment arms as a function of z_{cg0} .

The optimization functions formulated in this study can also be conveniently applied to derive optimal geometric parameters of the conventional modified-oval cross-sections, symmetric about both axes. A modified-oval cross-section can be uniquely defined by five independent parameters, radii of the top/bottom (R_2) and side (R_1) surfaces, blend radii (R_3), overall height (H_2) and overall width (H_1). Figure 2.17 presents a comparison of a symmetric optimal cross-section ($H_1=2.29$ m, $H_2=1.55$ m, $Z_{cg}=0.78$ m, $R_1=4.55$ m, $R_2=0.39$ m, $R_3=33.50$ m, $R_4=0.39$ m, $R_5=4.55$ m, $L_p=6.76$ m) obtained for 50% to 90% fill volume range with those of the currently used circular and modified-oval tanks. Compared with the currently used modified-oval cross-section, the symmetric optimization (referred to as Optimal-oval) yields tank geometry with moderately larger radii for arcs 1 and 5, and considerably larger radii for arcs 3 and 7. The blend radii approach the limiting value of 0.39 m, resulting in reduced cross-section height and width. The shape approaches that of a modified-square.

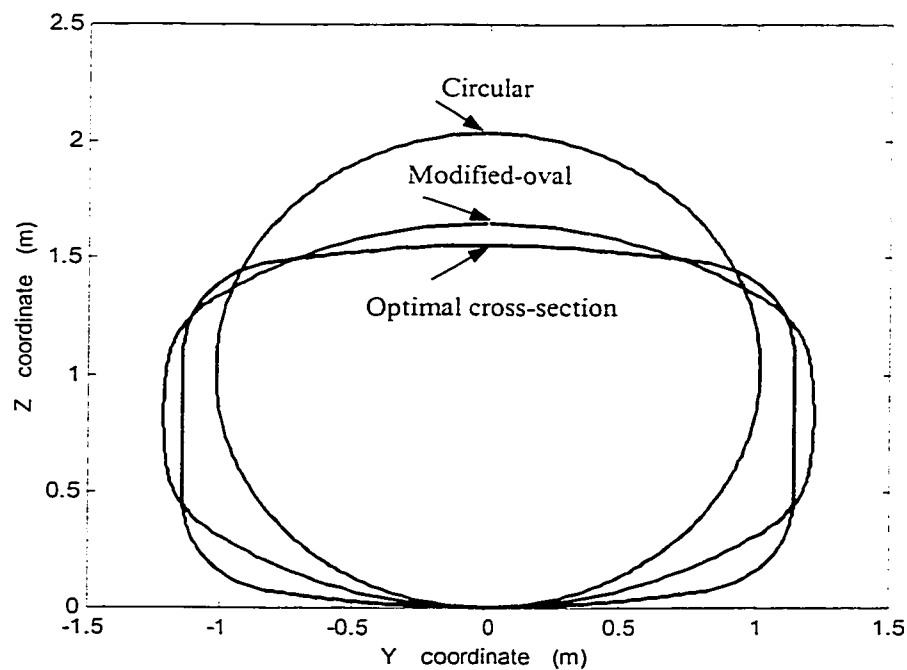


Figure 2.17: Comparison of symmetric optimal tank cross-section with those of the circular and modified-oval tanks.

2.7 SUMMARY

A generic tank cross-section is proposed to describe the geometry of currently used tanks employed in transportation of liquid bulk products. A kineto-static roll plane model of the partially-filled generic cross-section tank is developed and analyzed to study the lateral and vertical shifts in cargo c.g. under application of lateral acceleration and tank tilt. Three different multivariable constrained optimization functions are formulated and solved numerically to minimize the tank cross-section c.g. height and lateral movement of the liquid bulk, and thus the resulting overturning moment as a function of fill volume. The optimization functions are solved subject to constraints imposed on the total cross-section area, overall width and height, and perimeter. Five different optimal cross-sections are derived corresponding to 40%, 50%, 60%, 70% and 100% fill volumes. Two optimal cross-sections are identified corresponding to 50% to 70% and 70% to 90% liquid fill volume ranges, respectively. The influence of perimeter constraint on the optimal solutions are also investigated. The optimal solutions in all the cases invariably converge towards nearly conical shape, resulting in simultaneous reduction in liquid c.g. height and lateral load transfer. The potential benefits of optimal cross-sections in enhancing the roll stability of partly-filled tank vehicle combinations are investigated in the following Chapters.

CHAPTER 3

STATIC ROLL STABILITY ANALYSIS OF VEHICLES WITH PARTLY-FILLED OPTIMAL TANKS

3.1 INTRODUCTION

The likelihood of a vehicle rollover during steady turning is strongly related to its rollover threshold or overturning limit. Heavy vehicles, in general, exhibit lower rollover threshold than the other road vehicles due to their high c.g. location, and large weight and dimensions [72, 73]. Moreover, the static rollover threshold limits of tank trucks are adversely influenced by the liquid cargo shift under partial fill conditions [7, 8]. The static roll performance of such vehicles can be considerably enhanced by minimizing lateral load shift, specifically in case of low to medium fill conditions. The potential performance benefits of various optimal tank configurations, derived in Chapter 2, are thus investigated in view of the liquid load shift and static roll stability of an articulated tank vehicle combination subject to steady turning maneuvers. The potential performance benefits of vehicles with optimal tanks are assessed under varying fill volumes by comparing their roll stability limits with those equipped with conventional tanks. The static roll stability limits of partly-filled articulated tank vehicles can be effectively derived through development and analysis of a static roll plane model of the vehicle.

A static roll analysis model of a five-axle tractor-tank-semitrailer vehicle is developed by integrating the roll plane steady state fluid model of a partially-filled generic tank, developed in Chapter 2, with a roll plane model of the articulated vehicle, reported in the literature [78, 82]. The liquid load shift occurring within the partially-filled optimal tank cross-sections under various fill volumes and lateral accelerations

encountered during a steady turn is computed using the iterative algorithm formulated in Chapter 2. The equations describing the static roll equilibrium of the vehicle equipped with a partially-filled generic tank are derived and solved simultaneously to evaluate the steady turning response and rollover threshold of the vehicle equipped with optimal and conventional tanks. The roll performance characteristics of the vehicle with different optimal cross-section tanks are then compared with those of the vehicle with currently used tanks to identify optimal cross-section tanks for various liquid fill conditions. The structural integrity of the proposed optimal cross-section tanks is preliminarily investigated to evaluate the influence of optimal tank geometry on the stress distribution of the tank structure.

3.2 STATIC ROLL PLANE MODEL OF AN ARTICULATED TANK VEHICLE

A wide range of heavy vehicle configurations are used in transportation of bulk liquid products. The most commonly used vehicle configurations include five-, six- or seven-axle tractor semitrailers, and seven- or eight-axle B-trains [11]. A survey conducted by Rohm and Haas Company [7] concluded that bulk transportation of liquid products is mostly performed by five-axle tractor-tank semitrailer combinations. A five-axle tractor semitrailer combination equipped with a tank of generic cross-section is thus considered for the analysis of steady turning rollover threshold as a function of fill volume and tank geometry. Many studies have reported that rollover threshold limits of heavy vehicles can be effectively derived from a static analysis characterizing the vehicle response in a steady turn maneuver [78, 80, 81-84]. The dynamic roll response of the vehicle can thus be neglected in the analysis. The roll response of the combination in a steady turn can be conveniently derived by solving the static equilibrium equations under

small successive increments in roll angle of the trailer sprung weight. In the analysis, the entire combination is represented by three roll planes comprising three composite axes: the front- and equivalent rear-axes of the tractor, and an equivalent composite-axis of the trailer axes, as shown in Figure 3.1. The composite axes are derived upon grouping axles with similar suspension properties [78]. The two composite tractor axes, representing the front- and equivalent rear-axes, are considered to support the sprung weights W_f and W_r , respectively, due to tractor. These sprung weights are coupled through torsional compliance (K_{tr}) of the tractor frame. The trailer sprung weight is represented by two sprung weights: sprung weight of the tank-semitrailer structure (W_t) and the sprung weight (W_l) due to liquid cargo in the tank. The sprung weight due to tank-semitrailer is coupled to the tractor sprung weight (W_r) through the torsional compliance of fifth wheel and trailer structure (K_c), as shown in Figure 3.1. The weight W_5 shown in the figure represents portion of the cargo and trailer weight supported by the fifth wheel.

The static roll plane model of the partially-filled tank vehicle is developed by integrating the steady state roll plane fluid model of a partially-filled generic tank, developed in Chapter 2, and roll plane model of the articulated vehicle, shown in Figure 3.2. In the figure, j_{si} and k_{si} represent the lateral and vertical axes of sprung mass-fixed coordinate system, while j_{ui} and k_{ui} denote the lateral and vertical axes of unsprung mass-fixed system i . j_n and k_n are lateral and vertical axes of an earth-fixed inertial system. The position of c.g. of liquid cargo in the tank is represented by $C_l(Y_l, Z_l)$ with respect to tank body-fixed coordinate system (YZO). a_y represents lateral acceleration imposed on liquid cargo during a steady turn and W_{ui} is unsprung weight of axle i . F_{si1} and F_{si2} are forces developed by left and right suspension springs on axle i . H_{ri} is height of the i th roll center

Composite Axle 1 Composite Axle 2 Composite Axle

-95-

The major highlights of the model and various simplifying assumptions made in the process of deriving the underlying equations are summarized below [11, 172, 184]:

- The relative roll motion between the sprung and unsprung weight occurs about the roll center, which is located at a fixed distance beneath the sprung weight center. Each sprung weight rotates about its respective roll center.
- The suspension springs deflect along directions normal to the respective unsprung weight, and transmit only compressive or tensile forces. All the axle forces acting in a direction normal to the axis of the axles are balanced by the suspension forces, while all axle forces acting along a direction parallel to the axle axis are assumed to act through the respective roll centers.
- The nonlinear force-displacement characteristics of the suspension springs, such as backlash and interleaf friction are incorporated through tabular load-deflection input. The force-deflection characteristics are linearized about the operating point to compute the suspension forces and spring rates during simulation. The force-displacement characteristics of the suspension springs of the three composite axles are presented in Figure 3.3 [172].
- The lateral and vertical stiffness characteristics of tire j ($j=1, 2, 3, 4$) of composite axle i ($i=1, 2, 3$), KY_{ij} and KT_{ij} , are assumed to be linear.
- At lateral accelerations close to the rollover limit of the vehicle, the load transfer to the tires located on the outside of the turn is quite significant. The lateral forces developed by tires on the inside of the turn are assumed to be negligible when compared to those developed by tires on the outside of the turn. The lateral deflections of tires are thus computed only for those tires on

the outside of the turn. The lateral stiffness of tires on axle i is considered as $KY_{i3} + KY_{i4}$, oriented along the earth-fixed lateral axis j_n .

- The roll resisting moments developed due to camber are represented through torsional springs of stiffness $KOVT_{ij}$, existing at the tire/road interface.
- Roll angles are assumed to be small for both the sprung and unsprung weights, such that the small angle assumptions $\sin\theta \approx \theta$ and $\cos\theta \approx 1$ hold, where θ denotes roll angle.
- The influence of articulation on roll response of the tank vehicle is neglected, assuming small articulation angle. The sprung weights supported by different composite axles are allowed to experience different vertical deflections. The total vertical load carried by each composite axle, however, is assumed to remain constant.
- The tractor frame and the combined fifth wheel and tank-semitrailer structure are assumed to possess ideal hysteretic properties, as shown in Figure 3.4 [172]. The figure also represents the torsional compliance of the structure.
- The liquid cargo can be represented by n sprung weights to study the roll behavior of tank vehicles with n independent compartments.

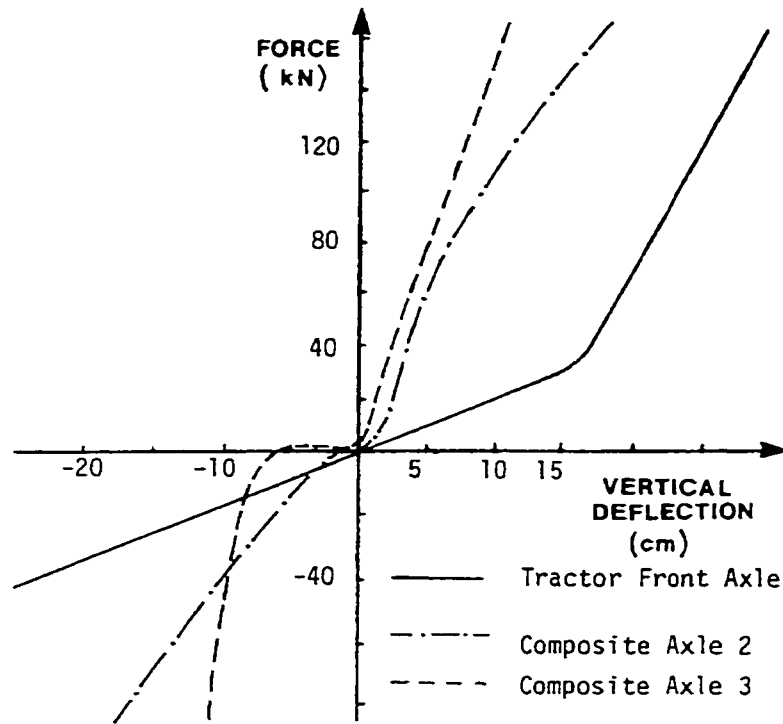


Figure 3.3: Force-displacement characteristics of suspension springs of composite axles [172].

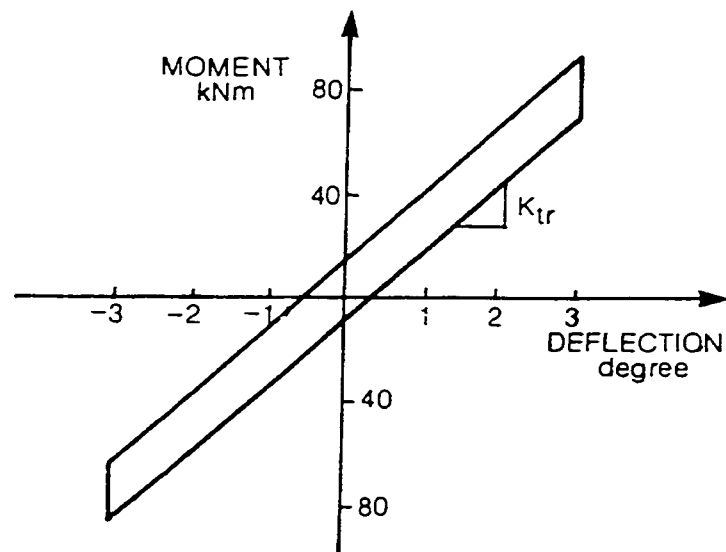


Figure 3.4: Idealized representation of tractor frame compliance [172].

3.3 EQUATIONS OF STATIC ROLL EQUILIBRIUM

A total of 15 algebraic equations along with two equations describing the load shift within a cleanbore tank are required to describe the static roll equilibrium of an articulated tank vehicle. The static roll equilibrium of an n -compartmented vehicle is described by $15+2n$ equations. The 15 algebraic equations are obtained by balancing the roll moments acting on the sprung and unsprung weights, vertical suspension and tire forces, and lateral forces acting on the tires of each composite axle. The set of algebraic equations describing the static roll equilibrium of a five-axle tractor-tank-semitrailer vehicle are expressed in terms of small variations in roll angles, lateral and vertical translations of the sprung and unsprung weights, lateral and vertical translations of c.g. of the liquid bulk in the tank and vehicle lateral acceleration. A detailed derivation of equations of roll equilibrium of an articulated vehicle is presented in [11, 172]. The final equilibrium equations of a five-axle tractor-semitrailer tank vehicle are presented below. It should be noted that, in all the equations, the roll angles are expressed in radians and the lateral acceleration (a_y) is normalized with g .

Roll moments acting on the sprung weights

The roll moments acting on the sprung weight of a composite axle include moments due to suspension forces, torsional compliance of the tractor and trailer structure, lateral forces acting through the roll center, lateral component of the sprung weight, and moment due to movement of the liquid cargo within the tank.

$$(FS_{i1} - FS_{i2})s_i + (FS_{i1} + FS_{i2})Z_{ri}(\theta_{si} - \theta_{ui}) - F_{ri}Z_{ri} + M_{r1i} + M_{r2i} + M_{r3i} + M_{r4i} + M_{rli} = 0 \quad (3.1)$$

where FS_{ij} is the force due to suspension springs on axle i , given by

$$FS_{ij} = K_{ij}[Z_{ui} + (-1)^i s_i(\theta_{si} - \theta_{ui})]; (j=1, 2) \quad (3.2)$$

where $i=1, 2, 3$ denotes the sprung weights and composite axles on the tractor front, tractor rear and trailer respectively, K_{i1} and K_{i2} are the equivalent linear spring rates of the left and right springs on the i th suspension. Z_{ui} is vertical distance between the unsprung weight c.g. and roll center of axle i along the k_{ui} axis, as shown in Figure 3.2. s_i is half the suspension lateral spread of axle i and θ_{ui} is roll angle of the i th unsprung weight. F_{ri} is the lateral force acting through the roll center of axle i , in a direction parallel to j_{ui} axis, expressed as:

$$F_{ri} = W_{si}(a_y - \theta_{ui}) \quad (3.3)$$

where the three sprung weights are given by

$$\begin{aligned} W_{s1} &= W_f + W_{fr} \\ W_{s2} &= W_r + W_5 - W_{fr} \\ W_{s3} &= W_t + W_l - W_5 \end{aligned} \quad (3.4)$$

The term W_{fr} in above equations defines the vertical shear force acting through the tractor frame. M_{r1i} , M_{r2i} , M_{r3i} , M_{r4i} , and M_{rli} are the roll moments due to torsional compliance of the tractor frame (K_{tr}), shear force acting on the tractor frame (W_{fr}), vertical load on the fifth wheel (W_5), torsional compliance of the fifth wheel and trailer structure (K_c), and the liquid load (W_l), respectively, acting on axle i . These additional roll moments are derived from following relationships:

$$\begin{aligned} M_{r1i} &= \begin{cases} (-1)^{i+1} K_{tr}(\theta_{s2} - \theta_{s1}); (i = 1, 2) \\ 0; i = 3 \end{cases} \\ M_{r2i} &= \begin{cases} (-1)^{i+1} W_{fr}(a_y - \theta_{si})Z_{fi}; (i = 1, 2) \\ 0; i = 3 \end{cases} \end{aligned}$$

$$\begin{aligned}
M_{r3i} &= \begin{cases} 0; i=1 \\ (-1)^i W_s Z_{si} (a_y - \theta_{si}); (i=2, 3) \end{cases} \\
M_{r4i} &= \begin{cases} 0; i=1 \\ (-1)^i K_c (\theta_{s3} - \theta_{s2}); (i=2, 3) \end{cases} \\
M_{rli} &= \begin{cases} 0; i=1, 2 \\ W_l [Y_l (1 + a_y \theta_{si}) + Z_l (\theta_{si} - a_y)]; (i=3) \end{cases} \quad (3.5)
\end{aligned}$$

where Z_{fi} is vertical height of the tractor frame with respect to c.g. of the i th sprung weight and Z_{si} is vertical distance between fifth wheel and c.g. of the i th sprung weight.

Roll moments acting on the unsprung weights

The equation for roll moment of the unsprung weight i includes moments arising from suspension and tire forces, lateral forces acting through the roll center and lateral forces developed at the tire-road interface. The equation for roll equilibrium of the i th unsprung weight can be expressed as:

$$\begin{aligned}
& - (FS_{i1} - FS_{i2})s_i + (FT_{i1} - FT_{i4})(b_i + d_i) - (FT_{i3} + FT_{i4})y_i + OVT_{i3} + OVT_{i4} \\
& (FT_{i2} - FT_{i3})b_i + F_{ri}z_{ui} + F_{yi}H_{ui} + \left(\sum_{j=1}^4 FT_{ij} \right) R_{ti} \theta_{ui} = 0; \quad (i=1, 2, 3) \quad (3.6)
\end{aligned}$$

where OVT_{i3} and OVT_{i4} are roll-resisting moments developed at the tire-road interface of outboard tires, FT_{ij} is vertical force developed by tire j of axle i , b_i is half the track width of inner tires, d_i is dual tire spacing and y_i is lateral displacement of the tires on the outside of the turn. F_{yi} is lateral force developed by the tires of axle i , R_{ti} is effective radius of tires on axle i and H_{ui} is height of the i th unsprung weight center from the ground plane.

Forces developed by suspension springs

The forces generated by compression/extension of suspension springs must

satisfy the following relationship to maintain equilibrium along the k_{ui} axis:

$$F_{si1} + F_{si2} = W_{si}(1 + a_y \theta_{ui}) \quad (3.7)$$

Vertical forces generated by tires

The vertical load carried by each composite axle is assumed to remain constant, while neglecting the influence of road grade and vehicle pitch. The forces developed by tires of a composite axle are thus required to satisfy the following equilibrium equation:

$$W_{si} + W_{ui} = \sum_{j=1}^4 FT_{ij} \quad (3.8)$$

Lateral forces generated by tires

When vehicle lateral acceleration approaches its rollover limit, the tires on the outside of the turn carry almost entire axle load. This results in lateral translation of the centroid of normal pressure distribution at the tire-road interface. For a dual tire set, the lateral force experienced by axle i is expressed as:

$$F_{yi} = (KY_{i3} + KY_{i4})y_i \quad (3.9)$$

where KY_{i3} and KY_{i4} are the linear spring rates of tires 3 and 4 on axle i , oriented along the earth-fixed lateral axis j_n , and y_i is the change in the effective trackwidth of the i th axle due to lateral translation of the centroid of interface pressure. Balancing the total lateral (inertial) forces due to the i th axle and its supported sprung weight by the lateral forces generated by the tires yields:

$$(KY_{i3} + KY_{i4})y_i = (W_{si} + W_{ui})a_y \quad (3.10)$$

Equations (3.1) through (3.10) provide a total of 15 algebraic equations representing the force and moment equilibrium of an articulated tractor-semitrailer

vehicle in the roll plane. Equation (2.18) provides a set of two equations required to compute the instantaneous coordinates of the center of mass of liquid within a cleanbore tank of generic cross-section. A total of 17 equations are therefore developed to describe the static roll plane model of the tank vehicle. These equations of static roll equilibrium are further rewritten in terms of variations in roll angles, vertical motions of sprung weights, lateral and vertical motions of unsprung weights, lateral and vertical translations of the c.g. of the liquid cargo and vehicle lateral acceleration, to express the effects of a small variation in roll angle of the tank semitrailer sprung weight ($\Delta\theta_{s3}$). The algebraic equations can be written in matrix notation in the following manner:

$$[A_v]\{\Delta X\} = \{Q_v\}\Delta\theta_{s3} \quad (3.11)$$

where $[A_v]$ is a 17×17 matrix of coefficients, which are functions of vehicle parameters, and $\{Q_v\}$ is a vector of dimension 17×1 , and $\{\Delta X\}$ is the vector of vehicle response variables due to $\Delta\theta_{s3}$, expressed as:

$$\{\Delta X\}^T = \{\Delta a_y, \Delta\theta_{s1}, \Delta\theta_{s2}, \Delta\theta_{ui}, \Delta Z_{ui}, \Delta H_{ui}, \Delta y_i, \Delta Y_l, \Delta Z_l\}; \quad (i=1, 2, 3) \quad (3.12)$$

where T indicates transpose, and $i=1, 2, 3$ represents the three composite axes.

Equation (3.11) is solved for small variations in the trailer roll angle ($\Delta\theta_{s3}$) to simulate the steady tuning performance of the partially-filled tank vehicle. The simulation begins with the vehicle in the upright position. Initially, the lateral acceleration, and roll angles of the sprung and unsprung weights are set to zero ($\theta_{si}=\theta_{ui}=0$; $i=1, 2, 3$). The roll angle of trailer sprung weight is then gradually increased in small increments. For each increment in the sprung weight roll angle, Equation (3.12) is solved to determine the corresponding response vector $\{\Delta X\}$. The lateral and vertical coordinates of the liquid

cargo c.g. are then evaluated, and the matrix $[A_v]$ and vector $\{Q_v\}$ are updated to reflect changes in roll properties of the vehicle due to nonlinearities of the suspension springs. The calculations are terminated when normal loads on the inside tires of the tractor rear and trailer composite axles approach zero, indicating the condition of relative rollover [78, 94]. The vehicle rollover is thus detected as the tires on these two composite axles experience lift-off. The highest lateral acceleration encountered during the computing process determines the rollover threshold acceleration of the tank vehicle combination.

Computer simulations are carried out for tanks of circular, modified-oval and various optimal cross-sections, derived in Chapter 2. For multiple compartment tanks, it is assumed that all compartments are filled to identical height. The parameters of the simulation vehicle are listed in Table 3.1.

Table 3.1: Simulation parameters of the tank vehicle used in the analysis [172].

<i>Tractor</i>	
<i>Type:</i>	<i>Three Axle</i>
Sprung Weight:	46882 N
Unsprung Weight (front axle):	9340 N
Unsprung Weight (rear axle):	22240 N
Wheel Base:	4.37 m
<i>Tank and Trailer</i>	
<i>Type:</i>	<i>Triaxle</i>
Sprung Weight (empty):	87448 N
Tank Length:	12.19 m
Vertical spring rate of tires:	788 kN/m
Lateral spring rate of tires:	876 kN/m

3.4 LOAD SHIFT IN PARTLY-FILLED OPTIMAL TANKS

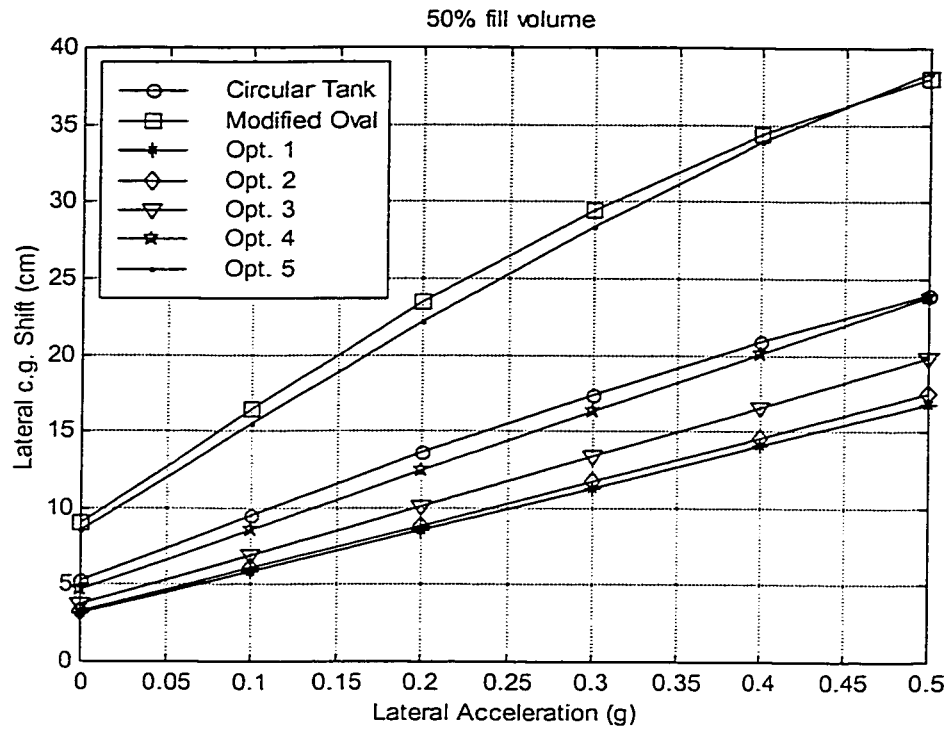
A tank truck undergoing a steady turn maneuver experiences a steady lateral acceleration field and sprung mass roll angle. The application of this lateral acceleration field may yield considerable load shift under partial fill conditions. The magnitude of cargo shift is strongly dependent upon tank cross-section, fill volume and amplitude of lateral acceleration as described earlier in Sections 2.2. The liquid load shift, experienced in terms of deviations in vertical and lateral coordinates of the cargo c.g., occurring within the partly-filled optimal cross-sections is investigated through analysis of the steady roll-plane model, developed in Section 2.4. The instantaneous coordinates of cargo c.g. and deviations in c.g. coordinates are evaluated as functions of vehicle lateral acceleration and tank semitraiiler roll angle, and compared with those of the currently used circular (MC307 and MC312, $R=2.03/2$ m) and modified-oval (MC306 A1, $R_1=1.78$ m, $R_2=0.39$ m, $R_3=1.78$ m, $H_1=2.44$ m, $H_2=1.65$ m) tanks. It should be noted that conventional and optimal tank cross-sections are selected to yield identical volume. The analyses are initially performed for optimal configurations derived for specific fill volume ratio, as described in Section 2.6.1 (*Opt. 1* to *Opt. 5*). The load shift encountered in two optimal configurations derived for specific fill volume range, described in Section 2.6.2 (*OPT1* and *OPT2*), is then analyzed and compared with those of the conventional tanks. The results are discussed in following subsections.

3.4.1 Load Shift Analysis of Optimal Tanks for Typical Fill Volumes

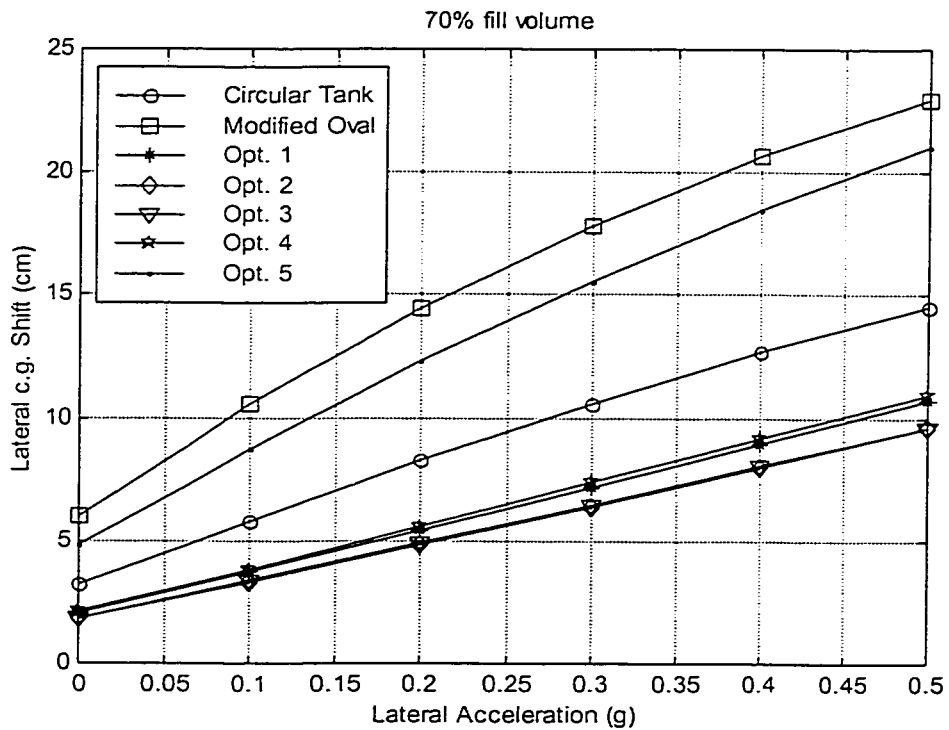
Figures 3.5 and 3.6 illustrate the shift in lateral and vertical c.g. coordinates of liquid cargo within *Opt. 1* through *Opt. 5* tanks, and the conventional circular and modified-oval tanks. The deviations in coordinates are evaluated for 50% and 70% fill

volumes, and lateral acceleration ranging from 0. to 0.5 g under a constant sprung weight roll angle of 7 degrees. The results show considerable increase in deviations in the lateral and vertical c.g. coordinates of the cargo with increase in lateral acceleration, irrespective of tank cross-section and fill volume considered in the analysis, as a result of increase in the magnitude of liquid free surface gradient with increase in a_y . The results further show that magnitude of lateral deviation of the c.g. coordinates is considerably larger than that obtained in the vertical axis, irrespective of fill volume and tank cross-section, due to influence of gravity acceleration. Higher fill volume, however, yields considerably smaller deviations in both lateral (ΔY_l) and vertical (ΔZ_l) coordinates, attributed to significant reduction in free surface area under high fill volumes.

The optimal configurations, Opt. 1, Opt. 2 and Opt. 3, yield considerably lower magnitudes of lateral and vertical deviations in c.g. coordinates under both fill volumes, when compared with those obtained for the circular and modified-oval tanks. This reduction in load shift is primarily ascribed to considerably narrower cross-section of these three optimal tanks, since they are obtained based upon relatively low reference fill volumes of 40%, 50% and 60%, respectively, as described in Section 2.6.1. The Opt. 4 configuration yields deviations that are similar to those obtained for the circular tank under 50% fill volume, due to their comparable cross-section width, and lower shifts under 70% fill volume, due to less free surface area of the liquid within Opt. 4. The Opt. 5 configuration, derived for 100% fill volume, yields considerably larger deviations in the c.g. coordinates of liquid cargo than the other optimal configurations and circular cross-section tanks, attributed to its relatively wider cross-section resulting from disregard of liquid shift in the optimization solution, as described in Section 2.6.1. The magnitudes of



(a)



(b)

Figure 3.5: Comparison of lateral deviations in c.g. coordinates of liquid cargo within optimal and currently used tanks.

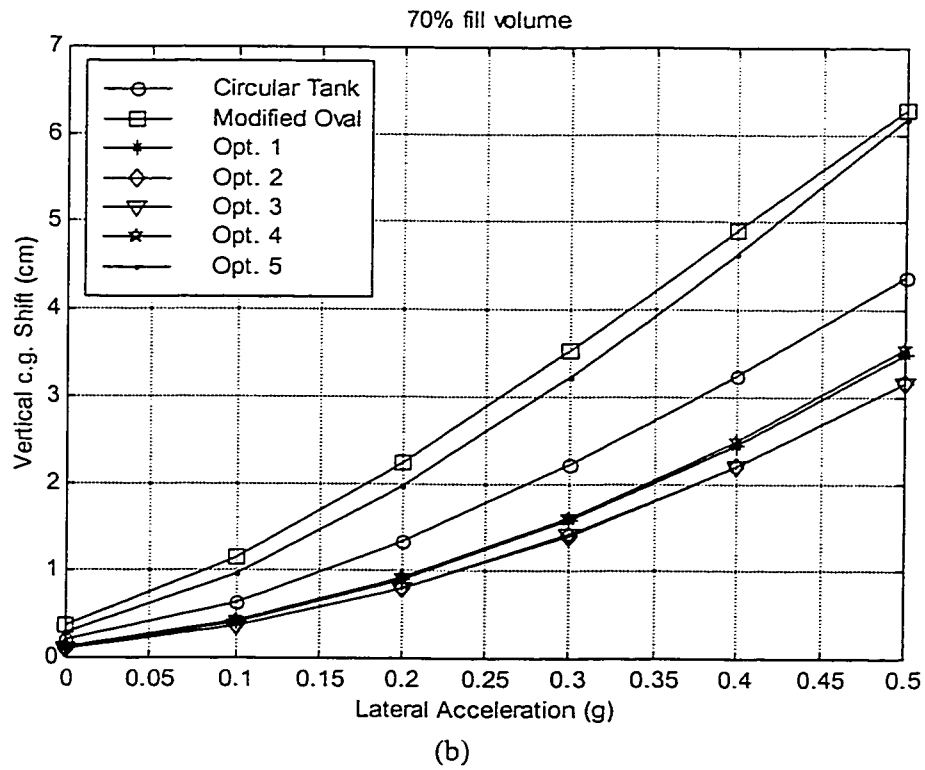
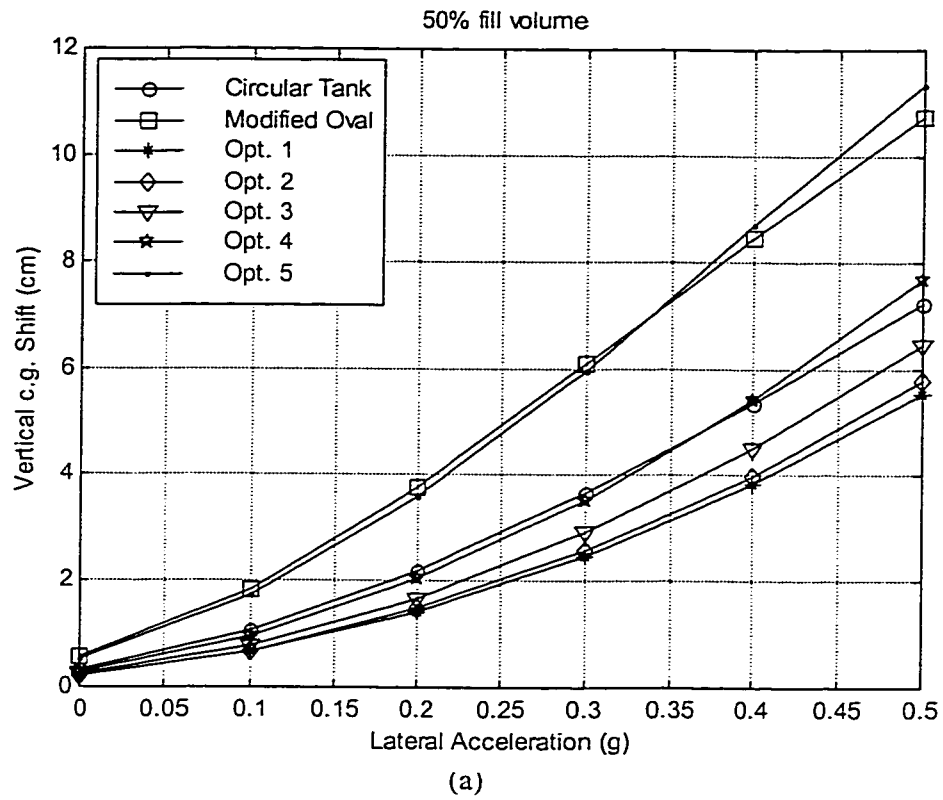


Figure 3.6: Comparison of vertical deviations in c.g. coordinates of liquid cargo within optimal and currently used tanks.

deviations attained for this configuration, however, are lower than those obtained for the modified-oval cross-section, because of the considerably narrower upper portion of its cross-section, as shown in Figure 2.9. These results suggest that the Opt. 5 design may be considered as optimal in cases where partial fill condition does not occur.

3.4.2 Load Shift Analysis of Optimal Tanks for Typical Fill Ranges

The liquid load shift encountered in two optimal configurations (*OPT1* and *OPT2*) derived for 50-70% and 70-90% fill volume ranges, described in Section 2.6.2, is analyzed for the fill ranges considered in the optimization (50%-90%). The analyses are performed under varying magnitudes of constant lateral acceleration (a_y) ranging from 0. to 0.5 g and tank roll angle (θ_{s3}) of 7 degrees.

Figure 3.7 illustrates the trajectories of the c.g. of the liquid cargo within the optimal configurations, *OPT1* and *OPT2*, with 50% and 80% fill volumes. The figure also illustrates a comparison of resulting trajectories with those attained for conventional circular and modified-oval tanks under identical fill volumes. Each curve shown in Figure 3.7 illustrates the coordinates of cargo c.g. corresponding to a_y in the range of 0. to 0.5 g with increments of 0.1 g . The leftmost symbol on each curve relates to $a_y=0.$, while the rightmost relates to $a_y=0.5$ g . The magnitudes of deviations in lateral and vertical coordinates of the liquid cargo c.g. for both fill volumes under $a_y=0.4$ g and $\theta_{s3}=7$ degrees are summarized in Table 3.2.

The lower fill volume ($\beta=0.5$) yields considerably lower c.g. height in the absence of lateral acceleration ($a_y=0.$), the corresponding magnitudes of lateral deviation tend to be significant under a steady lateral acceleration field. Higher fill volume on the other hand yields higher c.g. location but considerably less lateral deviations. A comparison of

the c.g. heights of the liquid cargo within different tanks, shown in Figure 3.7, reveals that *OPT2* tank yields the lowest c.g. height for both fill volumes in the entire range of a_y considered. The cargo c.g. height in the *OPT2* tank remains well below those of the conventional cross-sections under both fill volumes, as a result of its considerably low cross-section c.g. height, as shown in Figure 2.13 and Table 2.3. The circular tank yields the highest values of vertical coordinate of the liquid c.g. for both fill volumes, due to its excessive cross-section c.g. height. The modified-oval tank yields relatively lower c.g. height, comparable to that of the *OPT2* tank under 80% fill volume, but causes considerable lateral cargo shift under application of a_y , attributed to its excessive wide cross-section. The *OPT1* cross-section results in c.g. heights of the liquid cargo slightly higher than those attained for the modified-oval tank under 80% fill volume, due to its relatively large c.g. height arising from the considerably narrow cross-section.

A comparison of the c.g. trajectories of the liquid cargo within different tanks reveals that while the proposed optimal cross-section *OPT1* yields a moderate increase in cross-sectional c.g. height when compared to that of the modified-oval tank under relatively high fill volume (80%), it leads to significant reduction in lateral and vertical liquid load shift under both 50% and 80% fill volumes. The load shift is considerably lower than that attained for the conventional tanks, as shown in Figure 3.7 and Table 3.2, attributed primarily to its considerably narrower cross-section. Under lower fill volume ($\beta=0.5$), this configuration yields lower c.g. height than the modified-oval cross-section, and the corresponding variation in the lateral c.g. coordinate of the cargo under extreme lateral acceleration ($a_y=0.5\text{ g}$) is nearly 50% of that attained in a modified-oval tank. While *OPT2* design yields liquid c.g. variations somewhat similar to those attained for

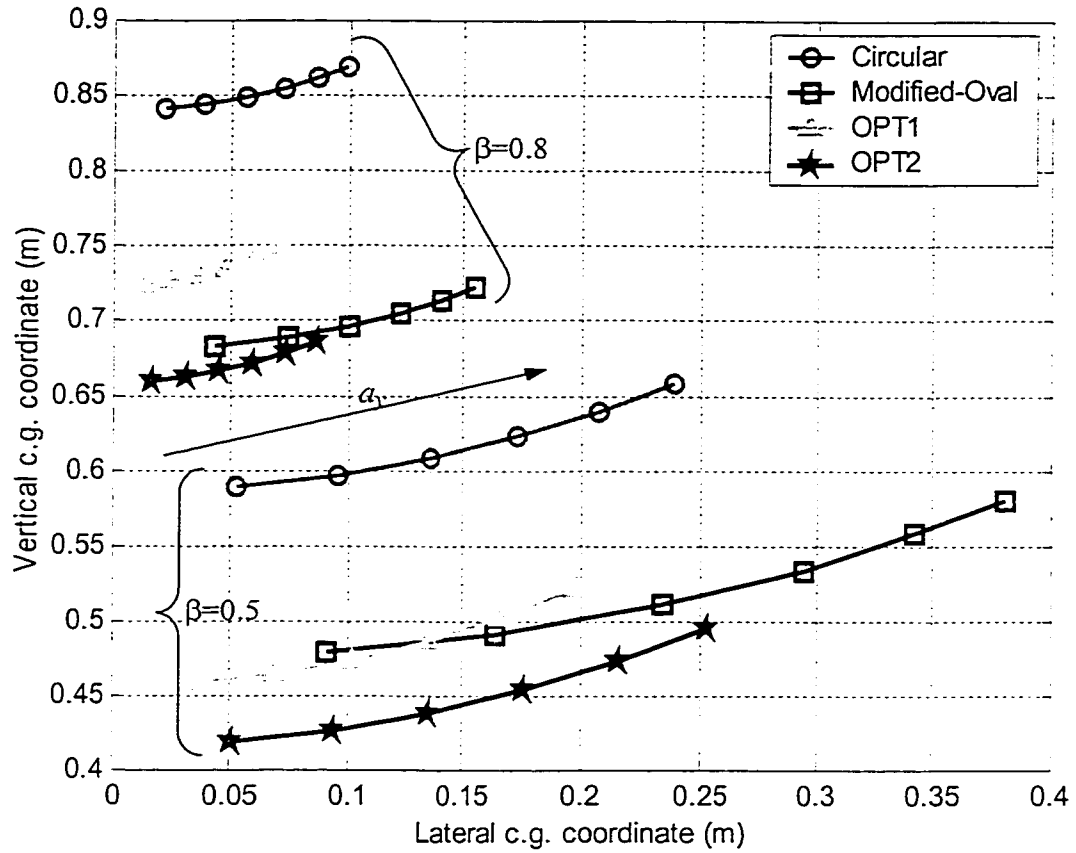


Figure 3.7: Comparison of trajectories of liquid cargo c.g. within optimal and conventional tanks ($0 \leq \alpha_1 \leq 0.5$ g).

Table 3.2: Comparison of load c.g. shift within tanks of various cross-sections ($\alpha_1=0.4$ g and $\theta_{s,j}=7$ degrees).

Tank configuration	Geometric parameters (m)	Variation in the c.g. coordinates (m)			
		$\beta=0.5$		$\beta=0.8$	
		ΔY_l	ΔZ_l	ΔY_l	ΔZ_l
Circular tank	$R=1.015$; $H_1=2 R$; $H_2=2 R$	0.208	0.053	0.086	0.022
Modified-oval	$R_1=1.78$, $R_2=0.39$, $R_3=1.78$; $R_4=R_2$; $R_5=R_1$; $H_1=2.44$; $H_2=1.65$	0.343	0.085	0.140	0.032
<i>OPT1</i>	$R_1=24.97$; $R_2=0.45$; $R_3=10.50$; $R_4=0.72$; $R_5=1.66$; $H_1=1.98$; $H_2=2.03$	0.168	0.046	0.059	0.016
<i>OPT2</i>	$R_1=24.96$; $R_2=0.39$; $R_3=2.60$; $R_4=0.80$; $R_5=1.70$; $H_1=2.14$; $H_2=1.88$	0.216	0.058	0.073	0.020

the circular tank due to comparable cross-section, it results in considerably less c.g. shifts than the modified-oval tank under both fill volumes, as is evident from Table 3.2, ascribed mostly to its relatively narrow cross-section. Lower fill volumes coupled with *OPT2* tank, however, can result in considerable lateral load shift, larger than that attained in a circular tank, due to the relatively wide lower portion of the *OPT2* cross-section. Although the modified-oval tank exhibits c.g. height comparable to that of the *OPT2* cross-section, it yields the largest lateral and vertical load shift for both fill volumes, owing to its excessively wide cross-section.

The liquid load shift is further analyzed for optimal configurations obtained without a constraint on the perimeter, as described in Section 2.6.2. Figure 3.8 presents a comparison of the trajectories of the liquid cargo c.g. within the optimal and conventional tanks, where *OPT1_n* and *OPT2_n* refer to those attained without the additional perimeter constraint for 50% to 70% and 70% to 90% fill ranges, respectively. Table 3.3 summarizes the magnitudes of the shift in the lateral and vertical c.g. coordinates of the liquid cargo within the *OPT1_n* and *OPT2_n* and relative gain with respect to the *OPT1* and *OPT2* as well as the conventional tanks under $a_y=0.4\ g$ and $\theta_{s3}=7$ degrees. An examination of Figure 3.8 and Table 3.3 reveals the similar behavior of the two sets of optimal configurations obtained with and without the perimeter constraint (i.e., *OPT1* & *OPT2* and *OPT1_n* & *OPT2_n*). The *OPT1_n* and *OPT2_n*, however, result in considerably lower c.g. heights of liquid than *OPT1* and *OPT2*, respectively, under both fill volumes, due to the relatively lower c.g. heights of *OPT1_n* and *OPT2_n* cross-sections with wider bottom and narrower top. While *OPT1_n* and *OPT2_n* yield moderately lower liquid c.g. shift at 80% fill volumes due to their relatively narrower top, they cause slightly higher

load shift under 50% fill volume, when compared to *OPT1* and *OPT2*, respectively, attributed mostly to the larger liquid free surface areas resulting from the relatively wider bottom of their cross-sections.

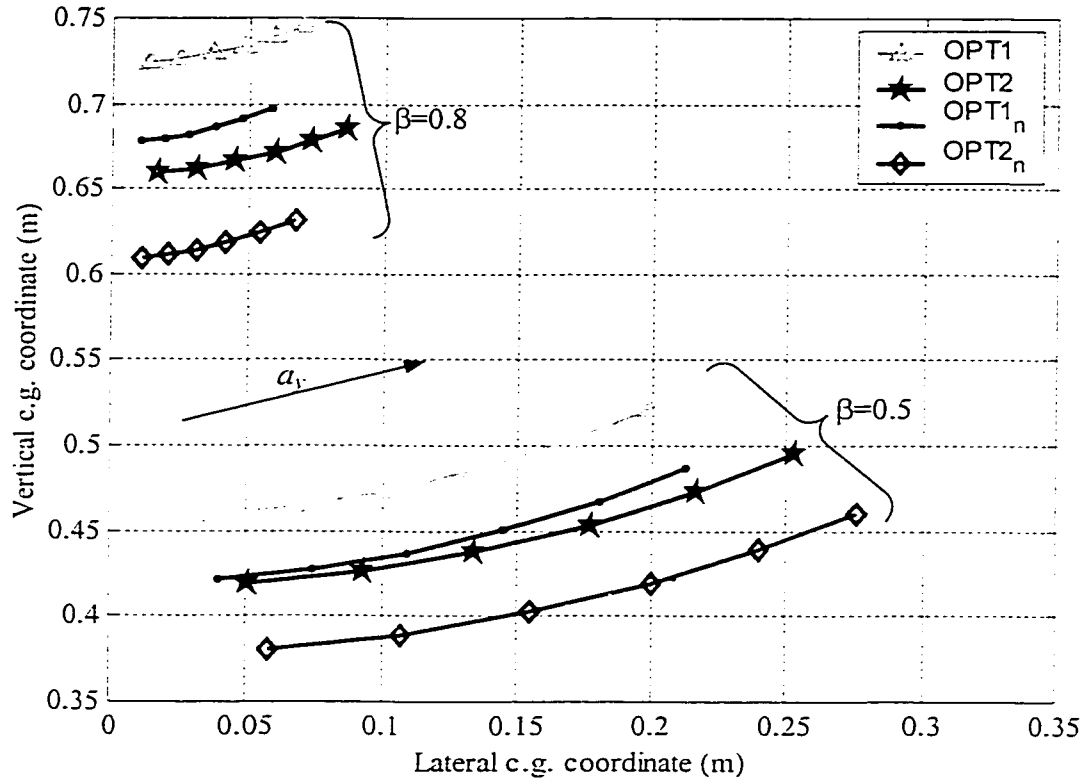


Figure 3.8: Comparison of trajectories of liquid cargo c.g. within the two sets of optimal tanks obtained with and without the perimeter constraint ($0 \leq a_y \leq 0.5 \text{ g}$).

Table 3.3: Comparison of load c.g. shift within the two sets of optimal tanks.

Optimal tank configuration	Variation in the c.g. coordinates (m)			
	$\beta=0.5$		$\beta=0.8$	
	ΔY_l	ΔZ_l	ΔY_l	ΔZ_l
<i>OPT1</i>	0.168	0.046	0.059	0.016
<i>OPT2</i>	0.216	0.058	0.073	0.020
<i>OPT1_n</i>	0.180	0.049	0.048	0.013
<i>OPT2_n</i>	0.240	0.062	0.054	0.015

3.5 ROLLOVER THRESHOLD LIMITS OF PARTLY-FILLED ARTICULATED VEHICLES WITH DIFFERENT TANKS

The potential performance benefits of the proposed optimal tank cross-sections are further investigated in terms of static roll stability of the articulated tank vehicle, based upon static roll plane analysis of the tank vehicle. Equation (3.11) is solved for different tank cross-sections and fill volumes to derive the rollover threshold limits, while cross-section parameters are selected to ensure identical volume of all the tanks.

The partial fill condition in a tank-vehicle combination may occur in two modes: (i) variable load partial-fill condition, which occurs in vehicles involved in local delivery of gasoline or fuel oils; and (ii) constant load partial-fill condition, which is encountered in general-purpose tank vehicles due to variations in weight density of different liquid products and axle load regulations. The steady turning rollover threshold lateral acceleration limits of the vehicle with different tanks are evaluated for both types of partial fill conditions. The results are discussed in following subsections.

3.5.1 Optimal Cross-sections Obtained for Typical Fill Volumes

Figure 3.9 presents the static rollover threshold acceleration limits of the tractor-semitrailer vehicle equipped with tanks of various cross-sections, including circular, modified-oval and the five optimal configurations (Opt.1 through Opt.5) obtained corresponding to 40% to 70%, and 100% fill volumes, respectively. The rollover threshold is evaluated for various fill volumes, while the total cargo load is allowed to vary with the fill volume. The weight density of the liquid cargo (a kind of fuel oil) is taken as 6800 N/m^3 (0.025 lb/in^3).

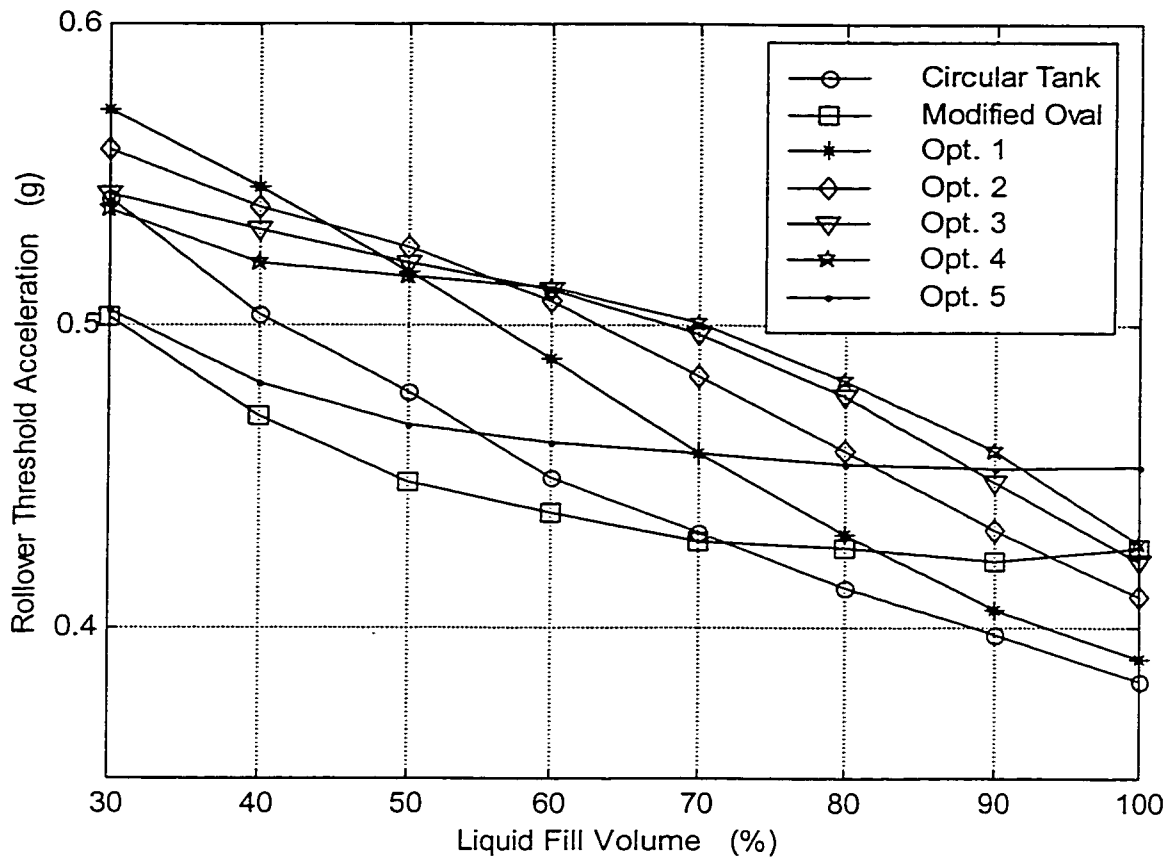


Figure 3.9: Rollover threshold acceleration limits of an articulated vehicle with various tanks as a function of fill volume (variable cargo load).

The results show that the rollover threshold of the vehicle combination with all the tanks decreases monotonously as the liquid fill volume increases. This is attributed to increase in c.g. height with increase in fill volume. The rollover threshold of the vehicle equipped with two wide cross-section tanks (the modified-oval and Opt. 5), however, approaches nearly steady values for fill volumes exceeding 70%. This is attributed to their low c.g. height over the entire range of fill volume considered in the analysis. The Opt. 5 configuration, however, yields rollover threshold lateral acceleration higher than that of the currently used modified-oval configuration over the entire fill range. The results further show that the circular cross-section tank, employed in general purpose transportation of bulk liquids, yields considerably lower values of rollover threshold

under fill volumes exceeding 70%, which is mostly caused by higher c.g. location and considerable lateral load shift. The modified-oval tank yields lowest values of rollover threshold limits for fill volumes below 70%, due to significant lateral load shift. The rollover threshold of the vehicle equipped with Opt. 5 tank reveals trend similar to that of the modified oval tank, due to its relatively wider cross-section.

From the figure, it is further evident that Opt. 3 and Opt. 4 cross-sections yield considerably larger values of rollover threshold for fill volumes in the 30% to 90% range, when compared with those of the currently used cross-sections. The Opt. 5 configuration, however, yields nearly constant rollover threshold at fill volumes exceeding 55%, which is larger than those of the vehicles equipped with circular or modified-oval tanks. While Opt. 2, Opt. 3 and Opt. 4 cross-sections reveal considerably larger roll stability, the rollover threshold tends to decrease with increase in fill volume due to their narrow cross-section. The Opt. 5 configuration may thus be considered most suited for vehicles equipped with partially-filled tanks with variable load. This configuration results in rollover threshold, which is 7% higher than that of the modified-oval tank at fill volumes above 60%, and 7% to 20% higher than the circular tank for fill volumes above 60%.

Figure 3.10 shows static rollover threshold acceleration limits of the vehicle equipped with various tanks as a function of the fill volume, while the cargo load is held constant (265.3 kN or 59633 lbs.). The weight density of the cargo is varied to realize fill volume variations in the 40% to 90% range under the selected cargo load.

A lower fill volume, realized with high density liquid cargo, yields lower c.g. height. The static rollover threshold of the vehicle under this condition is thus expected to be largely affected by the lateral load shift. The cargo with light density, on the other

hand, yields high fill volume and thus high c.g. location. In this case, the static rollover threshold limit is mostly determined by the c.g. height.

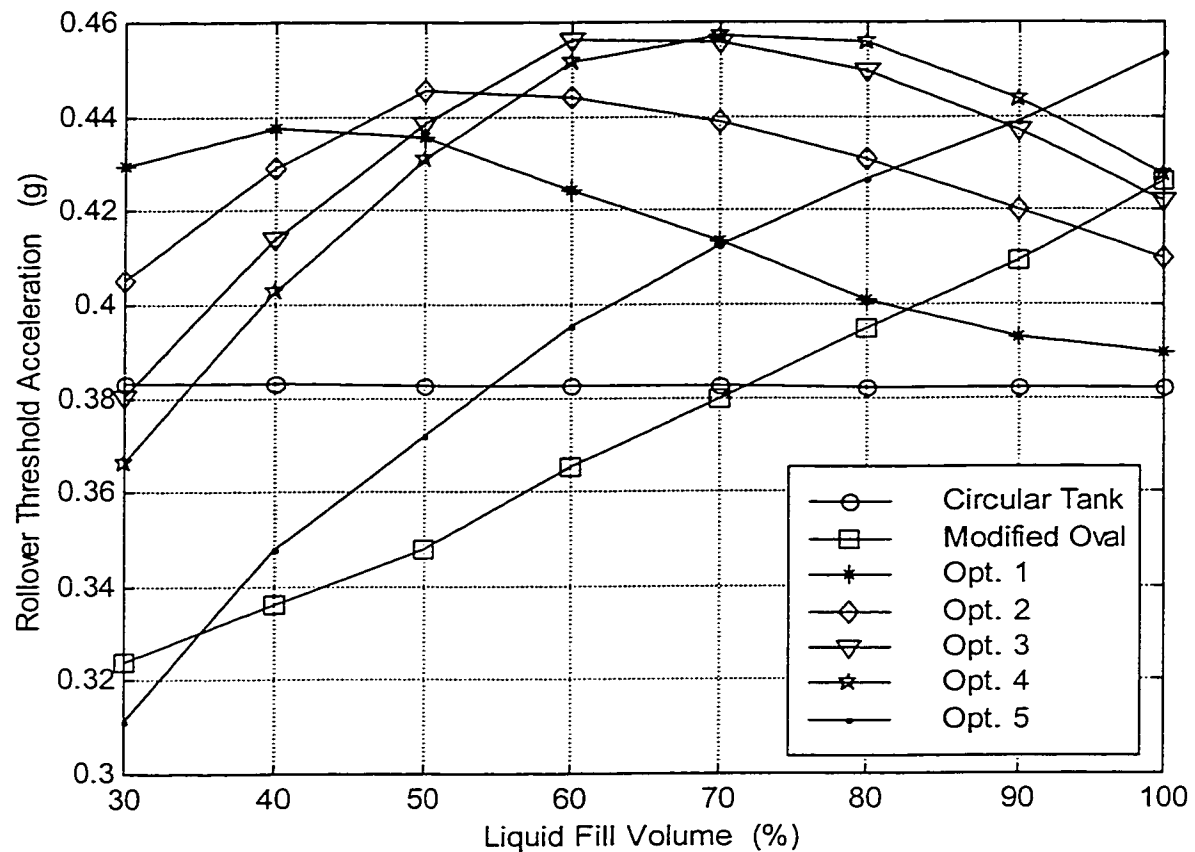


Figure 3.10: Comparison of rollover threshold acceleration limits of an articulated vehicle equipped with optimal and conventional tanks as a function of fill volume (constant cargo load).

Under constant cargo load condition, the vehicle with a circular cross-section tank yields nearly constant value of rollover threshold limit over the entire fill range. The anticipated increase in the rollover threshold limit under low fill volume is mostly offset by significant increase in lateral load shift. The high c.g. location of the circular cross-section under higher fill volume yields relatively lower value of rollover threshold limit. Under low fill volumes, the modified-oval cross-section tank yields the lowest rollover threshold limit, which is primarily attributed to high overturning moment caused by excessive load shift within its considerably wide cross-section. The rollover threshold

acceleration limit increases considerably with increase in the fill volume despite the increase in liquid c.g. height. This increase is mostly attributed to significantly lower lateral cargo shift with the increasing fill volume and lower c.g. height. These results suggest that the relative loss in roll stability limits of wider tanks is considerably larger than the corresponding gain arising from their lower cross-sectional c.g. height, especially under low fill volumes.

The rollover threshold of the vehicle with Opt. 5 tank exhibits trends similar to that of the vehicle with the modified-oval tank. This is attributed to its wider cross-section that is comparable with the modified-oval cross-section. The rollover threshold of the vehicle combination with Opt. 5 tank, however, is larger than that with the modified-oval tank for fill volumes exceeding 35%, as shown in Figure 3.10.

The optimal configurations, Opt. 1 through Opt. 4, reveal vehicle rollover threshold larger than that of the vehicle with the circular tank for fill volume greater than 35%, and the modified-oval tank for fill volume below 82%. While Opt. 2, Opt. 3 and Opt. 4 configurations yield considerably higher values of rollover threshold in nearly entire fill volume range, the Opt. 4 configuration reveals the highest vehicle rollover threshold for fill volume exceeding 70%. In the 30% to 100% fill volume range, the rollover threshold of the vehicle varies from a low value of approximately 0.31 g to a high value of approximately 0.456 g, depending upon the tank cross-section. All the tank cross-sections, with the exception of Opt. 2, exhibit considerable variation in the vehicle rollover threshold with fill volume. The Opt. 2 cross-section reveals relatively less variation in the rollover threshold limit, which remains above 0.405 g for the entire range of fill volume. The rollover threshold of the vehicle equipped with this optimal tank is

approximately 10% to 17% higher than that of the vehicle equipped with the currently used circular tank in a wide range of fill volume (40%-90%). The Opt. 2 design may thus be considered a suitable option for general purpose cleanbore tanks, which frequently encounter wide range of partial fill conditions due to variations in weight density of liquid products.

3.5.2 Optimal Tanks Obtained for Typical Fill Ranges

Figure 3.11 illustrates the static rollover threshold acceleration limits of the vehicle equipped with conventional tanks and the two optimal configurations (*OPT1* and *OPT2*) derived for two fill ranges (50% to 70% and 70% to 90%) upon imposing a limit constraint on the tank perimeter. The figure illustrates the rollover limits for 40% to 100% fill volume range, while the cargo load is held constant (269.3kN) by varying weight density of the cargo. The rollover threshold values of the vehicle combination equipped with the optimal tanks are also summarized in Table 3.4 together with the percent change with reference to the currently used circular and modified-oval tanks.

The results show that the vehicle with both optimal cross-section tanks (*OPT1* and *OPT2*) yields rollover threshold values larger than those of the vehicle with the circular tank for the entire fill range, and with the modified-oval tank for fill volumes below 92%. The *OPT1* design ($Z_{cg}=0.92$ m) yields largest values of rollover threshold limits for fill volumes below 67%, while the *OPT2* design ($Z_{cg}=0.84$ m) results in the largest values for fill volumes ranging from 67% to 97%. Both the optimal cross-sections yield relatively less variations in the rollover threshold with variations in fill volume, while the rollover threshold limits remain above 0.4 g for the entire fill range. The results summarized in Table 3.4 show that both *OPT1* and *OPT2* cross-section tanks can enhance the rollover

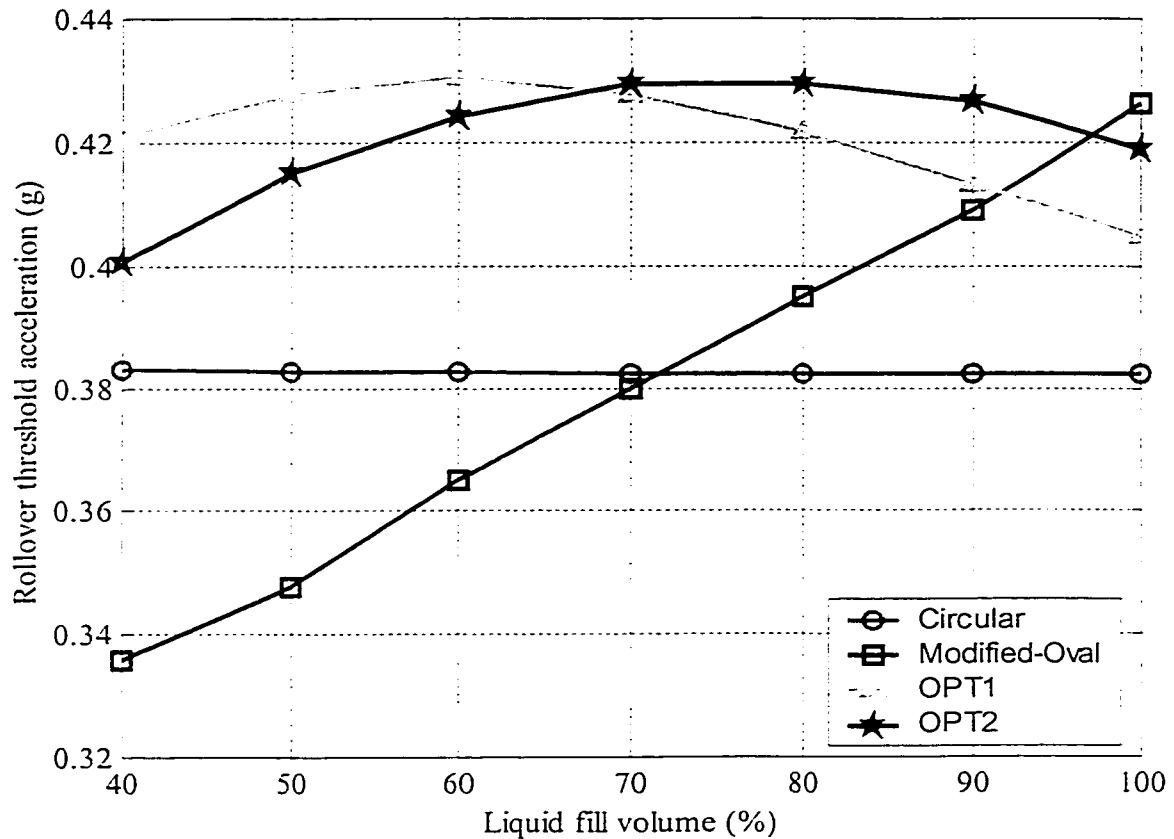


Figure 3.11: Comparison of rollover threshold acceleration limits of a partly-filled articulated vehicle with optimal and conventional tanks (constant cargo load).

Table 3.4: Relative gains in rollover threshold limits of the vehicle with optimal tanks (*OPT1* & *OPT2*): constant cargo load.

Fill volume ratio, β	Weight density (N/m^3)	Rollover threshold (g) and percent change					
		<i>OPT1</i>			<i>OPT2</i>		
		$a^*_{y_1}$ (g)	Percent change with respect to that of		$a^*_{y_2}$ (g)	Percent change with respect to that of	
			Circular	Modified-oval		Circular	Modified-oval
0.4	16965	0.421	10	25	0.401	5	19
0.5	13572	0.428	12	23	0.415	8	19
0.6	11310	0.431	13	18	0.424	11	18
0.7	9694	0.428	12	13	0.429	12	13
0.8	8483	0.422	10	7	0.429	12	9
0.9	7540	0.413	8	1	0.427	12	4

threshold limits by as much as 19-25% under low fill volume when compared to that of the vehicle with the modified-oval tank. This gain, however, decreases gradually with increase in fill volume. The *OPT2* tank yields approximately 12% higher rollover threshold limit than the circular tank under higher fill volume.

Figure 3.12 presents a comparison of the static rollover threshold acceleration limits of the vehicle equipped with the two sets of optimal tanks (*OPT1* & *OPT2*, and *OPT1_n* & *OPT2_n*) obtained for 50% to 70% and 70% to 90% fill volume ranges, with and without the additional perimeter constraint, while the cargo load is held constant (269.3kN). Table 3.5 summarizes the rollover threshold values of the vehicle equipped with *OPT1_n* and *OPT2_n* configurations together with the percent change with reference to *OPT1* and *OPT2* as well as the conventional tanks. The results reveal that the *OPT1_n* design ($Z_{cg}=0.88$ m) yields the largest values of rollover threshold limits for fill volumes ranging from 45% to 68%, due to its narrow cross-section, while the *OPT2_n* design ($Z_{cg}=0.80$ m) results in the largest values of threshold limits for fill volumes ranging from 68% to 100%, attributed mostly to its low cross-section c.g. height. The optimal tanks obtained without the perimeter constraint, *OPT1_n* and *OPT2_n*, yield slightly higher rollover threshold limits than those attained for the optimal tanks obtained with the perimeter constraint, *OPT1* and *OPT2*, respectively, under high fill volumes (60%-100%), due to less overturning moments caused by relatively lower c.g. heights of the liquid within the *OPT1_n* and *OPT2_n* cross-sections, as indicated in Section 3.4.2, while they result in somewhat lower rollover threshold limits than *OPT1* and *OPT2*, respectively, for fill volumes below 50%, attributed primarily to larger overturning moments arising from relatively larger liquid load shift associated with the wider lower

portion of their cross-sections. Table 3.5 show that both $OPT1_n$ and $OPT2_n$ cross-section tanks can enhance the rollover threshold limits by as much as 15-24% under low fill volume when compared to that of the vehicle with a modified-oval tank. This gain, however, decreases gradually with increase in fill volume, similar to that observed for the $OPT1$ and $OPT2$ cross-sections, as discussed earlier in this Section. The $OPT2_n$ tank yields approximately 16% higher rollover threshold limit than the circular tank under higher fill volume.

The slight difference (0.2% to 4.7%) in the rollover threshold acceleration limits of the vehicle equipped with the partially-filled optimal tanks achieved with and without the perimeter constraint indicates that the influence of the perimeter constraint on the roll stability performance of the optimal tanks is trivial. The optimal tanks achieved with the perimeter constraint (i.e., $OPT1$ and $OPT2$) are thus considered to be more cost-effective designs, as they yield less tank weight due to the perimeter constraint. The $OPT1$ and $OPT2$ designs may therefore be considered most suitable for general purpose cleanbore tanks under medium and high fill volumes, respectively.

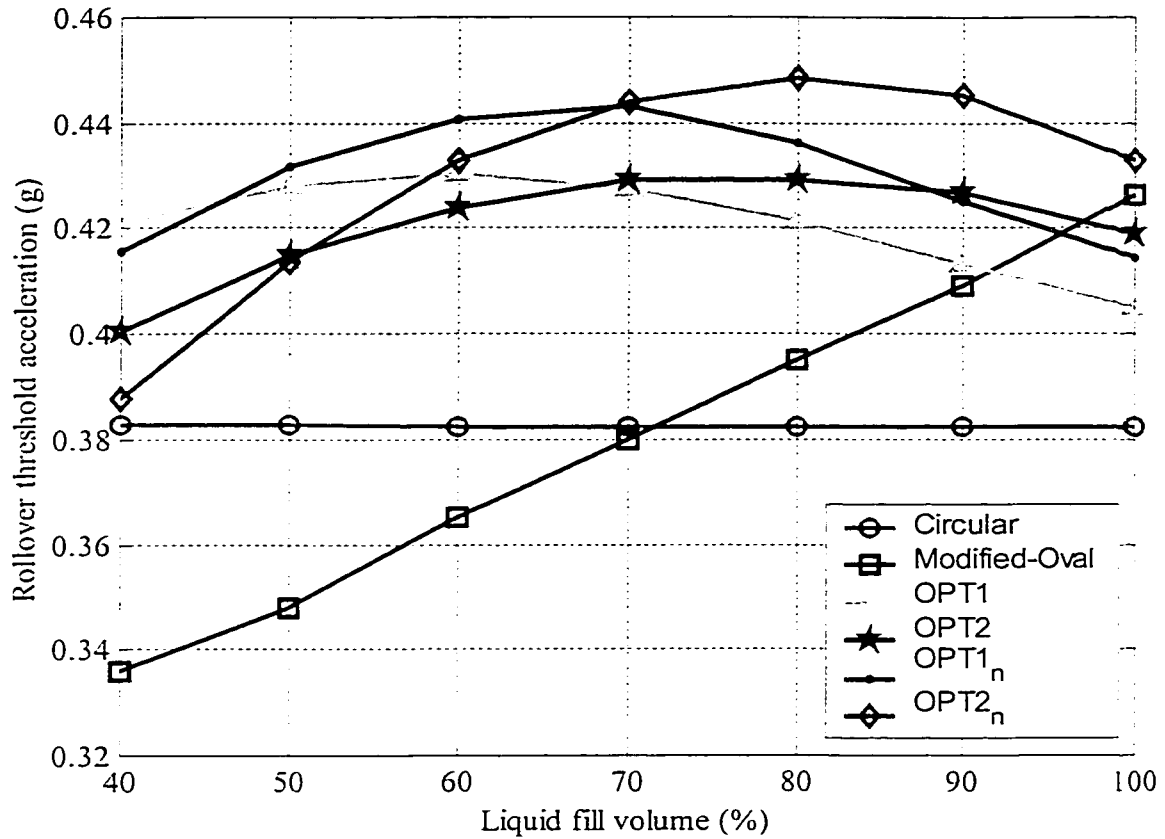


Figure 3.12: Rollover threshold acceleration limits of the vehicle with optimal tanks obtained with and without the perimeter constraint, and conventional tanks.

Table 3.5: Relative gains in rollover threshold limits of the vehicle with optimal tanks ($OPT1_n$ and $OPT2_n$): constant cargo load.

Fill volume ratio, β	Weight density (N/m^3)	Rollover threshold (g) and percent change							
		$OPT1_n$				$OPT2_n$			
		a^*_y (g)	Percent change with respect to that of			a^*_y (g)	Percent change with respect to that of		
			Circular	Modified-oval	$OPT1$		Circular	Modified-oval	$OPT2$
0.4	16965	0.416	9	24	-1	0.388	1	15	-3
0.5	13572	0.432	13	24	0.9	0.414	8	19	-0.2
0.6	11310	0.441	15	21	2.3	0.433	13	19	2.1
0.7	9694	0.443	16	17	3.5	0.444	16	17	3.5
0.8	8483	0.436	14	10	3.3	0.449	17	14	4.7
0.9	7540	0.425	11	4	2.9	0.445	16	9	4.2

Figure 3.13 presents the static rollover threshold acceleration limits of the tractor-semitrailer vehicle equipped with conventional tanks and the symmetric optimal configuration (referred to as Optimal-oval) obtained corresponding to 50% to 90% fill volume ranges. The rollover threshold is evaluated for various fill volumes under variable load condition, where cargo weight density is taken as 6800 N/m^3 . Compared with the conventional modified-oval tank, the optimal-oval tank yields an increase in vehicle rollover threshold limit in the range of 2.4% to 3.7% for the entire range of fill volumes. This slight increase in rollover threshold limit of the vehicle is ascribed mostly to the relatively narrow cross-section of the optimal-oval tank as compared to that of the modified-oval.

Figure 3.14 illustrates the static rollover threshold acceleration limits as functions of fill volume of the vehicle equipped with the conventional and symmetric optimal (Optimal-oval) tank configurations under constant load condition (269.3 kN). The results show that the vehicle with Optimal-oval configuration yields consistently higher values of rollover threshold acceleration limit than those of the vehicle with the modified-oval tank over the entire fill range. The increase is in the range of 2.2% to 5.8% for the entire fill volume, due to the same reason as for the variable load case. This slight improvement in static roll stability of the vehicle with an optimal-oval tank further indicates the limitations associated with oval cross-sections and potential advantages of optimal configurations derived on the basis of the generic cross-section proposed in Chapter 2.

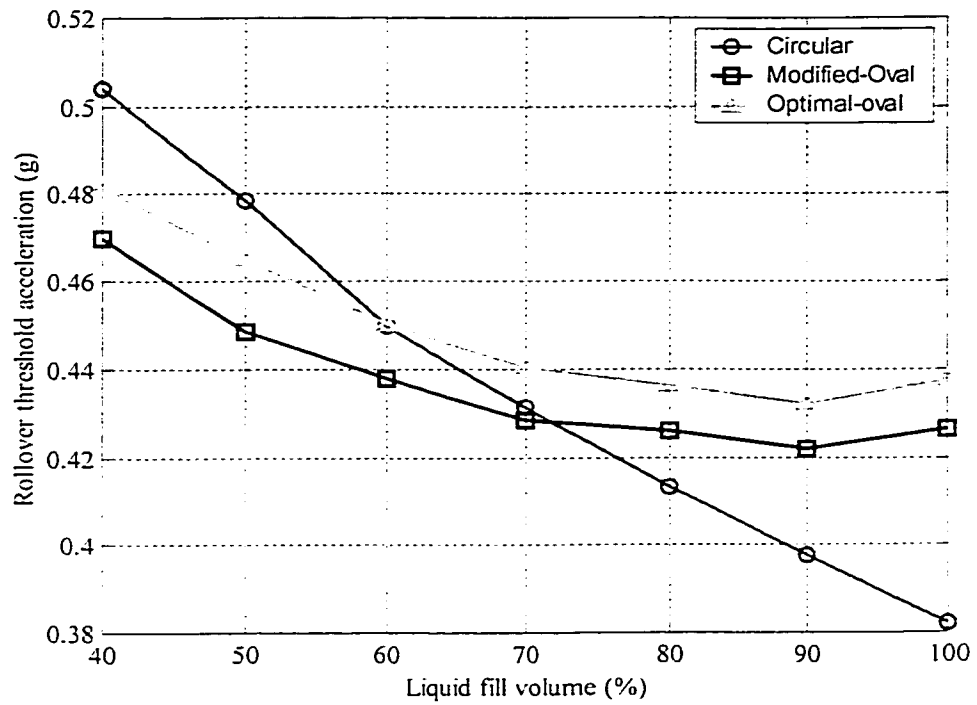


Figure 3.13: Rollover threshold acceleration limits of the vehicle with conventional and optimal-oval tanks (variable cargo load).

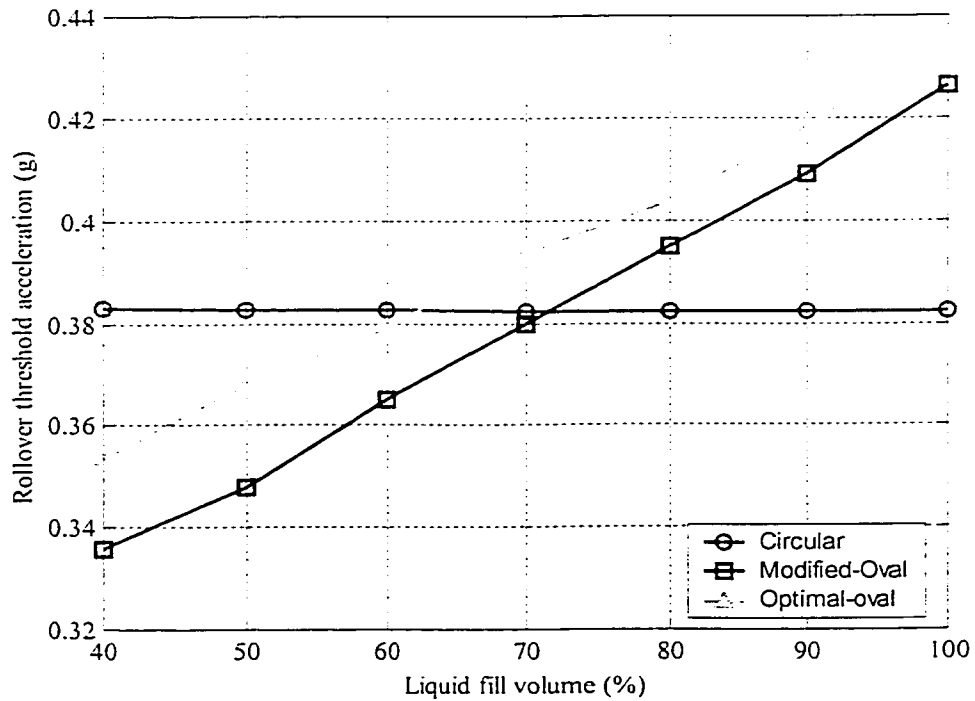


Figure 3.14: Rollover threshold acceleration limits of the vehicle with conventional and optimal-oval tanks (constant cargo load).

3.6 INFLUENCE OF OPTIMAL TANK GEOMETRY ON THE STRESS DISTRIBUTION OF THE TANK STRUCTURE

In this Section, the three optimal cross-sections proposed in the previous Sections, Opt.5 for relatively insignificant partial fill conditions, and OPT1 and OPT2 for 50%-70% and 70%-90% fill volume ranges, respectively, are further evaluated from tank structural integrity point of view.

A simple finite element model for a cleanbore cylindrical tank of generic cross-section and its supports is developed using the ANSYS software. The model allows static stress analysis of cylindrical tank of different cross-sections under various cargo fill conditions. The stress distributions of various optimal and conventional tanks in terms of equivalent stress contour and stress patterns along defined paths on the tank longitudinal direction are preliminarily analyzed and compared to investigate the influence of tank cross-section. The preliminary analysis results are presented in Appendix A.

The results reveal that tank supports yield the most significant influence on the stress distribution of the tank structure, regardless of tank cross-section, and that the optimal tanks proposed for typical fill ranges, OPT1 and OPT2, yield only moderately higher stress on both the lower and upper portions of the tank shell than the conventional tanks, under identical cargo load and nearly identical supports, due to the asymmetric feature of the optimal geometry and its complex interaction with the supports. The low c.g. tank proposed for relatively insignificant partial fill conditions, Opt.5, however, exhibits considerably higher stress concentration around the supports than the other tanks, attributed to the most significant geometry variation and considerably high curvature of its cross-section and support saddles.

Due to the idealized simplifications in developing the finite element model and the difficulty in achieving identical support geometry for different tank cross-sections, this comparative study should only be considered as qualitative and inconclusive. Further work is needed to model and analyze more realistic tanks with relatively detailed internal and external structures

3.7 SUMMARY

A static roll plane model of an articulated tank vehicle equipped with a generic tank is developed by integrating the roll plane model of the partially-filled tank with that of the articulated vehicle. The coupled model is then analyzed to investigate the rollover threshold acceleration limit of the vehicle as functions of the tank geometry, fill volume and type of partial-fill condition, such as variable and constant load. The performance characteristics of different optimal and conventional tanks are evaluated in terms of deviations of the c.g. coordinates caused by a steady lateral acceleration field, and rollover threshold acceleration limits of the vehicle combination.

From the results, it is concluded that wide bottom tanks yield low overturning moments under high fill volumes due to relatively lower c.g. height, while tanks with approximately conical geometry result in low overturning moments under medium fill volumes due to low lateral load shift. Under partial-fill conditions, the current tank configurations exhibit extensive lateral movement of the cargo, specifically under low fill volumes. The anticipated reduction in overturning moment under low fill volumes and thus lower c.g. height is largely offset by an increase in overturning moment due to the unrestricted lateral movement of the liquid load. These results suggest that the

conventional tanks are far from optimum in view of static roll stability of a partly-filled tank vehicle combination.

The vehicle with proposed optimal tank cross-sections in-general results in significant enhancement of roll stability limit over the entire fill range. This increase is attributed primarily to considerable reductions in lateral load shift and c.g. height of optimal cross-sections. For partial-fill condition involving variable loads, optimal cross-section with the lowest c.g. height (Opt .5) yields considerably higher and near constant values of rollover threshold limits for fill volumes exceeding 55%. The increase in the rollover threshold limit is in the order of 7% when compared with that of the vehicle with the modified-oval tank for fill volumes above 60%. Under partial-fill condition involving constant cargo load, the proposed optimal cross-sections with a perimeter constraint (*OPT1* and *OPT2*) yield considerable increase in the vehicle rollover threshold for 50% to 90% fill volumes. These two tanks further yield nearly constant rollover threshold limits for fill volumes ranging from 40% to 90%, which is approximately 12% higher than that of the vehicle equipped with a circular cross-section tank under high fill volumes and approximately 13% to 25% higher than that of the vehicle with a modified-oval tank in the 40% to 70% fill volume range.

From the analyses, it is concluded that for tank vehicles involving insignificant partial fill conditions, the Opt. 5 design obtained under 100% fill volume ratio may be considered as optimal, as it yields the least cross-section c.g. height, while for those involving large variations in liquid fill volume, optimal solutions achieved under 50%-90% fill volume range with a perimeter constraint (*OPT1* and *OPT2*) may be considered most suitable and cost-effective for general purpose cleanbore tanks under medium and

high fill volumes, respectively, since they yield considerably higher and nearly constant rollover threshold limits of the vehicle over a large range of fill volumes. The potential benefits of these two optimal cross-sections in enhancing the directional and roll dynamic characteristics of partly-filled tank vehicle combinations are further investigated in the following Chapters.

CHAPTER 4

CONSTANT SPEED DIRECTIONAL DYNAMIC RESPONSE ANALYSES OF PARTLY-FILLED TANK VEHICLES

4.1 INTRODUCTION

The directional dynamics and roll stability characteristics of a partly-filled tank vehicle are strongly dependent upon vehicle response to directional maneuvers and dynamic interactions between the moving liquid cargo and the vehicle. The lateral load shift coupled with relatively low stability limits of the articulated vehicle tends to further reduce the stability limits under partial-fill conditions. The reduced roll stability poses higher rollover risks under transient directional maneuvers. While the directional dynamics and roll stability characteristics of various configurations of freight vehicles have been extensively reported in the literature, dynamic analysis of partly-filled tank vehicles under the influence of additional forces and moments arising from liquid cargo movement has been addressed in only few studies due to associated complexities in modeling of fluid-vehicle interactions [11].

A quasi-static roll plane fluid model, described in Section 2.3, has been applied in conjunction with a constant speed yaw/roll plane model of articulated vehicles to evaluate the mean roll dynamic response of partly-filled tank vehicles [11, 173]. The analytical model of liquid cargo is based upon the assumption of inviscid fluid and negligible contributions due to fundamental oscillation frequency of fluid slosh. Although this approach does not predict oscillatory sloshing forces and moments that may arise under a transient steering maneuver, the computed response quantities were observed to be in

good agreement with mean values of the road measured response of a scale model truck for different fill levels, vehicle speeds, and typical steering maneuvers [193].

Dynamic roll stability limits of partly-filled tank vehicle combinations may be enhanced by reducing the magnitude of overturning moments caused by lateral fluid slosh under a directional maneuver, as described in the previous Chapter. It has also been reported that dynamic rollover limits of heavy vehicles are strongly related to their static rollover threshold values [93, 137]. The optimal tank cross-sections derived in the previous Chapters are thus considered to offer considerable benefits in enhancing the dynamic roll response behavior under partial-fill conditions.

In this Chapter, the optimal tank cross-sections, *OPT1* and *OPT2*, proposed in Chapter 3, are employed to study the effects of tank geometry on the directional response and roll stability characteristics of partly-filled articulated tank vehicles. A quasi-static roll plane model of liquid bulk within a partially-filled tank of generic cross-section is developed and integrated to a three-dimensional yaw/roll model of a five-axle tractor semitrailer vehicle to investigate the directional and roll dynamic performance of the vehicle. The analyses are performed for the combination with partly-filled tanks of various cross-sections, including conventional and optimal. The directional and roll response characteristics of different tank and vehicle combinations are evaluated under steady as well as transient directional maneuvers, and different fill volumes. The dynamic response characteristics of the combinations, evaluated in terms of defined performance measures, are compared to study the potential performance benefits of optimal cross-section tanks.

4.2 CONSTANT SPEED YAW/ROLL MODEL OF A PARTLY-FILLED ARTICULATED TANK VEHICLE

A vast number of constant speed vehicle models of varying complexities have been developed to study directional response and dynamic roll stability limits of commercial vehicles [11, 128, 129]. Such models can not be directly applied for directional dynamic analysis of partly-filled tank trucks due to lack of consideration of dynamic interactions of the moving cargo. A directional dynamic model for response analysis of a partly-filled tank vehicle can be effectively developed by integrating a quasi-static fluid slosh model into a proven model of the rigid cargo vehicle. From the review of reported dynamic models and other studies, described in Chapter 1, the Yaw/Roll model developed by UMTRI (The University of Michigan Transportation Research Institute) [98] is considered for further development to study dynamic roll response of tank vehicle combinations. It should be noted that instantaneous values of roll and yaw mass moments of inertia of moving cargo vary considerably with variations in vehicle response to a steering maneuver. The kineto-static roll plane model of the generic tank, described in Section 2.3, is therefore further analyzed to derive mass moments of inertia of the deflected liquid cargo.

4.2.1 Quasi-Static Model of a Partly-Filled Tank of Generic Cross-section

The roll plane of a partly-filled tank of generic cross-section, mounted on its support, is illustrated in Figure 4.1, which is similar to Figure 2.6 presented in Chapter 2. The weights due to liquid cargo and empty tank trailer structure are represented by W_1 and W_2 , respectively. The vertical distance from the tank base to the c.g. of the empty tank trailer is denoted by Z_b . Y_i and Z_i ($i=1, \dots, 5$) are the coordinates of the intersection

$$z = \frac{a_{lv} + \theta_{s2}}{1 - a_{lv}\theta_{s2}} y + h_0 \quad (4.1)$$

-133-

The lateral and vertical coordinates of c.g. of the deflected liquid bulk, with respect to the tank body fixed coordinate system (YZO), Y_l and Z_l , are evaluated from Equation (2.24), as discussed in Chapter 2. The instantaneous values of mass moments of inertia of the shifted liquid cargo about the tank body-fixed coordinate system are further computed from the following volume integrals:

$$I_{xl} = \iiint_V (y^2 + z^2) \rho dv; I_{yl} = \iiint_V (x^2 + z^2) \rho dv; \text{ and } I_{zl} = \iiint_V (x^2 + y^2) \rho dv \quad (4.2)$$

where ρ is mass density of liquid cargo, and V is domain of volume integration, i.e., the deflected liquid volume corresponding to area integral domain Q . Assuming constant forward speed and negligible pitch motion of the tank, the domain of area integral (Q) can be used to describe the domain of volume integral (V) in the roll plane. The integral limit along the longitudinal axis of the tank is defined as $(0, L)$, where L is the tank length. Equations (4.2) thus reduce to:

$$\begin{aligned} I_{xl} &= \rho L \iint_Q (y^2 + z^2) dy dz \\ I_{yl} &= \frac{\rho L^3}{3} \iint_Q dy dz + \rho L \iint_Q z^2 dy dz \\ I_{zl} &= \frac{\rho L^3}{3} \iint_Q dy dz + \rho L \iint_Q y^2 dy dz \end{aligned} \quad (4.3)$$

Equation (4.3) is then evaluated numerically in the specific area domain (Q) corresponding to the particular liquid free surface configuration, as described in Chapter 2. The mass moments of inertia of the deflected liquid bulk with respect to the trailer sprung mass-fixed coordinate system are then computed in the following manner:

$$\begin{aligned}
I_{xl2} &= I_{xl} + \frac{W_l}{g} (Z_b^2 + 2Z_b Z_l) \\
I_{yl2} &= I_{yl} + \frac{W_l}{g} (X_b^2 - 2X_b X_l + Z_b^2 + 2Z_b Z_l) \\
I_{zl2} &= I_{zl} + \frac{W_l}{g} (X_b^2 - 2X_b X_l)
\end{aligned} \tag{4.4}$$

where X_b denotes the longitudinal distance between origin of the tank body axis system and c.g. of the tank-trailer sprung mass.

It should be pointed out that instantaneous values of mass moments of inertia of the deflected liquid bulk may be strongly affected by fluid slosh and oscillation frequency. In the above formulations, the fundamental slosh frequency is assumed to lie away from the typical steering frequencies. It has been reported that fundamental frequency of fluid slosh is dependent upon tank size, cross-section and fill volume. This frequency is reported to occur in the 0.52 to 0.67 Hz frequency range for commonly used tanks under 40% to 70% fill ranges [187]. The fluid response may be largely considered as quasi-static when frequency of fluid slosh is well above the steering frequency. In situations where steering frequency is in the vicinity of the natural frequency of fluid slosh, the mass moments of inertia would be expected to vary considerably. The formulations derived from quasi-static liquid model should thus be considered applicable only when the steering frequency is reasonably below the corresponding slosh frequency.

4.2.2 Constant Velocity Directional Dynamic Model of the Vehicle Combination

The vehicle model is derived on the basis of Yaw/Roll model reported in [98]. In this model, the five-axle tractor semitrailer vehicle is modeled as two sprung masses: the sprung mass of tractor, m_1 , and the tare mass of semitrailer structure and empty tank, m_2 . Quasi-static model is used to represent liquid cargo as a floating mass, m_l , with respect to

c.g. of trailer sprung mass. The axles are modeled as independent unsprung masses, m_{ui} ($i=1, 2, \dots, 5$). The sprung masses of the vehicle are characterized as rigid bodies with five degrees of freedom: lateral, vertical, yaw, roll and pitch. The unsprung masses are treated as beam axles, which are free to roll and bounce with respect to the sprung masses to which they are attached. The articulation is modeled as a rigid coupling in translation but relatively compliant in roll. Figure 4.2 illustrates roll plane of the three dimensional model of the tractor-semitrailer tank vehicle, where W_{ui} and θ_{ui} represent the weight and roll angle, respectively, of axle i . Figure 4.3 presents the pitch plane of the vehicle model and various coordinate systems attached to sprung and unsprung masses. The yaw/roll model of the articulated tank vehicle is developed subject to a number of simplifying assumptions, which are well documented in [11, 184]. The major assumptions include: (i) the vehicle is assumed to move at a constant forward speed on a horizontal surface possessing even frictional properties; (ii) the pitch rotations of sprung masses and relative roll motions between sprung and unsprung masses are considered to be small, such that small angle simplifications are applicable; (iii) the load transfers among various axles are neglected and thus the total load on each axle is held constant throughout the simulation; (iv) the relative roll motions between the sprung and unsprung masses take place about the respective roll centers, which are located at a fixed distance beneath the sprung mass c.g.; and (v) the suspension forces act along the vertical axis of the associated unsprung mass. The forces developed by suspension springs are considered to be nonlinear functions of suspension deflections. The non-linear suspension characteristics are represented in the program through a tabular input comprising the suspension force and corresponding spring deflection, which are linearized about the operating point. The

cornering force and aligning moment characteristics of the tires are expressed as nonlinear functions of normal load and side-slip angle, while the influence of wheel camber on lateral force generation is neglected. The vertical load on a tire is computed from its instantaneous deflection using the linear vertical tire stiffness. The cornering force and aligning moment characteristics of commonly used radial tires of heavy vehicles (11R22.5) as a function of normal load and side-slip angle are illustrated in Figures 4.4 and 4.5, respectively.

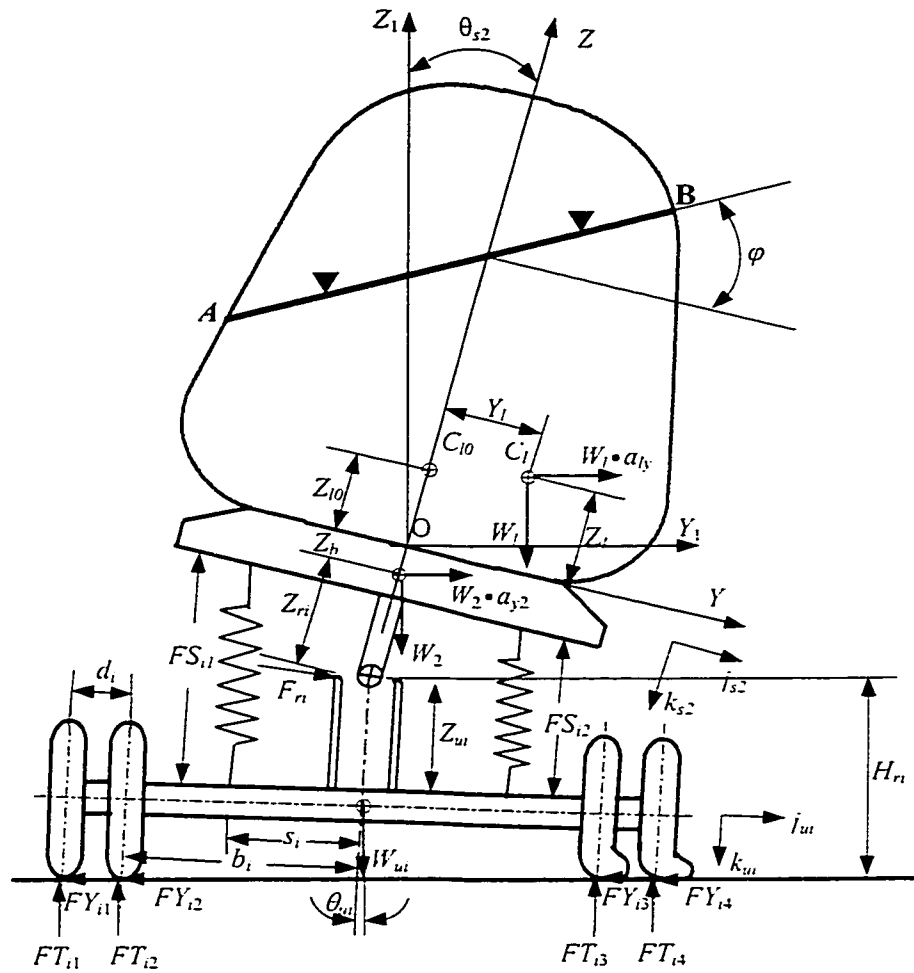


Figure 4.2 Roll plane representation of the partially-filled tank vehicle model.

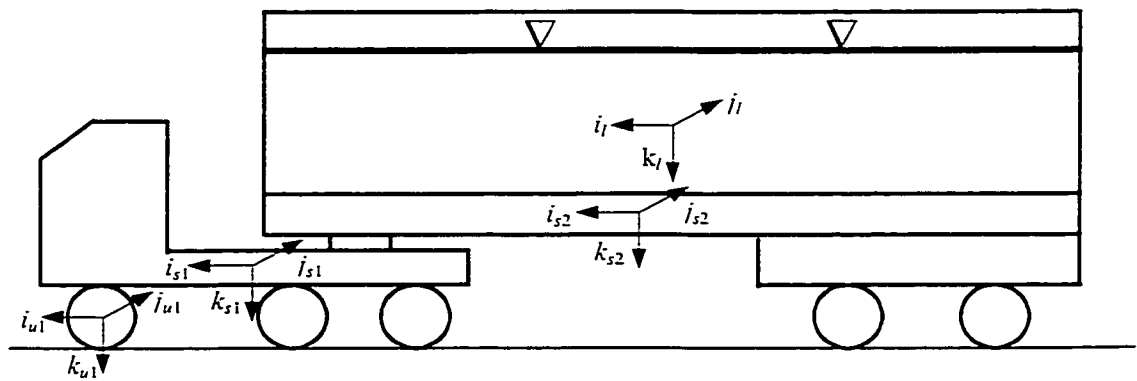


Figure 4.3: Pitch plane representation of the tank vehicle model and the attached coordinate frames.

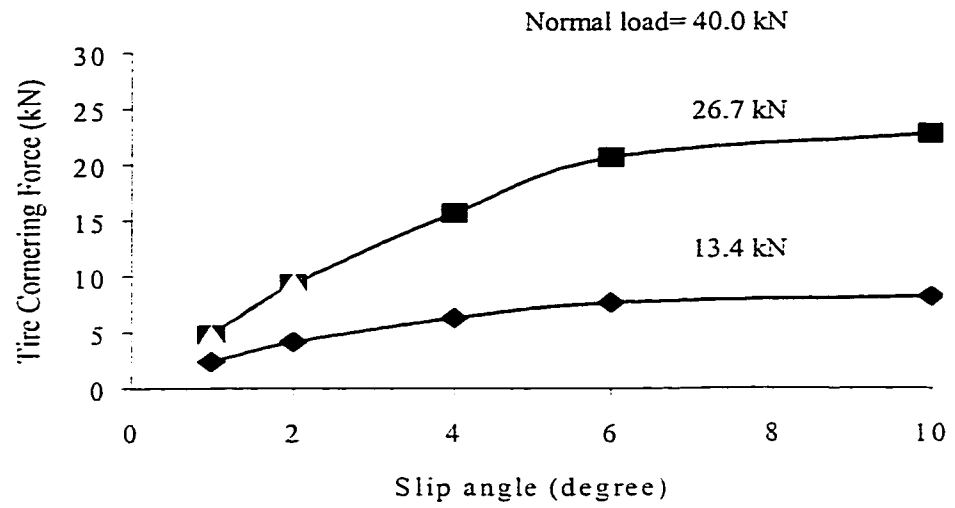


Figure 4.4: Cornering force properties of a radial truck tire as a function of load and side-slip angle [101].

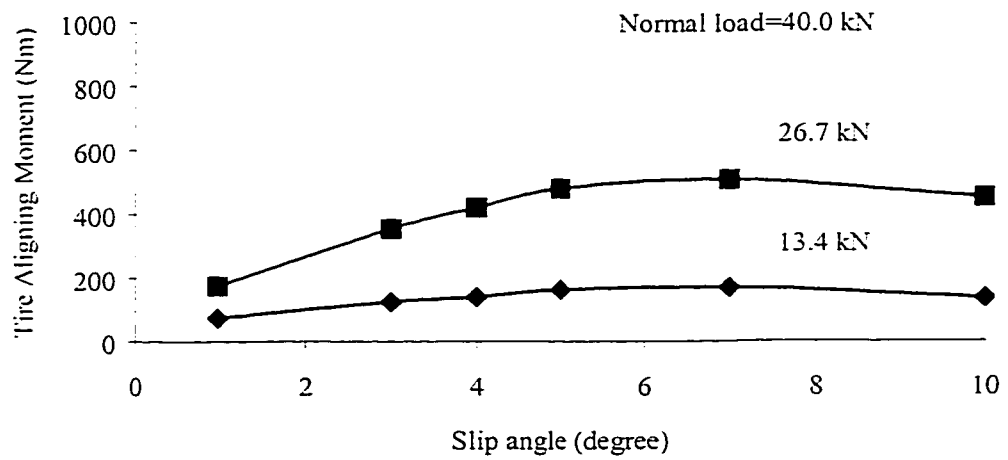


Figure 4.5: Aligning moment property of a radial truck tire as a function of load and side-slip angle [101].

4.2.3 Equations of Motion of the Articulated Tank Vehicle

The equations of motion of yaw/roll model of the partly-filled articulated tank vehicle are derived upon considering equilibrium for both the quasi-static fluid slosh and the rigid bodies representing the vehicle. The motion of each sprung mass is described by five second-order differential equations and that of each unsprung mass is described by two second differential equations, which are derived using the respective body-fixed coordinate system. The resulting equations of motion of the tank vehicle model incorporating liquid forces and moments are presented below.

The five second-order differential equations describing the motion of each of the two sprung masses are given by:

Lateral force equations:

$$m_f a_f \ddot{j}_{sf} + m_{lf} a_{lf} \ddot{j}_{sf} = (\text{Lateral components of constraint forces}) + \sum_{i=N_1}^{N_2} [F_{ri} \cos(\theta_{sf} - \theta_{ui}) - (FS_{i1} + FS_{i2}) \sin(\theta_{sf} - \theta_{ui})] + (m_f + m_{lf})g \sin \theta_{sf}; (f=1, 2) \quad (4.5)$$

Vertical force equations:

$$m_f a_f \ddot{k}_{sf} + m_{lf} a_{lf} \ddot{k}_{sf} = (\text{Vertical components of constraint forces}) + \sum_{i=N_1}^{N_2} [F_{ri} \sin(\theta_{sf} - \theta_{ui}) + (FS_{i1} + FS_{i2}) \cos(\theta_{sf} - \theta_{ui})] + (m_f + m_{lf})g \cos \theta_{sf}; (f=1, 2) \quad (4.6)$$

Roll moment equations:

$$(I_{xf} + I_{xlf}) \dot{p}_f - (I_{yf} + I_{ylf} - I_{zf} - I_{zlf}) q_f r_f = (\text{Roll moments from constraints}) + \sum_{i=N_1}^{N_2} [(FS_{i1} + FS_{i2}) Z_{ri} \sin(\theta_{sf} - \theta_{ui}) + (FS_{i1} - FS_{i2}) s_i \cos(\theta_{sf} - \theta_{ui}) - F_{ri} Z_{ri} \cos(\theta_{sf} - \theta_{ui})] + m_{lf} [(Z_{lf} + Z_{b_f}) a_{lf} \ddot{j}_{sf} + Y_{lf} a_{lf} \ddot{k}_{sf}] + m_{lf} g [Y_{lf} \cos \theta_{sf} + (Z_{lf} + Z_{b_f}) \sin \theta_{sf}]; (f=1, 2) \quad (4.7)$$

Pitch moment equations:

$$\begin{aligned}
 & (I_{yf} + I_{ylf}) \dot{q}_f - (I_{zf} + I_{zlf} - I_{xf} - I_{xlf}) p_f r_f = (\text{Pitch moments from constraints}) \\
 & + \sum_{i=N_1}^{N_2} [(FS_{i1} + FS_{i2}) \cos(\theta_{sf} - \theta_{ui}) + F_{ri} \sin(\theta_{sf} - \theta_{ui})] X_{ui} \\
 & - m_{lf} [X_{bf} a_{lf} \bar{k}_{sf} + (Z_{lf} + Z_{bf}) a_{lf} \bar{i}_{sf}] + m_{lf} g [-X_{bf} \cos \theta_{sf} + (Z_{lf} + Z_{bf}) \sin \alpha_{sf}]; (f=1, 2)
 \end{aligned} \tag{4.8}$$

Yaw moment equations:

$$\begin{aligned}
 & (I_{zf} + \sum_{i=N_1}^{N_2} I_{zui} + I_{zlf}) \dot{r}_f - (I_{xf} + I_{xlf} - I_{yf} - I_{ylf}) p_f q_f = (\text{Yaw moments from constraints}) \\
 & + \sum_{i=N_1}^{N_2} \left\{ [F_{ri} \cos(\theta_{sf} - \theta_{ui}) - (FS_{i1} + FS_{i2}) \sin(\theta_{sf} - \theta_{ui})] X_{ui} + \sum_{j=1}^4 AT_{ij} \right\} \\
 & + m_{lf} (-Y_{lf} a_{lf} \bar{i}_{sf} + X_{bf} a_{lf} \bar{j}_{sf}) + m_{lf} g (X_{bf} \sin \theta_{sf} + Y_{lf} \sin \alpha_{sf}); (f=1, 2)
 \end{aligned} \tag{4.9}$$

where m_f ($f=1, 2$) represents the sprung masses of the vehicle combination, and m_{lf} the liquid cargo mass due to unit f . It should be noted that cargo mass is considered for the second sprung unit alone, such that $m_{l1}=0$. a_f and a_{lf} are the acceleration vectors of the sprung mass and liquid cargo mass of unit f . \bar{i}_{sf} , \bar{j}_{sf} and \bar{k}_{sf} are the unit vectors describing the body coordinate system fixed to sprung mass unit f . θ_{sf} and α_{sf} are the roll and pitch angles, respectively, of sprung unit f , and p_f , q_f and r_f are the roll, pitch, and yaw rates. I_{xf} , I_{yf} and I_{zf} are the roll, pitch and yaw mass moments of inertia of sprung unit f with respect to the (i_{sf}, j_{sf}, k_{sf}) coordinate system. I_{xlf} , I_{ylf} and I_{zlf} are the roll, pitch and yaw mass moments of inertia of the liquid cargo with respect to the (i_{sf}, j_{sf}, k_{sf}) coordinate system, and I_{zui} is the yaw mass moment of inertia of unsprung mass i about k_{ui} coordinate of the unsprung mass i ($i=1, 2, \dots, 5$). Y_{lf} and Z_{lf} ($f=2$) are instantaneous coordinates of liquid cargo c.g. in the tank-body fixed coordinate system (YZO), while X_{bf} ($f=2$) denotes the longitudinal distance between origin of the tank body axis system and c.g. of the tank-

trailer sprung mass. Z_{bf} ($f=2$) represents the vertical distance from tank base to c.g. of the empty tank trailer, as defined in Section 4.2.1. N_1 and N_2 denote the axle numbers on each sprung mass unit ($N_1=1$ and $N_2=3$ for $f=1$; and $N_1=4$ and $N_2=5$ for $f=2$). The forces and moments due to liquid cargo vanish for the tractor unit ($f=1$) due to absence of the liquid cargo.

The two second-order differential equations describing the vertical and roll motions of each of the five unsprung masses are given by:

Roll moment equations:

$$I_{xui} \dot{p}_{ui} = -(FS_{i1} - FS_{i2})s_i - F_{ri}Z_{ui} - \sum_{j=1}^4 (FT_{ij} \sin \theta_{ui} + FY_{ij} \cos \theta_{ui})(H_{ri} - Z_{ui} \cos \theta_{ui}) + (FT_{i1} - FT_{i4})(b_i + d_i) + (FT_{i2} - FT_{i3})b_i; (i=1, \dots, 5) \quad (4.10)$$

Vertical force equations:

$$m_{ui} a_{uzi} = (FS_{i1} + FS_{i2}) - \sum_{j=1}^4 (FT_{ij} \cos \theta_{ui} + FY_{ij} \sin \theta_{ui}) + m_{ui} g \cos \theta_{ui}; (i=1, \dots, 5) \quad (4.11)$$

where I_{xui} is roll mass moment of inertia of axle i and p_{ui} is its roll velocity. m_{ui} is mass due to axle i and a_{uzi} is the vertical acceleration in the respective unsprung mass axis system. Other symbols used in Equations (4.5) through (4.11) are listed in Table 4.1.

The acceleration of the fluid bulk (a_{f2}) within the tank semitrailer is computed using the semitrailer acceleration and velocity through kinematic relationship [11]. The constraint forces at the coupling are also evaluated from kinematic expressions, relating the accelerations at the constraint or articulation points attached to sprung masses of the two coupled units. The constraint moments are determined from relative angular

displacements between the two sprung masses. The detailed derivations of terms on the right hand side of Equations (4.5) through (4.11) are presented in references [11, 184].

Table 4.1: Description of symbols used in constant speed yaw/roll model.

AT_{ij}	Aligning moment due to tire j ($j=1, 2, 3, 4$) on axle i ($i=1, 2, \dots, 5$)
b_i	Half track width of inner tires on axle i
d_i	Dual tire spacing of tires on axle i
F_{ri}	Lateral force acting through the roll center of axle i
FS_{i1}, FS_{i2}	Forces due to suspension springs on axle i
FT_{ij}	Vertical force due to tire j on axle i
FY_{ij}	Lateral force developed at the j th tire-road interface on axle i
H_{ri}	Height of the roll center of axle i from the ground plane
s_i	Half the lateral suspension spread of axle i
X_{ui}	Longitudinal location of axle i from c.g. of the sprung mass to which the axle is attached
Z_{ri}	Vertical distance between the roll center and c.g. of the sprung weight
Z_{ui}	Vertical distance between c.g. of unsprung weight and the roll center

The differential equations of motion of the partly-filled articulated tank vehicle are solved in the time domain under a specified steer input. The steer input is described either by the time-history of front wheel steer angle (denoted by δ_f) in an open-loop manner or by the path coordinates in a closed-loop manner. The solution procedure is initiated by solving the differential equations of motion for a given steer input during a small time increment. The resulting roll angle and lateral acceleration response of the semitrailer sprung mass are then used in the roll plane model of the partly-filled tank to evaluate instantaneous values of c.g. coordinates and mass moments of inertia of the deflected liquid cargo. The equations of motion for the vehicle model are solved at the subsequent time step using the computed values of cargo c.g. coordinates and mass

moments of inertia. Validity of the proposed tank vehicle model is examined by comparing its response under 100% fill volume with that of a vehicle loaded with an equivalent rigid cargo obtained using the well-known constant velocity Yaw/Roll model [98].

4.3 DIRECTIONAL MANEUVERS AND PERFORMANCE MEASURES

From the safety-related performance measures summarized by EI-Gindy et al. [136] and the correlation analysis conducted by McFarlane et al. [137], it has been established that most controllability and maneuverability measures are strongly related to stability measures, especially the load transfer ratio. The roll dynamic performance of heavy vehicles is often evaluated in terms of lateral dynamic load transfer ratio (LTR) and rearward amplification (RWA).

Articulated vehicles, especially multiple articulated vehicles, often exhibit relatively large magnitudes of lateral motion of the rearmost unit during high-speed directional maneuvers, which may be further amplified by the motion of the liquid cargo within a partly-filled tank trailer. This phenomenon is characterized by the rearward amplification (RWA), defined as ratio of the maximum value of lateral acceleration (and/or roll angle) at c.g. of the sprung weight of the rearmost trailer to that developed at c.g. of the tractor sprung weight during a transient directional maneuver [136], expressed as:

$$RWA = \max(RWA_{max}, RWA_{min}) \quad (4.12)$$

For a tractor semitrailer combination, $RWA_{max} = \max(a_{y2}) / \max(a_{y1})$ and $RWA_{min} = \min(a_{y2}) / \min(a_{y1})$, where a_{y1} and a_{y2} are instantaneous lateral accelerations encountered at the c.g.'s of the tractor and semitrailer sprung weights, respectively. The

RWA may also be expressed by ratio of roll angle response of the two units, $RWA_{\theta} = \max(\theta_{s2})/\max(\theta_{s1})$. The RWA describes the vehicle's tendency to amplify the severity of maneuver-induced motions of the tractor. A larger value of RWA indicates an increased likelihood of rollover of the rearmost trailer of a combination.

The likelihood of vehicle rollover has also been described in terms of lateral load transfer tendency of the vehicles. This tendency is often expressed in terms of dynamic load transfer ratio (LTR) and dynamic vertical load factor (DLF) [11, 136]. The dynamic vertical load factor is defined as ratio of instantaneous vertical load on the left or right track of a given axle to the static vertical load on that track, expressed as:

$$DLF_r = \frac{2F_{zr}}{F_{zr} + F_{zl}} \text{ and } DLF_l = \frac{2F_{zl}}{F_{zr} + F_{zl}} \quad (4.13)$$

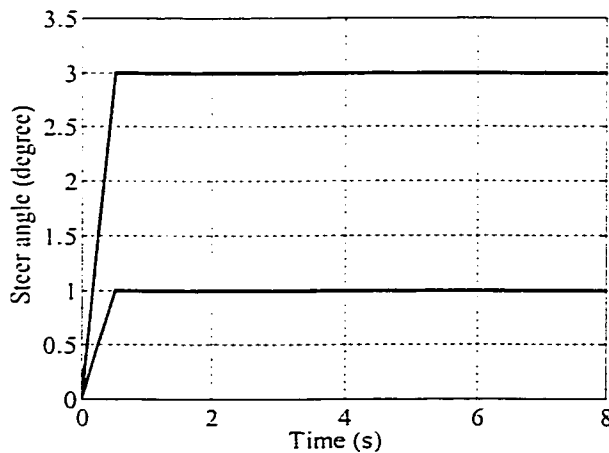
where F_{zr} and F_{zl} are instantaneous vertical loads on the right- and left-wheels of an axle. The DLF assumes a unity value under static conditions and may approach zero during a directional maneuver, when tires on the inner track lose contact with the road. The DLF due to outer track tires in this situation will attain a maximum value of two. This measure describes the roll dynamics of a particular axle. The roll dynamic performance of a vehicle combination has also been evaluated in terms of the dynamic load transfer ratio (LTR), defined as ratio of the sum of instantaneous absolute value of the difference between right-wheel loads and left-wheel loads, to the sum of all the wheel loads, and is expressed as [136]:

$$LTR = \sum_{i=1}^N \frac{|F_{zri} - F_{zli}|}{F_{zri} + F_{zli}} \quad (4.14)$$

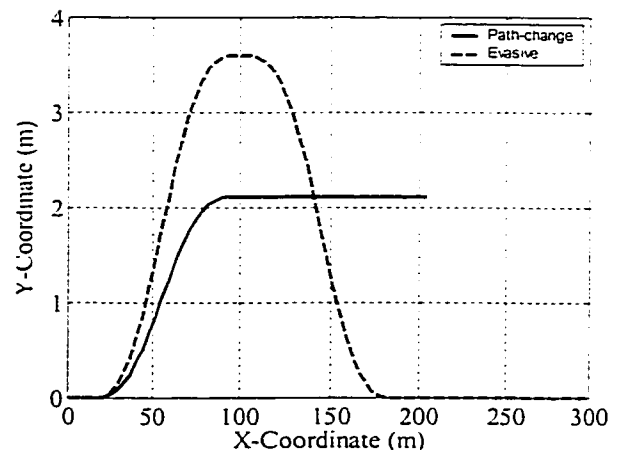
where N is number of axles of the combination. For vehicles with trailer units that are uncoupled in roll, load transfer ratio calculations apply only within the independent units.

The front steering axle is usually excluded from the calculations because of its relatively high roll compliance. The LTR assumes an initial value of zero and approaches unity when the wheels on the inside track lift off the ground.

The above performance measures are evaluated under prescribed directional maneuvers. Apart from these proposed measures, the performance potentials of the optimal tanks are evaluated in terms of variations in c.g. coordinates and mass moments of inertia of the cargo, and lateral acceleration, roll angle, yaw rate, articulation angle and the path trajectory response of the vehicle. In this study, steady and transient steer maneuvers, including ramp-step steer inputs, and path-change and evasive maneuvers, are considered to study the steady-state and transient directional performance of partly-filled tank vehicle combinations. Figure 4.6(a) and (b) illustrate the time-histories of ramp-step steady steer inputs, and path coordinates for single and double lane change transient maneuvers [11, 136].



(a) Ramp-step steer inputs.



(b) Path coordinate.

Figure 4.6: Time history of steady ramp-step steer inputs and path coordinates of transient maneuvers.

4.4 DYNAMIC RESPONSE TO STEERING INPUTS

The directional response characteristics of a five-axle tractor-semitrailer vehicle with partly-filled tanks of different cross-sections are analyzed for both variable and constant load conditions. Since partial fill condition in cleanbore tanks is most frequently realized due to variations in product density, the results of the analyses are emphasized for constant load situations. Computer simulations are initially performed to investigate the dynamic response characteristics of the tank vehicle with 50% fill volume (industrial acid, weight density= 13572 N/m^3 or 0.050 lb/in^3) and 80% fill volume (diesel oil, weight density= 8482 N/m^3 or 0.031 lb/in^3). The axle loads under both fill volumes remain constant near the permissible values. The simulations are then carried out for variable load partial fill conditions, where the axle loads vary with fill volume due to constant density of the liquid cargo. The analyses are performed for four different tank cross-sections, including circular, modified-oval, *OPT1* and *OPT2*. The performance measures are evaluated and compared to examine potential performance benefits of the optimal cross-sections. The simulation parameters of the five-axle tractor semitrailer vehicle combination are summarized in Table 4.2.

Table 4.2: Simulation parameters of a five-axle tank vehicle combination.

<u>Tractor</u>	
Type:	Three-Axle
Sprung Weight:	52486 N (11800 lb)
Unsprung Weight (front axle):	5338 N (1200 lb)
Unsprung Weight (rear axle):	11120 N (2500 lb)
Wheel Base:	4.42 m (174 in)
Tare Center of Gravity Height:	1.12 m (44 in)
Roll Mass Moment of Inertia:	2938 Nms ² (26000 lb-in.s ²)
Yaw Mass Moment of Inertia:	19207 Nms ² (170000 lb-in.s ²)
Pitch Mass Moment of Inertia:	19207 Nms ² (170000 lb-in.s ²)

<u>Tank-Semitrailer</u>	
Type:	Two-Axle
Sprung Weight (Empty):	51828 N (11652 lb)
Unsprung Weight:	13344 N (3000 lb)
Tank Length:	7.85 m (309 in)
Tare Center of Gravity Height:	1.54 m (60.79 in)
Roll Mass Moment of Inertia:	9039 Nms ² (80000 lb-in.s ²)
Yaw Mass Moment of Inertia:	11298 Nms ² (100000 lb-in.s ²)
Pitch Mass Moment of Inertia:	11298 Nms ² (100000 lb-in.s ²)

4.4.1 Constant Load Partial Fill Conditions

The dynamic response of a tank vehicle is a function of various tank design and operating parameters. The transient directional response and thus the stability characteristics of the vehicle with the currently used tanks are compared with those of the vehicle equipped with the proposed optimal tanks in order to study the influence of tank design. The influence of steer input, fill volume and vehicle speed on the dynamic response of the tank vehicle are also investigated .

4.4.1.1 Response to steady steer inputs

The directional response characteristics of the vehicle combination, equipped with different partly-filled tanks, is initially evaluated under steady (ramp-step) steer inputs of 1 and 3 degrees, respectively. The steady steer response is evaluated at a constant forward speed of 60 km/h. The response characteristics are derived in terms of deviations in the coordinates of cargo c.g. (ΔY_l and ΔZ_l), mass moments of inertia (I_{xl2} , I_{yl2} and I_{zl2}) of the cargo about the tank trailer sprung mass system; roll deflection (θ_{s2}), lateral acceleration (a_{y2}) and yaw rate (r_2) of the semitrailer sprung mass; articulation angle (γ); wheel dynamic load factor (DLF) and load transfer ratio (LTR) of the combination.

Liquid Load Shift and Roll Mass Moment of Inertia

Figures 4.7 and 4.8 illustrate the instantaneous lateral load shift in terms of ΔY_l and variations in roll mass moment of inertia (I_{xl2}) of the cargo as a function of the fill volume, tank cross-section, and magnitude of steer angle input, respectively. The parameter β denotes the fill volume ratio, defined as ratio of wetted cross-sectional area to total cross-sectional area of the tank. It should be noted that the variations in β are induced by change in the weight density of the liquid cargoes, since the payload is held constant.

The results show that the magnitude of ΔY_l increases considerably with increase in steer angle. This increase is attributed to higher sprung mass roll angle and lateral acceleration response of the trailer caused by larger steady steer input. The magnitude of ΔY_l , however, decreases with increase in fill volume ratio. The results show trends similar to those derived from static roll analyses, namely higher fill volume yields considerably

lower lateral load shift. The results further show that both optimal cross-sections yield considerably lower magnitudes of load shift, when compared to those attained for the circular and modified-oval tanks, irrespective of the fill volume and magnitude of steer input. The lateral load shift response of the *OPT2* tank is similar to that of the circular tank under 1 degree steer input, but considerably lower than that of the modified-oval tank for 50% fill volume. The *OPT1* cross-section yields lowest magnitude of ΔY_l under both fill volumes and steer angles, while the modified-oval tank, due to its wider cross-section, yields the largest magnitude of ΔY_l . The magnitude of ΔY_l increases rapidly with magnitude of steer input and approaches steady values in all cases, except for 50% filled modified-oval tank under steer input of 3 degrees, where it rises rapidly with time due to its relatively large width, as shown in Figure 4.7, indicating the tank trailer instability.

The roll mass moment of inertia of the cargo ($I_{x/l2}$) also tends to be considerably larger in circular and modified-oval tanks, when compared with those attained for both optimal tanks, irrespective of the fill volume and steer angle. The considerably lower values of $I_{x/l2}$ of the deflected cargo within optimal cross-sections are attributed to relatively lower values of ΔY_l and liquid c.g. height. The values of $I_{x/l2}$ vary only slightly with time under low steer angle input of 1 degree for both fill volumes, regardless of the tank cross-section. The variations in magnitudes $I_{x/l2}$ of cargo within the circular and modified-oval tanks, however, become pronounced under a relatively large steer input of 3 degrees. These significant changes are mostly attributed to the considerable deflections of liquid cargo within the conventional tanks, and high trailer roll angle and lateral acceleration excitations. Similar to ΔY_l , under 50% fill volume and 3 degree steer input, the $I_{x/l2}$ response of the cargo within the modified-oval tank exhibits an instability, as

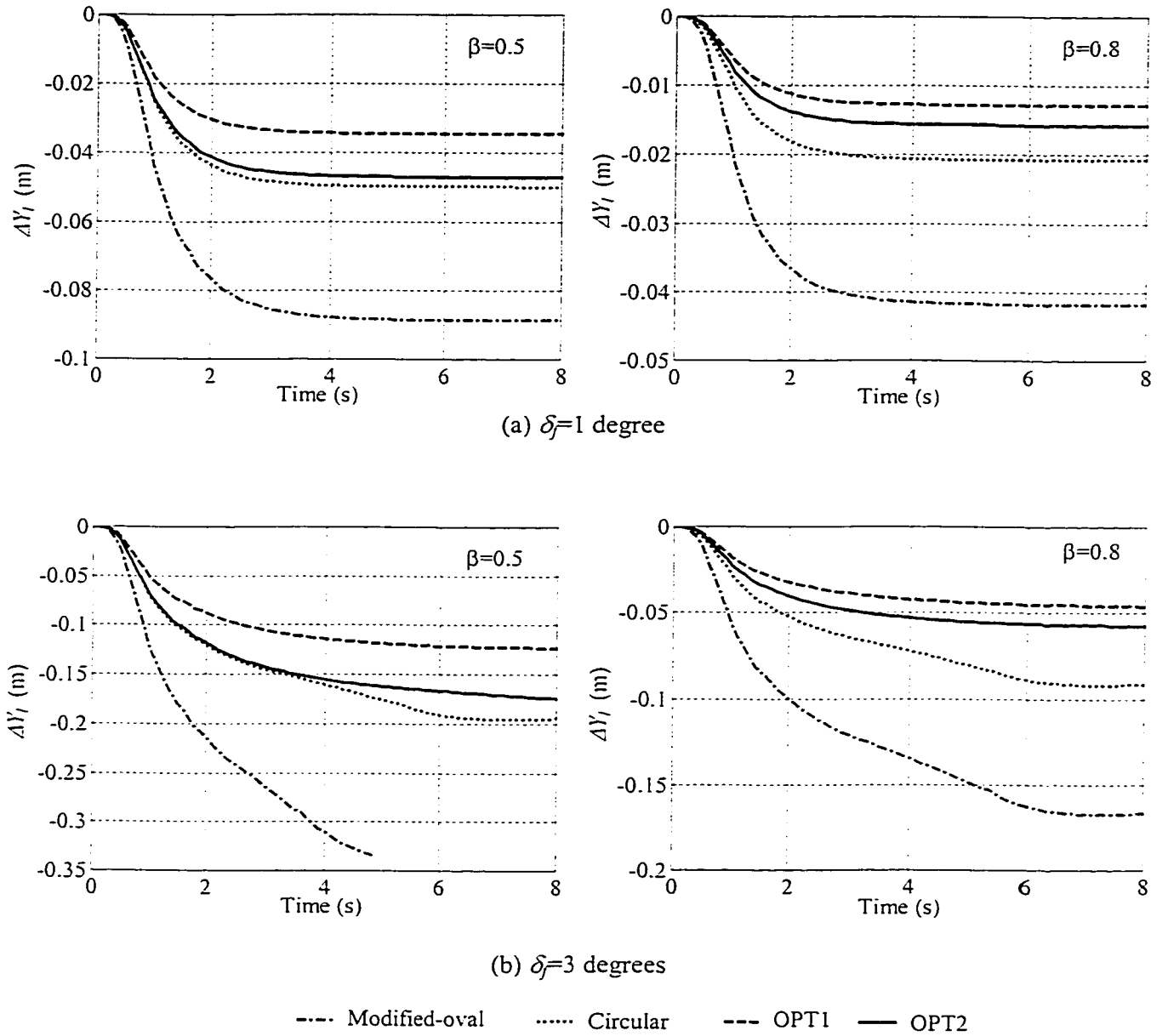
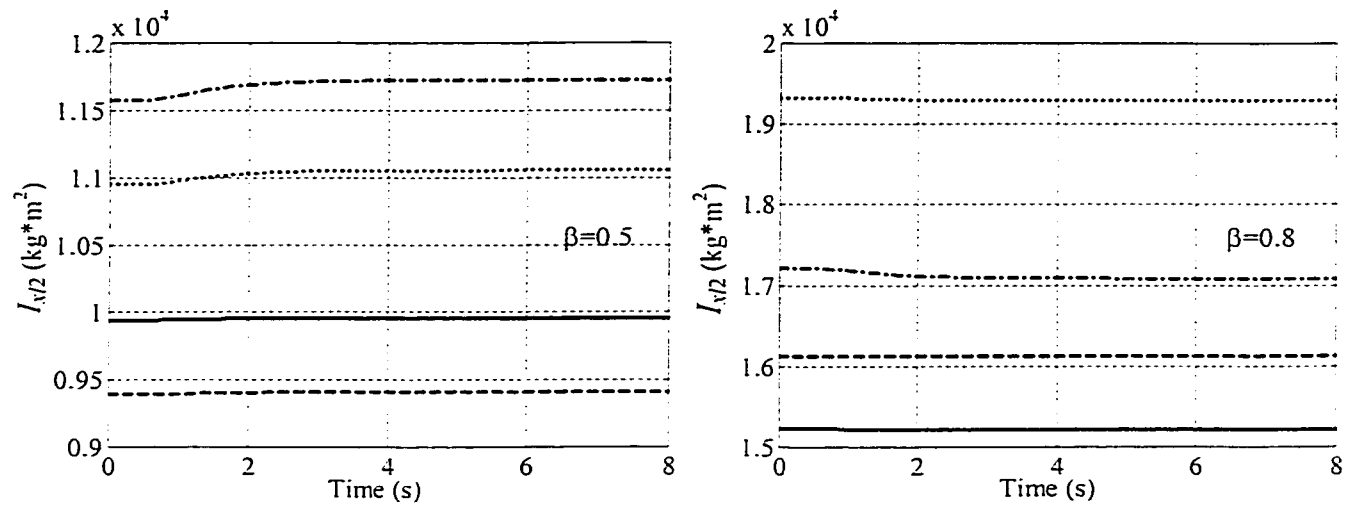
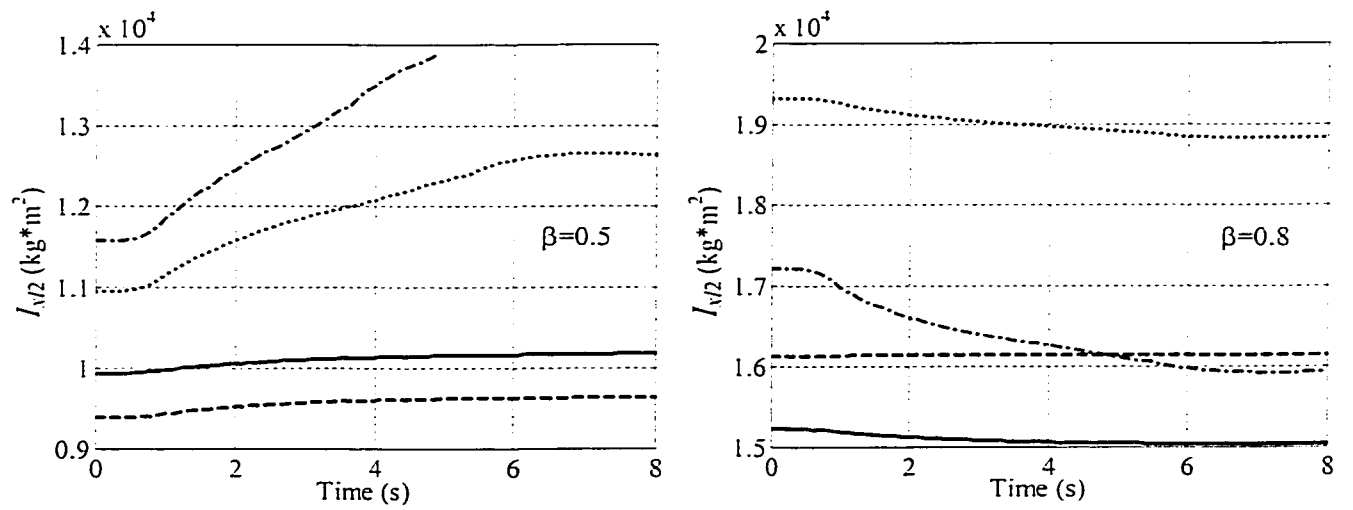


Figure 4.7: Influence of tank cross-section, fill volume and steer angle on the lateral load shift of liquid cargo within conventional and optimal tanks ($U=60$ km/h).



(a) $\delta_f = 1$ degree



(b) $\delta_f = 3$ degrees

--- Modified-oval Circular -.- OPT1 — OPT2

Figure 4.8: Influence of tank cross-section, fill volume and steer angle on the roll mass moment of inertia of liquid cargo within conventional and optimal tanks ($U=60$ km/h).

shown in Figure 4.8. It is interesting to note that the magnitudes of $I_{x/2}$ increase with time under 50% fill volume, while they tend to decrease under 80% fill volume, irrespective of the tank cross-section and steer input. This is mostly due to the different deflection patterns of the liquid cargo in the roll plane under medium and high fill volumes. The magnitudes of $I_{x/2}$ of liquid cargo within the optimal tanks remain nearly constant as compared with those computed for the conventional tanks, irrespective of the steer input and fill volume. The slight variations in $I_{x/2}$ of cargo within optimal tanks can be mostly attributed to considerably less shifts in the c.g. coordinates of the liquid within the optimal tank cross-sections.

Dynamic Roll Response

Under a relatively low steer input of 1 degree, the magnitudes of roll angle, yaw rate and lateral acceleration response of the vehicle with conventional tanks are quite small and thus do not depart significantly from those of the vehicle with optimal tanks. This is attributed to low sprung mass roll angle and lateral acceleration excitation induced by the low steady steer input. Significant variations in ΔY_l and $I_{x/2}$ of the cargo within the conventional circular and modified-oval tanks, observed under a higher steer input of 3 degrees, however, yield considerably high magnitudes of roll motion, yaw rate and lateral acceleration response of the trailer sprung mass, as shown in Figure 4.9 (the lateral acceleration and yaw rate response of the circular and modified-oval tank vehicles overlaps under 80% fill volume). The magnitudes of these response variables of the vehicle equipped with the optimal tanks are considerably lower, irrespective of the fill volume. The high magnitude response of conventional tank vehicles results in significant variations in wheel DLF and LTR, and thus deviations in the path trajectory, as illustrated

in Figure 4.10 (the path trajectory response of the circular and modified-oval tank vehicles overlaps).

It is interesting to note that fill volume influences the behavior of different tanks quite differently. The vehicle with the modified-oval tank exhibits considerably higher response at 50% than at 80% fill volume. The pronounced response under low fill volume is primarily attributed to excessive lateral load transfer associated with its wide cross-section. The circular and *OPT1* tanks yield slightly lower vehicle response at 50% than at 80% fill volume, owing to the relatively higher cargo c.g. locations associated with their relatively narrow cross-sections. The vehicle with the relatively low c.g. conical tank (*OPT2*), however, reveals slightly higher response at 50% than at 80% fill volume, due to relatively large liquid load shift resulting from the relatively wide tank cross-section. The insignificant impact of fill volume on the response characteristics of the vehicle with circular, *OPT1* and *OPT2* tanks is primarily attributed to the combined effects of cargo c.g. height and load shift associated with the three tank cross-sections. Under low fill volumes, the expected decrease in vehicle response due to low overturning moment from a lower c.g. height is greatly offset by considerable increase in overturning moment caused by large lateral shift in the c.g. location of the liquid cargo. Higher fill volumes, on the other hand, lead to larger overturning moment attributed to higher cargo c.g. location and considerably lower overturning moment due to relatively smaller load shift.

Under 80% fill volume, the circular and modified-oval tanks yield quite similar response. This similarity in vehicle response is principally attributed to the combined influence of cargo c.g. heights and load shifts associated with these two conventional tank cross-sections. Under high fill volume, the relatively large response of the circular

tank vehicle is primarily attributed to its higher c.g. location arising from the high cross-section c.g. height. The decreased response of the modified-oval tank vehicle under higher fill volume is mostly ascribed to significant reduction in load shift and relatively low liquid c.g. location resulting from its wider cross-section. Under the steer input of 3 degrees, the vehicle with 50% filled modified-oval tank exhibits roll instability near $t=5$ s, as evident from the rapid growth in roll angle response of the trailer shown in Figure 4.9. The corresponding values of LTR and DLF approach 1 and 0, respectively, as shown in Figure 4.10. This instability is mostly induced by the considerable overturning moment resulting from excessive magnitude of ΔY_l , as shown in Figure 4.7. In this case, the rearmost right track of the combination loses contact with the road due to excessive lateral transfer of the normal load, as observed from the rearmost right wheel dynamic load factor response shown in Figure 4.10. The lower degree of cargo shift under 80% fill volume, however, yields marginally stable response of the vehicle. The value of LTR approaches nearly 0.95.

Under a steady steer input of 3 degrees, the peak values of the dynamic load transfer ratio (LTR) of the vehicle combination equipped with the optimal tanks are approximately 20-30% lower than those of the vehicle equipped with the conventional tanks. Under both steer inputs, the vehicle equipped with the modified-oval tank, which exhibits the lowest cross-sectional c.g. height among the four tanks, reveals the largest LTR response. The relative roll stability of this vehicle is thus considered to be lowest, which is primarily caused by excessive lateral load shift property of the wider cross-section. These results suggest that liquid load shift within a partly-filled wide tank is the

predominant factor affecting the dynamic response and thus roll stability of the tank vehicle, irrespective of the fill volume.

Under a 3 degree ramp-step steer input, the destabilizing moment caused by the lateral cargo shift within a 50% filled modified-oval tank leads to complete transfer of normal load from the inner to the outer track at approximately $t=5$ s, as is evident from the LTR response of the vehicle combination, shown in Figure 4.0. This total lateral transfer of the normal load in turn causes a rapid increase in the trailer roll angle and thus the liquid load shift, and a decrease in the lateral acceleration and yaw rate response, as shown in Figure 4.9. The vehicle equipped with the optimal and circular tanks exhibits stable behavior under identical conditions of fill volume and steer input. The significant lateral transfer of the normal load resulting from partly-filled conventional tanks also yields considerable departure of the vehicle path from that attained with the optimal cross-sections. This path deviation is caused by the lateral load shift and nonlinear cornering force properties of the tires.

A comparison of response characteristics of the vehicle with different cross-section tanks under different magnitudes of steady steer inputs and fill volumes clearly illustrates the superior performance of the vehicle with both optimal tanks. This improved performance is mostly due to significantly reduced lateral shift of the cargo within the proposed optimal cross-section tanks.

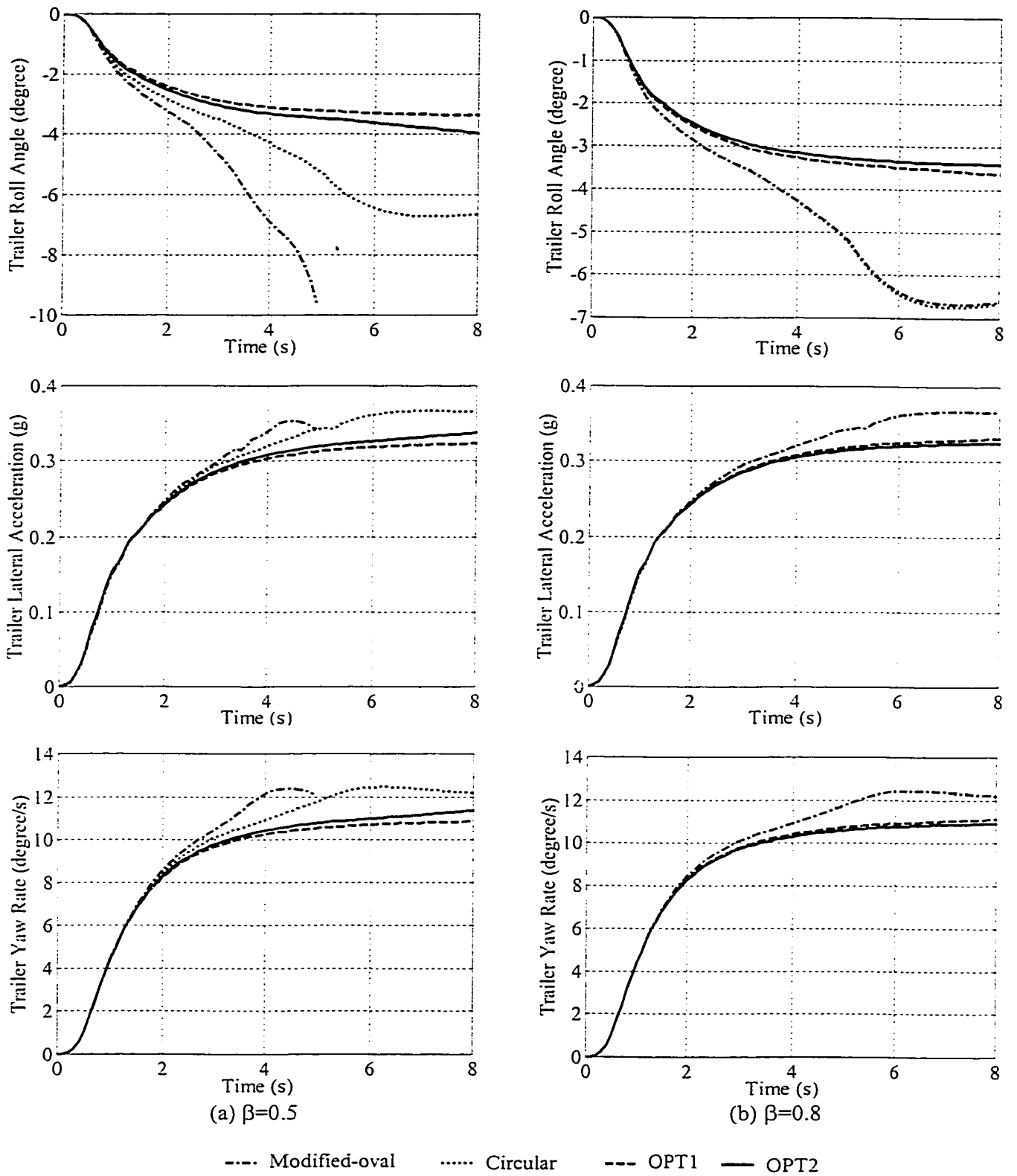
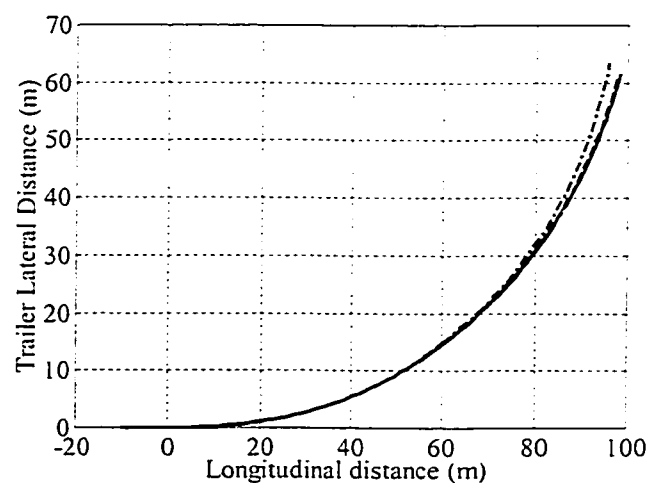
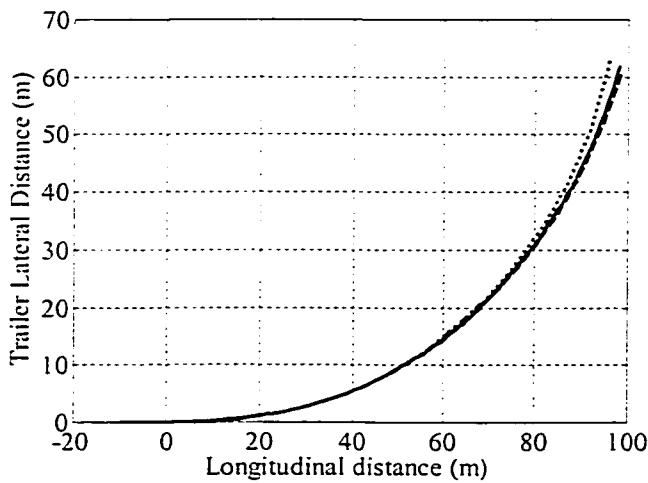
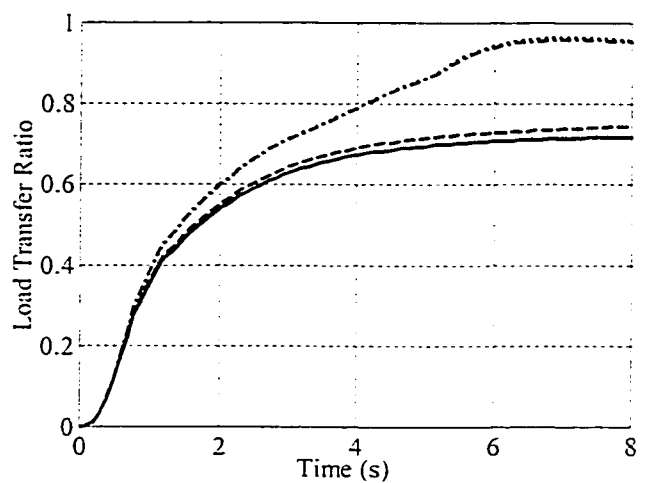
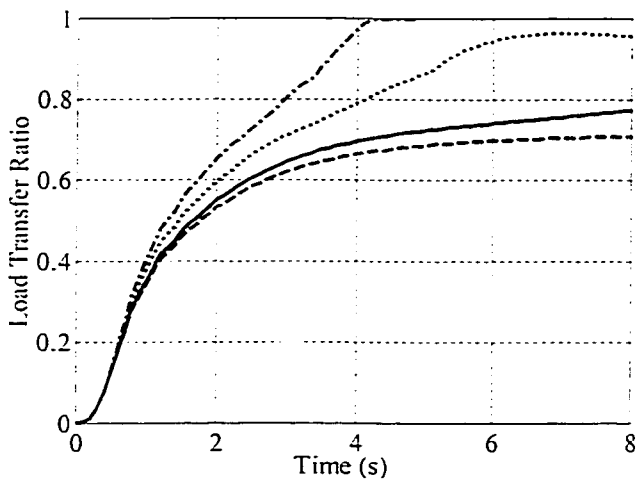
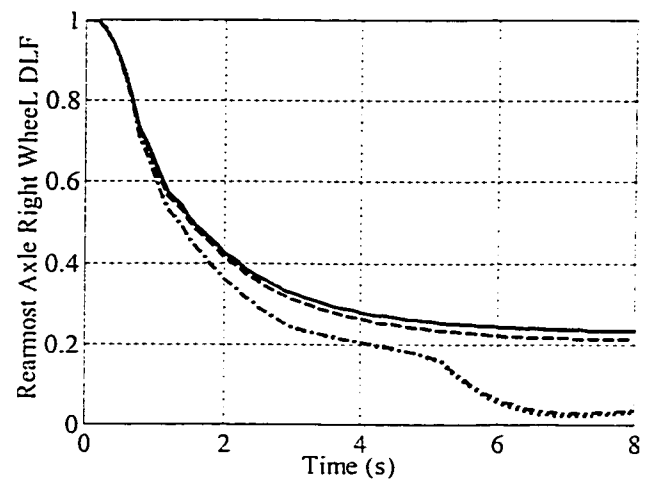
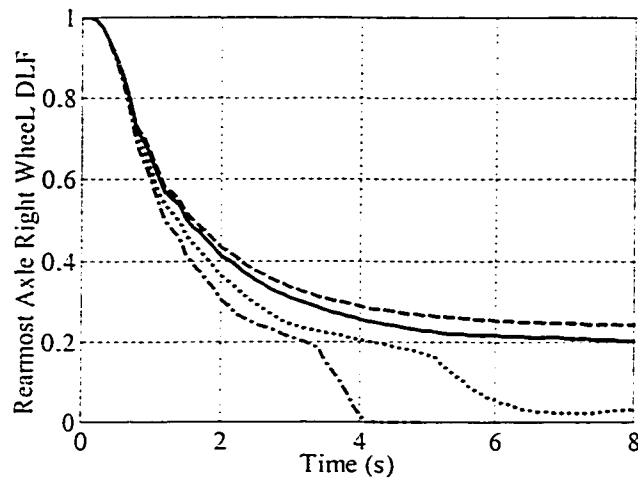


Figure 4.9: Influence of tank cross-section and fill volume on the directional response of the vehicle ($U=60$ km/h, $\delta_f=3$ degrees).



(a) $\beta=0.5$

(b) $\beta=0.8$

--- Modified-oval Circular -.-.- OPT1 — OPT2

Figure 4.10: Influence of tank cross-section and fill volume on the lateral load transfer and path trajectory of the vehicle ($U=60$ km/h, $\delta_f=3$ degrees).

Influence of Vehicle Speed on the Directional and Roll Response

The roll angle, lateral acceleration, yaw rate, load transfer ratio and path trajectory response of the vehicle with the currently used circular and modified-oval tanks does not deviate significantly from that of the vehicle with the optimal tanks under low level steering input ($\delta_f=1$ degree) and forward speed of 60 km/h. The vehicle combination exhibits stable roll dynamic behavior, irrespective of the fill volume and tank cross-section. The directional dynamic response characteristics of the vehicle combination with different tanks, however, differ considerably at a higher forward speed. Figures 4.11 and 4.12 illustrate the time histories of roll angle, lateral acceleration and yaw rate response of the trailer sprung mass, and load transfer ratio (LTR) of the vehicle combination to a steady steer of 1 degree and a forward speed of 90 km/h. The figures illustrate the vehicle response under two different fill volume ratios, $\beta=0.5$ and $\beta=0.8$, respectively. The figures also illustrate the time-histories of ΔY_l and $I_{x/l2}$ due to the cargo. Figures 4.13 further illustrates the semitrailer path trajectory and articulation angle response of the vehicle.

The maximum values of the vehicle response parameters tend to increase considerably with increase in forward speed, irrespective of the tank cross-section and fill volume, as a result of rapid increase in the magnitude of lateral acceleration with forward speed. An examination of the results shows that the vehicle equipped with the optimal tanks experiences significantly less magnitudes of roll angle, lateral acceleration, yaw rate, articulation angle, and LTR response than that with conventional tanks, irrespective of the fill volume. The response parameters of the vehicle with the optimal tanks invariably approach their steady values near 6 s. The magnitudes of the response

variables of the vehicle equipped with the circular and modified-oval tanks, however, continue to increase with time over the simulation period (12 s) considered in the study, with LTR exceeding the recommended value of 0.6 for the circular tank vehicle and reaching the losing-contact value of 1.0 for the modified-oval tank vehicle after about 7.5 s, as shown in Figures 4.11 and 4.12. This increasing response suggests possible roll instability of the vehicle combination, which is evident in case of the modified-oval tank vehicle. The magnitudes of deviations in lateral coordinate of cargo c.g. and roll mass moment of inertia, and response variables of the vehicle equipped with a 50% filled modified-oval tank increase significantly, with LTR reaching 1.0 after about 7.5 s, and the vehicle approaches roll instability, as shown in Figure 4.11. This impending instability is mostly attributed to the excessive overturning moment caused by considerable lateral load transfer in liquid cargo and lateral acceleration filed developed at a higher speed. The vehicles with the circular and modified-oval tanks also exhibit significant departure in the path trajectory when compared with that of the vehicles with the optimal tanks, as shown in Figure 4.13.

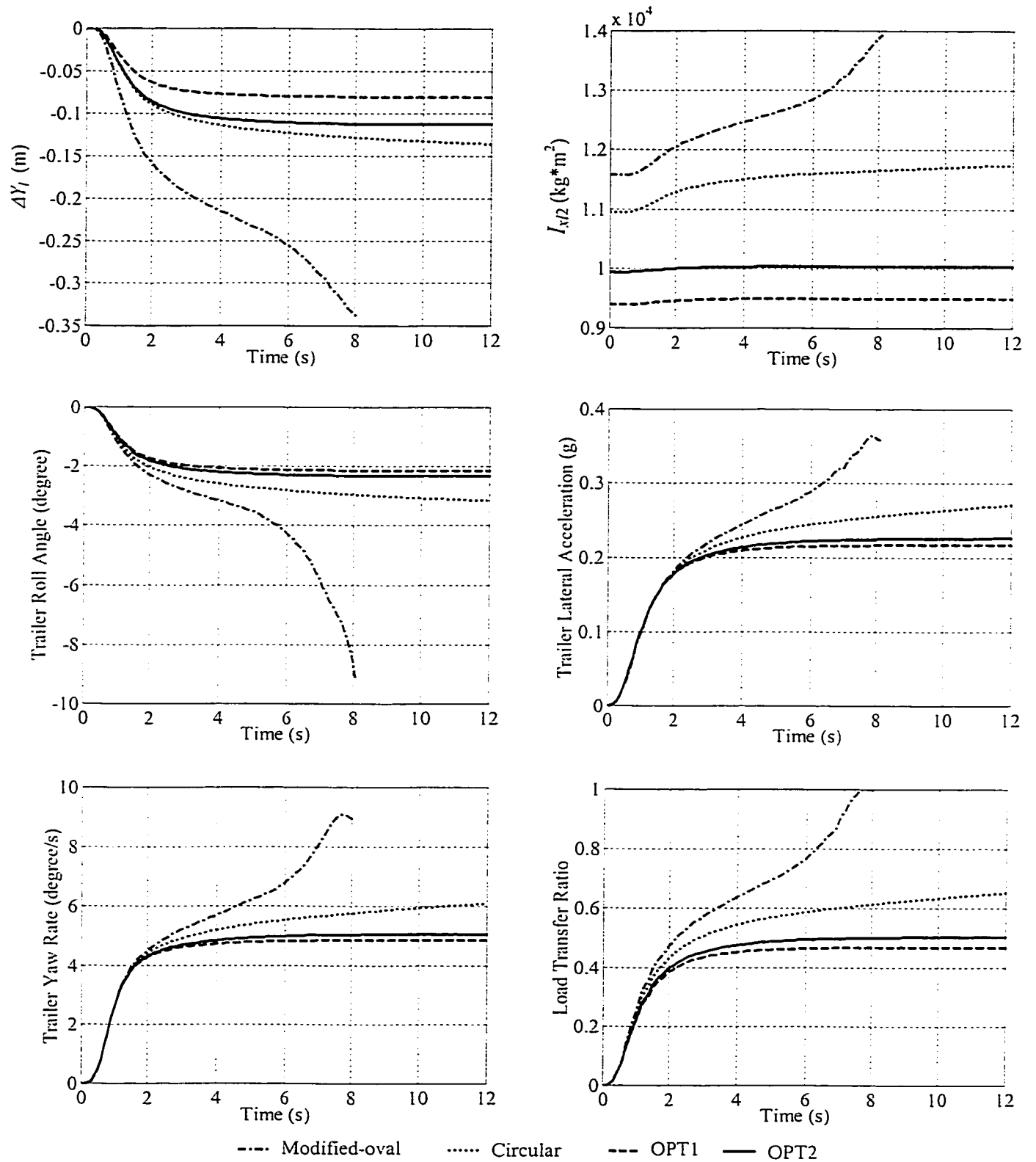


Figure 4.11: Directional response of the vehicle combination with different tanks to a steady steer input of 1 degree ($U=90$ km/h, $\beta=0.5$).

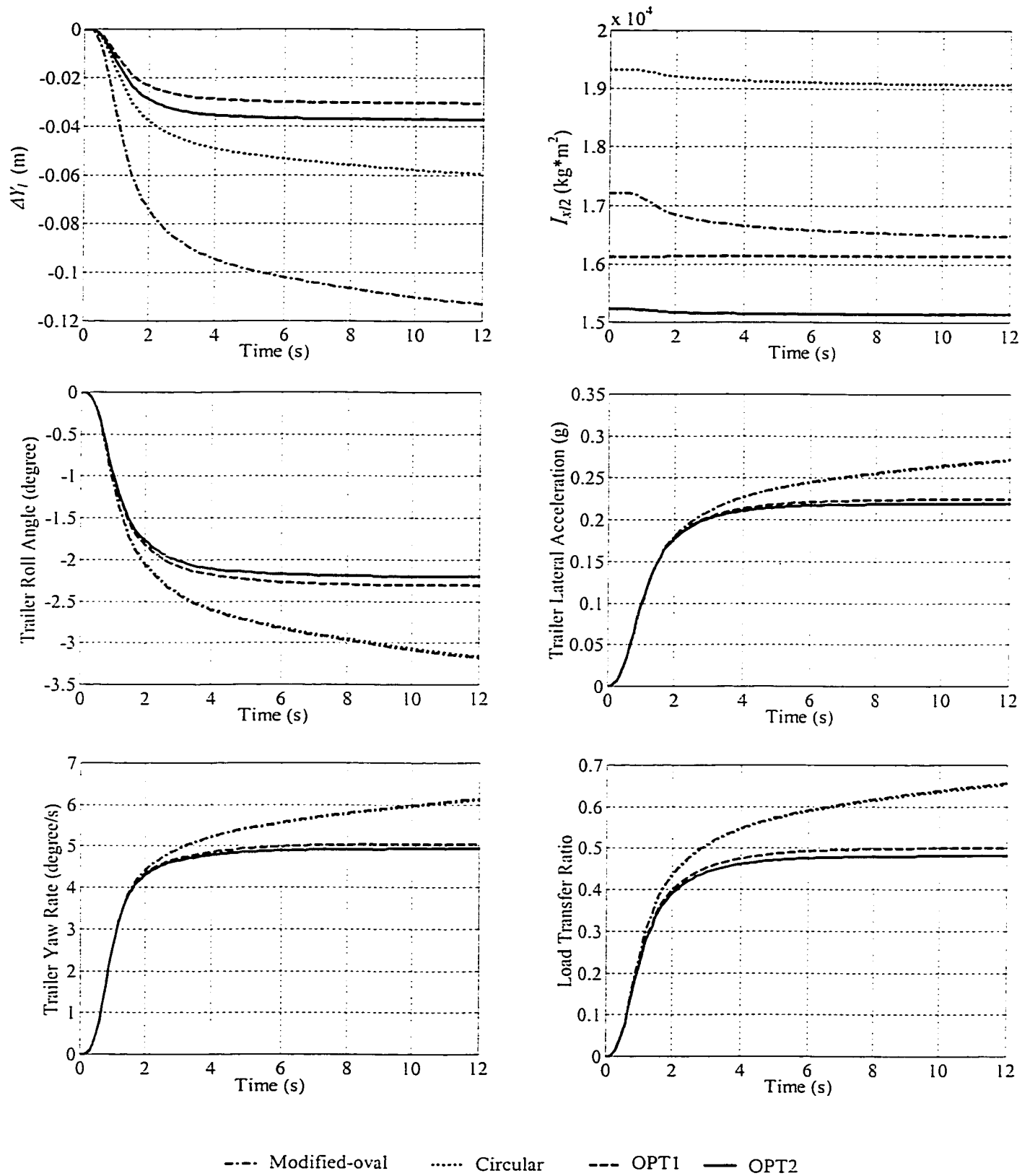
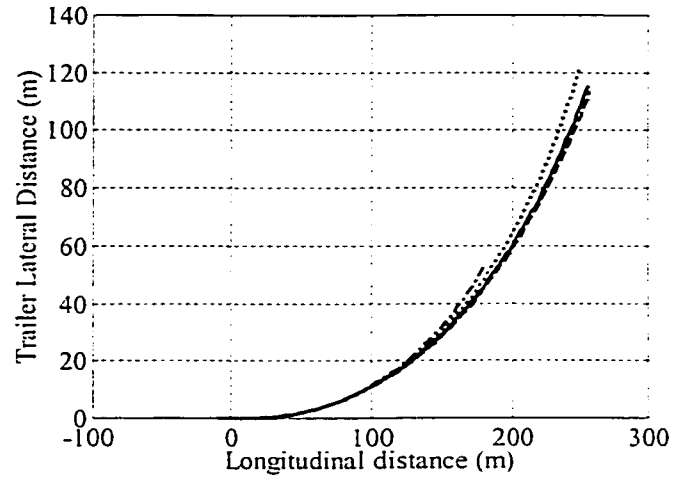
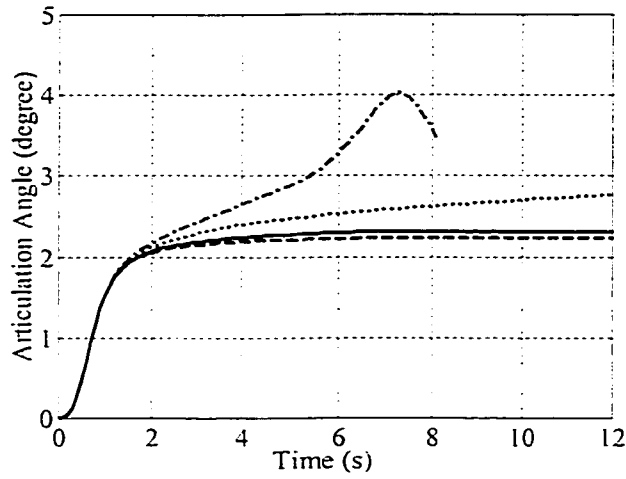
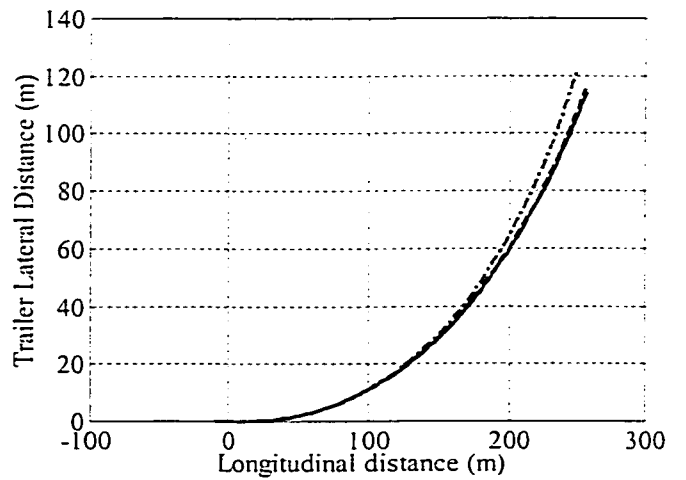
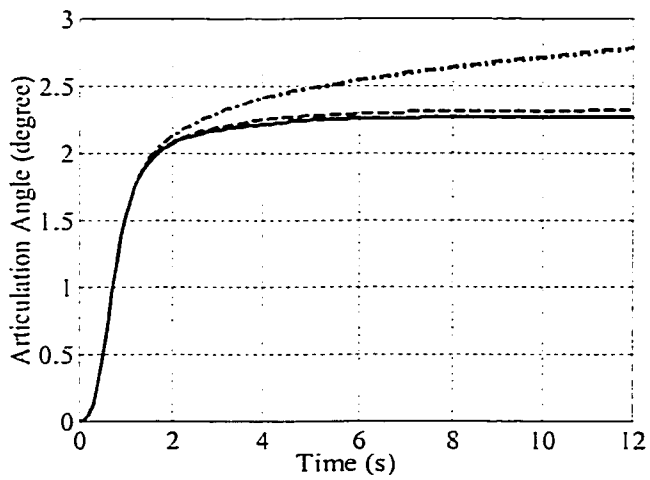


Figure 4.12: Directional response of the vehicle combination with different tanks to a steady steer input of 1 degree ($U=90$ km/h, $\beta=0.8$).



(a) $\beta=0.5$



(b) $\beta=0.8$

--- Modified-oval Circular -.- OPT1 — OPT2

Figure 4.13: Articulation angle and path trajectory response of the vehicle combination with different tanks to a steady steer input of 1 degree ($U=90$ km/h).

4.4.1.2 Transient steer inputs

The directional and roll response characteristics of the partly-filled tractor-semitrailer tank vehicle are further investigated under path-change and evasive maneuvers using a closed-loop driver model [11]. The analyses are performed for 50% and 80% fill volumes, and the results are compared to examine the potential performance benefits of the optimal cross-section tanks under transient directional maneuvers. Figures 4.14 through 4.17 illustrate the liquid cargo lateral c.g. shift (ΔY_l) and roll mass moment of inertia (I_{x2}), trailer roll angle (θ_{s2}) and load transfer ratio (LTR) response of the vehicle equipped with the four different cross-section tanks, while negotiating path-change and evasive maneuvers, respectively, at a forward speed of 100 km/h.

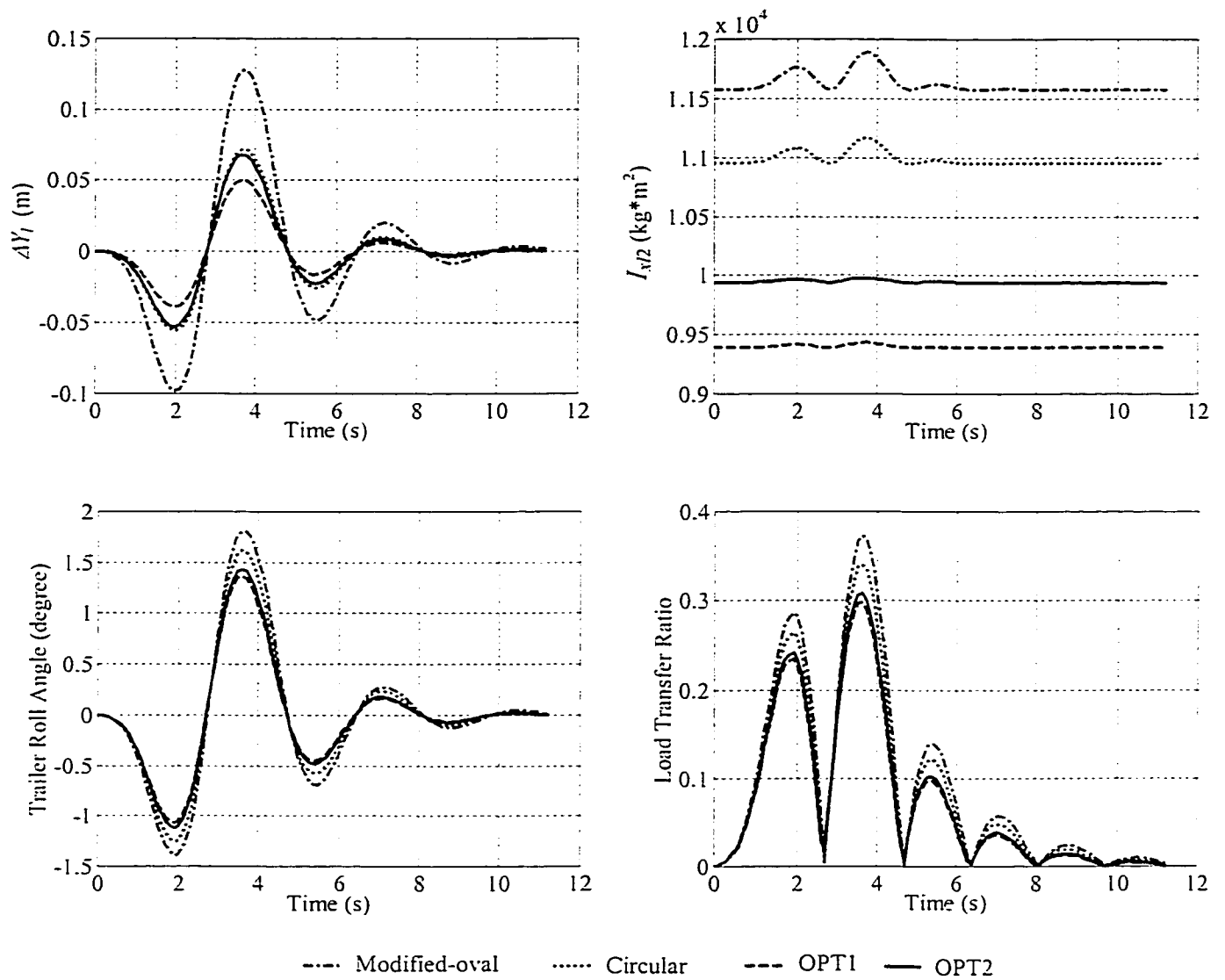


Figure 4.14: Directional response of partly-filled tank vehicles to a path-change maneuver performed at 100 km/h ($\beta=0.5$).

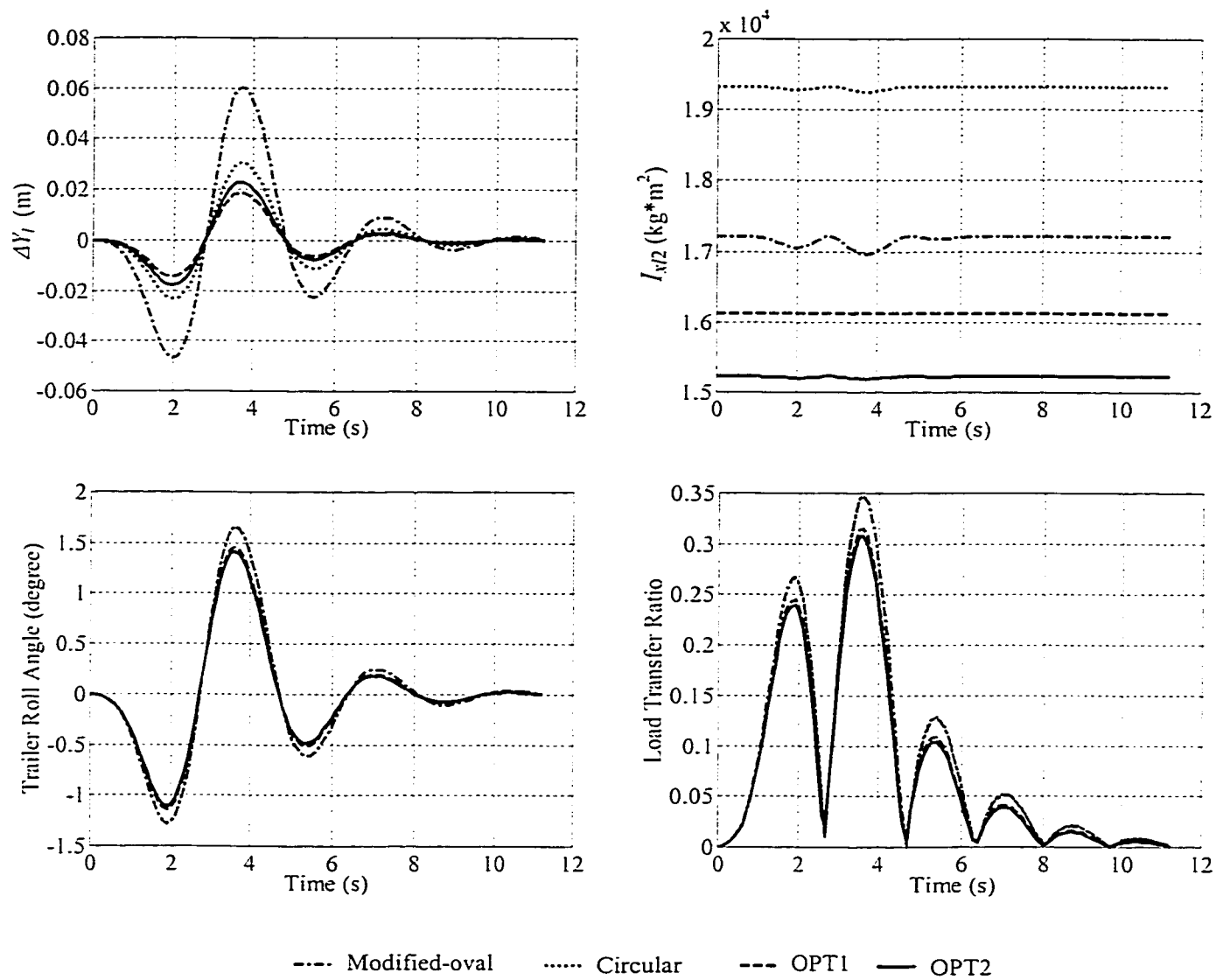


Figure 4.15: Directional response of partly-filled tank vehicles to a path-change maneuver performed at 100 km/h ($\beta=0.8$).

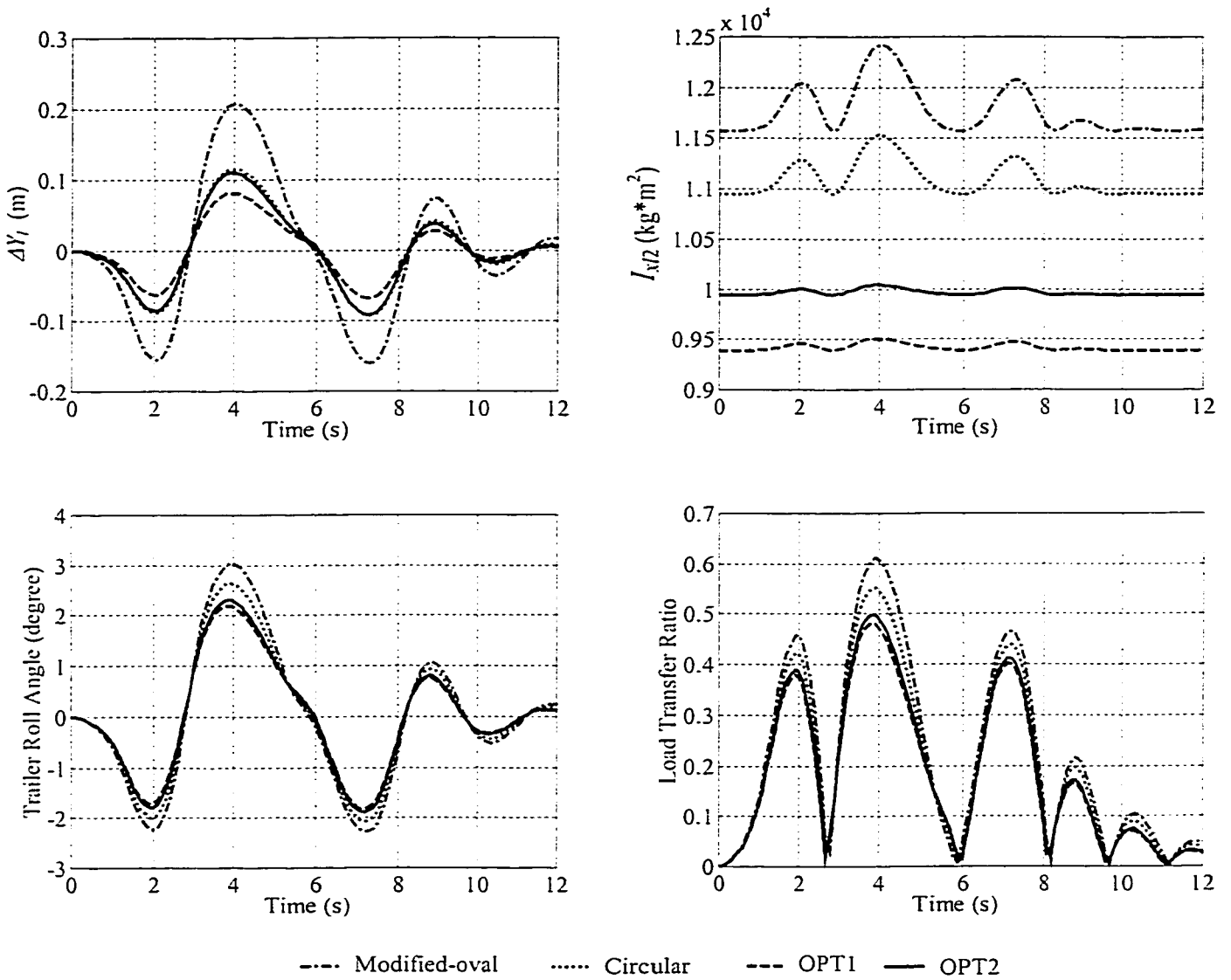


Figure 4.16: Directional response of partly-filled tank vehicles to a evasive maneuver performed at 100 km/h ($\beta=0.5$).

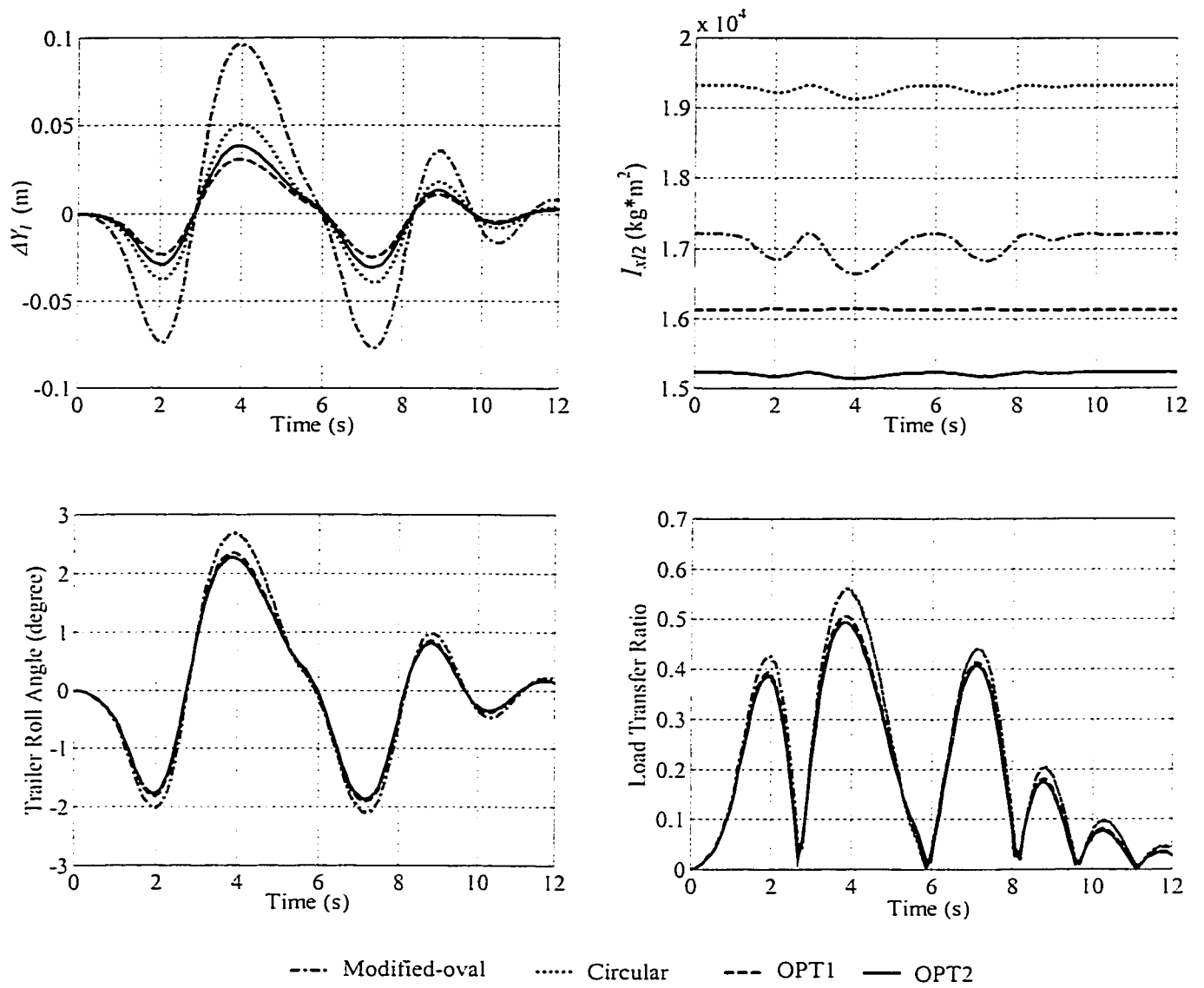


Figure 4.17: Directional response of partly-filled tank vehicles to a evasive maneuver performed at 100 km/h ($\beta=0.8$).

As observed from the response to steady steer inputs in Section 4.4.1.1, both optimal cross-sections yield considerably lower magnitudes of load shift and less variations in roll mass moment of inertia of the cargo, when compared to those attained for the circular and modified-oval tanks, under identical conditions of fill volume and directional maneuver. The vehicle with *OPT1* tank yields the least lateral load transfer under both fill volumes. This combination also yields the lowest peak response in roll angle and load transfer ratio under 50% fill volume, while the vehicle with the *OPT2* tank exhibits the minimal response of these variables under 80% fill volume. The peak roll angle response of the trailer ($\theta_{s,2}$) and load transfer ratio (LTR) response of the vehicle with the circular and *OPT1* tanks under 50% fill volume are slightly lower than those attained under 80% fill volume. This behavior is attributed to the relatively high c.g. location of liquid cargo associated with the two narrow cross-sections, while the vehicle with the *OPT2* reveals lightly higher response at 50% fill volume, due to its relatively wide cross-section. The trivial influence of fill volume on the response characteristics of the vehicle with circular, *OPT1* and *OPT2* tanks are principally attributed to only small variations in the overturning moments, resulting from both the c.g. height and lateral load shift properties, as discussed in Section 4.4.1.1. Under 80% fill volume, the circular and modified-oval tanks yield similar roll angle and LTR response, as illustrated in Figures 4.15 and 4.17 (the roll angle and LTR response of the circular and modified-oval tank vehicles overlaps under 80% fill volume in both Figures).

The larger liquid load shift encountered within the conventional tanks, especially the wide modified-oval cross-section, leads to considerably larger peak values of directional response quantities ($\theta_{s,2}$ and LTR), when compared with those obtained for the

optimal tanks. The difference in the peak response parameters of the vehicle with different tank cross-sections is not significant under the mild path-change maneuver, due to relatively low lateral acceleration excitation induced by the mild steering maneuver. This disparity, however, becomes evident under the evasive maneuver and 50% fill volume, as shown in Figure 4.16, as a result of considerably larger lateral acceleration disturbance caused by the severe steering operation. The maximum values of trailer LTR of the vehicle equipped with the optimal tanks are approximately 20% lower than that of the vehicle with the modified-oval tank, and 10% lower than that with the circular tank. The influence of tank cross-section on the rearward amplification (RWA) of the lateral acceleration response of the vehicle under the path-change and evasive maneuvers is summarized in Table 4.3. The results show that the optimal tanks yield certain reduction in the RWA response of the vehicle, due to relatively lower overturning moment of the liquid cargo. The results further indicate that the RWA values increase under a relatively severe evasive maneuver, owing to increase in the destabilizing moment with increase in maneuver severity. The magnitudes of RWA of the vehicle with all the tanks are quite small, as is typical of tractor semitrailer vehicle combinations [36]. The potential benefits of the optimal cross-section tanks are thus not evident.

Table 4.3: Lateral acceleration rearward amplifications of the vehicle with various tanks.

Maneuvers	Modified-oval	Circular	<i>OPT1</i>	<i>OPT2</i>
Path change ($\beta=0.5$)	1.1167	1.1070	1.089	1.0930
Path change ($\beta=0.8$)	1.1099	1.1098	1.097	1.0938
Evasive ($\beta=0.5$)	1.1331	1.1224	1.108	1.1102
Evasive ($\beta=0.8$)	1.1247	1.1278	1.115	1.1126

It should be pointed out that the highest steering frequencies for the path-change and evasive maneuvers are identified as 0.3 *Hz* and 0.26 *Hz*, respectively, which are well below those of the corresponding fundamental frequencies of the liquid slosh within a tank [187]. This suggests that the quasi-static fluid slosh model can be considered valid for the analysis of transient directional maneuvers considered in this Chapter.

4.4.2 Variable Load Partial Fill Conditions

Figures 4.18 and 4.19 present a comparison of the variations in liquid load shift and roll mass moment of inertia, roll angle, lateral acceleration, yaw rate and load transfer ratio of the vehicle equipped with different tanks, at a constant forward speed of 60 km/h and subject to a steady steer input of 3 degrees. These results are derived for 50% and 80% fill volumes, while the cargo load is permitted to vary with the fill volume. The weight density of the liquid cargo is considered as 6800 N/m³.

Similar to the vehicle response under constant load partial fill conditions, the *OPT1* tank yields the least lateral shift of the cargo under both fill volumes, owing to its narrow cross-section. The vehicle with 50%-filled *OPT1* tank reveals the least response in roll angle, lateral acceleration, yaw rate and load transfer ratio of the vehicle. Under 80% fill volume, however, the vehicle with *OPT2* tank reveals the minimal response. The 50%-filled vehicle, in general, exhibits relatively lower response than the 80%-filled vehicle, irrespective of the tank cross-section. Although the magnitude of lateral cargo shift under 50%-fill condition is considerably larger, the 80%-fill condition yields significantly larger overturning moment due to increase in both the payload and the c.g. height. Under a low fill volume, the expected reduction in the vehicle response due to

decrease in both c.g. height and cargo load is largely offset by the increase in liquid load shift.

Under both fill volumes, the vehicles with the optimal tanks exhibit quite similar behavior, and the response approaches steady values after approximately 6 s. Under 50% fill volume, the vehicle equipped with the modified-oval tank yields the largest response due to excessive lateral shift of liquid load, while the vehicle with the circular tank reveals the second largest response due to its high c.g. The directional response of both vehicles approaches steady values near 6 s, as shown in Figure 4.18. Under 80% fill volume, the vehicle with conventional tanks yields similar steady-state response (the roll angle, lateral acceleration, yaw rate and LTR response of the circular and modified-oval tank vehicles overlaps), which is considerably higher than that of the vehicle with optimal tanks, as shown in Figure 4.19. This response behavior is attributed to the combined effect of reduced lateral shift and higher cg. of the liquid cargo.

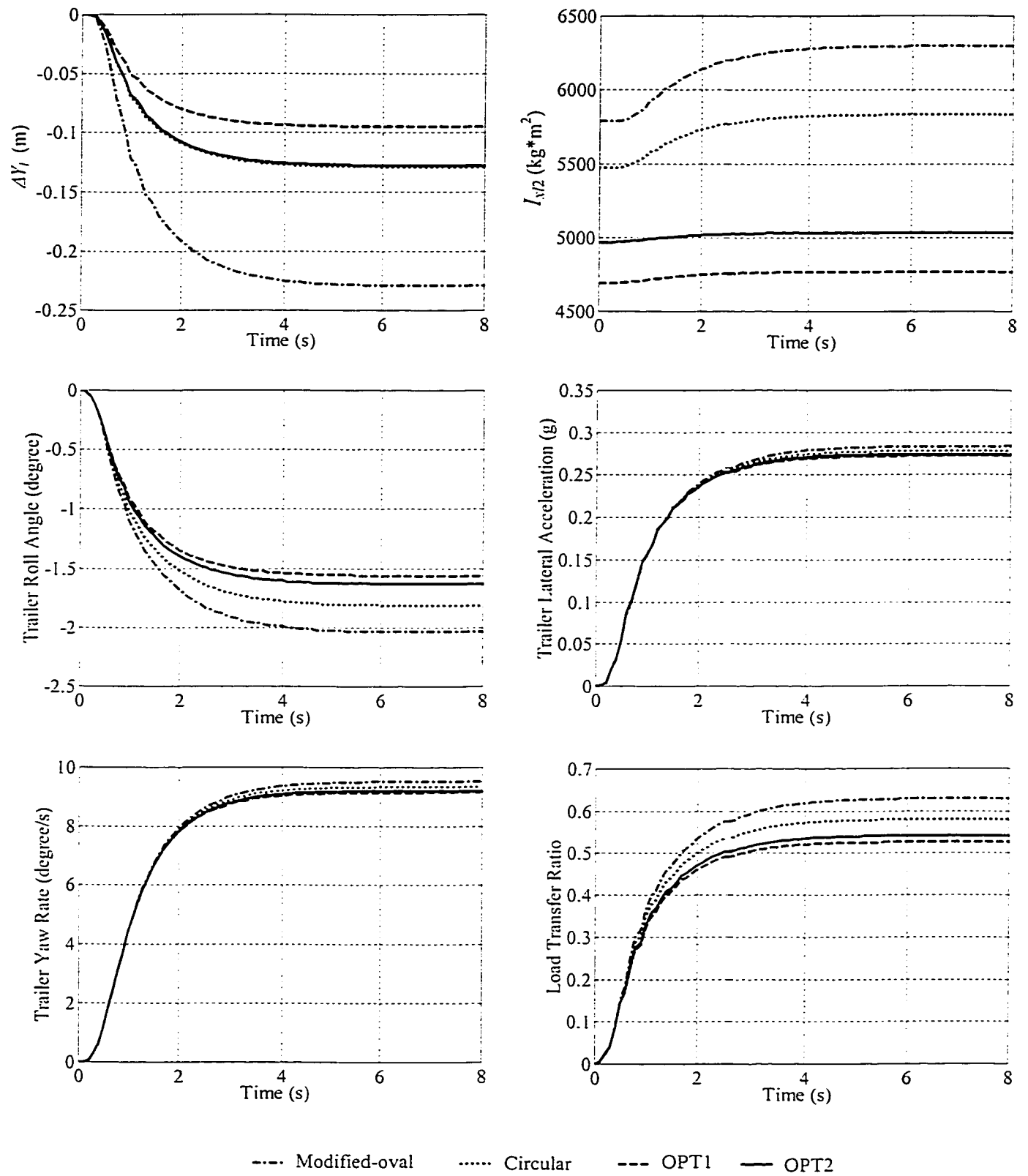


Figure 4.18: Directional response of the vehicle with different tanks to a steady steer input of 3 degrees (variable cargo load, $\beta=0.5$).

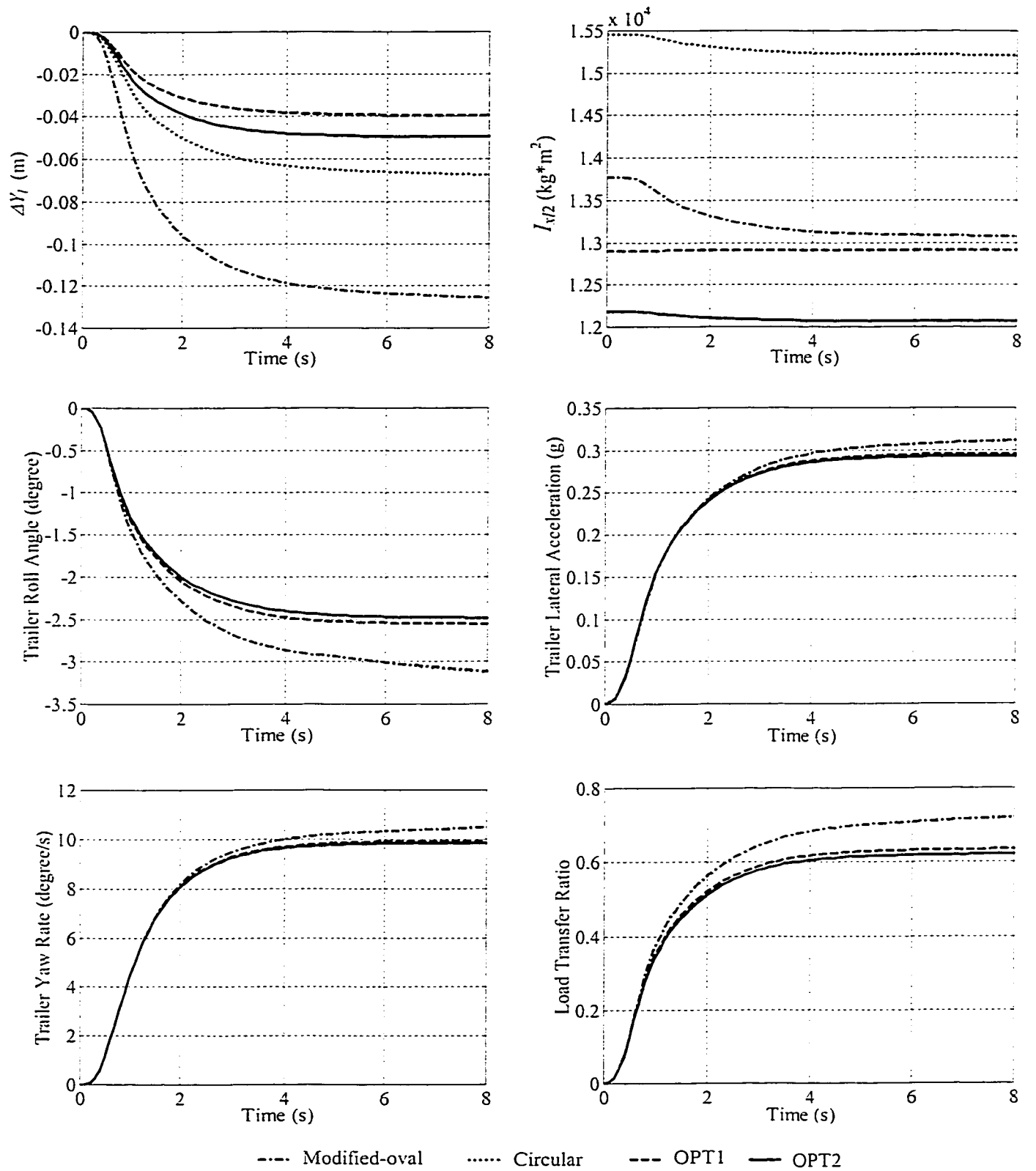


Figure 4.19: Directional response of the vehicle with different tanks to a steady steer input of 3 degrees (variable cargo load, $\beta=0.8$).

4.5 SUMMARY

A quasi-static roll plane model of a partly-filled generic tank is developed and integrated into a three-dimensional dynamic model of articulated vehicles to investigate the influence of optimal tank geometry on the directional response and roll stability characteristics of a five-axle tractor semitrailer tank vehicle. The dynamic characteristics of the vehicle equipped with two optimal tanks are compared with those of the vehicle equipped with the currently used tanks to demonstrate the performance potentials of the optimal tank geometry, in terms of load shift and mass moments of inertia of liquid cargo as well as roll angle, lateral acceleration, yaw motion, load transfer ratio and path trajectory response of the vehicle combination. Parametric sensitivity analyses are further carried out to study the influence of liquid fill condition, steer input and vehicle speed on the directional behavior of the vehicle combination.

The comparative study revealed that liquid load shift within a partially-filled tank plays a dominant role in influencing the dynamic response characteristics of a tank vehicle, especially under relatively low fill volumes. While the c.g. height of liquid cargo yields somewhat moderate contribution to the directional response characteristics of the vehicle combination under high fill volumes, its impact becomes relatively insignificant under low fill volumes. From the results, it is further concluded that the optimal tanks can considerably improve the directional and roll dynamic response characteristics of the partially-filled tank vehicle, which is primarily attributed to their relatively low c.g. height and considerably low derivations in lateral c.g. coordinate of the cargo. The benefit potentials of the optimal tanks increase with increase in the severity of the directional maneuver. Under constant load partial fill conditions, although the vehicle

with all the tanks reveals stable behavior under small levels of steady steer inputs, the vehicle with the modified-oval tank subject to larger steer inputs and relatively low fill volumes approaches unstable state. Under a small steer input, the increase in vehicle forward speed leads to rapidly increased roll response of the vehicle with the conventional tanks and possible rollover, while the vehicle with the optimal tanks remains stable and exhibits considerably lower response. The vehicle with the optimal as well as the currently used tanks exhibit stable behavior during the mild path-change and evasive maneuvers at typical highway speeds. However, the response of the vehicle with the conventional tank cross-sections is considerably larger than that of the vehicle with the optimal tank cross-sections.

CHAPTER 5

VARIABLE SPEED DYNAMIC MODEL OF A PARTLY-FILLED ARTICULATED TANK VEHICLE

5.1 INTRODUCTION

The dynamic behavior and operational safety performance characteristics of various configurations of heavy vehicles carrying rigid cargoes have been extensively reported in the literature. Majority of these studies, however, have been performed under either steering or braking inputs [105-112]. The directional dynamics of articulated vehicles under simultaneous braking and steering have been addressed in a few studies [113, 116, 119]. The variations in speed and tire properties under simultaneous braking and steering result in considerable complexities in the analysis. The combination of variable speed operations, together with cornering, is one of the most commonly encountered highway maneuvers, which has been associated with most vehicle accidents. During variable speed directional maneuvers, the load transfer in the longitudinal direction coupled with the lateral load transfer due to steering, can lead to wheel lock-up resulting in possible yaw instability and/or loss of directional control of the vehicle. The load transfer in the longitudinal and lateral directions is further exaggerated in the case of partly-filled tank vehicles due to unrestricted liquid cargo movement in the roll and pitch planes. This may cause considerable reduction in stability limits and safety performance of the vehicle combinations.

While a number of comprehensive variable speed directional dynamics models of heavy vehicles have been reported in the literature [113, 119, 121, 123], they can not be directly applied for dynamic analysis of partly-filled tank vehicles under combined

braking and steering maneuvers due to lack of consideration of cargo-vehicle interactions. The cargo is generally assumed to be rigidly attached to the trailer structure and thus the cargo interactions with the dynamics of the vehicles are neglected. Dynamic analysis of partially-filled tank vehicles has been addressed in only few studies and under limited maneuvers. Most of the reported studies on dynamics of tank vehicles have considered the movement of liquid cargo in the roll plane alone under constant speed steering maneuvers [172, 173, 178, 183, 187-196]. Few studies have also investigated the fluid motion in the pitch plane alone under straight line braking [197, 198]. The fluid slosh analyses in these studies are mostly based upon either steady-state motion of inviscid fluid or equivalent mechanical models. The cargo movement within a partly-filled tank and its influence on dynamic characteristics of the vehicle combination under simultaneous application of steering and braking, however, have not been addressed due to complexities associated with modeling of fluid dynamic behavior inside the moving tanks.

The three-dimensional tank vehicle model described in Chapter 4 is based upon the assumption of constant vehicle forward speed, and thus can not be used to predict the directional response and stability characteristics of partly-filled tank vehicles under simultaneous steering and braking inputs. A variable-speed tank vehicle model is thus formulated to study the vehicle response under braking and turning maneuvers.

5.2 THREE-DIMENSIONAL MODEL OF A PARTLY-FILLED TANK OF GENERAL CROSS-SECTION

The lateral and longitudinal accelerations, experienced by a tank semitrailer under steering and braking maneuvers, impose equal and opposite inertial accelerations on the

liquid cargo, causing the motion of the liquid in both the lateral (roll plane) and longitudinal (pitch plane) directions. Assuming steady-state and inviscid fluid flow conditions, the entire liquid bulk within a partly-filled tank is considered to move as a rigid bulk. The equation of liquid free surface can thus be determined from the pressure variations in a static fluid. The coordinates of the liquid bulk c.g., corresponding magnitudes of liquid load shift along the lateral, vertical and longitudinal axes, and variations in liquid bulk mass moments of inertia can then be computed based on the equation of the liquid free surface.

5.2.1 Liquid Free Surface Equation

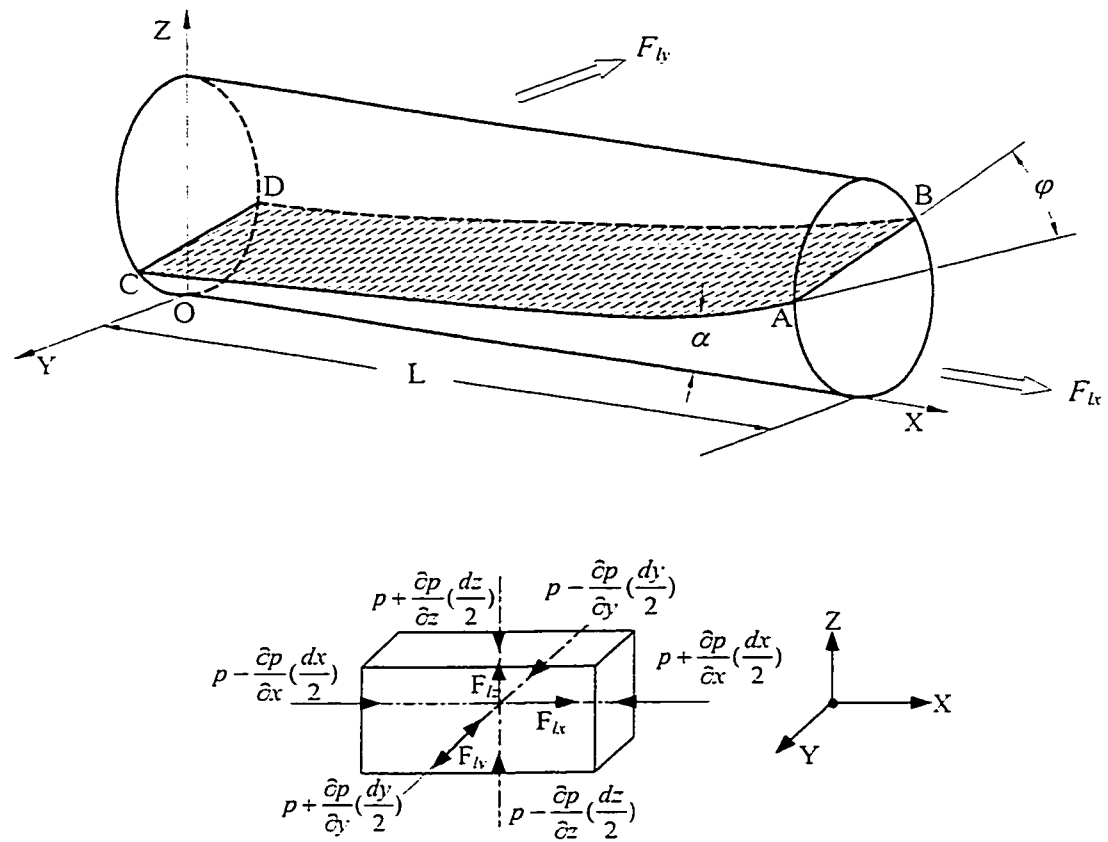


Figure 5.1: Free surface of liquid cargo under application of longitudinal (F_{Lx}) and lateral (F_{Ly}) accelerations, and free body diagram of a liquid element.

The variations in pressure at the center of an element of the liquid bulk in the tank-fixed coordinate system, $XYZO$, can be expressed as [213]:

$$dP = \frac{\partial P}{\partial x} dx + \frac{\partial P}{\partial y} dy + \frac{\partial P}{\partial z} dz \quad (5.1)$$

The forces acting on the element can be expressed by the following equilibrium equation [213]:

$$\frac{1}{\rho} \frac{\partial P}{\partial x} = F_{lx}; \quad \frac{1}{\rho} \frac{\partial P}{\partial y} = F_{ly}; \quad \text{and} \quad \frac{1}{\rho} \frac{\partial P}{\partial z} = F_{lz} \quad (5.2)$$

where F_{lx} , F_{ly} and F_{lz} represent body forces per unit mass of the liquid element along OX , OY and OZ directions, respectively, and ρ is mass density of the liquid cargo. Equations (5.1) and (5.2) yield following expression for the pressure differential for the element:

$$dP = \rho(F_{lx} dx + F_{ly} dy + F_{lz} dz) \quad (5.3)$$

Since the pressure differential due to element vanishes at the free surface, Equation (5.3) reduces to:

$$F_{lx} dx + F_{ly} dy + F_{lz} dz = 0 \quad (5.4)$$

and

$$F_{lx} x + F_{ly} y + F_{lz} z = c_0 \quad (5.5)$$

where c_0 is a constant. The equation of the liquid free surface in terms of x and z coordinates in the three-dimensional tank axis system, shown in Figure 5.1, can be expressed as:

$$f_s(x, z) = \frac{(c_0 - F_{lx} x - F_{lz} z)}{F_{ly}} \quad (5.6)$$

When the liquid cargo experiences pure lateral body force in the roll plane, as in the case of constant speed turning, Equation (5.6) reduces to:

$$f_s(z) = \frac{(c_0 - F_{Lz}z)}{F_{Ly}} \quad (5.7)$$

For the roll plane motion of the liquid within the tank, the lateral and vertical liquid body forces are derived as:

$$F_{Ly} = a_{Ly} \cos \theta_{s2} + \sin \theta_{s2} \text{ and } F_{Lz} = \cos \theta_{s2} - a_{Ly} \sin \theta_{s2} \quad (5.8)$$

where a_{Ly} and θ_{s2} represent the liquid lateral acceleration (in g units) and tank-trailer roll angle, respectively. Equation (5.7) can thus be expressed as:

$$f_s(z) = \frac{a_{Ly} + \tan \theta_{s2}}{1 - a_{Ly} \tan \theta_{s2}} z + \frac{c_0}{1 - a_{Ly} \tan \theta_{s2}} \quad (5.9)$$

For small roll angles, Equation (5.9) reduces to the liquid free surface equation in the roll plane similar to that developed by Rakheja et al. [189]:

$$f_s(z) = \frac{a_{Ly} + \theta_{s2}}{1 - a_{Ly} \theta_{s2}} z + h_0 \quad (5.10)$$

where the tank roll angle, θ_{s2} , is expressed in radians, and the constant term,

$h_0 = \frac{c_0}{1 - a_{Ly} \theta_{s2}}$, represents the intercept of the liquid free surface with the Z -axis.

Under the application of longitudinal acceleration alone, as in the case of straight-line braking, the free surface equation in terms of x coordinate can be derived from Equation (5.5), by letting $F_{Ly}=0$., such that:

$$f_s(x) = \frac{c_0 - F_{Lx}x}{F_{Lz}} \quad (5.11)$$

For small pitch angles, F_{Lx} can be approximated by the liquid longitudinal acceleration (a_{Lx}), while F_{Lz} can be considered as -1 (in g unit). Equation (5.11) then

reduces to the liquid free surface equation in the pitch plane similar to that developed in [196, 197]:

$$f_s(x) = a_{tx}x + h_0 \quad (5.12)$$

where the constant term, $h_0 = -c_0$, represents the intercept of the liquid free surface with the Z-axis.

5.2.2 Patterns of Free Surface and Wetted Volume

Figure 5.2 illustrates some of the patterns of the deflected liquid cargo in the pitch and roll planes of a cleanbore tank, subject to lateral and longitudinal accelerations, respectively. During a straight-line braking maneuver, the liquid free surface may assume one of four possible patterns, depending on fill volume, tank geometry and magnitude of deceleration. The pattern ① could be realized under medium fill volume and low deceleration, while patterns ② and ③ could occur under very low and high fill volumes, respectively. The pattern ④ of the deflected fluid volume corresponds to medium fill condition and high levels of deceleration. The liquid free surface in the roll plane may assume three possible patterns under steady turning maneuvers, as shown in Figure 5.2(b). Pattern ❶ corresponds to medium fill volume, and relatively low levels of roll angle and lateral acceleration excitations. The free surface of liquid under low and high fill volumes may lie on only one side of the vertical axis of the tank, as shown by patterns ❷ and ❸. In case of the generic tank cross-section, the liquid free surface in the roll plane may assume more than 20 specific configurations, depending upon the lateral liquid force and fill volume, as discussed in Chapter 2.

Figure 5.3 illustrates the contours of the free surface under simultaneous application of longitudinal and lateral accelerations. In the absence of the lateral body

force, the plane of liquid free surface is normal to the XOZ plane, while the angle (α) between the two planes defines the liquid free surface gradient in the pitch plane, caused by the longitudinal deceleration. The two intersecting lines of the free surface in the roll planes (tank heads) are thus symmetric about the vertical axis in the YOZ plane, as shown in Figure 5.2(a). Under application of a lateral body force, caused by a steering input, the liquid bulk shifts laterally towards outside of the turn. The resulting angle (ϕ) between the liquid free surface and a horizontal line in the YOZ plane defines the free surface gradient in the roll plane. The resulting liquid free surface is thus no longer normal to the XOZ plane, as shown in Figs. 5.3(a)-(d). The isometric representations of the free surface shown in the figure correspond to four pitch plane patterns illustrated in Figure 5.2(a). The intersections of the free surface with the YOZ planes (tank heads) are indicated by straight lines AB and CD, which may assume three possible patterns illustrated in Figure 5.2 (b).

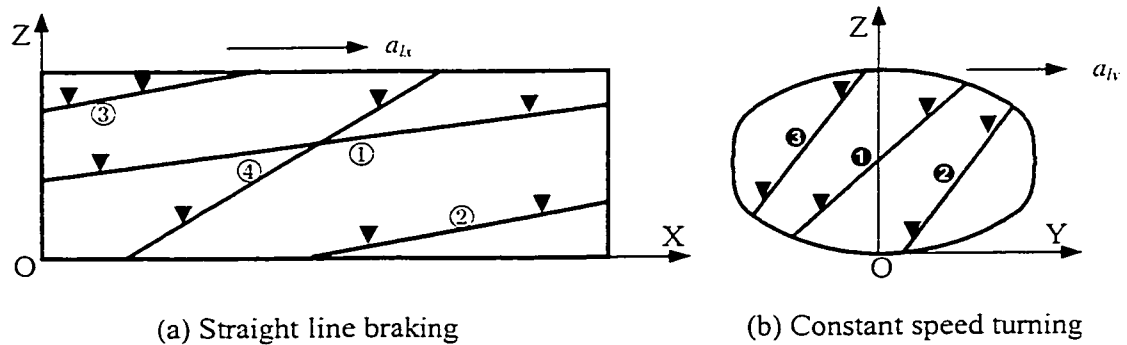
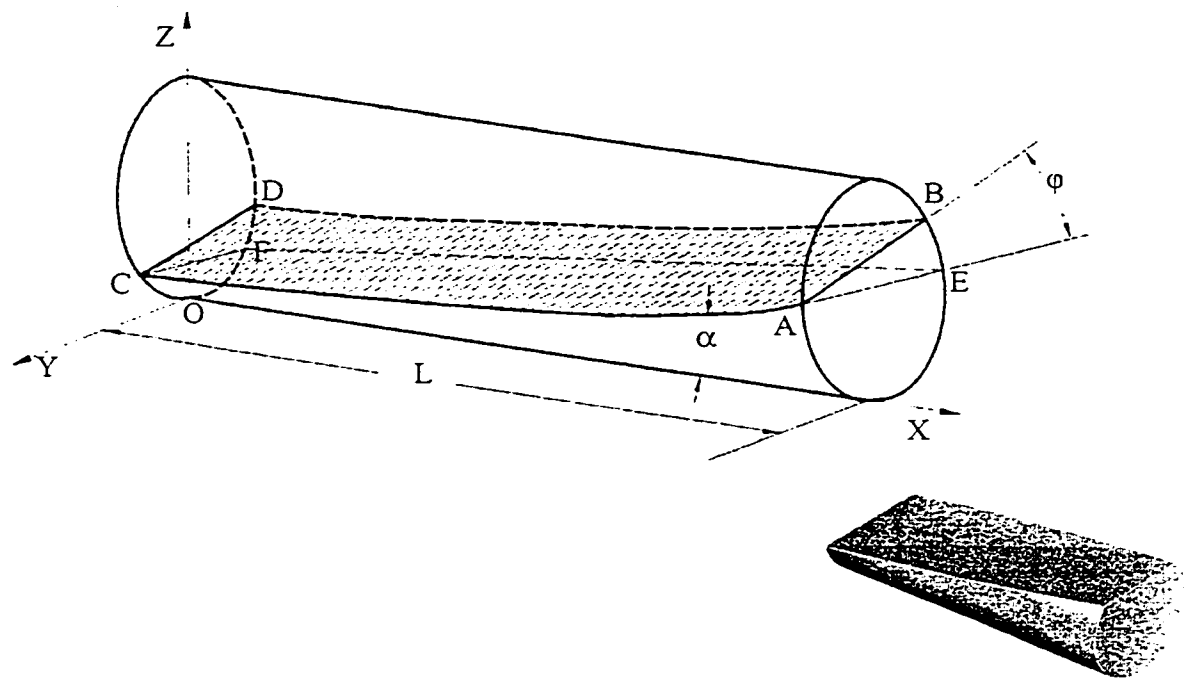
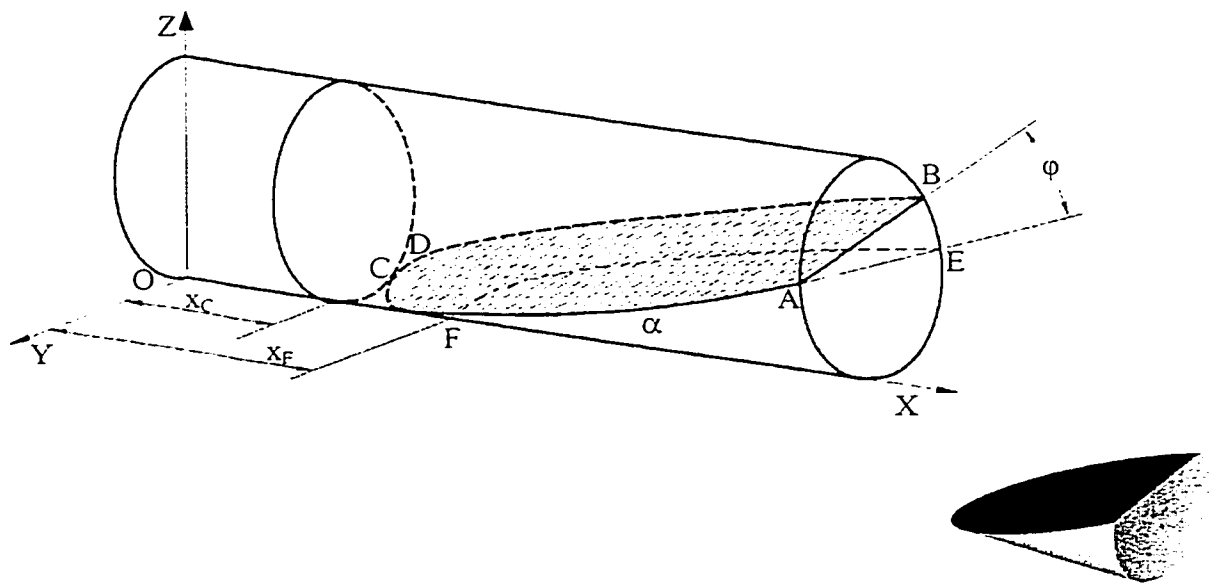


Figure 5.2: Liquid free surfaces under longitudinal and lateral accelerations.

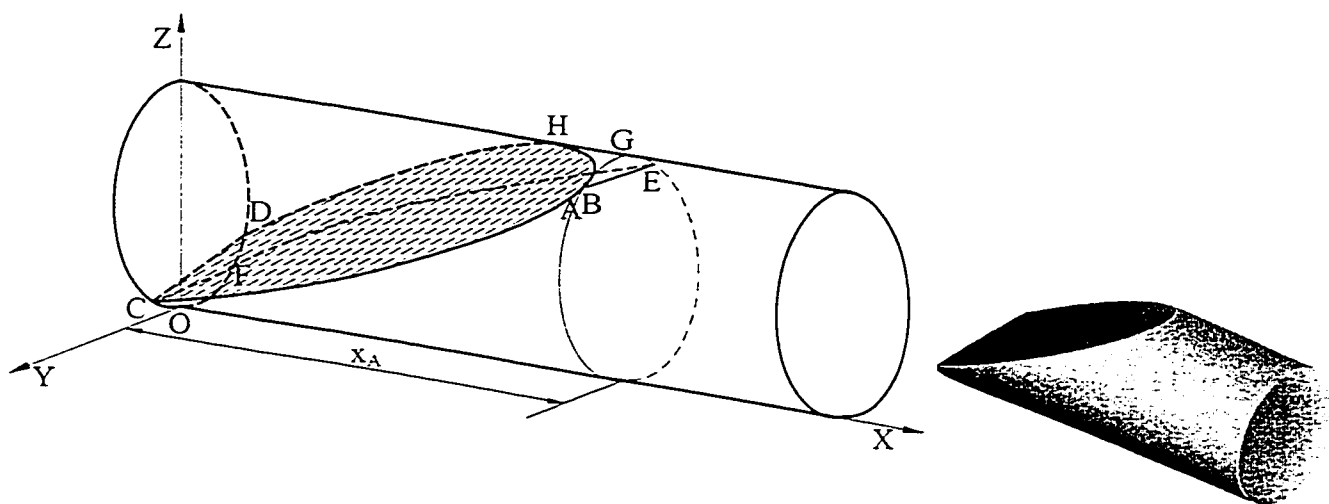


(a) Configuration 1

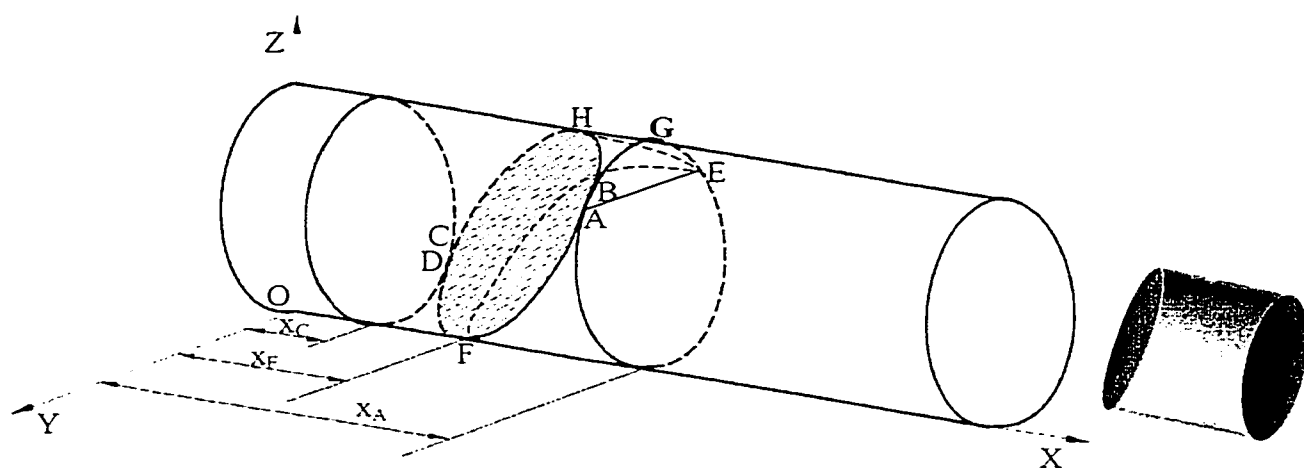


(b) Configuration 2

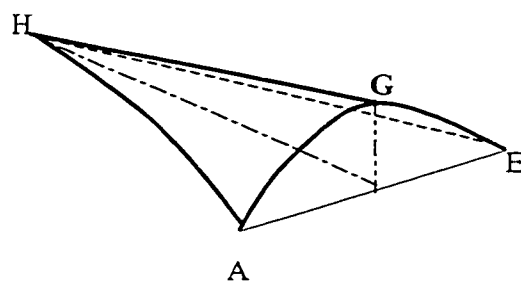
Figure 5.3: Patterns of liquid free surface in a partly-filled circular tank under simultaneous application of longitudinal and lateral accelerations.



(c) Configuration 3



(d) Configuration 4



(e) Enlarged geometry of volume AHEG present in configurations 3 and 4

Figure 5.3: Patterns of liquid free surface in a partly-filled tank under simultaneous application of longitudinal and lateral accelerations.

In Figure 5.3(a), the liquid free surface intersects the two heads of the tank at points A, B, C, and D. The plane of the free surface is presented by a plane ACFE, normal to the XOZ plane, and a deflected wedge shaped volume formed by the planes ABE and CDF. The plane ACFE represents the free surface pattern similar to that realized under application of straight line braking alone. The liquid volume in the tank thus consists of two components, the volume beneath the plane ACFE, and the volume between the plane of free surface ABDC and plane ACFE. Under low fill volumes, the free surface of liquid may assume a pattern shown in Figure 5.3(b). The free surface intersects the right head of the tank at points A and B, and the shell at point C (coincident with D). Point F represents the lowest intersection point of the free surface. The straight line AE and curve EF are defined in order to express the liquid volume in two components: beneath the plane AEF, and between the free surface plane and plane AEF.

Under high fill volumes, the free surface intersects the left head of the tank at points C and D, and the rightmost intersection point with the tank surface (shell) is denoted by A(B), while H represents the highest point on the intersecting curves, as shown in Figure 5.3(c). In this case, the liquid volume in the tank is composed of four components: (i) the volume underneath plane AEFC normal to the plane XOZ; (ii) between the free surface AHDC and AEFC plane; (iii) within the curved area AHEG, shown in Figure 5.3(e), and plane AHE; and (iv) the filled volume on the right side of the plane AGE. In Figure 5.3(d), the free surface is denoted by plane AHCF, where points A and C overlap points B and D, respectively. The left- and right-most points on the intersecting curves are represented by points C(D) and A(B), respectively, while points H and F represent the highest and lowest intersection points with the tank surface. The

liquid volume within the partly-filled tank consists of four components: (i) the volume underneath the plane AEF; (ii) between the plane of free surface AHCF and plane AEF; (iii) between the curved surface AHEG, shown in Figure 5.3(e), and plane AHE; and (iv) the completely filled volume on the right side of plane AGE.

For a particular liquid free surface configuration, the volume of liquid V_f within the tank can be derived from the following volume integral:

$$V_f = \iiint_V dV \quad (5.13)$$

where V defines the domain of volume integration. The volume integrals and domains of integration corresponding to the four different free surface patterns, shown in Figure 5.3, are summarized in Table 5.1.

Table 5.1: Domains of volume integration.

Free surface configuration	Integral limits
1	$2 \int_0^L \int_0^{Z_{AC}} \int_0^{f_c} dV + \int_0^L \int_{Z_{AC}}^{Z_{BD}} \int_{f_c} dV$ <p>Z_{AC} and Z_{BD} are computed from equations of lines AC and BD as functions of x</p>
2	$2 \int_{x_F}^L \int_0^{Z_{AF}} \int_0^{f_c} dV + \int_{x_C}^L \int_{Z_{AC}}^{Z_{BD}} \int_{f_c} dV$ <p>Z_{AF} is computed from the equation of intersecting curve AF as a function of x</p>
3	$2 \int_0^{x_A} \int_0^{Z_{AC}} \int_0^{f_c} dV + \int_0^{x_A} \int_{Z_{AC}}^{Z_{BD}} \int_{f_c} dV + 2 \int_{x_H}^{x_A} \int_{Z_{BH}}^{H_2} \int_0^{f_c} dV + 2 \int_0^{L-x_A} \int_0^{H_2} \int_0^{f_c} dV$ <p>Z_{BH} is computed from the equation of intersecting curve BH as a function of x</p>
4	$2 \int_{x_F}^{x_A} \int_0^{Z_{AC}} \int_0^{f_c} dV + \int_{x_C}^{x_A} \int_{Z_{AC}}^{Z_{BD}} \int_{f_c} dV + 2 \int_{x_H}^{x_A} \int_{Z_{BH}}^{H_2} \int_0^{f_c} dV + 2 \int_0^{L-x_A} \int_0^{H_2} \int_0^{f_c} dV$

The integration limits x_A , x_C , x_F and x_H in Table 5.1 define the x -coordinates of intersecting points A, C, F and H, respectively, as shown in Figure 5.3. The lower limit of integration f_s is computed from Equation (5.6) for the liquid free surface, while the upper limit f_c denotes the right-hand-side equation of the tank cross-section and is derived from the equation for each circular arc of the generic tank geometry (Equation (2.2)), given by:

$$f_c = Y_{ci} + \sqrt{R_i^2 - (z - Z_{ci})^2} \quad \text{subject to } Z_{i-1} \leq z < Z_i; (i=1, \dots, 5) \quad (5.14)$$

where Y_{ci} and Z_{ci} represent the coordinates of center of arc i , and R_i is its radius, while Z_i denotes the maximum value of vertical coordinate of arc i . For a circular cross-section tank, Equation (5.14) reduces to:

$$f_c = \sqrt{2Rz - z^2} \quad (5.15)$$

where R is tank radius. The vertical coordinates, Z_{AC} and Z_{BD} , of the intersecting curves, AC and BD, are derived as functions of x from simultaneous solution of Equations (5.6) and (5.14). The vertical coordinates, Z_{AF} and Z_{BH} , of the intersecting curves, AF and BH, are computed in a similar manner. For a circular cross-section tank, the magnitudes of the vertical coordinates Z_{AC} and Z_{BD} are derived as:

$$\begin{aligned} Z_{AC} &= -\frac{1}{2} \left[B_0 + \sqrt{B_0^2 - 4 \left(\frac{F_z^2}{F_y^2} + 1 \right) \left(\frac{c_0 - F_x x}{F_y} \right)^2} \right]; \text{ and} \\ Z_{BD} &= -\frac{1}{2} \left[B_0 - \sqrt{B_0^2 - 4 \left(\frac{F_z^2}{F_y^2} + 1 \right) \left(\frac{c_0 - F_x x}{F_y} \right)^2} \right] \end{aligned} \quad (5.16)$$

where $B_0 = \frac{-2F_z}{F_y^2} (c_0 - F_x x) - 2R$.

A numerical algorithm is formulated to identify the configuration of the free surface of liquid within the tank and to solve the volume integral (Equation (5.13))

subject to a particular combination of longitudinal and lateral body force excitations. The magnitude of the unknown constant c_0 in Equation (5.6) is computed using an iterative algorithm, based upon constant fluid volume under the free surface. The initial fill volume of liquid within the partly-filled tank is computed from the fill height and the tank geometry, as $V_0 = LA_f$, where A_f is the wetted cross-section area under static conditions. The starting value of c_0 is assumed to be equal to the product of the initial free surface height and the z component of the body force (F_{tz}). The algorithm further computes the coordinates of all possible intersection points of the free surface with the tank cross-section by simultaneous solution of Equations (5.6) and (5.14) for each value of x coordinate in the integration process. The analysis then identifies the particular circular arc on which the liquid free surface intersects the tank cross-section by comparing the coordinates of the possible intersection points with the tank cross-section characteristic coordinates, (Y_i, Z_i) , which are described in Section 2.3. Based on this, the appropriate integral limits along the Z -axis and the corresponding arc equation, f_c , are selected for the volume integration. The total liquid volume under the deflected free surface is then evaluated numerically using the volume integrals corresponding to the particular free surface configuration, as described in Table 5.1. The value of c_0 is adjusted in an iterative manner until convergence is achieved between V_f and V_0 .

5.2.3 Liquid Load Shift and Mass Moments of Inertia

The instantaneous coordinates of c.g. of the liquid bulk, (X_l, Y_l, Z_l) , are evaluated from the following moment integrals:

$$X_l = \frac{1}{V_f} \iiint_V x dV; Y_l = \frac{1}{V_f} \iiint_V y dV; \text{ and } Z_l = \frac{1}{V_f} \iiint_V z dV \quad (5.17)$$

The shifts in the coordinates of liquid bulk c.g., caused by applications of lateral and longitudinal excitation, can be expressed as:

$$\Delta X_l = \frac{L}{2} - X_l; \Delta Y_l = Y_l; \text{ and } \Delta Z_l = Z_l - Z_{l0} \quad (5.18)$$

where Z_{l0} is the static c.g. height of the liquid cargo from the tank base. The liquid c.g. coordinates in terms of trailer sprung mass body-fixed coordinate system are expressed as:

$$X_{l2} = X_l - X_b; Y_{2l} = Y_l; \text{ and } Z_{l2} = -(Z_l + Z_b) \quad (5.19)$$

where X_b denotes the longitudinal coordinate of empty tank trailer c.g. with respect to the tank body-fixed coordinate system (a positive value indicates that c.g. lies ahead of the origin of the tank body-fixed system), and Z_b represents the distance between the tank base and c.g. of empty tank trailer structure.

The mass moments of inertia of the liquid cargo also vary considerably with variations in the free surface. The instantaneous values of mass moments of inertia of the deflected liquid bulk with respect to the tank body-fixed coordinate system are computed from three volume integrals, as expressed by Equation (4.3). The moments of inertia of the deflected liquid bulk with respect to the tank trailer body-fixed coordinate system are then computed from Equation (4.5).

5.3 VARIABLE SPEED YAW/ROLL MODEL OF AN ARTICULATED TANK VEHICLE

The dynamic model for directional response and stability analysis of a partly-filled tank vehicle under simultaneous braking and turning maneuvers can be effectively developed by integrating the three-dimensional quasi-static fluid slosh model, developed in Section 5.2, into a variable speed yaw/roll dynamic model of a rigid cargo vehicle

[119]. A five-axle articulated tank vehicle combination comprising of a three-axle tractor and a two-axle semitrailer is considered to study its dynamic characteristics under combined braking and turning maneuvers. The tractor consists of a single front axle with single tires that can be arbitrarily steered. All other axles on the vehicle combination can be represented as single or tandem axles with single or dual wheel sets.

The articulated tank vehicle combination is modeled as two sprung masses: the sprung mass of the tractor, m_1 , and the tare mass of the semitrailer structure and empty tank, m_2 . The liquid cargo mass, m_l , is considered as a floating mass with respect to c.g. of the trailer sprung mass. The axles are modeled as independent unsprung masses, m_{ui} ($i=1, 2, \dots, 5$). The two sprung masses of the vehicle are characterized as rigid bodies with six-DOF, including longitudinal, lateral, vertical, roll, pitch and yaw motions. The unsprung masses are free to roll and bounce (two-DOF) with respect to the sprung masses to which they are attached. A rotational DOF is defined for each of the ten wheel sets to perform braking analysis. The torsional flexibility due to tractor frame, and the coupling between the tractor and trailer sprung masses are represented by two lumped torsional compliances. The roll stiffness due to anti-sway bars and linkages is represented by auxiliary roll stiffness between the sprung and unsprung masses for each axle.

The brake system on each axle of the vehicle combination is represented by the input pressure and output torque characterized with the time lag (time delay between the time of pedal application and the onset of pressure rise in the brake chamber), rise time (time required to reach 63% of the steady-state step response) and the brake torque ratio (the resulting brake torque per unit of air pressure in the brake chamber). These properties are described either in a linear fashion by a brake torque coefficient or by their

nonlinear characteristics using lookup tables. Although the model development is carried out for pneumatic brake systems commonly used in heavy vehicles, the characteristics of hydraulic brake systems can also be incorporated through appropriate brake system models, where the brake lag and rise times are considered negligible [119]. In the simulation model, the brake torque is applied to the wheel causing it to decelerate, while the tire brake force is derived from longitudinal slip in conjunction with the tire model. At a given instant, a portion of the brake torque may thus be devoted to achieving deceleration of the wheel.

The directional dynamic model of the articulated tank vehicle is developed subject to a number of simplifying assumptions, namely: (i) the sprung and unsprung masses move as one rigid body in yaw, however, they experience independent roll and pitch motions; (ii) the suspension springs experience deflection along the unsprung mass fixed k -direction and roll about the user-defined suspension roll center, located at a fixed distance below the sprung mass c.g.; the longitudinal and lateral forces arising from tires are thus applied directly at the spring locations resulting in forces and moments about the sprung mass c.g.; (iii) the suspension spring forces are modeled as nonlinear functions of suspension deflections using look-up tables, while the dissipative properties are characterized by Coulomb friction (CF_{ij}) and viscous damping coefficient (C_{ij}); (iv) sprung mass roll and pitch rotations are assumed to be small in the implementation of the mathematical equations, such that the simulations can be considered valid only up to a maneuver limit at which a wheel lift-off occurs; and (v) the cross-products of mass moments of inertia of the sprung masses are considered negligible to avoid dynamic coupling among the three rotational-DOF (roll, pitch and yaw).

The articulation is modeled as a force and moment constraint in which tractor and semitrailer are subject to equal and opposite forces and moments dependent on the difference in the fifth wheel position and orientation as measured on the tractor and semitrailer. Initially the fifth wheel position of the tractor and the semitrailer are assumed to be identical. As the simulation run proceeds, however, forces developed at the tire-road interface will cause disparate paths for the fifth wheel position of the tractor and the semitrailer; a distance will thus develop between them. A linear spring and dashpot are the assumed connection to model the force at the fifth wheel. The direction of the restraining hitch force is assumed to be along a line through the fifth wheel location of the tractor and semitrailer. The fifth wheel moment restraint is similarly represented by a torsional spring-damper connection between the tractor and semitrailer, and the effects of pitch rotation and the articulation angle are neglected, since the most commonly used fifth wheel and inverted fifth wheel couplings permit relative yaw and pitch rotations between the leading and the trailing units, but are considerably stiff in roll. The roll moment transmitted through the fifth wheel is assumed to be applied along the longitudinal axis of the tractor.

The roll and pitch planes of the three-dimensional model of the articulated tank vehicle are shown in Figures 5.4 and 5.5, together with the various coordinate systems. As shown in the figures, the entire liquid cargo within the tank is assumed to move as a rigid body, due to the lateral and longitudinal accelerations of the tank trailer subject to combined steering and braking operations, as described in Section 5.2. The motion of the liquid free surface creates a new deflected shape of the liquid bulk within the tank, resulting in shift of the coordinates of the liquid cargo c.g. from its static position C_{10}

$(L/2, 0, Z_{i0})$ to $C_l(X_l, Y_l, Z_l)$ in terms of the tank body-fixed coordinate system, and considerable variations in its mass moments of inertia properties.

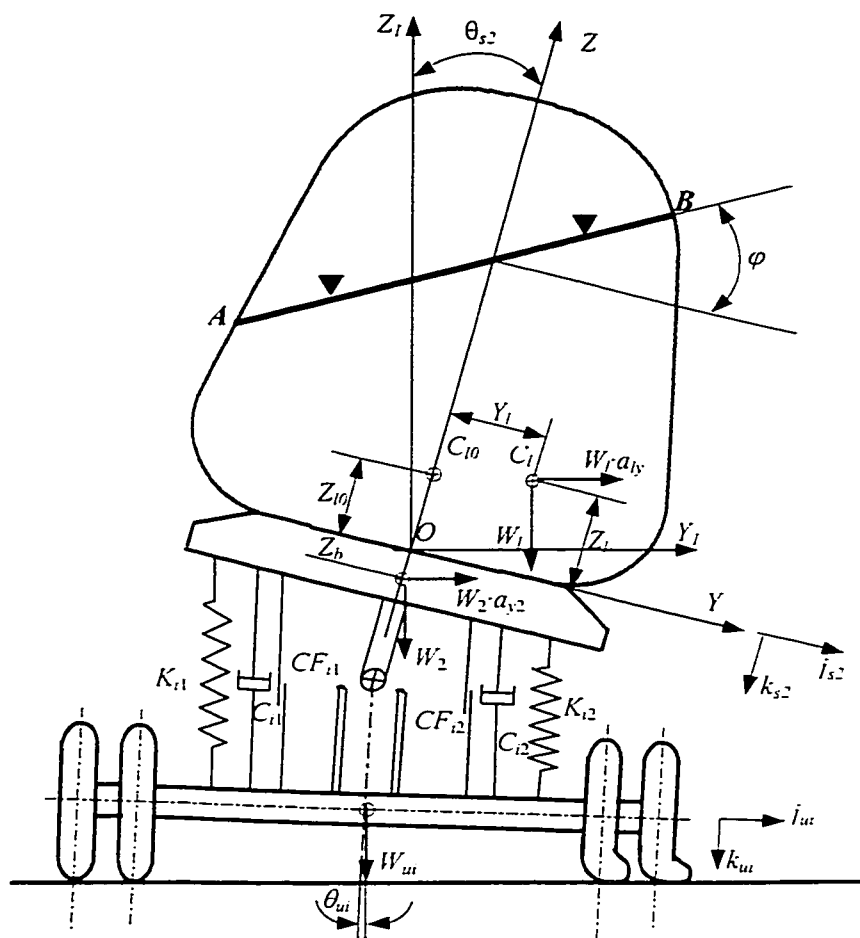


Figure 5.4: Roll plane representation of the partially-filled three-dimensional tank vehicle model.

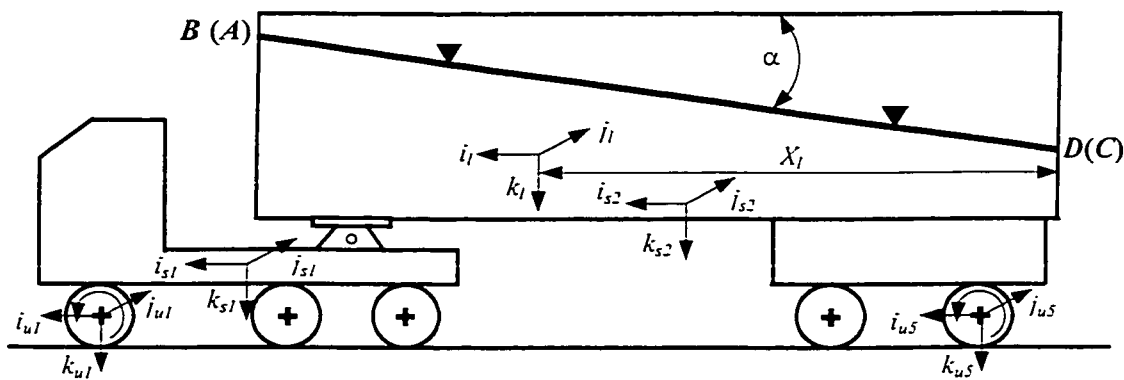


Figure 5.5: Pitch plane representation of the partially-filled three-dimensional tank vehicle model and attached coordinate systems.

5.4 EQUATIONS OF MOTION

The equations of motion of the variable speed three-dimensional model of the articulated tank vehicle system are derived upon consideration of dynamics of several subsystems and their interactions. In order to interpret the equations of motion of the vehicle system, it is convenient to define appropriate coordinate systems. The dynamics of the vehicle subsystems are thus described in orthogonal coordinate systems defined in the following subsection.

5.4.1 Coordinate Systems

Three orthogonal coordinate systems are defined as following:

- (1) An inertial coordinate system: a right-hand orthogonal coordinate system (i_n, j_n, k_n) fixed in space is used as a reference point from which vehicle motions and attitudes are defined. The origin is placed at the tractor sprung mass c.g. at the beginning of the simulation. The inertial coordinate system is aligned with the gravity vector and the horizontal projection of the tractor longitudinal axis. The axes are defined according to the SAE convention, where i_n is horizontal axis out of the front of the vehicle, j_n is horizontal axis emerging from right side of the vehicle and k_n is vertical axis pointing downwards.
- (2) Body fixed coordinate systems: a vehicle-fixed coordinate system is attached to each of the sprung mass c.g. ($i_{sf}, j_{sf}, k_{sf}; f=1, 2$), which defines the location and attitude of the sprung mass with respect to the inertial coordinate system. The three angles required to define the orientation of each of the sprung mass axis system with respect to the inertial coordinate system are roll (θ_{sf}), pitch (α_{sf}) and yaw (φ_{sf}).

- (3) Axle axis systems: an axle axis system is fixed to each axle ($i_{ui}, j_{ui}, k_{ui}; i=1, 2, \dots, 5$) and defines the direction of the unsprung mass, relative to the respective sprung mass-fixed coordinate system.

The axis system of each sprung mass is related to the inertial system by the following transformation:

$$\begin{Bmatrix} \overline{i}_n \\ \overline{j}_n \\ \overline{k}_n \end{Bmatrix} = D_{sf} \begin{Bmatrix} \overline{i}_s \\ \overline{j}_s \\ \overline{k}_s \end{Bmatrix}_f \quad (f=1, 2) \quad (5.20)$$

where the transformation matrix D_{sf} can be derived using three sequential steps of rotations (roll, pitch and yaw) [184].

$$D_{sf} = D_{roll}, D_{pitch}, D_{yaw}, \quad (5.21)$$

where D_{rollf} , D_{pitchf} and D_{yawf} represent roll, pitch and yaw rotation matrices, respectively, and are given by:

$$\begin{aligned} D_{roll,} &= \begin{bmatrix} 1 & 0 & 0 \\ 0 & \cos \theta_s & -\sin \theta_s \\ 0 & \sin \theta_s & \cos \theta_s \end{bmatrix}_f \\ D_{pitch,} &= \begin{bmatrix} \cos \alpha_s & 0 & \sin \alpha_s \\ 0 & 1 & 0 \\ -\sin \alpha_s & 0 & \cos \alpha_s \end{bmatrix}_f \\ D_{yaw,} &= \begin{bmatrix} \cos \varphi_s & -\sin \varphi_s & 0 \\ \sin \varphi_s & \cos \varphi_s & 0 \\ 0 & 0 & 1 \end{bmatrix}_f \end{aligned} \quad (5.22)$$

where θ_{sf} , α_{sf} and φ_{sf} are the roll, pitch and yaw angles, respectively, of sprung unit f . Assuming small pitch angles of the sprung masses, matrix D_{pitchf} can be simplified by replacing $\sin\alpha_{sf}$ by α_{sf} and $\cos\alpha_{sf}$ by 1.0. Expanding Equation (5.21) thus yields:

$$D_{sf} = \begin{bmatrix} \cos\varphi_s & -\sin\varphi_s \cos\theta_s + \alpha_s \cos\varphi_s \sin\theta_s & \sin\varphi_s \sin\theta_s + \alpha_s \cos\varphi_s \cos\theta_s \\ \sin\varphi_s & \cos\varphi_s \cos\theta_s + \alpha_s \sin\varphi_s \sin\theta_s & -\cos\varphi_s \sin\theta_s + \alpha_s \sin\varphi_s \cos\theta_s \\ -\alpha_s & \sin\theta_s & \cos\theta_s \end{bmatrix}_f \quad (5.23)$$

Each unsprung mass is permitted to roll and bounce with respect to the sprung mass to which it is attached. The orientation of unsprung mass i fixed system with respect to associated sprung mass f axis system can be defined by the following transformation:

$$\begin{Bmatrix} \overline{i}_s \\ \overline{j}_s \\ \overline{k}_s \end{Bmatrix}_f = D_{fi} \begin{Bmatrix} \overline{i}_u \\ \overline{j}_u \\ \overline{k}_u \end{Bmatrix}_i \quad (f=1, 2; i=1, 2, \dots, 5) \quad (5.24)$$

where the transformation matrix D_{fi} is defined by roll (θ_{sf} and θ_{ui}) and pitch (α_{sf}) angles, given by [184]:

$$D_{fi} = \begin{bmatrix} 1 & -\alpha_{sf} \sin\theta_{ui} & -\alpha_{sf} \cos\theta_{ui} \\ \alpha_{sf} \sin\theta_{sf} & \cos(\theta_{sf} - \theta_{ui}) & \sin(\theta_{sf} - \theta_{ui}) \\ \alpha_{sf} \cos\theta_{sf} & -\sin(\theta_{sf} - \theta_{ui}) & \cos(\theta_{sf} - \theta_{ui}) \end{bmatrix} \quad (f=1, 2; i=1, 2, \dots, 5) \quad (5.25)$$

5.4.2 Equations of Motion

Equations of motion of the variable speed three-dimensional model of the partially-filled articulated tank vehicle are derived by integrating forces and moments arising from the quasi-static fluid equations, Equations (4.5) and (5.17), and the articulated vehicle. The motion coordinates of each of the sprung masses are determined from the summation of forces and moments in the respective body-fixed axis system,

arising from tires (acting through the unsprung mass of the axle and suspension), articulation constraint, gravity and the liquid cargo shift.

The dynamics of each sprung mass is described by six second-order differential equations. Application of Newton's law of motion yields six equations for each of the sprung masses. The equations of translational motions of the sprung masses are derived in the following general form, while the force components for rigid cargo vehicles are derived in details in [218, 219].

Longitudinal force equations:

$$m_f a_f \vec{i}_{sf} + m_{lf} a_{lf} \vec{i}_{sf} = (\text{Longitudinal components of constraint forces}) + (\text{Longitudinal components of suspension forces}) + \text{Longitudinal component of forces due to gravity}; (f=1, 2) \quad (5.26)$$

Lateral force equations:

$$m_f a_f \vec{j}_{sf} + m_{lf} a_{lf} \vec{j}_{sf} = (\text{Lateral components of constraint forces}) + (\text{Lateral components of suspension forces}) + (\text{Lateral component of forces due to gravity}); (f=1, 2) \quad (5.27)$$

Vertical force equations:

$$m_f a_f \vec{k}_{sf} + m_{lf} a_{lf} \vec{k}_{sf} = (\text{Vertical components of constraint forces}) + (\text{Vertical components of suspension forces}) + (\text{Vertical component of forces due to gravity}); (f=1, 2) \quad (5.28)$$

where $f=1, 2$, represent tractor and trailer sprung mass units, respectively, and m_f and m_{lf} are the sprung and liquid cargo masses, respectively, of unit f , while $m_{ll}=0$. $\vec{i}_{sf}, \vec{j}_{sf}$ and \vec{k}_{sf} are the three unit vectors describing the body coordinate system fixed on unit f , and a_f is the acceleration vector at c.g. of the sprung mass f , expressed by:

$$a_f = (\ddot{u}_f + q_f w_f - r_f v_f) \bar{i}_{sf} + (\ddot{v}_f + r_f u_f - p_f w_f) \bar{j}_{sf} + (\ddot{w}_f + p_f v_f - q_f u_f) \bar{k}_{sf}; (f=1,2) \quad (5.29)$$

a_{lf} ($f=2$) is the acceleration vector of the liquid bulk c.g., $a_{l2} = a_{lx} \bar{i}_{s2} + a_{ly} \bar{j}_{s2} + a_{lz} \bar{k}_{s2}$,

derived as:

$$\begin{aligned} a_{l2} = & \{a_{x2} + \dot{q}_2 Z_{l2} - \dot{r}_2 Y_{l2} + q_2(p_2 Y_{l2} - q_2 X_{l2}) - r_2(r_2 X_{l2} - p_2 Z_{l2})\} \bar{i}_{s2} \\ & + \{a_{y2} + \dot{r}_2 X_{l2} - \dot{p}_2 Z_{l2} + r_2(q_2 Z_{l2} - r_2 Y_{l2}) - p_2(p_2 Y_{l2} - q_2 X_{l2})\} \bar{j}_{s2} \\ & + \{a_{z2} + \dot{p}_2 Y_{l2} - \dot{q}_2 X_{l2} + p_2(r_2 X_{l2} - p_2 Z_{l2}) - q_2(q_2 Z_{l2} - r_2 Y_{l2})\} \bar{k}_{s2} \end{aligned} \quad (5.30)$$

where u_f , v_f and w_f are the translational (longitudinal, lateral and vertical) velocities of unit f along its body-fixed coordinates \bar{i}_{sf} , \bar{j}_{sf} and \bar{k}_{sf} ($f=1, 2$), respectively. \dot{u}_f , \dot{v}_f and \dot{w}_f are the corresponding translational accelerations, which are solved from the equations of motion at the beginning of each integration time step in the computer program. a_{x2} , a_{y2} and a_{z2} are the components of trailer sprung mass acceleration (a_2) along the trailer body-fixed coordinate system. p_f , q_f and r_f are the rotational velocities (roll, pitch and yaw rates) of sprung mass f with respect to the inertial coordinate system, while \dot{p}_f , \dot{q}_f and \dot{r}_f are the corresponding angular accelerations. X_{l2} , Y_{l2} and Z_{l2} are the coordinates of the instantaneous c.g. of the liquid bulk in terms of tank trailer body-fixed system.

The three components of forces due to gravity of the trailer sprung mass and liquid cargo are computed as:

$$\begin{Bmatrix} F_{gx} \\ F_{gy} \\ F_{gz} \end{Bmatrix} = D_f^{-1} \begin{Bmatrix} 0 \\ 0 \\ (m_f + m_{lf})g \end{Bmatrix} = (m_f + m_{lf})g \begin{Bmatrix} -\alpha_{sf} \\ \sin \theta_{sf} \\ \cos \theta_{sf} \end{Bmatrix} \quad (5.31)$$

The equations of rotational motions of each sprung mass are expressed in the following general form:

Roll moment equations:

$$(I_{xf} + I_{xlf})\dot{p}_f - (I_{yf} + I_{ylf} - I_{zf} - I_{zlf})q_f r_f = (\text{Roll moment due to constraint}) + (\text{Roll moments due to suspensions}) + (\text{Roll moment due to liquid forces}); \quad (f=1, 2) \quad (5.32)$$

Pitch moment equations:

$$(I_{yf} + I_{ylf})\dot{q}_f - (I_{zf} + I_{zlf} - I_{xf} - I_{xlf})p_f r_f = (\text{Pitch moment due to constraint}) + (\text{Pitch moments due to suspensions}) + (\text{Pitch moment due to liquid forces}); \quad (f=1, 2) \quad (5.33)$$

Yaw moment equation:

$$(I_{zf} + \sum_{i=N_1}^{N_2} I_{zui} + I_{zlf})\dot{r}_f - (I_{xf} + I_{xlf} - I_{yf} - I_{ylf})p_f q_f = (\text{Yaw moment due to constraint}) + (\text{Yaw moments due to tires}) + (\text{Yaw moment due to liquid forces}); \quad (f=1, 2) \quad (5.34)$$

where I_{xf} , I_{yf} and I_{zf} are the roll, pitch and yaw mass moments of inertia of sprung mass f , and I_{xlf} , I_{ylf} and I_{zlf} are the roll, pitch and yaw mass moments of inertia of the liquid cargo with respect to the body-fixed system of sprung mass f . I_{zui} is the yaw mass moment of inertia of unsprung mass i . N_1 and N_2 are the axle numbers on each sprung mass unit, i.e., $N_1=1$ and $N_2=3$ for $f=1$; and $N_1=4$ and $N_2=5$ for $f=2$. The forces and moments due to liquid cargo, however, vanish for the tractor unit ($f=1$).

The three moment components due to inertial forces in the trailer sprung mass axis system are computed by:

$$\begin{Bmatrix} M_{lx} \\ M_{ly} \\ M_{lz} \end{Bmatrix} = \begin{Bmatrix} X_{l2} \\ Y_{l2} \\ Z_{l2} \end{Bmatrix} \times \left[m_{l2} \begin{Bmatrix} a_{lx} \\ a_{ly} \\ a_{lz} \end{Bmatrix} + D_2^{-1} \begin{Bmatrix} 0 \\ 0 \\ m_{l2}g \end{Bmatrix} \right]$$

$$= m_{l2} \left\{ \begin{array}{l} Y_{l2}a_{lz} - Z_{l2}a_{ly} + g(Y_{l2} \cos \theta_{sf} - Z_{l2} \sin \theta_{sf}) \\ Z_{l2}a_{lx} - X_{l2}a_{lz} - g(Z_{l2}\alpha_{sf} + X_{l2} \cos \theta_{sf}) \\ X_{l2}a_{ly} - Y_{l2}a_{lx} + g(X_{l2} \sin \theta_{sf} + Y_{l2}\alpha_{sf}) \end{array} \right\} \quad (5.35)$$

where a_{lx} , a_{ly} and a_{lz} are components of acceleration vector of the liquid cargo along the trailer sprung mass coordinates \bar{i}_{s2} , \bar{j}_{s2} and \bar{k}_{s2} , respectively.

The dynamics of each unsprung mass is described by two second-order differential equations, derived using the respective body-fixed coordinate system. The equations describing the motion of each of the unsprung masses are derived in the following form:

Unsprung mass vertical force equation:

$$m_{ui}a_{uzi} = (\text{Vertical forces due to suspension forces}) + (\text{Vertical forces due to tires}) + m_{ui}g : \quad (i=1, 2, \dots, 5) \quad (5.36)$$

Unsprung mass roll moment equation:

$$I_{xui}\dot{p}_{ui} = (\text{Roll moments due to suspension forces}) + (\text{Roll moments due to tire forces}) : \quad (i=1, 2, \dots, 5) \quad (5.37)$$

where a_{uzi} is vertical acceleration of unsprung mass i and I_{xui} is its roll mass moment of inertia. p_{ui} is roll rate of axle i .

The angular motion of each wheel is described by one differential equation. The equation of angular motion for each wheel is derived as:

$$J_k\dot{\omega}_k = F_{xk}R_{tk} - T_{bk} ; (k=1, 2, \dots, 10) \quad (5.38)$$

where T_{bk} is braking torque about the spin axis of the k th wheel, F_{xk} is longitudinal force developed at the tire-road interface, R_{tk} is height of the axle assumed to be equal to the effective rolling radius of the tire, and J_k is effective mass moment of inertia of the wheel

including tire, rim, and rotating components of the braking system. ω_k is wheel angular velocity about the spin axis. For convenience of analysis, the ten wheels of the vehicle are appropriately numbered, with 1, 3, 5, 7, 9 representing the wheels on the right track, and 2, 4, 6, 8, 10 representing the wheels on the left track of the vehicle, starting from the steering axle wheel.

In the case of a linear brake system model, the attempted brake torque on the k th moving wheel, T_{bk} , is calculated as $T_{bk}=B_{br} \cdot P_{bk}$, where P_{bk} represents the effective line pressure at the brake minus the pushout pressure, including time lag and rise time, while B_{br} represents the brake torque coefficient for the wheel. However, if the wheel approaches lock-up condition, the actual brake torque is limited by the tire-road friction. In the case of a brake system model with nonlinear characteristics, a brake lookup table (treadle pressure versus brake torque) is used to define the local brake torque coefficient [119].

The external forces and moments on the right-hand-side of the equations of motion due to suspensions, tires and articulation constraint are discussed in the following subsections.

5.4.3 Tire Forces

Vehicle motions are primarily caused by forces and moments developed at the tire-road interface. These forces arising from powertrain, brake system and steering inputs, directly influence the directional characteristics and braking performance of the vehicle. The braking and cornering forces, developed by a pneumatic tire, are strongly nonlinear functions of side-slip angle, camber angle, longitudinal deformation slip, normal load, road friction characteristics, and vehicle speed. A large number of tire

models based upon measured data and regression functions have been proposed to predict tire forces and moments, and considerable efforts are being made to develop more effective models to accurately predict the forces and moments under wide range of operating conditions [37, 214, 215]. Tire models for vehicle dynamic analysis, in general, may be grouped into two categories [215]: (i) physical models, which attempt to represent tire forces and moments based on analysis of tire mechanics; and (ii) empirical and semi-empirical models or black-box models, which predict tire forces and moments from measured data using regression techniques. In physical models, tire forces and moments are derived from a mathematical description of the tire structure and its deformation mechanisms. Such tire models, however, are usually not employed in vehicle modeling due to their complexity and poor computational efficiency. Black-box models, on the other hand, are widely used since they provide desired relations between input and output variables in a convenient manner on the basis of experimental data. The inputs to black-box models usually include normal load, lateral and longitudinal slip ratios, camber angle, and vehicle speed, derived from vehicle response parameters, while the outputs are tire forces and moments.

Tire forces and moments developed at the tire-road contact patch are represented by longitudinal traction/braking forces, lateral cornering force, vertical force, aligning moment, overturning moment and rolling resistance moment. While the overturning and rolling resistance moments yield only insignificant influence on directional dynamics of vehicles, the braking/traction and cornering forces, and aligning moment affect the directional performance most significantly.

The vertical force developed by a tire can generally be determined directly from instantaneous tire deflection and tire radial stiffness assuming linear vertical properties of the tire [119]. The longitudinal and lateral forces developed by the tire, however, are complex functions of many vehicle operating variables, such as normal load, side-slip angle, longitudinal slip, tire-road interface characteristics, and vehicle speed. In this study, a black-box model involving trigonometric functions and regression techniques, proposed by Pacejka et al. [37, 214], is employed to describe the braking and cornering force characteristics of the tires. The model has come to be known as the Magic Formula (MF) partly because of its complex and unusual structure, and partly due to its power to simulate many important tire performance functions with good accuracy.

In the Magic Formula, a desired tire response variable F_{tx} (longitudinal force, lateral force, aligning moment, etc.) is expressed in the following generic form:

$$F_{tx} = D_t \sin \{ C_t \arctan [B_t (x_t + S_h) - E_t x_t [B_t (x_t + S_h) - \arctan (B_t (x_t + S_h))]] \} + S_v \quad (5.38)$$

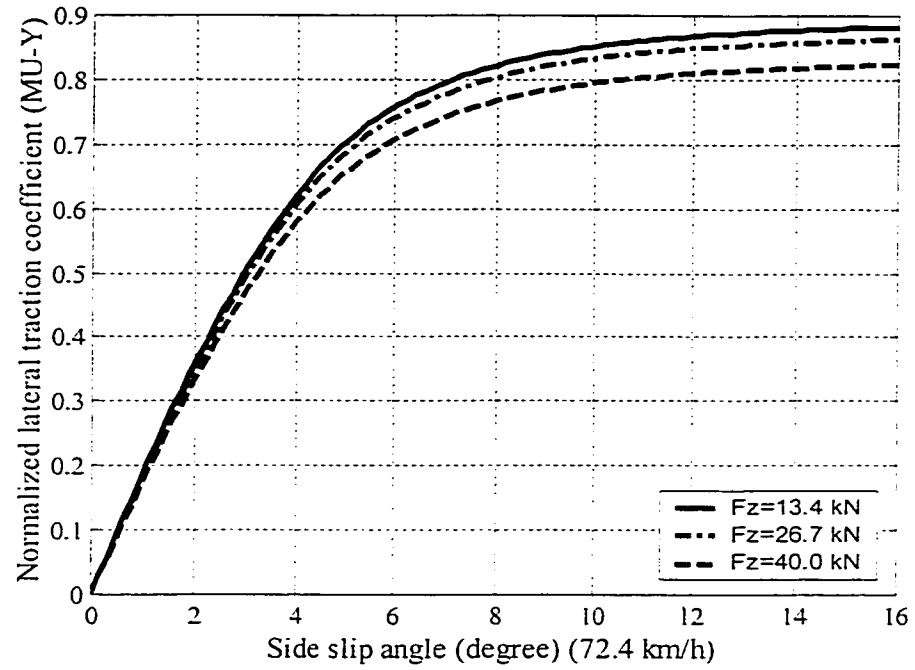
where the independent variable x_t represents a tire service variable, such as slip angle, camber angle, or longitudinal slip; S_h and S_v are referred to as horizontal and vertical shifts, respectively; B_t , C_t , D_t and E_t are constants referred to as stiffness factor, shape factor, peak value, and curvature factor, respectively [214]. The six constants, S_h , S_v , B_t , C_t , D_t and E_t , are identified from experimental data using nonlinear curve-fitting algorithms. The formula has been widely used and yields individual tire characteristics as a function of a tire service variable in a highly efficient and convenient manner. The estimates of the constants in the Magic Formula are conveniently derived by minimizing the following objective function:

$$U_{\alpha} = \sum_{i=1}^n [F_{\alpha}(x_{ti}) - F_{tm}(x_{ti})]^2 \quad (5.39)$$

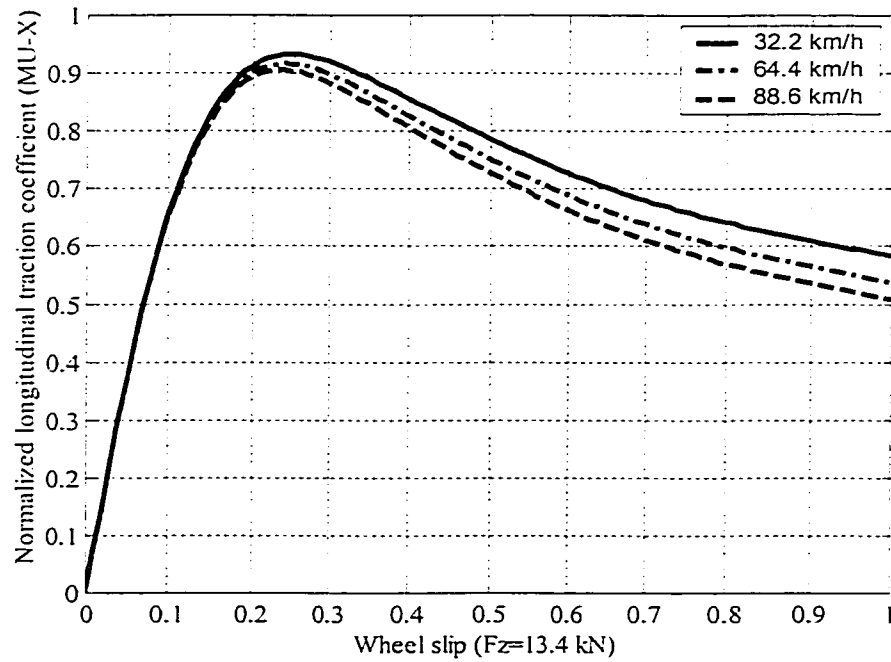
where F_{α} is output variable derived from Equation (5.38) and F_{tm} is the measured quantity as a function of input variable x_{ti} , while n is number of measured data points.

Application of the Magic Formula to available longitudinal force-slip data in the absence of cornering force yields expressions for longitudinal force, while its application to lateral force-sideslip angle data in the absence of traction/braking force yields expressions for cornering force functions.

The application of MF becomes more complex, however, when the response characteristics are derived as a function of many variables, such as normal load, sideslip angle, camber angle, longitudinal deformation slip and vehicle speed. The six constants of the MF are then expressed as functions of all the pertinent parameters. A dependent tire variable (such as lateral force, aligning moment, or longitudinal force) is then estimated as a nonlinear function of many independent variables (normal load, sideslip angle, inclination angle, longitudinal deformation slip and vehicle speed). Neglecting the effect of camber angle, for a fixed normal load or vehicle speed, the MF yields a series of cornering force-sideslip angle relationships in the absence of longitudinal slip and longitudinal force-slip functions without sideslip. Figures 5.6 (a) illustrates the normalized cornering forces (lateral frictional coefficients) as functions of side slip angle for three different vertical tire loads at a vehicle speed of 72.4 km/h of a truck tire, which are derived through solution of Magic Formula based on the measured data on a dry road [216]. Figure 5.6 (b) shows the corresponding normalized longitudinal forces (longitudinal frictional coefficients) as functions of slip for three different vehicle speeds under a vertical tire load of 13.4 kN.



(a) Normalized lateral force of a tire as a function of side-slip angle and normal load.



(b) Normalized braking force of a tire as a function of wheel-slip and speed.

Figure 5.6: Tire lateral and longitudinal friction coefficients on a dry road [216].

In the simulation program, the longitudinal and lateral tire forces are calculated using one of two user-specified tire model options: (i) a non-linear model, as described by Equation (5.38) and illustrated in Figure 5.6; and (ii) a linear model, which assumes negligible load- or speed-dependence and lateral and longitudinal force interaction. This linear tire model should thus be applied in situations involving moderate maneuvers.

The longitudinal and lateral forces developed by the tire under simultaneous application of braking and steering inputs can also be derived based on Equation (5.38), when measured data for combined longitudinal and lateral slips are available. The measurement of tire forces and moments in combined braking and steering maneuvers, however, is very intricate. Alternatively, forces from pure longitudinal and lateral slips can be manipulated to derive the forces under combined braking and steering maneuvers by using roll-off effect multiplication factors for cornering and longitudinal forces, respectively. The roll-off factors are defined as functions of longitudinal slip and sideslip angle of the tire on the basis of friction ellipse concept, and included in the tire model to allow for reduction in the free-rolling lateral forces under longitudinal slip conditions encountered with combined turning and braking. The longitudinal and cornering forces, and aligning moments are incorporated into the model as functions of instantaneous vertical load, wheel velocity along its plane, side-slip angle, longitudinal slip, nature of tire-road interface and roll-off functions.

5.4.4 Suspension Forces

Vehicle suspensions generate forces in three directions under simultaneous braking and cornering operations, as shown in Figure 5.7. In the figure, i_y , j_y and k_y represent a yaw plane system [119]. The direction of k_y always remains normal to the

road, and i_y and j_y follow the rotation of the vehicle around the k_y axis. FSX_{ij} (the first subscript indicates the axle, while the second subscript indicates left side or right side: 1 for left side and 2 for right side), FSY_i and FS_{ij} represent longitudinal, lateral and vertical suspension forces, respectively, while FX_{ij} denotes the longitudinal force developed at the j th tire-road interface on axle i . Various assumptions have been made concerning the forces between the sprung and unsprung masses [217].

- The reactions in the i_y direction are applied at the height of the axle center.
- The constraint in the j_y direction is assumed to be a point force applied at the roll center.
- The suspension forces, FS_{i1} and FS_{i2} , are assumed to act in the k_y direction.

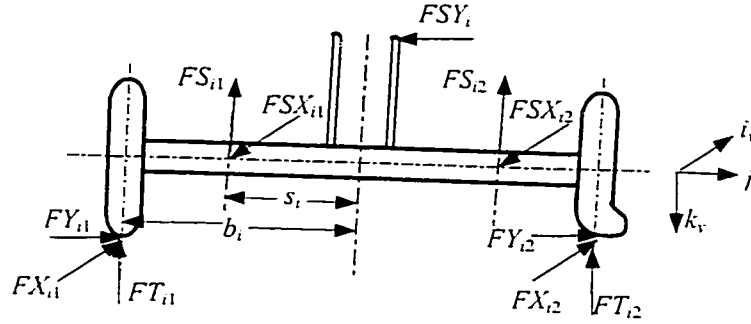


Figure 5.7: Suspension forces on a single axle

For a single axle i , the suspension forces, FS_{ij} , are computed from instantaneous spring deflections and the local equivalent linear spring rate, and the force components due to Coulomb friction and viscous damping:

$$FS_{ij} = K_{ij}\delta_{ij} + C_{ij}\dot{\delta}_{ij} + CF_{ij}; (i=1, 2, \dots, 5; j=1, 2) \quad (5.40)$$

where K_{ij} is linearized local spring rate, C_{ij} is viscous damping coefficient and CF_{ij} is suspension Coulomb friction, while δ_{ij} and $\dot{\delta}_{ij}$ are spring deflection and relative velocity,

respectively. The parameters K_{ij} and C_{ij} may be expressed as functions of δ_{ij} and $\dot{\delta}_{ij}$ for nonlinear springs and damping elements.

For tandem axles, the suspension force calculations use the same algorithms as the single axle. However, under application of braking, the suspension forces at the leading and trailing axles are derived in view of the brake torque and load transfer effect:

$$\begin{aligned} FS_i(lead) &= FS(lead) + \frac{F_{shift} * T_{bs}}{T_d} \\ FS_i(trail) &= FS(trail) - \frac{F_{shift} * T_{bs}}{T_d} \end{aligned} \quad (5.41)$$

where $FS_i(lead)$ and $FS_i(trail)$ are the total suspension forces on the leading and trailing axles, respectively, when braking is applied, while T_{bs} is the total brake torque due to all four brakes on the tandem set. F_{shift} represents a user-defined inter-tandem load transfer coefficient (a negative coefficient reduces the suspension force on the leading axle), which describes the percentage of total brake torque (generated on the rear axles) applied to transferring load from the trailing to the leading axle of the tandem set, and T_d is tandem spread of the axles. $FS(lead)$ and $FS(trail)$ are the suspension forces for the leading and trailing axles, as described by Equation (5.40).

The lateral and longitudinal suspension forces are viewed as constraint forces holding sprung and unsprung masses together in the yaw plane and calculated using the Phase II [217] procedure, as shown in Figure 5.7. In this method, it is assumed that the yaw plane acceleration components of the individual unsprung masses may be estimated from the acceleration of the mass center of the entire vehicle based upon the assumption that the entire vehicle is moving as a single rigid body in the yaw plane. The estimated lateral and longitudinal acceleration components as well as yaw acceleration are then

used to compute the yaw plane constraint forces between the sprung and unsprung masses, FSX_{ij} , FSY_i , based upon the known tire forces.

The lateral force on the sprung mass from unsprung mass i is computed by:

$$FSY_i = FY_{i1} + FY_{i2} - m_{ui}a_{uyi} \quad (5.42)$$

where a_{uyi} denotes the lateral acceleration of unsprung mass i in the yaw plane system.

The longitudinal forces on the sprung mass from unsprung mass i are derived as:

$$FSX_{i1} + FSX_{i2} = FX_{i1} + FX_{i2} - m_{ui}a_{uxi} \quad (5.43)$$

$$FSX_{i2} - FSX_{i1} = \frac{1}{s_i} [(FX_{i2} - FX_{i1})b_i - (AT_{i1} + AT_{i2}) - I_{zui}\ddot{\phi}_{ui}] \quad (5.44)$$

where a_{uxi} and ϕ_{ui} denote longitudinal acceleration and yaw rate of unsprung mass i in the yaw plane system, respectively. For axles with dual tire sets, the lateral and longitudinal suspension forces are derived as:

$$FSY_i = \sum_{j=1}^4 FY_{ij} - m_{ui}a_{uyi} \quad (5.45)$$

$$FSX_{i1} = \frac{1}{2} \left\{ \sum_{j=1}^4 FX_{ij} - m_{ui}a_{uxi} - \frac{1}{s_i} [(FX_{i4} - FX_{i1})(b_i + d_i) + (FX_{i3} - FX_{i2})b_i - I_{zui}\ddot{\phi}_{ui}] \right\}$$

$$FSX_{i2} = \frac{1}{2} \left\{ \sum_{j=1}^4 FX_{ij} - m_{ui}a_{uxi} + \frac{1}{s_i} [(FX_{i4} - FX_{i1})(b_i + d_i) + (FX_{i3} - FX_{i2})b_i - I_{zui}\ddot{\phi}_{ui}] \right\} \quad (5.46)$$

5.4.5 Constraint Forces and Moments

The constraint forces and moments appearing in the differential equations of motion for sprung masses of the tank vehicle combination, Equations (5.26) to (5.28) and (5.32) to (5.34), are determined based upon the assumed spring-damper connections

between the tractor and semitrailer, as described in Section 5.3. The transmitted force at the fifth wheel can be easily computed based on the spring-dashpot model as:

$$\bar{F}_c = K_c \bar{\delta}_p + C_c \dot{\bar{\delta}}_p \quad (5.47)$$

where \bar{F}_c and $\bar{\delta}_p$ represent constraint force vector and difference in path vector for the fifth wheel position of the tractor and semitrailer. K_c and C_c are constants describing the spring rate and dissipation. The complete computation of $\bar{\delta}_p$ and $\dot{\bar{\delta}}_p$ are presented in reference [217].

The relative roll angular displacement and velocity between the tractor and semitrailer are used, in conjunction with the torsional stiffness and damping factor (Coulomb damping), to calculate the roll moment transmitted through the fifth wheel. Thus

$$M_{xc} = K_{xc} (\theta_{s1} - \theta_{s2}) + C_{xc} (\dot{\theta}_{s1} - \dot{\theta}_{s2}) \quad (5.48)$$

where K_{xc} and C_{xc} denotes roll torsional stiffness and damping coefficient at the fifth wheel.

A complete derivation of the forces and moments produced by the suspensions and constraint mechanism are presented in details in references [217].

5.5 METHOD OF SOLUTION

The differential equations of motion of the partly-filled articulated tank vehicle combination, expressed by Equations (5.26) to (5.28), (5.32) to (5.34) and (5.36) to (5.38), are solved in the time domain under a specific combination of steering and braking inputs. The steering input is described either by the time-history of the steer

angle (δ_f) of the front wheels in an open-loop manner or by the path coordinates of the vehicle in a closed-loop manner using a driver model [11]. The braking input is represented by the time-history of the treadle pressure (P_b), which is further converted to braking torque using the brake system model. The solution procedure is initiated by solving the differential equations of motion for a given steer input and treadle pressure over a small time increment. The resulting acceleration and angular motion response variables of the trailer sprung mass are then utilized to compute the body forces imposed on the liquid bulk. The three-dimensional quasi-static fluid model is then solved to evaluate instantaneous values of the c.g. coordinates and mass moments of inertia of the deflected liquid cargo. The forces and moments caused by the movement of the liquid bulk are then computed and incorporated into the different equations describing dynamics of sprung and unsprung masses to compute the response characteristics of the vehicle combination during the subsequent time step. Validity of the proposed variable-speed three-dimensional dynamic model of the partly-filled tank vehicle is examined by comparing its response with that of an equivalent rigid cargo vehicle obtained using the widely used Phase IV model [119]. The results of the analyses are presented in following Chapter.

5.6 SUMMARY

A three-dimensional quasi-static model of a partly-filled tank of generic cross-section is developed and integrated into a comprehensive variable-speed three-dimensional model of an articulated vehicle to study cargo load shift and its influence on directional response and stability characteristics as well as braking performance of a partly-filled articulated tank vehicle combination under combined steering and braking

operations. The three-dimensional model of liquid cargo within a partly-filled tank is developed assuming inviscid fluid and negligible contributions due to fundamental slosh frequency. The resulting liquid load movement encountered under combined steering and braking is expressed in terms of variations in the instantaneous c.g. coordinates in the roll and pitch planes, and mass moments of inertia of the liquid bulk. The liquid free surface may assume four possible patterns, depending upon the fill volume and magnitudes of lateral and longitudinal acceleration excitation. The longitudinal, lateral and vertical translations of the c.g. coordinates of the cargo load and its mass moments of inertia are further derived as a function of longitudinal and lateral body forces imposed on the liquid bulk, fill volume and tank configuration.

The coupled tank vehicle model incorporates dynamics of air brake systems and comprehensive tire-road friction models, and is capable of simulating both open-loop and close-loop steering maneuvers, stopping distance performance, dynamic behavior in braking, and brake proportioning effects on braking limits. The variable speed dynamic model of the partly-filled articulated tank vehicle combination, developed in this Chapter, is analyzed in Chapter 6 to investigate the influence of cargo load shift on directional dynamic characteristics as functions of steering and braking input, cargo fill volume, road surface friction and tank cross-section.

CHAPTER 6

CARGO LOAD SHIFT AND ITS INFLUENCE ON DYNAMIC RESPONSE OF TANK VEHICLES UNDER BRAKING AND TURNING

6.1 INTRODUCTION

The directional response and safety performance characteristics of freight vehicles are influenced by many design and operating factors, such as weights and dimensions, suspension and tire properties, steering and braking maneuvers, road surface and vehicle speed. Apart from these design and operating factors, the forces and moments caused by moving liquid cargo strongly affect the dynamic response of tank vehicles. The directional response and safety performance of liquid cargo vehicles are thus dependent on factors other than the normal trucking practices, such as tank geometry, load fill volume, variation in center of gravity (c.g.) coordinates, lateral and longitudinal load shifts and liquid-structure interactions. Simultaneous applications of steering and braking cause considerable shifts in the cargo c.g. and thus dynamic load transfer in roll and pitch planes.

The dynamic characteristics of partly-filled tank vehicles have been investigated under either constant-speed steering or straight-line braking maneuvers [172, 173, 178, 183, 187-198]. These studies have clearly established that cargo movement within a partly-filled tank vehicle is a significant contributing factor leading to reduced roll stability limits and braking performance of the vehicle. The cargo movement within a partly-filled tank and its influence on the dynamic response and stability characteristics of the partially-filled tank vehicle under combined steering and braking maneuvers, however, has not been addressed. The lack of such studies is most likely attributed to

analytical complexities associated with three-dimensional fluid slosh within a partly-filled tank of complex geometry and its interactions with the vehicle.

In this Chapter, the variable-speed three-dimensional model of an articulated tank vehicle, developed in Chapter 5, is analyzed to study its directional response under steering and braking inputs. The three-dimensional quasi-static model of a partly-filled tank of generic cross-section, developed in Chapter 5, is initially solved to analyze the liquid load shift in the roll and pitch planes, and variations in mass moments of inertia of the deflected cargo under longitudinal and lateral acceleration fields encountered during braking-in-a-turn maneuvers. The load shift properties of conventional and optimal tank cross-sections are evaluated as functions of lateral and longitudinal body forces, fill volume and tank cross-section. The directional performance characteristics of the vehicle combination are then evaluated in terms of dynamic load transfer, yaw, roll and deceleration response. The response characteristics of a partially-filled conventional cleanbore tank of circular cross-section are compared with those of a corresponding equivalent rigid cargo vehicle to demonstrate the destabilizing effects of liquid load shift. Parametric sensitivity analysis is further carried out to examine the influence of steer and braking inputs, liquid load fill condition, tire-road friction property, and tank cross-section on the directional characteristics and braking behavior of the vehicle combination.

6.2 LIQUID LOAD SHIFT UNDER BRAKING AND STEERING INPUTS

As described in Chapter 5, the motion of the free surface of the liquid cargo within a partly-filled tank, caused by steering and braking inputs, can lead to considerable load shifts in the roll and pitch planes of the partly-filled tank. The magnitudes of the cargo load shift are complex functions of tank size, tank cross-section, fill volume, and

magnitudes of longitudinal and lateral accelerations imposed on the liquid bulk by the tank-trailer. Equation (5.17) describing the three-dimensional quasi-static model of a partly-filled generic tank, is solved to evaluate the load shift within partly-filled tanks of various cross-sections, including conventional circular and modified-oval, and the optimal (*OPT1* and *OPT2*) tanks, subject to different combinations of lateral and longitudinal acceleration fields.

6.2.1 Cargo Load Shift within a Partly-Filled Tank of Circular Cross-section

The three-dimensional quasi-static model of the liquid bulk is initially analyzed for a cleanbore tank of circular cross-section (MC 307, MC 312), which is most commonly employed in general purpose chemical transportation. Figures 6.1 and 6.2 illustrate the cargo load shift in terms of variations in coordinates of cargo c.g. (ΔX_l , ΔY_l , ΔZ_l) and variations in mass moments of inertia, respectively, as functions of lateral (a_{ly}) and longitudinal (a_{lx}) accelerations imposed on the liquid bulk. The results are derived for a 50%-filled cleanbore circular cross-section tank of 2.03 m (80 in) diameter and length of 12.91 m (480 in). Figures 6.3 and 6.4 illustrate variations in coordinates of the c.g. and mass moments of inertia (normalized with respective static values) of the liquid bulk under different magnitudes of lateral and longitudinal acceleration fields. The variation in vertical c.g. coordinate is presented in terms of the c.g. height ($Z_l = \Delta Z_l + Z_{l0}$) to take account of the static c.g. coordinate of the cargo. The results are presented for four discrete values of a_{ly} (0.1, 0.2, 0.3 and 0.4 g) for 50% ($\beta=0.5$) and 80% ($\beta=0.8$) fill volumes, respectively.

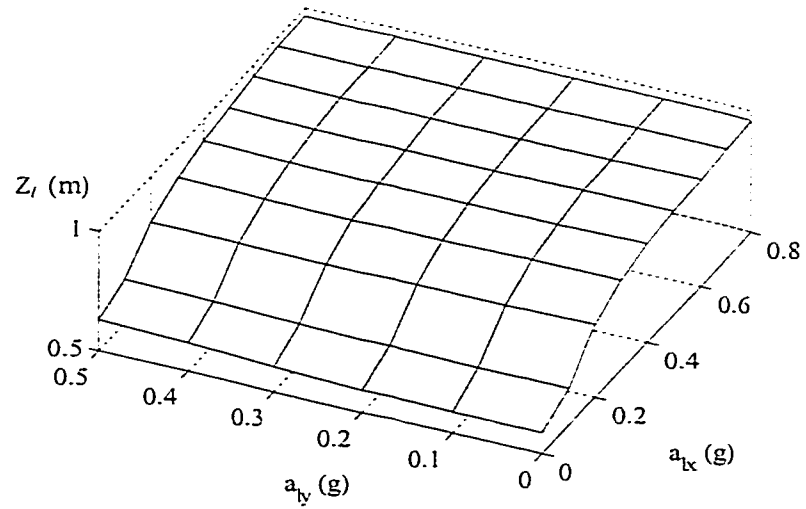
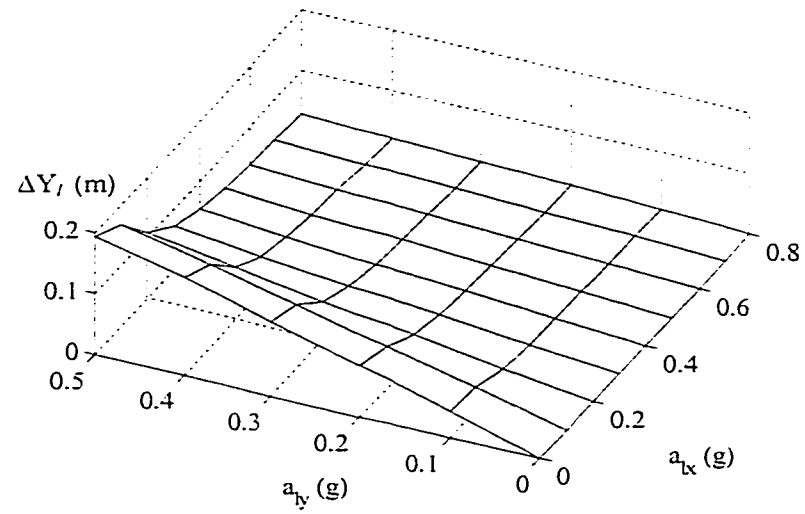
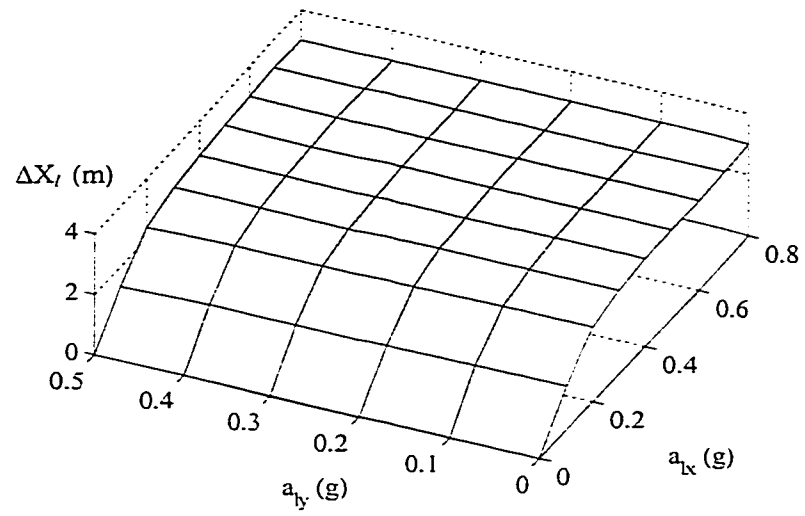


Figure 6.1: Variations in coordinates of liquid cargo c.g. as functions of longitudinal and lateral accelerations ($\beta=0.5$).

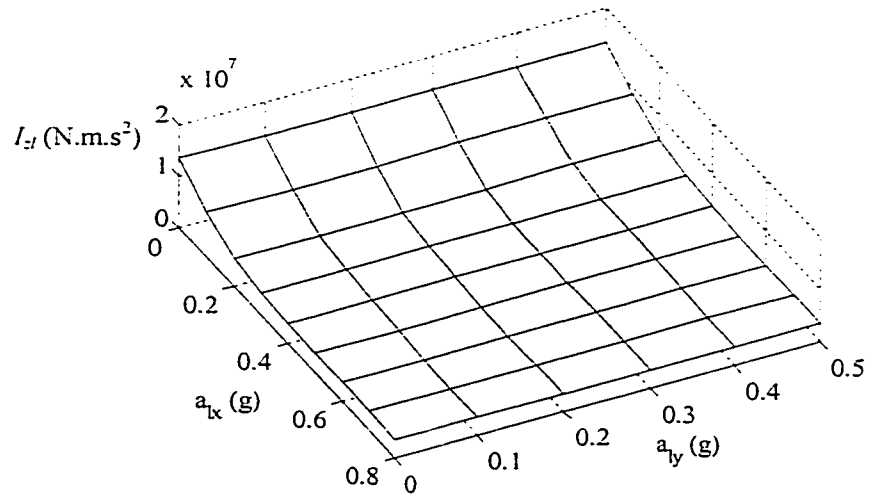
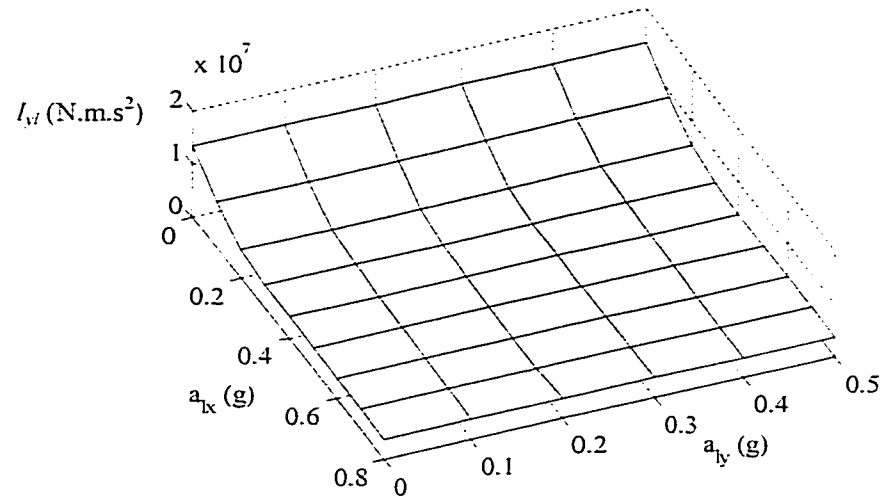
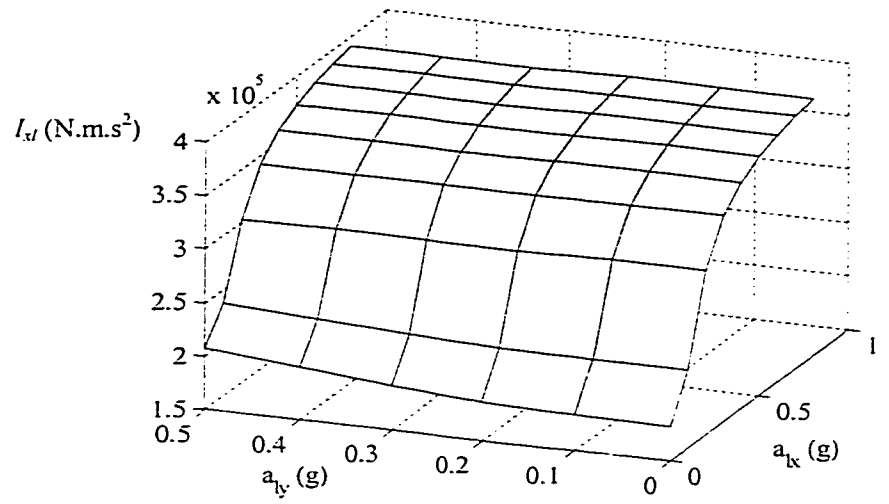


Figure 6.2: Variations in roll, pitch and yaw mass moments of inertia of liquid cargo as functions of longitudinal and lateral accelerations ($\beta=0.5$).

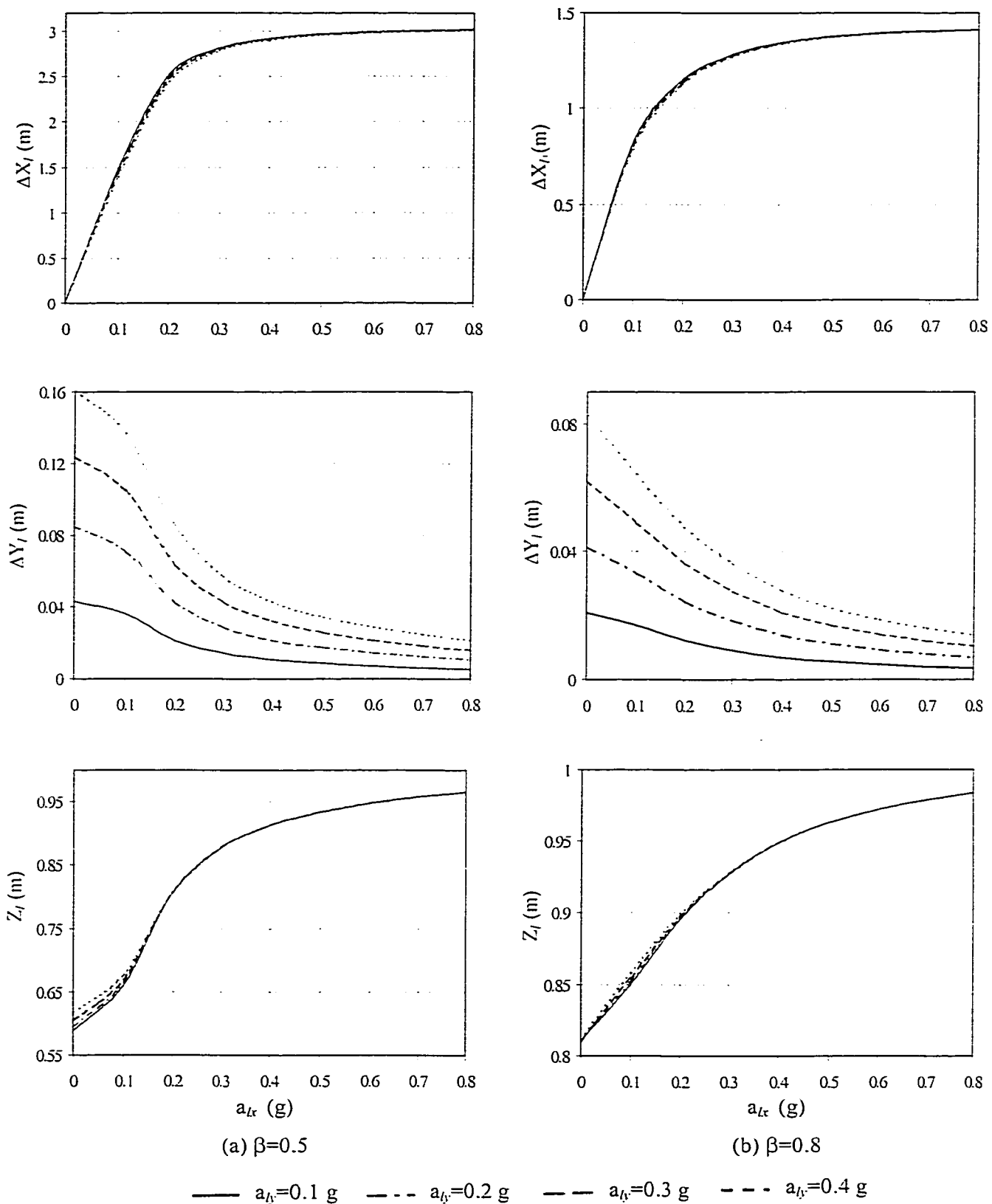


Figure 6.3: Variations in c.g. coordinates of liquid cargo under application of longitudinal and lateral acceleration fields.

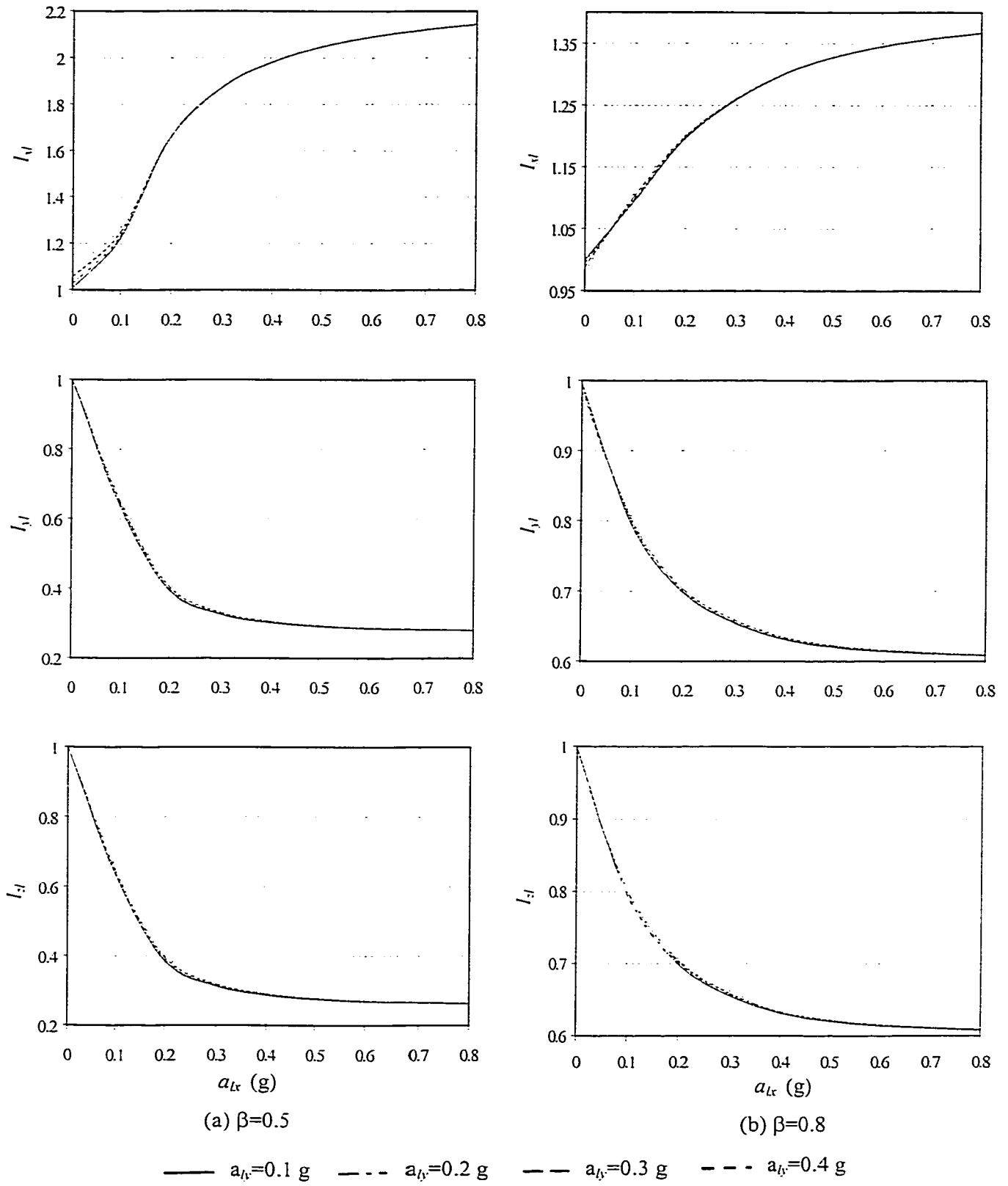


Figure 6.4: Variations in normalized mass moments of inertia of liquid cargo under application of longitudinal and lateral acceleration fields.

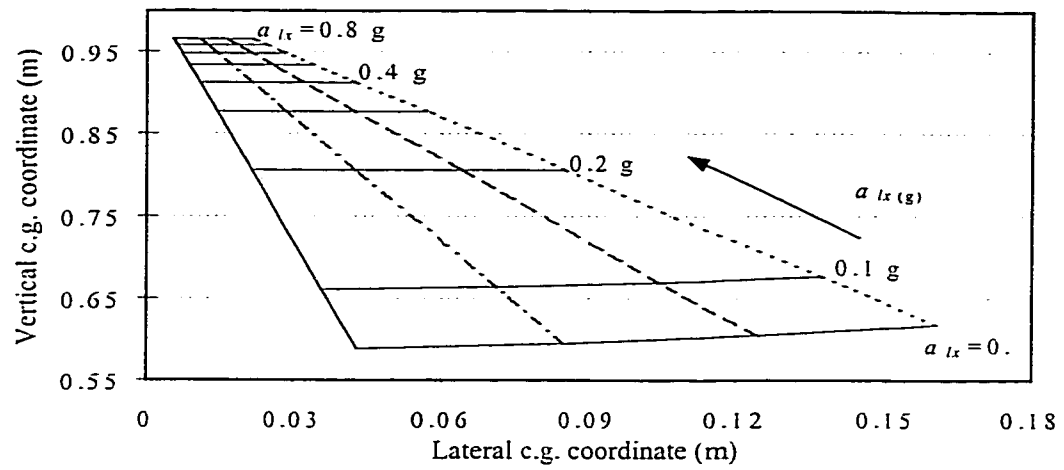
The results show considerable variations in coordinates of the cargo c.g., and roll, pitch and yaw mass moments of inertia of the liquid cargo under lateral and longitudinal acceleration fields. The variations are observed to be quite significant for lower fill volume, due to movement of the free surface. The mass moments of inertia of the liquid bulk vary most significantly under a_{lx} , while the influence of a_{ly} is relatively small. For a given value of a_{lx} , an increase in a_{ly} yields insignificant effect on ΔX_l , ΔZ_l , and normalized mass moments of inertia (I_{xl} , I_{yl} and I_{zl}). The roll mass moment of inertia of the liquid bulk (I_{xl}), however, increases most significantly under application of a_{lx} , irrespective of the magnitude of a_{ly} and fill volume. The I_{xl} increases rapidly under low to medium levels of a_{lx} , and approaches nearly steady values under higher levels of a_{lx} . The increase in I_{xl} approaches over 100% for $a_{lx} \geq 0.5$ g and $\beta=0.5$. The corresponding increase for 80% fill volume is approximately 30%. The pitch and yaw moments of inertia (I_{yl} and I_{zl}) tend to decrease with increase in a_{lx} . The decrease is observed to be quite rapid for $a_{lx} \leq 0.2$ g, due to relatively unconstrained movement of the liquid cargo under low levels of deceleration. The I_{yl} and I_{zl} decrease by 60% and 61%, respectively, under $a_{lx}=0.2$ g and $\beta=0.5$, while the corresponding reductions for 80% fill volume are in the order of 30% and 31%, respectively. A further increase in a_{lx} yields only minimal variations in I_{yl} and I_{zl} , attributed to considerably reduced motion of the liquid free surface.

While application of a pure lateral acceleration field yields most significant variations in ΔY_l of the liquid bulk, the application of a pure longitudinal acceleration causes most significant variations in ΔX_l and ΔZ_l . The variations in ΔX_l , however, are considerably large due to relatively large tank length. The variations in liquid bulk c.g. coordinates are observed to be considerably larger for $\beta=0.5$, when compared with those

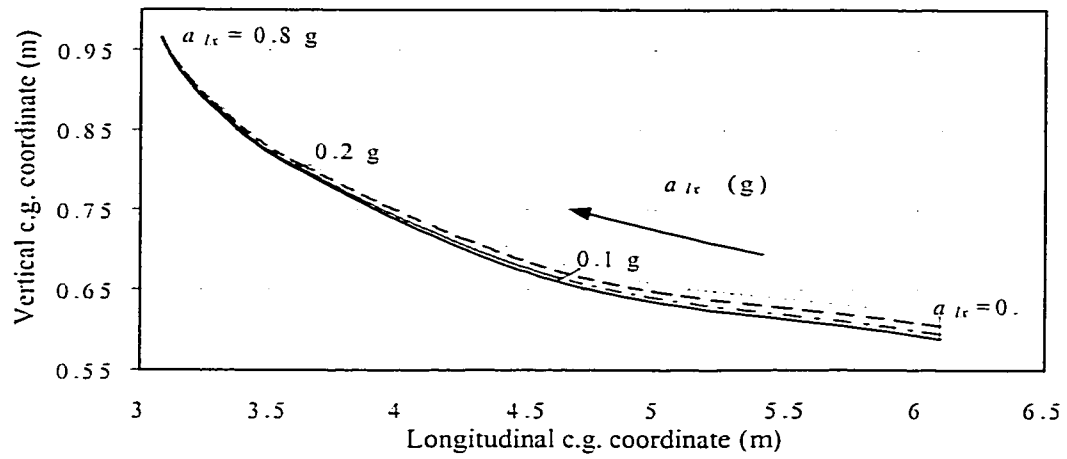
attained for $\beta=0.8$, due to increase in liquid motion with decrease in fill volume, as indicated previously. Application of $a_{lx}=0.6$ g to a 50%-filled tank yields ΔX_l in excess of 3 m, while Z_l increases from its static value of 0.59 m to approximately 0.95 m, irrespective of a_{ly} . For $\beta=0.8$ and $a_{lx}=0.6$ g, the ΔX_l is attained as 1.4 m, while the vertical c.g. coordinate (Z_l) increases from 0.81 m to 0.97 m, for the entire range of a_{ly} considered in the study. The large variations in ΔX_l caused by application of a_{lx} would cause significant variations in instantaneous axle loads and thereby the braking performance of the vehicle combination. Application of a pure lateral acceleration of 0.3 g yields an increase in the lateral coordinate of the cargo c.g. by 0.12 m for $\beta=0.5$ and 0.06 m for $\beta=0.8$. The magnitude of ΔY_l , however, decreases rapidly under application of a_{lx} for both fill volumes, as shown in Figures 6.1 and 6.3. This decrease is attributed to predominant liquid load shift along the longitudinal axis under a_{lx} and excessive tank length. From the results, it can be concluded that application of lateral acceleration (a_{ly}) and relatively low level longitudinal acceleration (a_{lx}) cause predominant fluid motion in the roll plane. The cargo load shift is dominant in the pitch plane, when a_{lx} exceeds 0.2 g, irrespective of the magnitude of a_{ly} .

Figures 6.5 and 6.6 illustrate the trajectories of the liquid cargo c.g. in the roll, pitch and yaw planes as functions of a_{lx} and a_{ly} , for four discrete values of a_{ly} (0.1, 0.2, 0.3 and 0.4 g) under 50% and 80% fill volumes, respectively. Each curve corresponding to a fixed value of a_{ly} represents the variations in c.g. coordinate under variation in a_{lx} ranging from 0. to 0.8 g. The results show that in the absence of a_{lx} the cargo c.g. shift in the roll plane mostly occurs along the lateral axis. For a given value of a_{ly} , the magnitude of ΔY_l decreases with increase in a_{lx} , while the magnitude of ΔZ_l increases significantly in

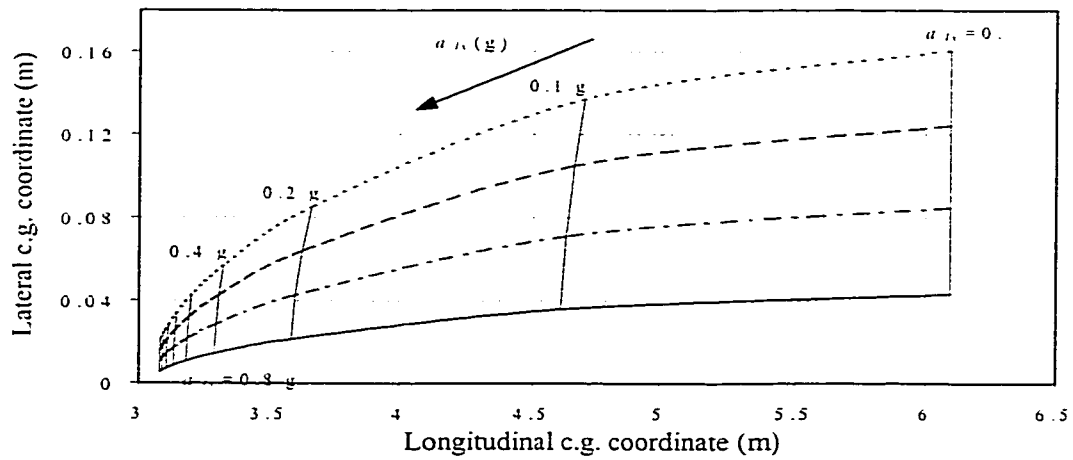
a nearly linear manner. The trajectories of the c.g. in the roll plane under both 50% and 80% fill volumes are thus observed to be nearly collinear, as shown in the figures. The influence of a_{ly} appears to be relatively insignificant under $a_{lx}=0.8$ g. This is further observed from the trajectory of the liquid cargo c.g. in the pitch and yaw planes. The trajectory of liquid cargo c.g. in the pitch plane reveals most significant variations along the longitudinal and vertical axes, irrespective of the fill volume and magnitude of a_{ly} , due to excessive longitudinal motion of the cargo.



(a) Roll plane



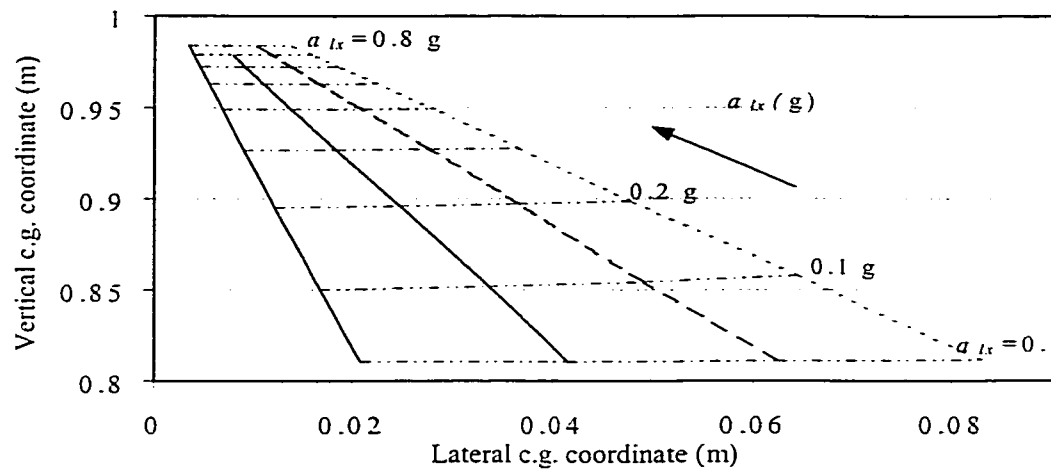
(b) Pitch plane



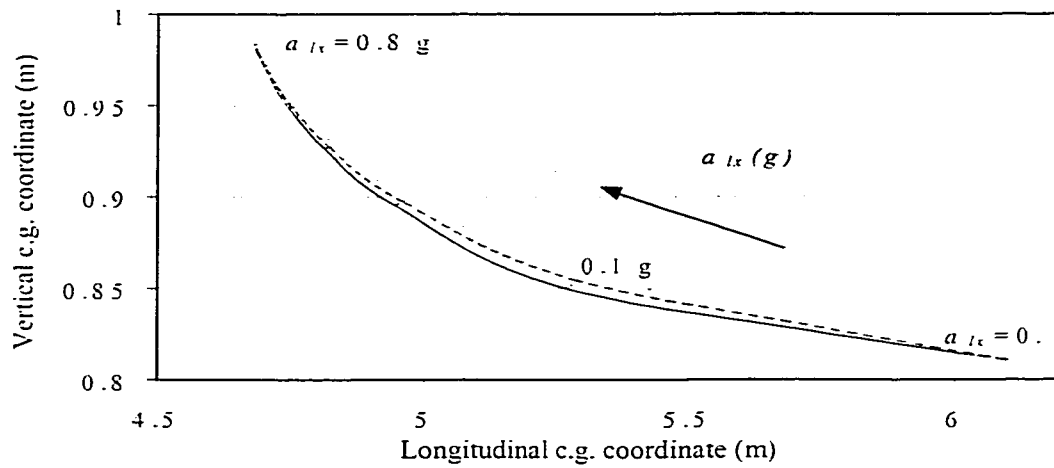
(c) Yaw plane

— $a_{ly}=0.1 \text{ g}$ - - - $a_{ly}=0.2 \text{ g}$ - - - $a_{ly}=0.3 \text{ g}$ - - - $a_{ly}=0.4 \text{ g}$

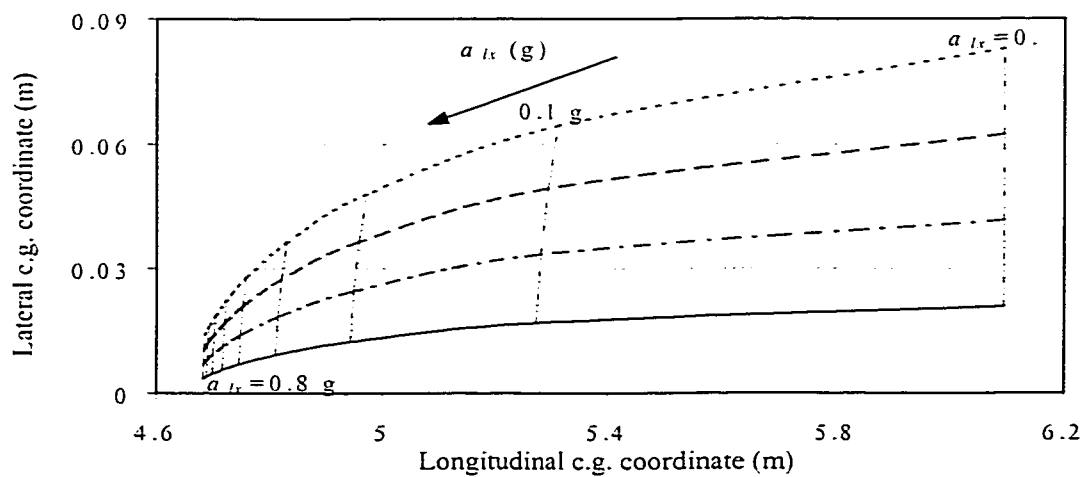
Figure 6.5: Trajectories of liquid cargo c.g. in the roll, pitch and yaw planes under applications of a_{lx} and a_{ly} ($\beta=0.5$).



(a) Roll plane



(b) Pitch plane



(c) Yaw plane

— $a_{ly}=0.1 g$ - - - $a_{ly}=0.2 g$ - - - $a_{ly}=0.3 g$ - - - $a_{ly}=0.4 g$

Figure 6.6: Trajectories of liquid cargo c.g. in the roll, pitch and yaw planes under applications of a_{lx} and a_{ly} ($\beta=0.8$).

6.2.2 Influence of Tank Cross-section on Cargo Load Shift

To evaluate the influence of tank cross-section on load shift and thus the trajectory of the c.g. of the liquid cargo under simultaneous application of lateral and longitudinal body forces, the fluid model is further analyzed for different tank cross-sections, including the conventional circular and modified-oval, and the two optimal tank (*OPT1* and *OPT2*) cross-sections, proposed in Chapter 3. The geometric parameters of these tank cross-sections have been presented in Chapter 3, while their length is taken as 12.91 m (480 in.). Figures 6.7 and 6.8 present the shift in c.g. coordinates of the liquid cargo as functions of longitudinal acceleration and tank cross-section for a fixed lateral acceleration of 0.3 g under 50% and 80% fill volumes, respectively. The corresponding trajectories of the liquid cargo c.g. in the roll, pitch and yaw planes are presented in Figures 6.9 and 6.10, when a_{lx} varies from 0 to 0.8 g.

The results show significant influence of a_{lx} on the shift in liquid c.g. coordinates, irrespective of tank cross-section and liquid fill volume, attributed to the dominant impact of a_{lx} , as discussed for the case of circular cross-section tank. The longitudinal and vertical c.g. shifts (ΔX_l and ΔZ_l) increase, while the lateral load shift (ΔY_l) decreases, rapidly with increase in the magnitude of a_{lx} . As a_{lx} increases beyond a certain level (approximately 0.5 g), the variations in c.g. coordinates of the cargo approach minimal, irrespective of the tank cross-section, due to considerably reduced liquid free surface and thus insignificant cargo load shift with further increase in a_{lx} . The results further reveal that under 50% fill volume, the influence of tank cross-section on longitudinal load shift (ΔX_l) is relatively small, specifically under high deceleration levels, as shown in Figure 6.7. The application of low level of deceleration, $a_{lx}=0.1$ to 0.4 g, however, reveals

considerable differences in the magnitudes of ΔX_l and ΔY_l attained for different tank cross-sections. A modified-oval tank cross-section yields largest values of ΔX_l and ΔY_l due to its wide cross-section and thus considerably large resulting free surface area. These variations are more significant under 80% fill volume shown in Figure 6.8. The *OPTI* cross-section induces least values of ΔX_l and ΔY_l owing to its relatively narrow cross-section. The magnitudes of ΔX_l attained for different tanks with 50% fill volume, however, are quite comparable, which can be mostly attributed to the identical tank cross-section area and length, and relatively low fill volume of the liquid cargo, which tends to fill the lower wider portion of the optimal cross-sections. Since the lower part of the optimal geometry is relatively wide, the optimal cross-sections provide little resistance to the movement of the free surface, especially in the longitudinal direction.

The variations in the c.g. coordinates of cargo within the 80%-filled conventional and optimal tanks reveal considerable difference in the magnitudes of ΔX_l (approximately 0.2 m) for $a_{tx} > 0.2$ g, as shown in Figure 6.8. Among the four tanks considered, the modified-oval tank yields the largest value of ΔX_l , while *OPTI* reveals the least value of ΔX_l , as observed in the case of 50% fill volume. It is interesting to note that both the conventional circular and modified-oval tanks yield quite similar response in ΔX_l with only slight difference in the range of $a_{tx} = 0.1$ to 0.4 g, and so do the two optimal tanks. The significant difference in the magnitudes of ΔX_l attained with the conventional and optimal tanks is primarily attributed to the difference in geometric features associated with upper-half of the different tanks and high fill volume of the liquid cargo. Since the liquid cargo free surface is located at the upper section of the tank, which in case of the optimal cross-sections is considerably narrower than the lower part, the optimal cross-

sections provide effective resistance to the motion of the free surface, resulting in significant reduction in ΔX_l .

The variations in the lateral coordinate of the cargo c.g. (ΔY_l) reveal trends similar to those observed from the roll plane analyses, presented in Chapters 3 and 4. Under identical longitudinal and lateral accelerations as well as fill volume, the modified-oval tank yields the most significant variation in ΔY_l due to its excessively wide cross-section, while the *OPT1* reveals the least magnitude of ΔY_l among the four tanks considered. Under 50% fill volume, the *OPT2* tank yields similar lateral load shift as the circular tank because of their comparable cross-section widths, but considerably lower shift than that attained for the circular tank under 80% fill volume and $a_{lx} < 0.3$ g, which is primarily attributed to its relatively narrower upper section. The difference in lateral load shift (ΔY_l) attained with the various tanks, however, decreases rapidly with increase in the longitudinal acceleration (a_{lx}). Under decelerations exceeding 0.4 g, the circular, *OPT1* and *OPT2* tanks yield similar magnitudes of ΔY_l , irrespective of the fill volume. The modified-oval cross-section, however, yields larger values of ΔY_l , irrespective of a_{lx} and fill volume. The rapid decrease in ΔY_l response of all the cross-sections is caused by the increase in a_{lx} due to its dominant influence and significant dimension of tanks in the longitudinal direction, as discussed earlier for the case of circular cross-section tank.

Similar to the pure roll plane analyses, under both fill volumes, the circular cross-section yields the highest value of Z_l , attributed to its high cross-section c.g. location. The *OPT2* yields the lowest value of Z_l under 50% fill volume due to its relatively low cross-section c.g. height and width. Its c.g. height under 80% fill volume, however, is comparable to that of the modified-oval tank. Under 50% fill volume, the modified-oval

tank reveals considerably larger Z_l than the optimal tanks under relatively low levels of a_{lx} ($a_{lx} < 0.2$ g), due to considerable roll plane load shift of the cargo arising from its excessively wide cross-section coupled with relatively significant influence of the lateral acceleration. The *OPTI* tank yields medium levels of Z_l under both fill volumes, except for $a_{lx} < 0.2$ g under 50% fill volume, as a result of its relatively high cross-section c.g. location.

It is interesting to note that the trajectories of the liquid cargo c.g. in the roll planes of partly-filled conventional tanks (circular and modified-oval) are almost linear functions of a_{lx} , as shown in Figures 6.9 and 6.10. The corresponding trajectories attained for the optimal cross-sections do not exhibit this linear variation, especially for relatively low levels of a_{lx} and 80% fill volume. This behavior can be attributed to their asymmetric geometry in the roll plane. The narrow cross-section of the upper half of the optimal cross-sections provides high resistance to motion of the free surface, specifically under higher fill volumes. An examination of the c.g. trajectory curves, illustrated in Figures 6.9 and 6.10, further indicates that the optimal geometry yields significant reduction in cargo c.g. shift in the roll plane for both fill volumes, as in the case of pure roll plane analyses, discussed in Chapters 3 and 4. The results further show considerably lower load shift of the optimal cross-sections in the yaw plane, specifically for 80% fill volume.

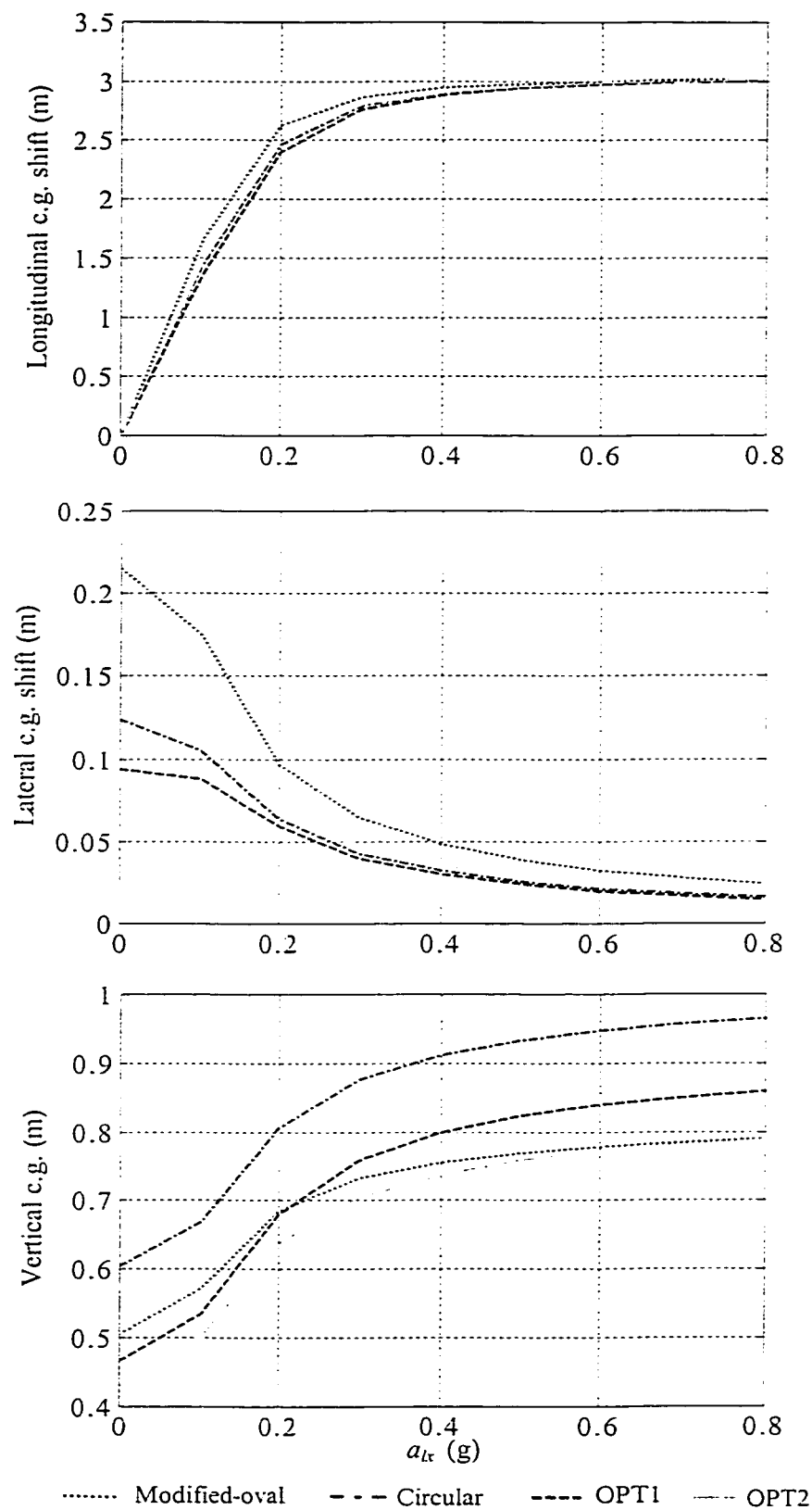


Figure 6.7: Variations in c.g. coordinates of the liquid cargo as functions of longitudinal acceleration and tank cross-section ($a_{ly}=0.3$ g and $\beta=0.5$).

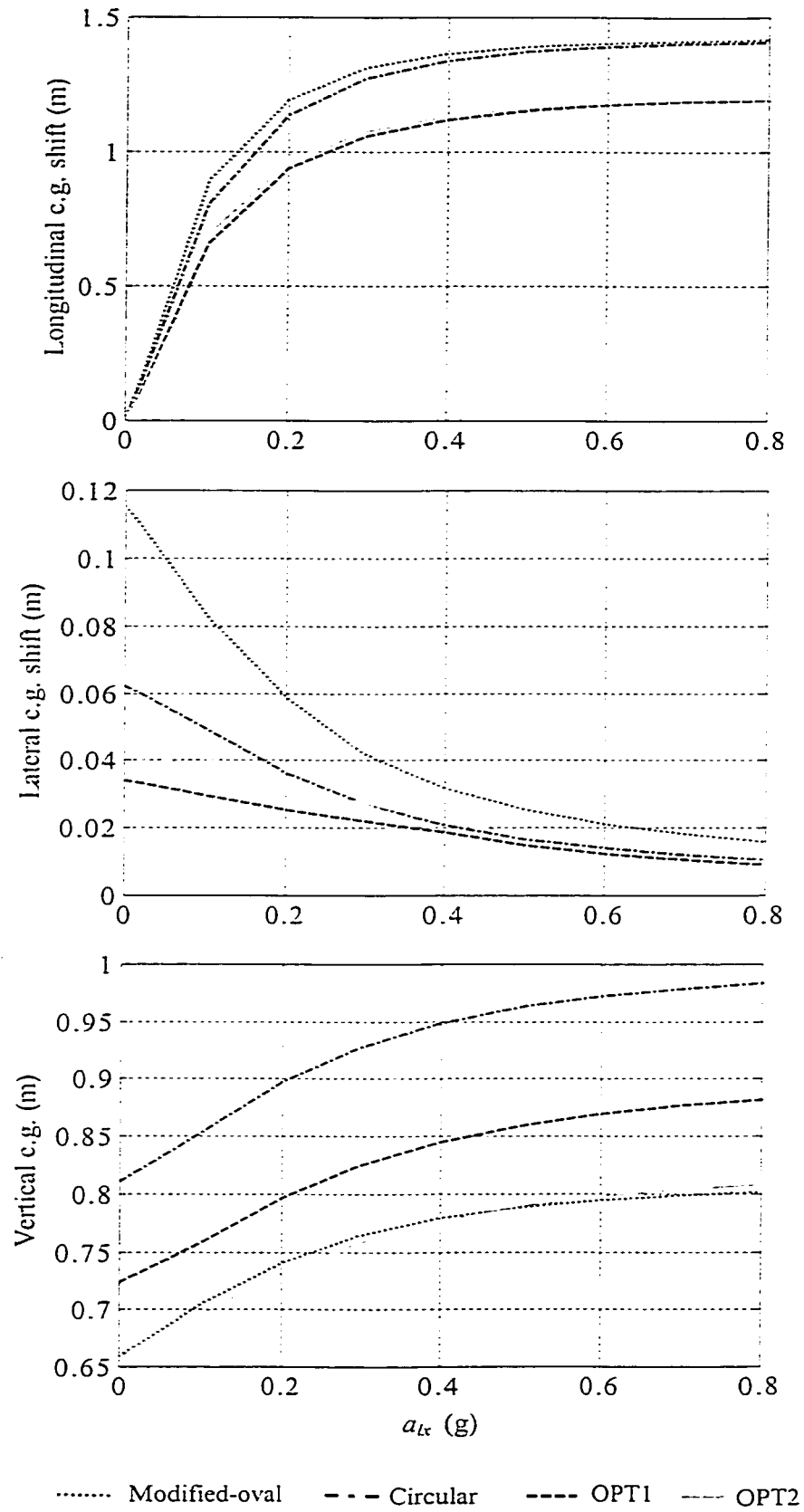


Figure 6.8: Variations in c.g. coordinates of the liquid cargo as functions of longitudinal acceleration and tank cross-section ($a_{Lx}=0.3$ g and $\beta=0.8$).

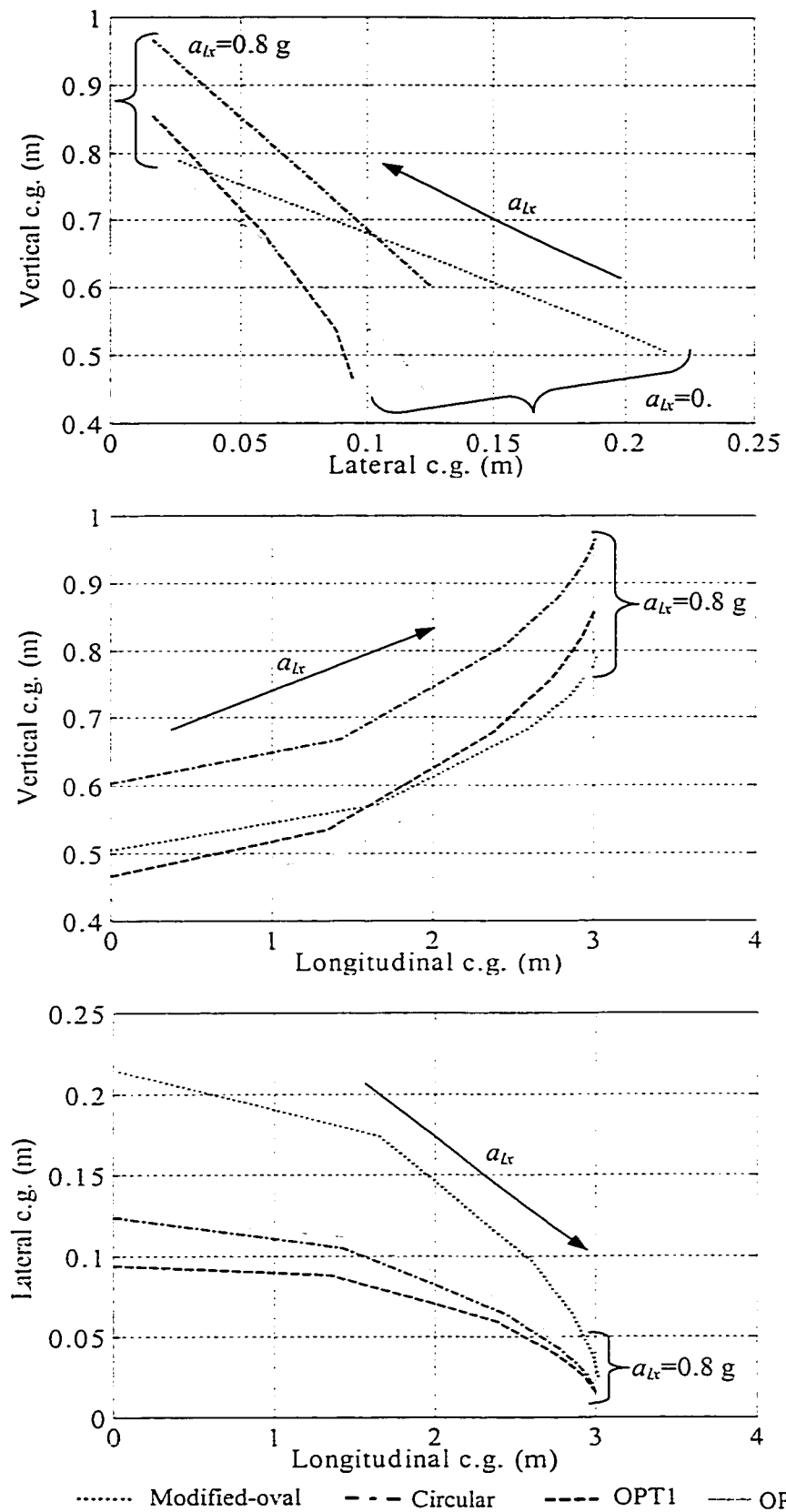


Figure 6.9: Trajectories of liquid cargo c.g. in the roll, pitch and yaw planes as functions of longitudinal acceleration and tank cross-section ($a_{Lx}=0.3 \text{ g}$ and $\beta=0.5$).

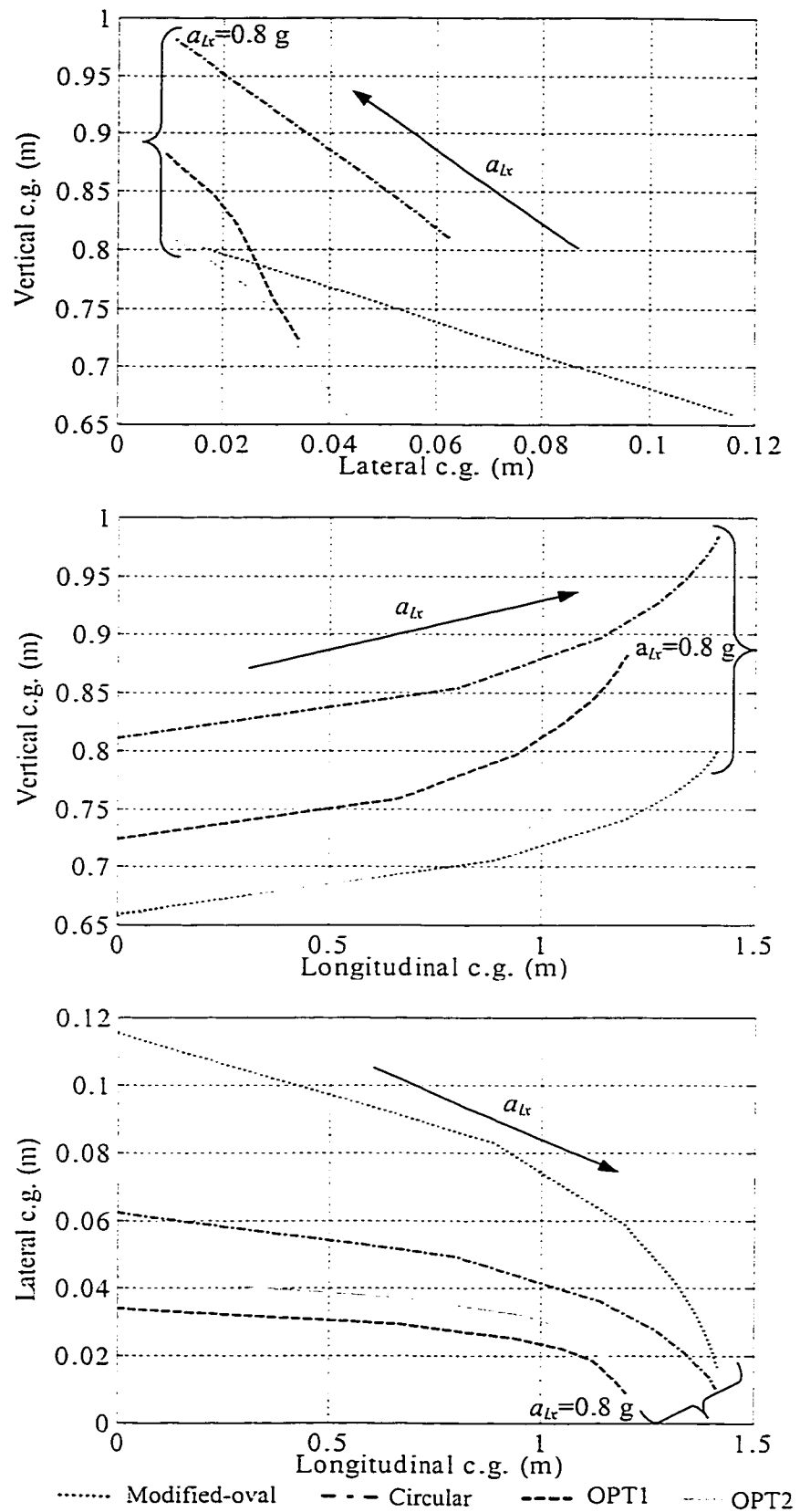


Figure 6.10: Trajectories of liquid cargo c.g. in the roll, pitch and yaw planes as functions of longitudinal acceleration and tank cross-section ($a_{tx}=0.3$ g and $\beta=0.8$).

6.3 VEHICLE MANEUVERS AND PERFORMANCE MEASURES

The equations of motion of the variable-speed dynamic model of the partly-filled articulated tank vehicle, developed in Chapter 5, are solved to evaluate its directional response characteristics under different braking and steering maneuvers. The directional response characteristics of the partly-filled tank vehicle are assessed in terms of liquid load shift and various established safety performance measures.

6.3.1 Simulation Conditions

The directional response characteristics of articulated vehicles are known to be strongly affected by various operating factors, such as loading, speed, braking, steering and road condition. The performance evaluations based upon simulations of vehicle models thus necessitate consideration of representative simulation conditions related to operating parameters. Simulation conditions selected for analysis of steering and braking performance of partly-filled articulated tank vehicles are described below.

The tank vehicle combination is assumed to move at a specified initial speed along a straight path on a level surface with even frictional property. A constant steering procedure is applied to bring the vehicle into a turn. A braking input is applied to achieve a constant deceleration brake as the vehicle approaches steady-turning condition [36, 113]. Two different magnitudes of steering inputs are considered for the analysis, as illustrated in Figure 6.11. Two different braking inputs are also considered by varying the magnitudes of treadle pressure, as shown in Figure 6.11. Two road surfaces with different friction characteristics are considered to study the influence of road surface properties [120, 216]: (i) a typical high friction dry road with $\mu=0.9$, referred to as road 'A'; and (ii)

a low friction wet or slippery road with $\mu=0.4$, referred to as road 'B'. The μ -slip curves for road A have been illustrated in Figures 5.6.

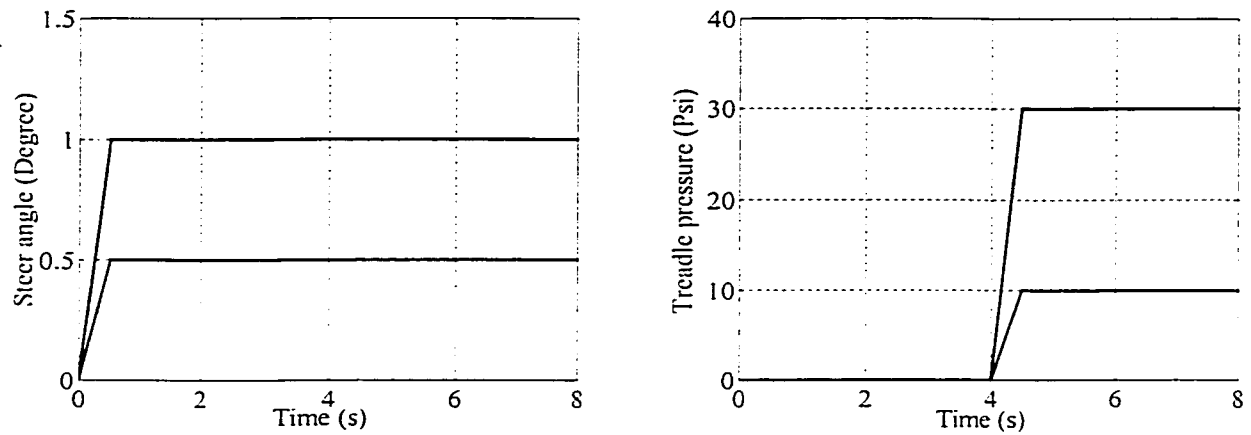


Figure 6.11: Steering and braking inputs.

Table 6.1 summarizes some of the simulation parameters of the candidate five-axle tractor semitrailer tank vehicle. The braking force (torque) distribution is selected as 14:43:43, which is proportional to the static weight distribution among the axles. The total braking gain is selected to be 262 Nm/kPa (16000 lb-in/psi) and the time lag and rise time of the braking systems are set as 0.05 s and 0.25 s, respectively [119, 216].

Table 6.1: Simulation parameters of a five-axle tractor-tank-semitrailer combination [100, 216].

Tractor

Type	Three-Axle
Curb Weight on Front Suspension:	41.86 kN (9410 lb)
Curb Weight on Rear Suspension:	27.09 kN (6090 lb)
Wheel Base:	4.42 m (174 in)
Tare Center of Gravity Height:	1.12 m (44 in)
Frame Roll Torsional Stiffness:	4519 Nm/degree (40000 lbin/degree)
Roll Mass Moment of Inertia:	2938 Nms ² (26000 lbins ²)
Yaw Mass Moment of Inertia:	19207 Nms ² (170000 lbins ²)
Pitch Mass Moment of Inertia:	19207 Nms ² (170000 lbins ²)

Tank-Semitrailer

Type	Two-Axle
Kingpin Static Load:	16.95 kN (3810 lb)
Curb Weight on Rear Suspension:	36.43 kN (8190 lb)
Wheel Base:	10.41 m (410 in)
Tare Center of Gravity Height:	1.52 m (60 in)
Payload:	233.53 kN (52500 lb)
Roll Mass Moment of Inertia:	9039 Nms ² (80000 lbins ²)
Yaw Mass Moment of Inertia:	11298 Nms ² (100000 lbins ²)
Pitch Mass Moment of Inertia:	11298 Nms ² (100000 lbins ²)

Axle and Suspension Parameters

	Axle 1	Axle 2	Axle 3	Axle 4	Axle 5
Unsprung Weight (kN):	5.34	11.12	11.12	6.67	6.67
Loaded Tire Radius (m):	0.516	0.516	0.516	0.546	0.546
Roll Center Height (m):	0.464	0.838	0.838	0.686	0.686
Axle Roll Mass Moment of Inertia (Nms ²):	418	576	576	463	463
Wheel Polar Moment of Inertia (Nms ²):	23	26	26	26	26
Tire Track Width (m):	2.045	1.829	1.829	1.829	1.829
Dual Tire Spacing (m):	-	0.330	0.330	0.330	0.330
Suspension Spring Spacing (m):	0.828	0.965	0.965	1.118	1.118
Static Axle Load (kN):	49.54	76.56	76.56	76.60	76.60

6.3.2 Performance Measures

An undesirable response of an articulated vehicle combination under combined cornering and braking maneuvers may occur in one of the two modes: (i) yaw instability, which may lead to loss of directional control, jackknifing and trailer swing; and (ii) roll instability that may result in vehicle rollover. A wide range of performance measures have been proposed to assess relative safety dynamics performance of articulated freight vehicles [101, 132-136]. These performance measures address the dynamic rollover potential, braking performance, jackknife and trailer swing potentials. In case of partly-filled tank vehicles, the safety performance measures may be strongly affected by the dynamic load shift and variations in mass moments of inertia of the moving cargo. The dynamic response characteristics of the partly-filled tank vehicle are thus evaluated in terms of dynamic load shift and different performance measures related to roll and yaw instabilities, such as rollover, jackknifing or trailer swing potentials of the vehicle combination.

Dynamic load shift properties of a partly-filled tank vehicle subject to simultaneous braking and steering are evaluated in terms of variations in the cargo c.g. coordinates and mass moments of inertia, moments induced by cargo shift, and dynamic normal load factor (DLF) of the wheels. The DLF is defined as the instantaneous ratio of dynamic vertical load on a wheel to its static vertical load, expressed as:

$$DLF_k = \frac{F_{zk}}{F_{zk0}}; (k=1, 2, \dots, 10) \quad (6.1)$$

where F_{zk} and F_{zk0} are the instantaneous dynamic and static vertical loads on wheel k , respectively. The dynamic load factor of a wheel is initially unity and may approach zero, when it loses contact with the road under a directional maneuver. The variations in c.g.

coordinates of the cargo cause additional roll, pitch and yaw moments on the vehicle, given by:

$$\begin{aligned} \begin{Bmatrix} M_{lx} \\ M_{ly} \\ M_{lz} \end{Bmatrix} &= \begin{Bmatrix} X_{l2} \\ Y_{l2} \\ Z_{l2} \end{Bmatrix} \times \begin{Bmatrix} a_{lx} \\ a_{ly} \\ a_{lz} \end{Bmatrix} m_{l2} \\ &= m_{l2} \begin{Bmatrix} Y_{l2}a_{lz} - Z_{l2}a_{ly} \\ Z_{l2}a_{lx} - X_{l2}a_{lz} \\ X_{l2}a_{ly} - Y_{l2}a_{lx} \end{Bmatrix} \end{aligned} \quad (6.2)$$

The yaw directional response or the potential yaw instability of a vehicle combination can be detected from the instantaneous values of yaw angles of the sprung masses and their rate of change with respect to time (yaw rates) [36, 101, 113, 120]. The vehicle model is thus analyzed to derive time-histories of yaw rates of the two units and their relative yaw motion (articulation angle) under simultaneous applications of steering and braking. The roll dynamic response of the vehicle combination is assessed in terms of the lateral acceleration, roll angle, and load transfer ratio (LTR) of the combination [93, 128, 136], as described in Chapter 4. The braking performance characteristics of the partly-filled tank vehicle are further evaluated in terms of braking deceleration and wheel-slip response characteristics, as in the case of straight-line braking [101, 197, 206].

6.4 DYNAMIC RESPONSE TO COMBINED BRAKING AND TURNING MANEUVERS: CYLINDRICAL TANK TRAILER

The variable-speed yaw/roll tank vehicle model is analyzed to simulate the dynamic characteristics of the five-axle tractor semitrailer tank vehicle combination under various steering and braking inputs, fill volumes, road conditions and tank cross-sections. The vehicle response characteristics to different steering and braking inputs are initially investigated for a cleanbore cylindrical tank trailer as a function of the fill volume. The analyses are performed for both the partly-filled liquid cargo trailer and an equivalent rigid cargo trailer, while the cargo load is held constant (233.53 kN or 52500 lb). An equivalent rigid cargo is described by an equal cargo mass with c.g. coordinates and inertia properties identical to those of the liquid cargo under static condition.

The results attained for the cleanbore cylindrical tank trailer combination are expressed in terms of the performance measures, and analyzed to enhance an understanding of the vehicle response to combined steering and braking maneuvers. The influence of alternate tank cross-section on the vehicle response is then analyzed to further study the performance benefit potentials of the optimal cross-section tanks under combined steering and braking maneuvers. The simulations are initially performed using the frictional properties of a typical dry road (road A), and the normalized cornering and braking force characteristics of the tires illustrated in Figure 5.6.

The articulated vehicle combination with both the liquid and equivalent rigid cargoes is initially considered to move at a constant forward speed of 80 km/h along a straight path with a uniform surface. A ramp-step steer input (0.5 and 1.0 degree) is then applied, while the speed is held constant. As the vehicle approaches a nearly steady-state

condition ($t \geq 4$ s), a braking input is applied to realize a constant deceleration, as shown in Figure 6.11.

6.4.1 Dynamic Load Shift under Steering and Braking Inputs

The dynamic load shift properties of a 50%-filled (cargo density: 13.57 kN/m^3) articulated tank vehicle equipped with a circular cross-section tank are evaluated under both steering and braking inputs. The dynamic load shift characteristics are assessed in terms of dynamic load factors (DLF) of different tires, using Equation (6.1). The analyses are performed for 0.5 and 1.0 degree ramp-step steer inputs and a braking treadle pressure of 68.95 kPa (10 psi). Figure 6.12 illustrates the time-histories of the DLF responses of tires on the different axles. The results also show the DLF responses of tires of the corresponding equivalent rigid cargo vehicle to illustrate the contributions due to the moving cargo.

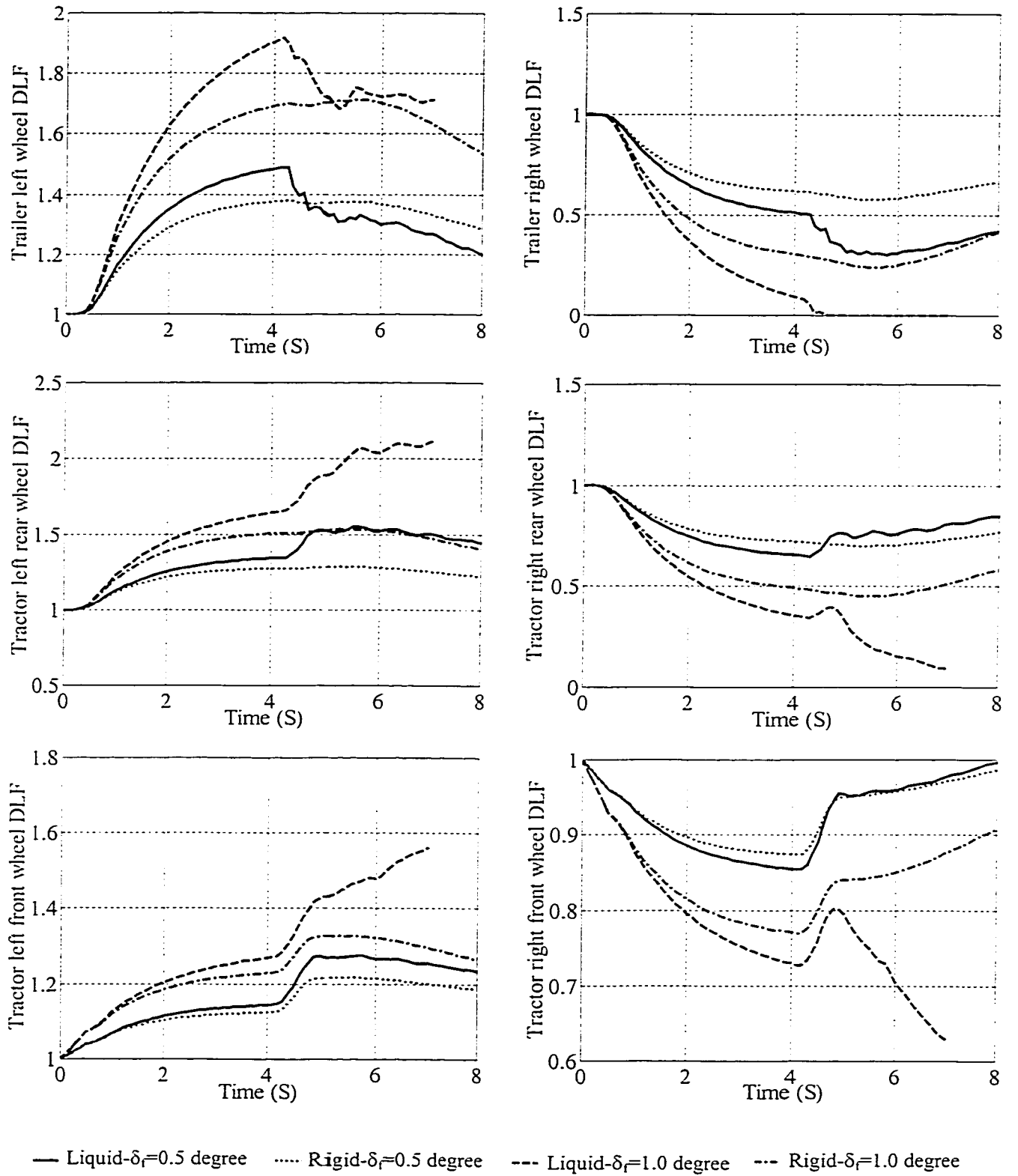


Figure 6.12: Dynamic load factor response of axle wheels under steering and braking input ($T_b=68.95$ kPa).

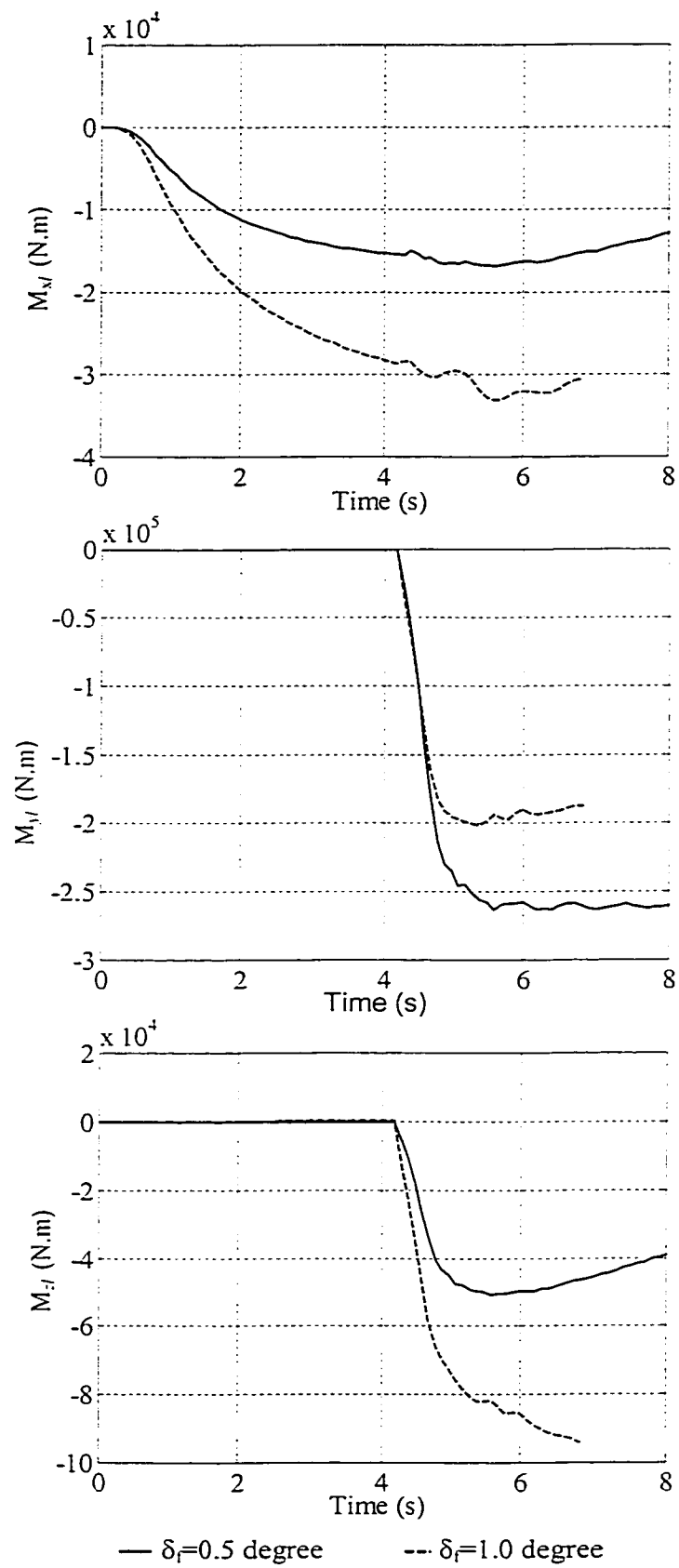


Figure 6.13: Moments induced by variations in the coordinates of the cargo c.g. under steering and braking input ($T_b = 68.95$ kPa).

The results show that the DLF response of different tires approach nearly steady-state values prior to application of braking input at $t=4$ s. The equivalent rigid cargo vehicle exhibits only slight variations in DLF responses of tractor axle tires after the application of braking. The DLF responses of the trailer tires, however, vary rapidly as the brake forces build up. The DLF responses of these tires then tend to approach a steady value in an asymptotic manner. In case of the liquid cargo vehicle, the liquid load shift in the roll plane (ΔY_l and ΔZ_l) results in considerably larger variations in the DLF responses of different wheels, as shown in Figure 6.12. The DLF responses of all the wheels exhibit rapid and significant variations under the application of braking (at $t=4$ s), irrespective of the magnitude of steering input. This rapid change in DLF responses is mostly attributed to the additional moments ($M_{x,l}$, $M_{y,l}$ and $M_{z,l}$) induced by the movement of the liquid cargo in the roll and pitch planes, as shown in Figure 6.13. The results further show that the magnitudes of roll and yaw moments increase considerably with increase in the magnitude of the steering input, while that of the corresponding pitch moment tends to decrease, due to increase in vertical load shift (ΔZ_l), as described in Equation (6.2).

Under a steady steering input of 0.5 degree, the liquid load shift along the longitudinal direction (ΔX_l) and thus the pitch moment ($M_{y,l}$) approach nearly steady values after application of braking input ($t \geq 5.2$ s), while the cargo shift in the roll plane (ΔY_l and ΔZ_l) and the corresponding roll and yaw moments ($M_{x,l}$ and $M_{z,l}$) decrease gradually, due to reduction in the forward speed and the corresponding lateral acceleration. The DLF responses of the wheels on the outer track thus decrease. The rigid cargo vehicle, however, exhibits only slight variations in the DLF responses of the tractor

rear- and trailer-axle wheels following the application of braking. The DLF responses of various wheels exhibit certain oscillations occurring at approximately 1.3Hz, which is most likely attributed to the pitch mode oscillation of the vehicle combination.

6.4.2 Directional Response under Steering and Braking Inputs

The directional response characteristics of the partly-filled and equivalent rigid cargo vehicles, evaluated under combined braking and steering inputs, are expressed in terms of lateral and longitudinal accelerations of the trailer sprung weight (a_{y2} , a_{x2}), roll angle and yaw rate of the trailer sprung weight (θ_{s2} , r_2), articulation angle (γ), LTR as evaluated from Equation (4.14), and wheel slip response of different tires. Figures 6.14 and 6.15 illustrate the time-histories of these measures under step steer inputs of 0.5 and 1.0 degrees, and treadle pressure of 68.95 kPa (10 psi).

Both the equivalent rigid and liquid cargo vehicles exhibit stable directional behavior under application of steering inputs, as determined from the measures illustrated in Figure 6.14. The vehicle with the liquid cargo, however, yields considerably larger magnitudes of trailer lateral acceleration, roll angle, yaw rate, articulation angle and LTR than the vehicle with the equivalent rigid cargo. This is mostly attributed to the additional roll moments caused by the liquid load transfer, illustrated earlier in Figure 6.13. Under application of braking at $t=4$ s, the cargo tends to further shift towards front of the trailer, resulting in rapid increase in ΔX_l and ΔZ_l . The magnitudes of ΔY_l , however, decrease under braking due to combined influence of the lateral and longitudinal forces imposed on the liquid bulk, as discussed in Section 6.2. This gives rise to pronounced pitch and yaw moments due to liquid load shift, resulting in rapid variations in the DLF of the tractor axle wheels near $t=4.3$ s, as shown in Figure 6.12.

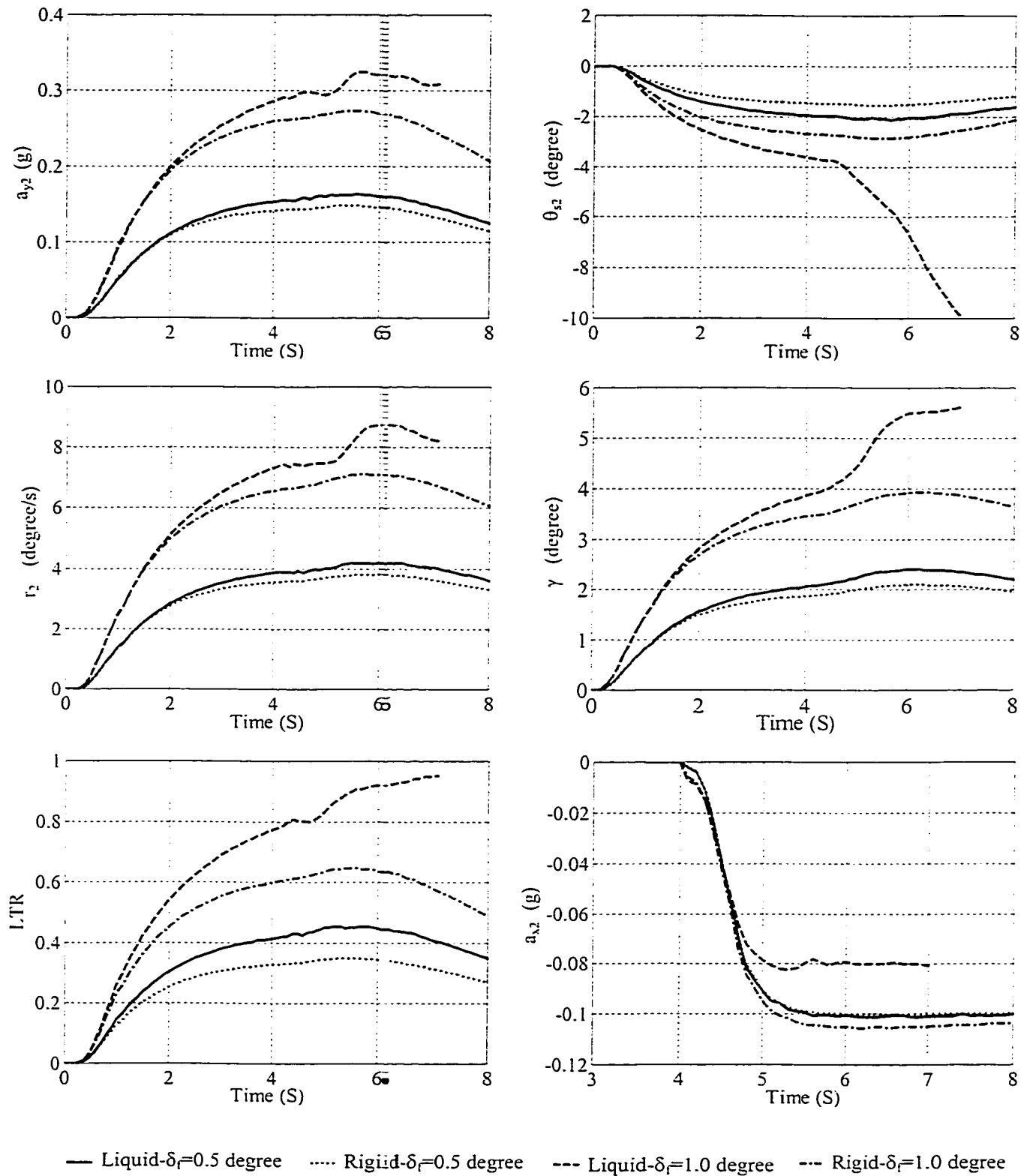


Figure 6.14: Directional response characteristics of the liquid and equivalent rigid cargo vehicles under steering and braking input ($T_b = 68.95$ kPa).

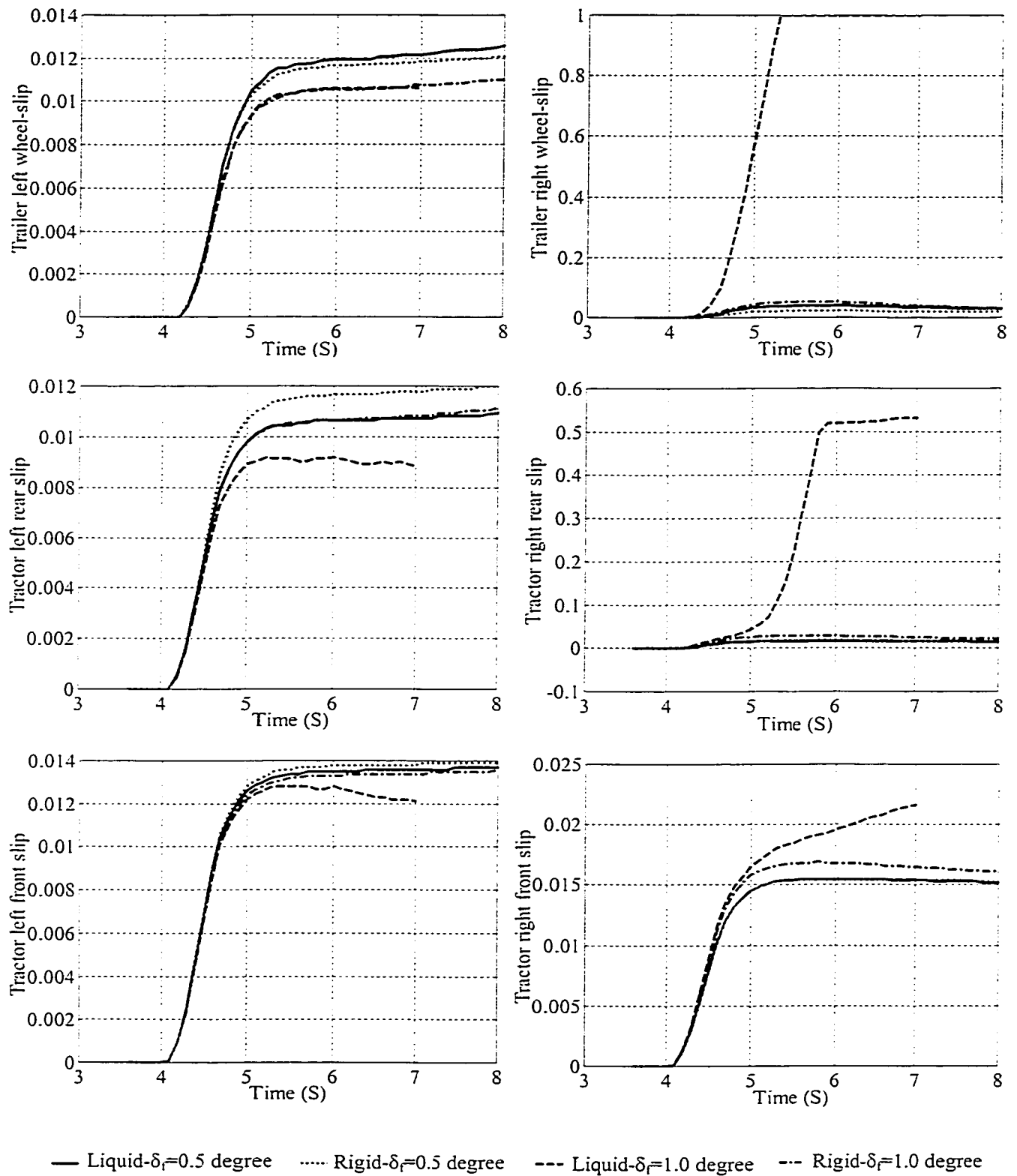


Figure 6.15: Wheel-slip responses under steering and braking input ($T_b=68.95$ kPa).

The application of braking in addition to the constant front wheel steer input causes a further increase in the directional response variables of both the liquid and rigid cargo vehicles. The magnitudes of all the response variables, with the exception of LTR response of liquid cargo vehicle under 1.0 degree steer input, approach their maximum values near 5.5 s and then decrease as the vehicle speed decreases under braking. It is also interesting to note that the LTR response of liquid cargo vehicle subjected to 1 degree steer input and braking approaches unity value near $t=7.0$ s, indicating potential roll instability.

The dynamic characteristics of the tank vehicle combination under braking-in-a turn maneuver are strongly influenced by the magnitudes of steering and braking inputs. Applications of higher levels of steering and braking inputs could cause more pronounced load shift in case of liquid cargo vehicles, and the response characteristics of such vehicles could deviate significantly from those of the corresponding rigid cargo vehicles. An increase in the steer angle from 0.5 degree to 1.0 degree causes dominant lateral load transfer in the roll plane as evident from the DLF responses of the wheels shown in Figure 6.12. The application of braking input causes significant shift in the longitudinal and vertical coordinates of the cargo c.g. and thus rapid variations in the DLF responses. Under application of larger steering input (1.0 degree), the inner (right) wheels of the trailer axles experience lock-up immediately after the braking is applied ($t=4.3$ s), due to rapid decrease in DLF or loss of wheel-road contact, as evident from the wheel slip responses shown in Figure 6.15. The wheel slip and DLF responses of inner wheels of the tractor axles also increase when the braking input is applied. As the shift in the vertical c.g. coordinate (ΔZ_l) increases to a steady value, the corresponding rise in the roll

moment causes the DLF of the inner wheels of the tractor axles to decrease rapidly at $t=4.8$ s. The LTR of the liquid cargo vehicle thus increases towards a unity value indicating a possible rollover, while that of the equivalent rigid cargo vehicle reaches a maximum value of approximately 0.65 and then decreases with forward speed, as shown in Figure 6.14. The possible rollover of the liquid cargo vehicle is further evident from the rapid increase in the magnitude of roll angle of the trailer, shown in the figure.

6.4.3 Influence of Brake Treadle Pressure

The directional response characteristics of liquid cargo vehicles are further investigated under different levels of braking strength. Two different values of brake treadle pressure (68.95 kPa and 206.85 kPa, or 10 psi to 30 psi) are used in the analyses, while the steady value of step-steer input is selected as 0.5 degree. Figure 6.16 illustrates the influence of brake treadle pressure on the roll, pitch and yaw moments (M_{x_l} , M_{y_l} and M_{z_l}) due to cargo load transfer within a 50%-filled tank trailer subject to 0.5 degree steer input. The results show that an increase in the braking treadle pressure from 10 psi to 30 psi causes more pronounced load shift in the pitch plane (ΔX_l and ΔZ_l), as evident from variations in M_{y_l} and M_{z_l} , which vary considerably immediately after the application of braking. The magnitude of ΔY_l under relatively higher braking treadle pressure input, however, decreases sharply, as observed earlier in Figure 6.3 and discussed in Section 6.2, resulting in decrease in the magnitudes of cargo shift induced yaw and roll moments. An increase in braking strength thus yields considerably larger variations in the DLF responses of different tires, as shown in Figure 6.17. In case of the liquid cargo vehicle, the magnitudes of the DLF responses of trailer wheels fall below unity, while those of tractor wheels rise above unity, irrespective of left or right tracks. This is mostly

attributed to the dominant influence of pitch plane load shift and thus the pronounced liquid induced pitch moment, as shown in Figure 6.16.

An increase in brake treadle pressure yields only moderate increase in the peak values of the directional response variables of the vehicles (a_{y2} , θ_{s2} , r_2 , γ and LTR), as illustrated in Figure 6.18. The most notable changes are observed immediately after the braking application. An increase in brake treadle pressure yields rapid decrease in response variables after the transient state, due to rapid decrease in forward velocity. The liquid cargo vehicle, although directionally stable ($LTR \leq 0.5$), yields considerably larger magnitudes of response variables than those attained for the equivalent rigid cargo vehicle. The increased pitch plane load shift, however, results in lockup of the inner trailer wheels of the liquid cargo vehicle soon after the application of braking ($t=5$ s), as observed from the wheel slip responses shown in Figure 6.19.

Under high levels of steering and braking inputs, the excessive load transfer in the roll and pitch planes and rapid lockup of the trailer inner wheels result in considerable decrease in the braking force, and consequently lower deceleration in case of the liquid cargo vehicles, as shown in Figures 6.14 and 6.18. The braking performance of a partly-filled liquid cargo vehicle is thus considerably inferior to that of the equivalent rigid cargo vehicle. The rapid lockup of the inner trailer wheels of the liquid cargo vehicle, however, affects the directional behavior of the vehicle combination only slightly, and the vehicle remains directionally stable. This can be attributed to two factors: (i) the trailer axle tires continue to transfer sufficient lateral force due to outer wheels, which are subject to considerably larger normal load; and (ii) the yaw moment generated by the uneven braking forces tends to offset the incipient outward yaw of the trailer.

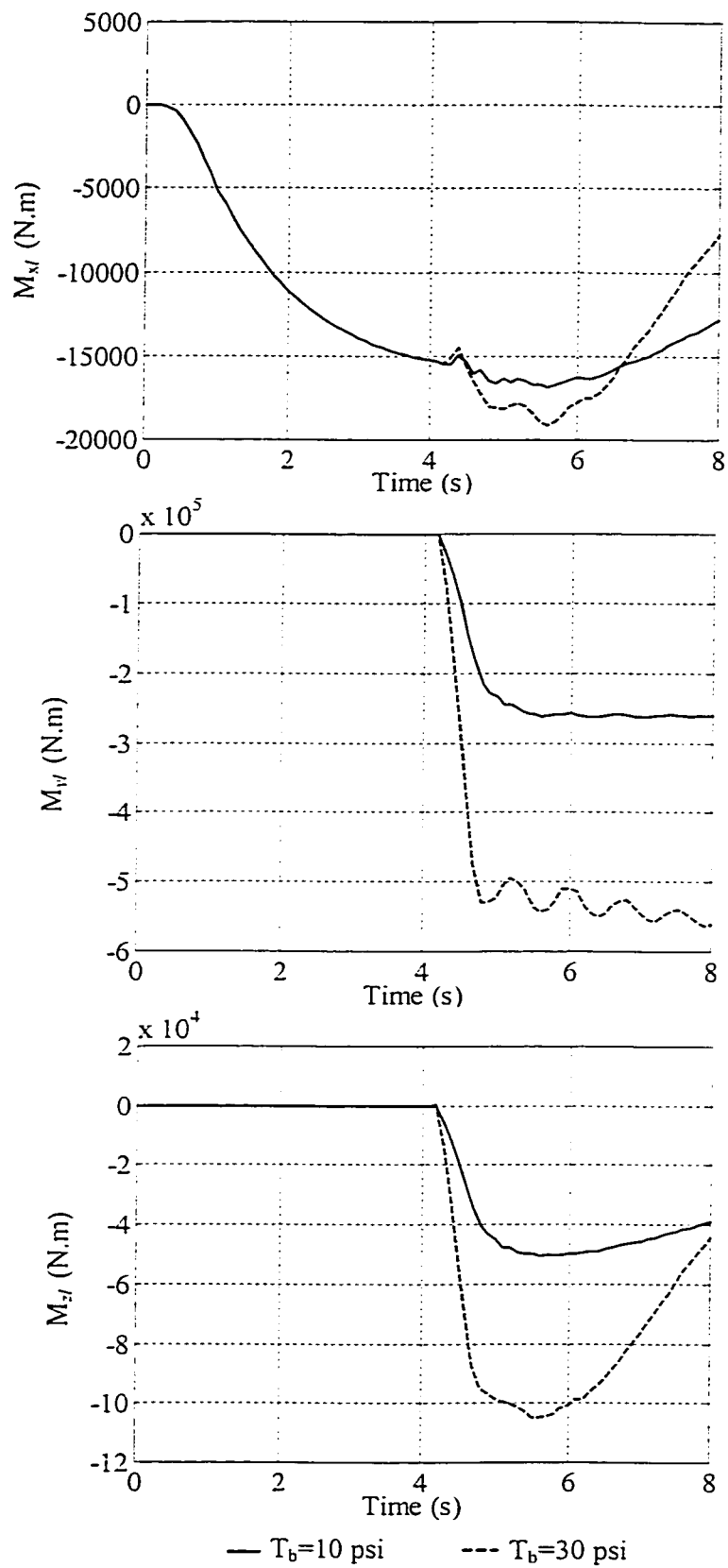


Figure 6.16: Influence of brake treadle pressure on the moments induced by variations in the coordinates of the cargo c.g. ($\delta_r = 0.5$ degree).

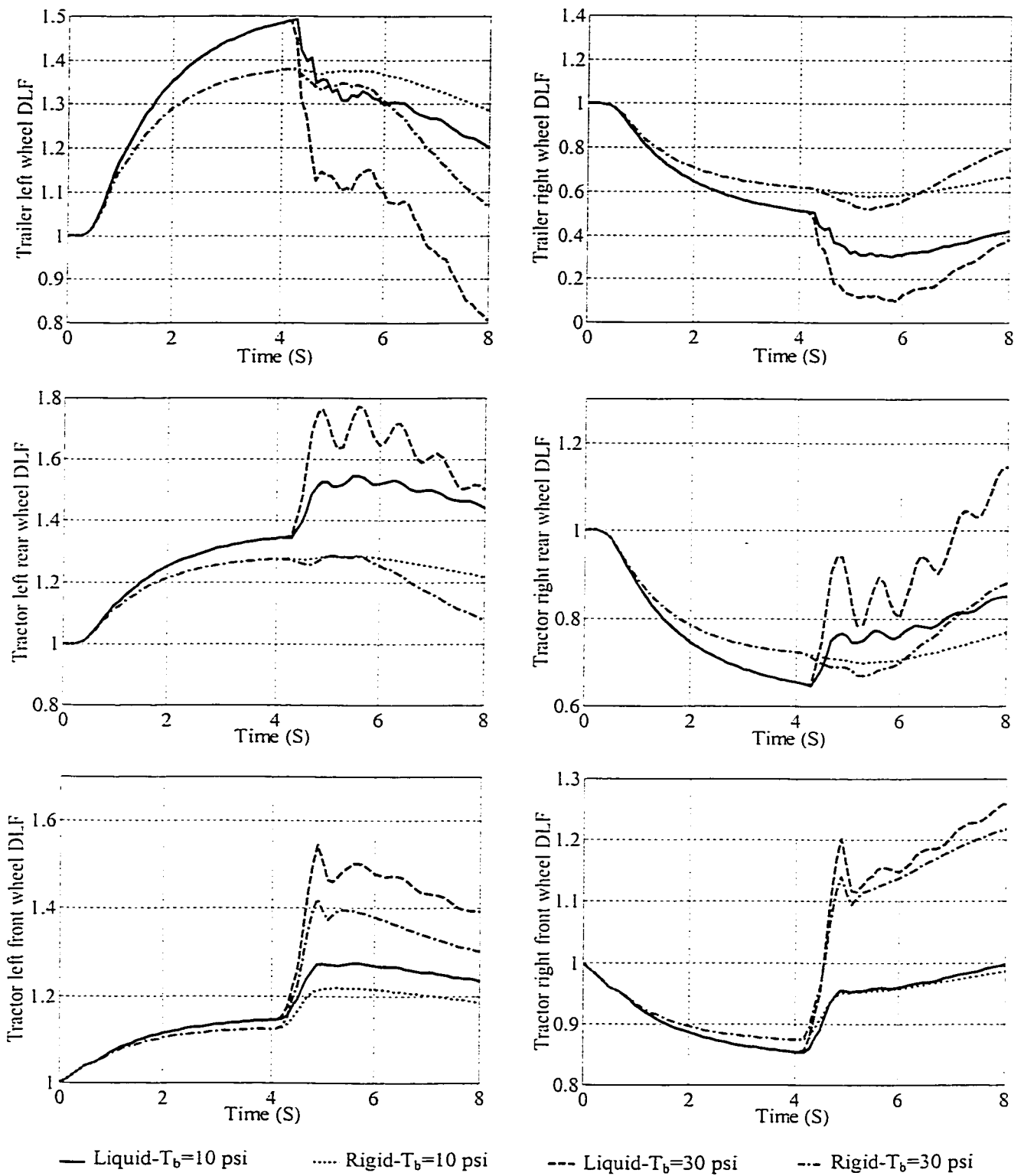


Figure 6.17: Influence of brake treadle pressure on the DLF responses of axle wheels ($\delta_f=0.5$ degree).

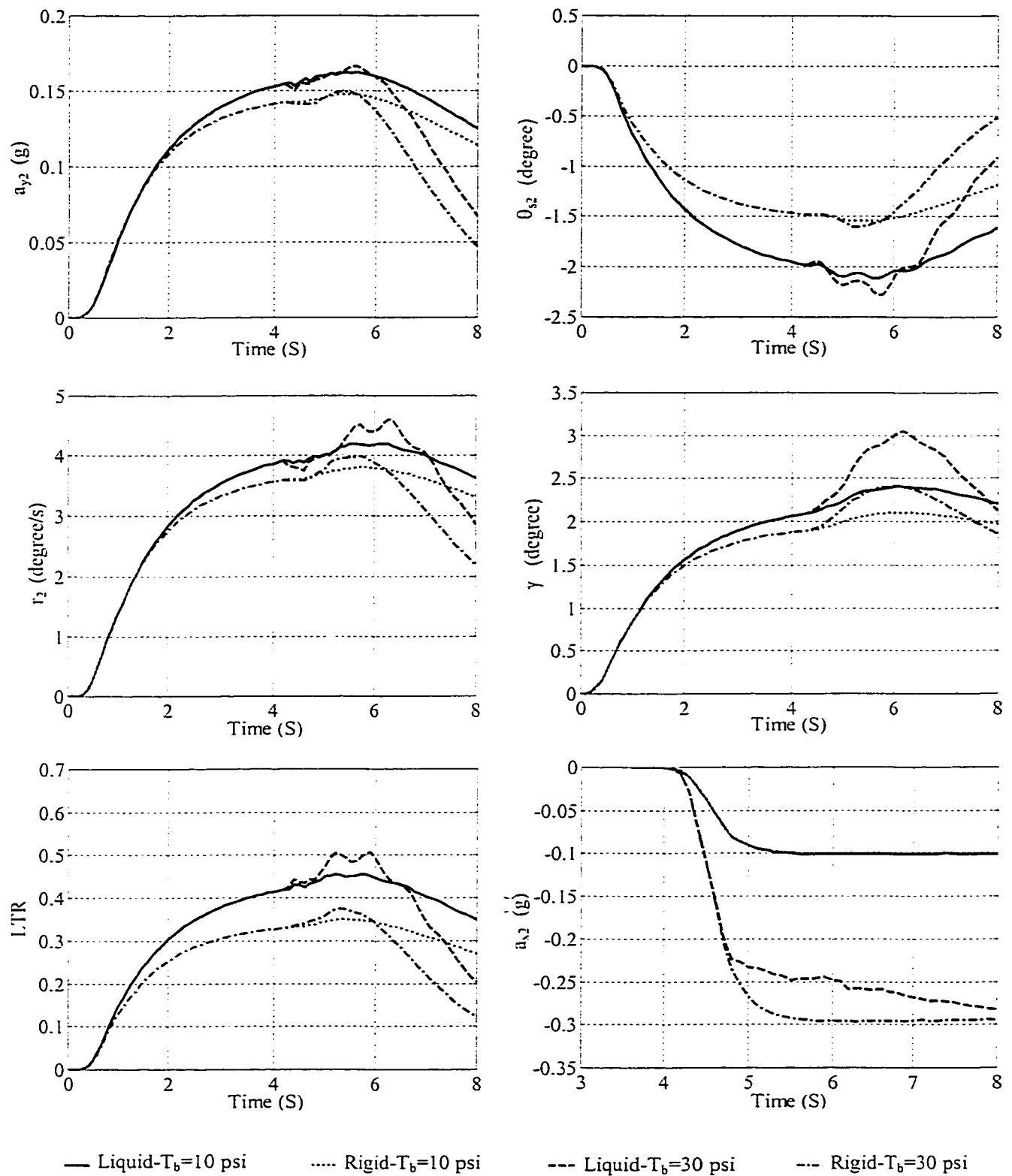


Figure 6.18: Influence of brake treadle pressure on the directional responses of the liquid and rigid cargo vehicles ($\delta_r=0.5$ degree).

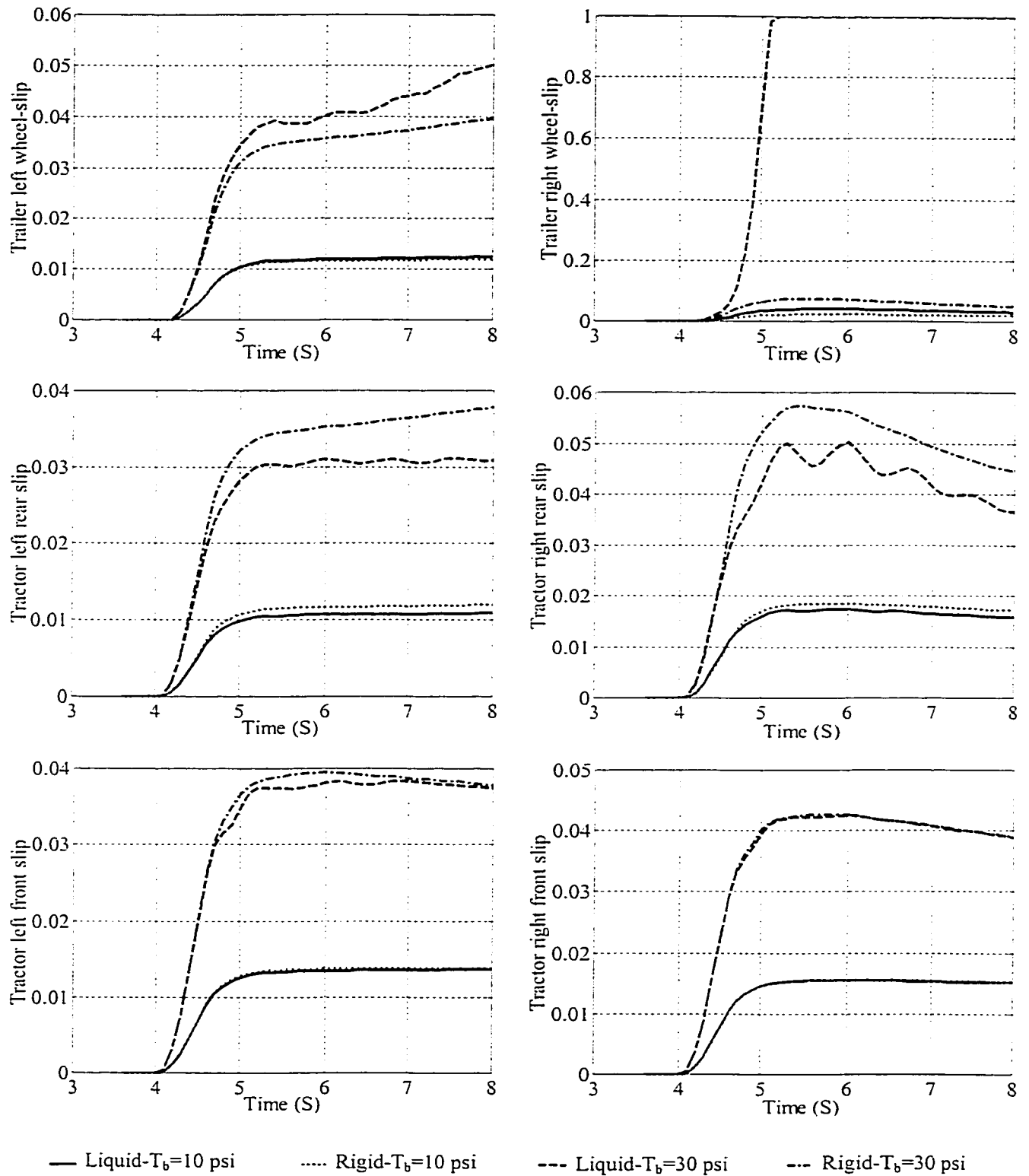


Figure 6.19: Influence of brake treadle pressure on the wheel-slip responses ($\delta_f=0.5$ degree).

6.4.4 Influence of Cargo Fill Volume

The simulations and analyses are further performed for the vehicle combination with different cargo fill volumes. The variations in the fill volume are achieved by varying the mass density of the liquid cargo, while the cargo load is held constant (233.53 kN). Figure 6.20 presents the directional responses of the 80%-filled (cargo density: 13.57 kN/m³) liquid and equivalent rigid cargo vehicles, subjected to 0.5 and 1.0 degree ramp-step steer inputs and a braking treadle pressure of 68.95 kPa (10 psi).

As expected for circular cross-section tank, an increase in fill volume yields considerable decrease in liquid load shift in the roll and pitch planes, and thus significant reduction in the moments induced by the liquid load shift. In case of the rigid cargo vehicle, a higher fill volume yields larger magnitudes of DLF, and the directional response variables (a_{y2} , θ_{s2} , r_2 , γ and LTR) due to increased cargo c.g. height, specifically for relatively larger steer input, while the liquid cargo vehicle yields only slight increase in the response magnitudes due to the combined influence of reduced liquid load shift and higher c.g. height of the circular cross-section. Under lower fill volumes, the expected decrease in the magnitudes of the response variables due to lower c.g. height is largely offset by the considerably larger cargo load shift, similar to the case of constant speed directional analyses, conducted in Chapter 4.

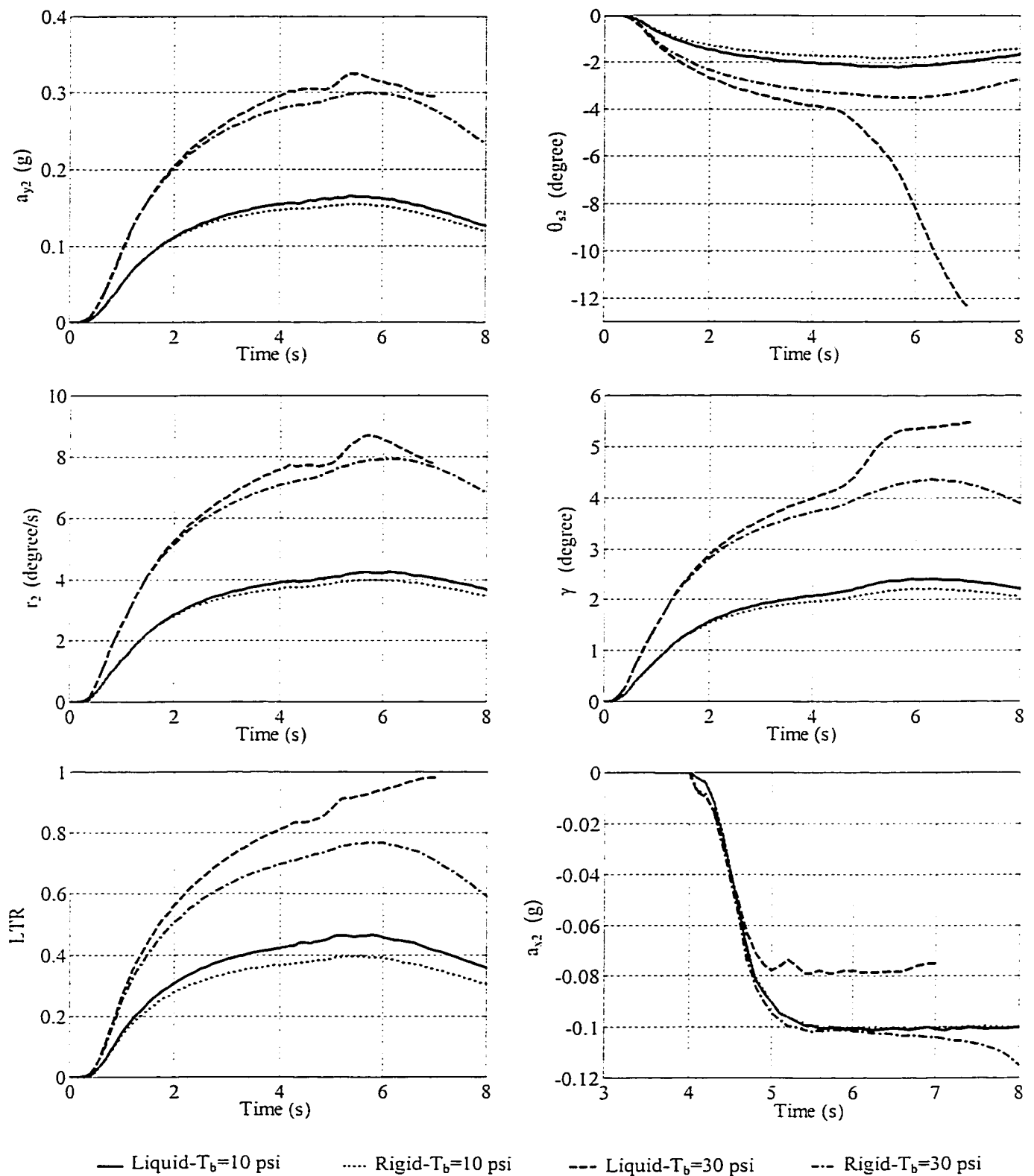


Figure 6.20: Directional response characteristics of the liquid and equivalent rigid cargo vehicles under steering and braking input ($\beta=0.8$, $T_b=68.95$ kPa).

6.4.5 Influence of Road Conditions

The traction, braking and cornering forces developed by tires are strongly influenced by the road friction properties. The dynamic characteristics of the vehicle combination under braking-in-a-turn maneuvers are therefore influenced by the road surface friction properties. The results presented in the previous Sections were derived for a dry road (road A) with a friction coefficient $\mu=0.9$. In this Section, the directional response characteristics of the vehicles are derived for a wet road (road B), assuming a friction coefficient of 0.4, to study the influence of road surface friction. Figures 6.21 through 6.22 present a comparison of the liquid induced moments and dynamic response of the vehicles equipped with a 50%-filled liquid tank (cargo density: 13572 N/m^3 , payload: 233.53 kN) and the corresponding equivalent rigid cargo, subject to a steer input of 0.5 degree and braking treadle pressures of 10 and 30 psi , respectively, on road B.

Similar to the results derived for road A, both vehicles exhibit stable behavior under the application of steering alone and the response variables approach their respective steady values near $t=4 \text{ s}$. The magnitudes of LTR approach 0.37 and 0.31 , respectively, for the liquid and rigid cargo vehicles, as shown in Figure 6.22. In case of the liquid cargo vehicle, application of braking yields a sharp increase in ΔX_l and ΔZ_l , with a decrease in ΔY_l during the transient stage, leading to rapid growth in the pitch and yaw moments, as shown in Figure 6.21. After the transient stage, the resulting roll and yaw moments, however, decrease due to reduction in the roll plane liquid load shift with decrease in forward speed and thus the lateral acceleration.

Under a braking treadle pressure of 10 psi , the dynamic response characteristics of both vehicles, expressed in terms of trailer lateral and longitudinal accelerations, roll

angle, yaw rate, articulation angle, LTR, and wheel-slip, are similar to those attained on road A, as illustrated in Figures 6.22 and 6.23. Under 30 psi braking treadle pressure, however, the pronounced liquid load shift in the pitch plane of the liquid cargo vehicle dominates the axle load transfer, leading to sharp increase in the tractor axle loads and sudden decrease in the trailer axle loads. The trailer axles thus experience lockup due to low friction coefficient available on road B, as evident from the wheel-slip response shown in Figure 6.23. The superimposition of the roll and pitch plane load transfers results in only slight increase in lateral acceleration, LTR and roll angle response of the vehicle following the application of braking, due to relatively low steer input. The trailer yaw rate and articulation angle, however, increase sharply, when the liquid cargo vehicle is subjected to a 30 psi treadle pressure input, as shown in Figure 6.22. The sudden increase in the yaw response on road B can be attributed to rapid increase in the wheel-slip of the trailer tires leading to wheel lockup, which in turn limits the available friction coefficient that could be used to generate the lateral forces, inducing a sharp drop and complete loss of the lateral force on the trailer axles in the case of the liquid cargo vehicle, as shown in Figure 6.24, and thus a rapid increase in the side-slip angle of the trailer. The sudden growth of the trailer side-slip angle results in a sharp increase in the trailer yaw rate and the articulation angle of the vehicle combination after 6s, as shown in Figure 6.22, an indication of an incipient trailer swing. For the liquid cargo vehicle, the inner trailer wheels experience lockup near $t=5$ s, while the outer trailer wheels exhibit lockup near $t=6$ s. The tractor rear inner wheels reveal lockup after 6.4 s. The rigid cargo vehicle also exhibits lockup of wheels at the inside of trailer and tractor rear axles, which occur almost simultaneously after 5.4 s due to rapid reduction in the wheel velocities and

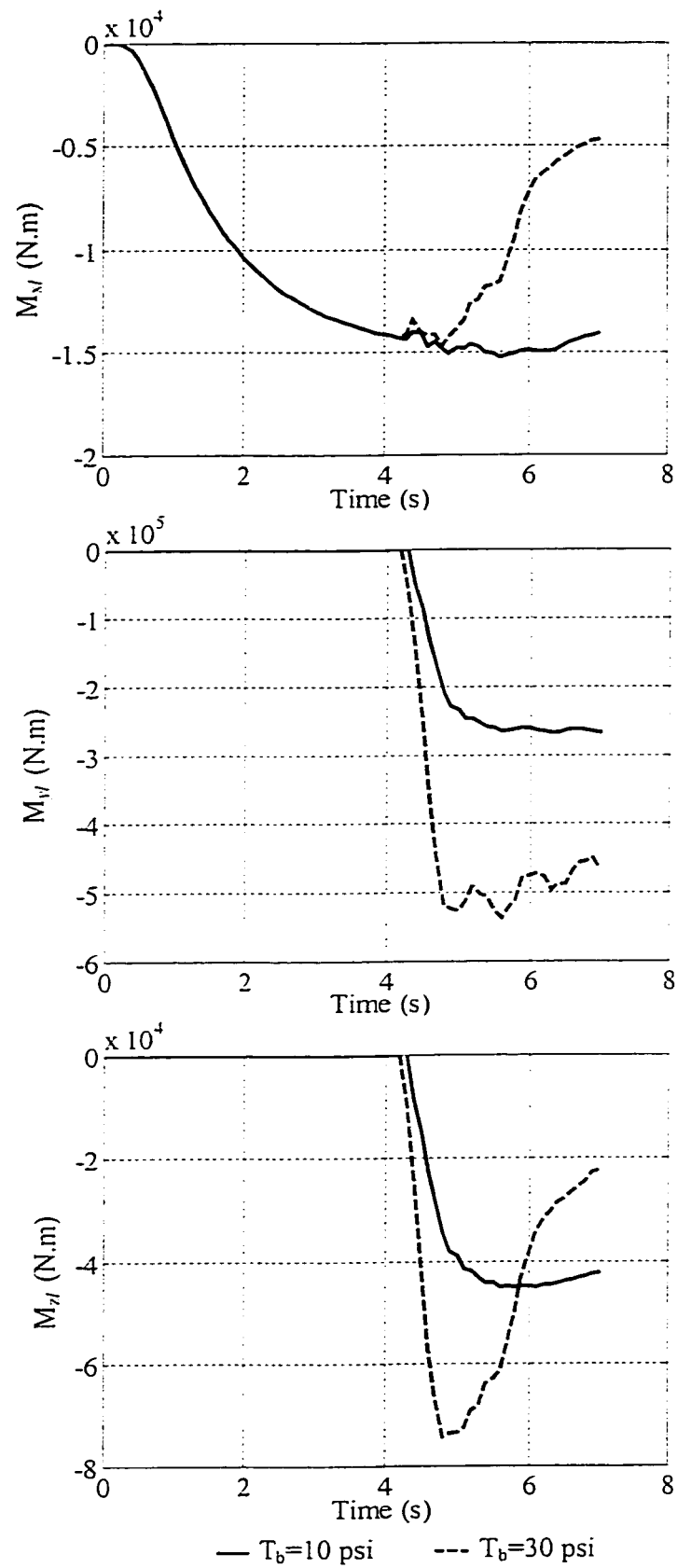


Figure 6.21: Moments induced by variation in the coordinates of the cargo c.g. under steering and braking input ($\delta_r = 0.5$ degree, road B).

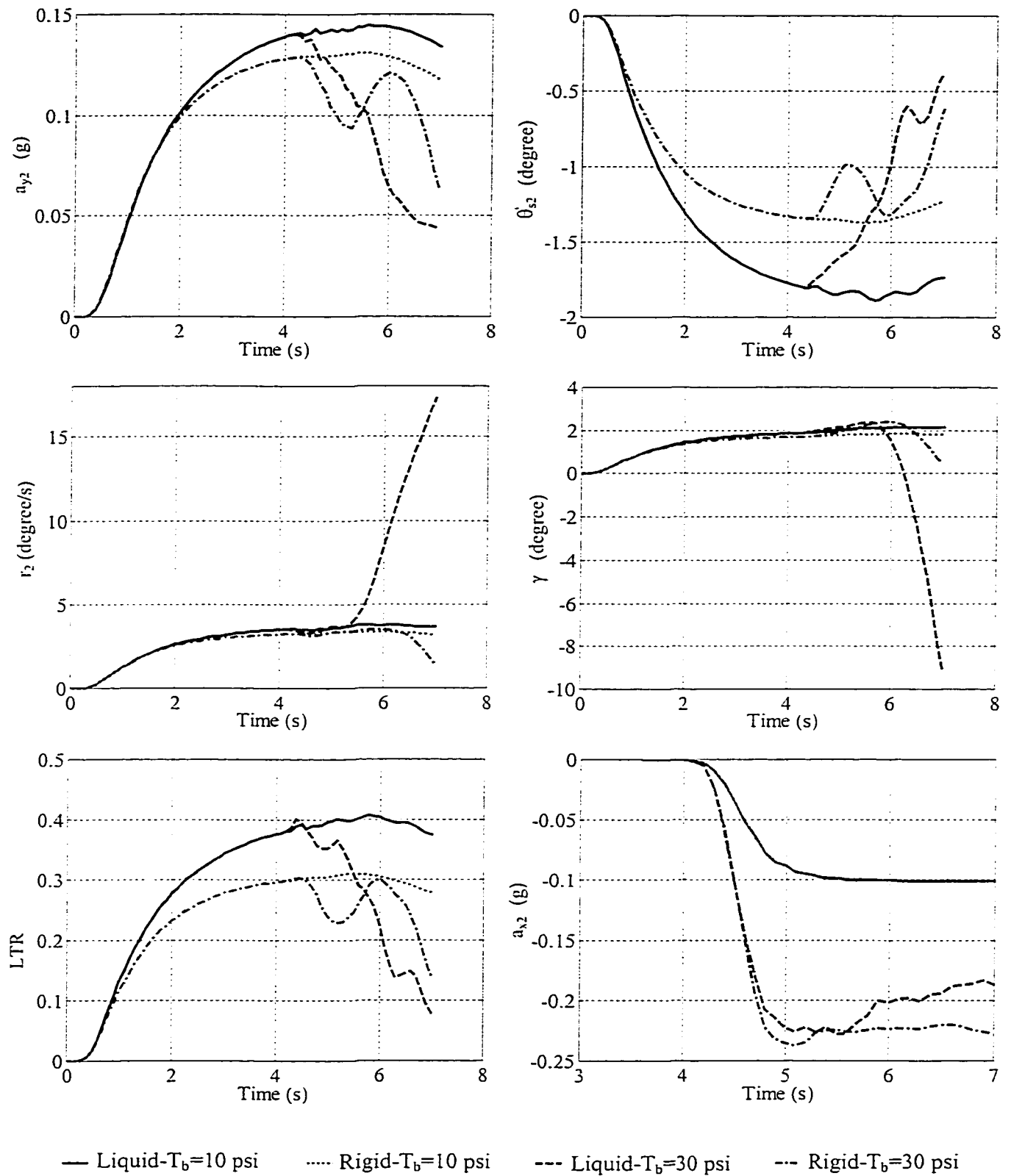


Figure 6.22: Directional and roll response of the liquid and rigid cargo vehicles under steering and braking input ($\delta_r=0.5$ degree, road B).

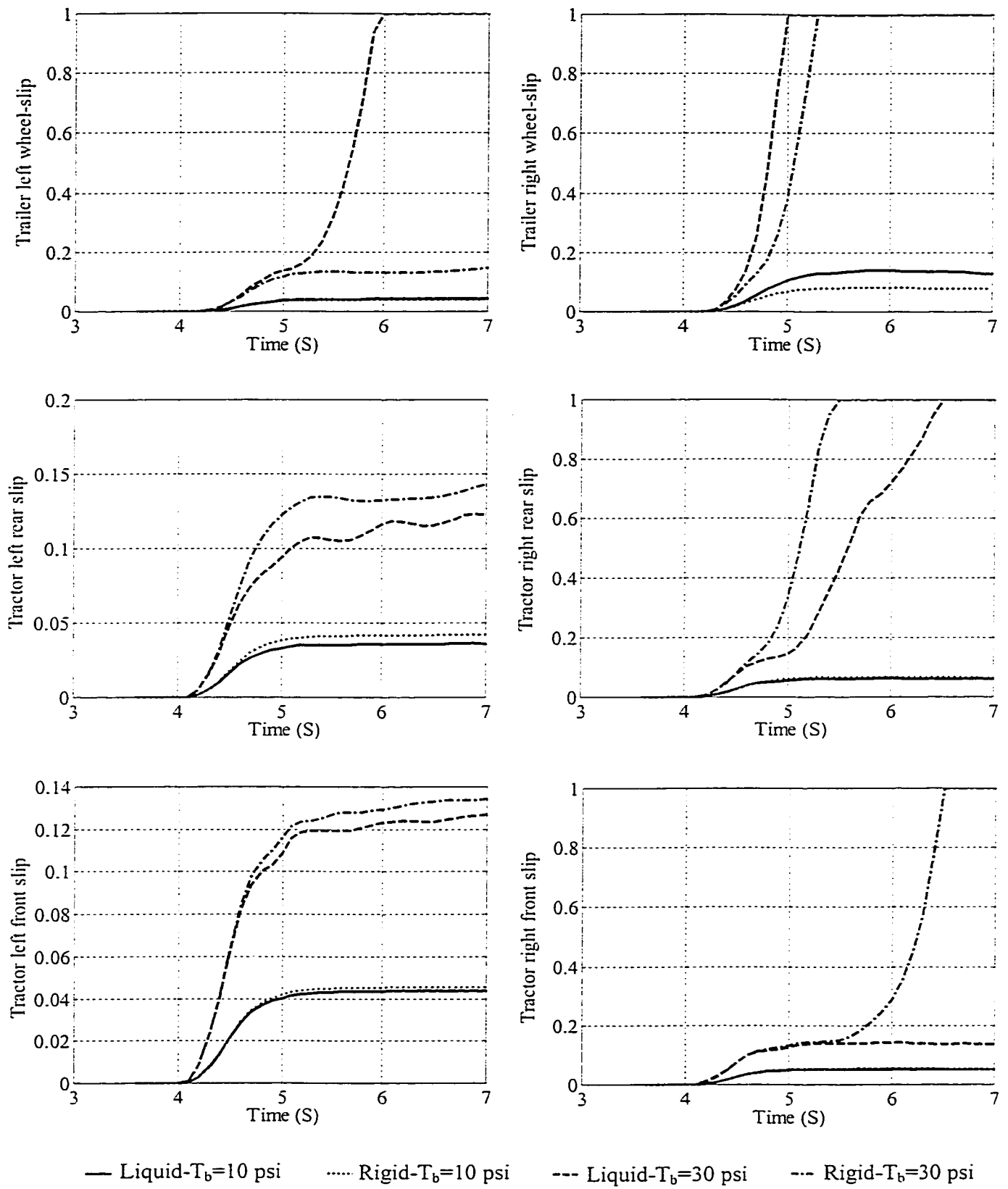
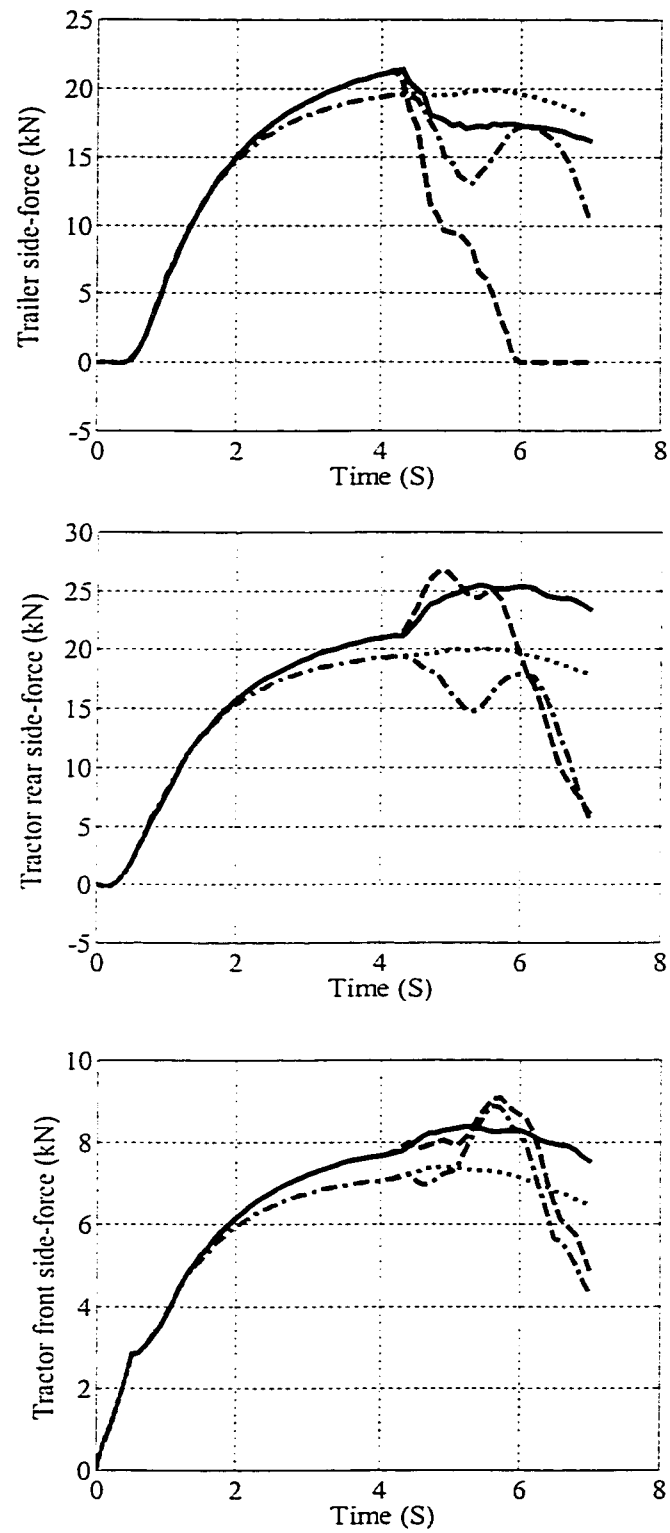


Figure 6.23: Wheel-slip response under steering and braking input ($\delta_f=0.5$ degree, road B).



— Liquid-T_b=10 psi Rigid-T_b=10 psi --- Liquid-T_b=30 psi --- Rigid-T_b=30 psi

Figure 6.24: Axle lateral force response under steering and braking input ($\delta_r=0.5$ degree, road B).

low friction coefficient of the road B. The vehicle, however, reveals stable directional behavior, as shown in Figure 6.22. It should be noted that the tractor rear axle of the rigid cargo vehicle locks up first, as shown in Figure 6.23, due to less forward-load-transfer from the trailer axles.

6.5 DIRECTIONAL RESPONSE OF TANK VEHICLES WITH OPTIMAL TANKS

The variable-speed tank vehicle model is further analyzed to evaluate the possible influence of tank cross-section on the dynamic characteristics of the articulated vehicle combination under combined steering and braking maneuvers. The directional response characteristics of the vehicles with different cross-section tanks are analyzed to assess the potential performance benefits of the optimal cross-sections under combined braking and steering inputs. The analyses are performed for vehicles equipped with the conventional circular and modified-oval tanks as well as the optimal tanks (*OPT1* and *OPT2*) under 50% fill volume (cargo density: 13572 N/m^3 , payload: 233.53 kN) and subject to a steer input of 0.8 degree and braking treadle pressures of 10 psi on road A ($\mu=0.9$). Figures 6.25 and 6.26 present a comparison of the DLF responses of the wheels and directional response characteristics of the vehicle.

All the vehicle combinations, irrespective of the tank geometry, exhibit steady turning response before $t=4 \text{ s}$, similar to the results derived for constant-speed steering maneuvers in Chapter 4. The modified-oval tank yields the most significant overturning moment (M_{xl}), due to the excessive lateral load shift within its wide cross-section. The modified-oval cross-section tank vehicle, therefore, yields largest variations in the DLF responses of the tires under steering, and steering and braking inputs, as shown in Figure 6.25. The vehicle with *OPT1* tank yields minimal variations in M_{xl} and the DLF

responses, which is mostly attributed to its considerably narrow cross-section. The vehicle with *OPT2* tank also exhibits quite similar responses in M_{xI} and the DLF. The vehicle combinations with the optimal tanks also reveal lower magnitudes of directional response variables when compared with those of the vehicles with circular and modified-oval tanks, as shown in Figure 6.26. At $t=4$ s, the magnitudes of LTR of the vehicles with modified-oval, circular, *OPT1* and *OPT2* tanks approach approximately 0.75, 0.68, 0.6 and 0.58, respectively.

Application of the braking yields somewhat similar trends in variations of the liquid induced moments and vehicle response variables, irrespective of the tank cross-section. The load shift in the pitch plane (ΔX_I and ΔZ_I) and thus the cargo-induced pitch and yaw moments increase rapidly, resulting in a rapid normal load transfer from the trailer axles to the tractor axles during the transient stage of the braking, as shown in Figures 6.25. The DLF responses of inner (right) wheels of the axles of the trailer with modified-oval and circular tanks approach zero at about 4.4 s and 5.1 s, respectively, indicating loss of tire-road contact. This is attributed to the combined effects of considerable liquid load shifts in the roll and pitch planes, as observed from the DLF responses in Figure 6.25. The loss of contact of the trailer inner wheels in turn causes a considerable variation in the DLF responses of the tractor wheels, which is most significant in the case of the modified-oval tank. This significant deviation in DLF is mostly attributed to relatively dominant influence of the liquid induced roll moment and considerably large value of LTR (0.75). The discrepancy in the responses of the vehicle with the conventional and optimal tanks is thus further exaggerated following the braking application, as shown in Figures 6.25 and 6.26.

As the braking forces build up and the vehicle assumes a nearly steady deceleration (a_{x2}), the variations in DLF responses of most of the tires reduce, except for the modified-oval tank vehicle. The magnitudes of selected directional response variables also tend to vary quite slowly, as shown in Figure 6.26, due to decrease in ΔY_l with decreasing vehicle speed. The vehicle with the circular tank reveals stable behavior, although the trailer right wheels lose contact with the road. The corresponding magnitudes of response variables, however, are considerably larger than those attained for both the optimal geometry tank cross-sections, owing to the relatively larger overturning moment arising from lateral load shift and higher c.g. height of the cargo within the circular tank.

The results also show that application of braking yields only minimal impact on the lateral load shift (ΔY_l) in the case of the modified-oval tank, due to relatively significant role of the lateral acceleration coupled with partly-filled liquid cargo within the wide cross-section, as discussed earlier in Section 6.2. The magnitudes of vehicle response variables thus continue to increase even after the inner trailer wheels lose contact with the road due to excessive roll moment caused by the liquid load shift. The vehicle combination with the modified-oval tank, therefore, exhibits an impending roll instability, as evident from the rapidly increasing roll angle and LTR responses shown in Figure 6.26. The magnitudes of deceleration of the vehicles with conventional tanks also approach relatively higher values due to loss of contact of the trailer inner wheels with the road.

The potential performance benefits of the optimal cross-section tanks in enhancing the directional response characteristics of partly-filled tank vehicles under

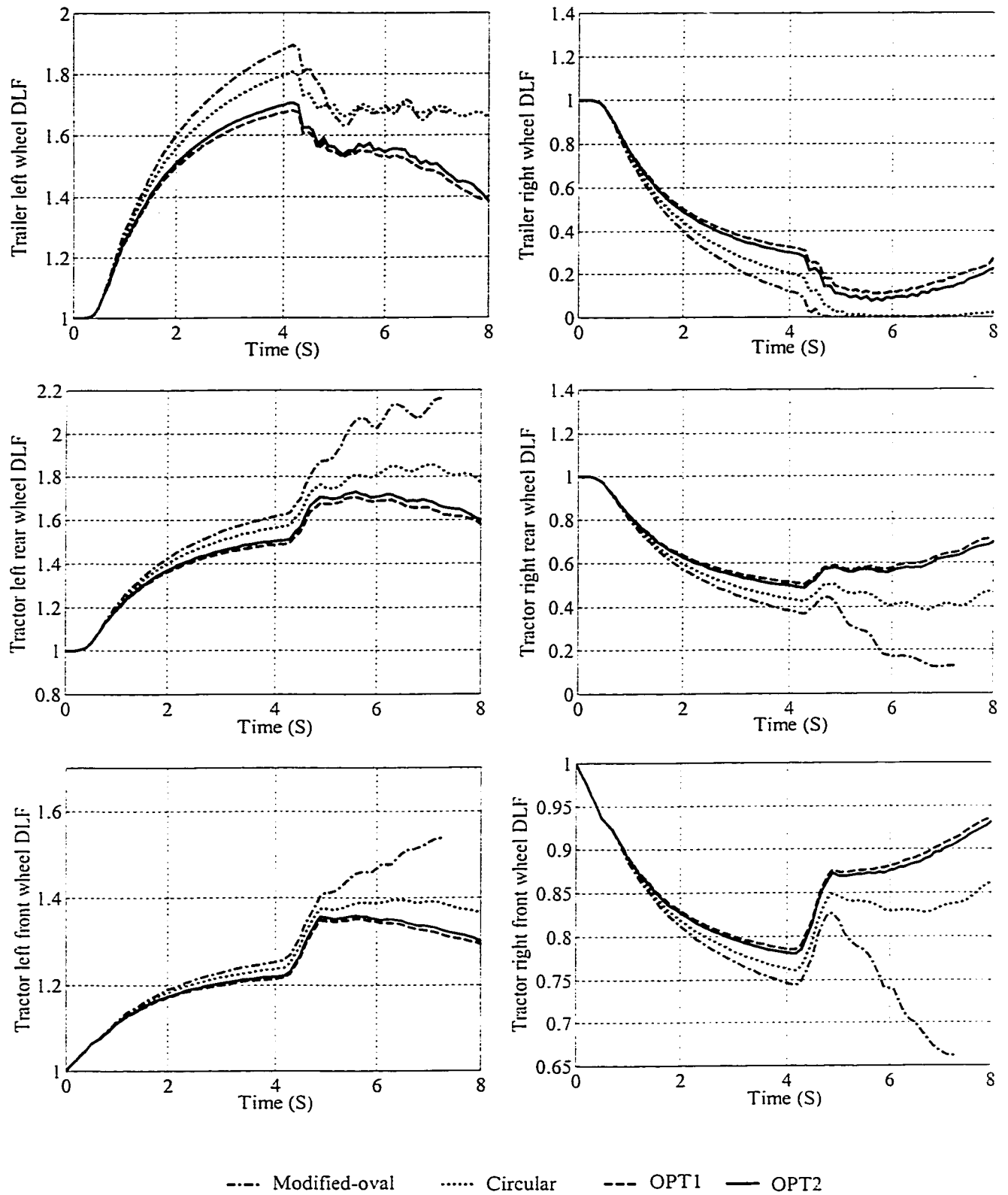


Figure 6.25: Dynamic load factor response of the vehicle with various tanks under steering and braking input ($\delta_r=0.8$ degree, $T_b=10$ psi, road A).

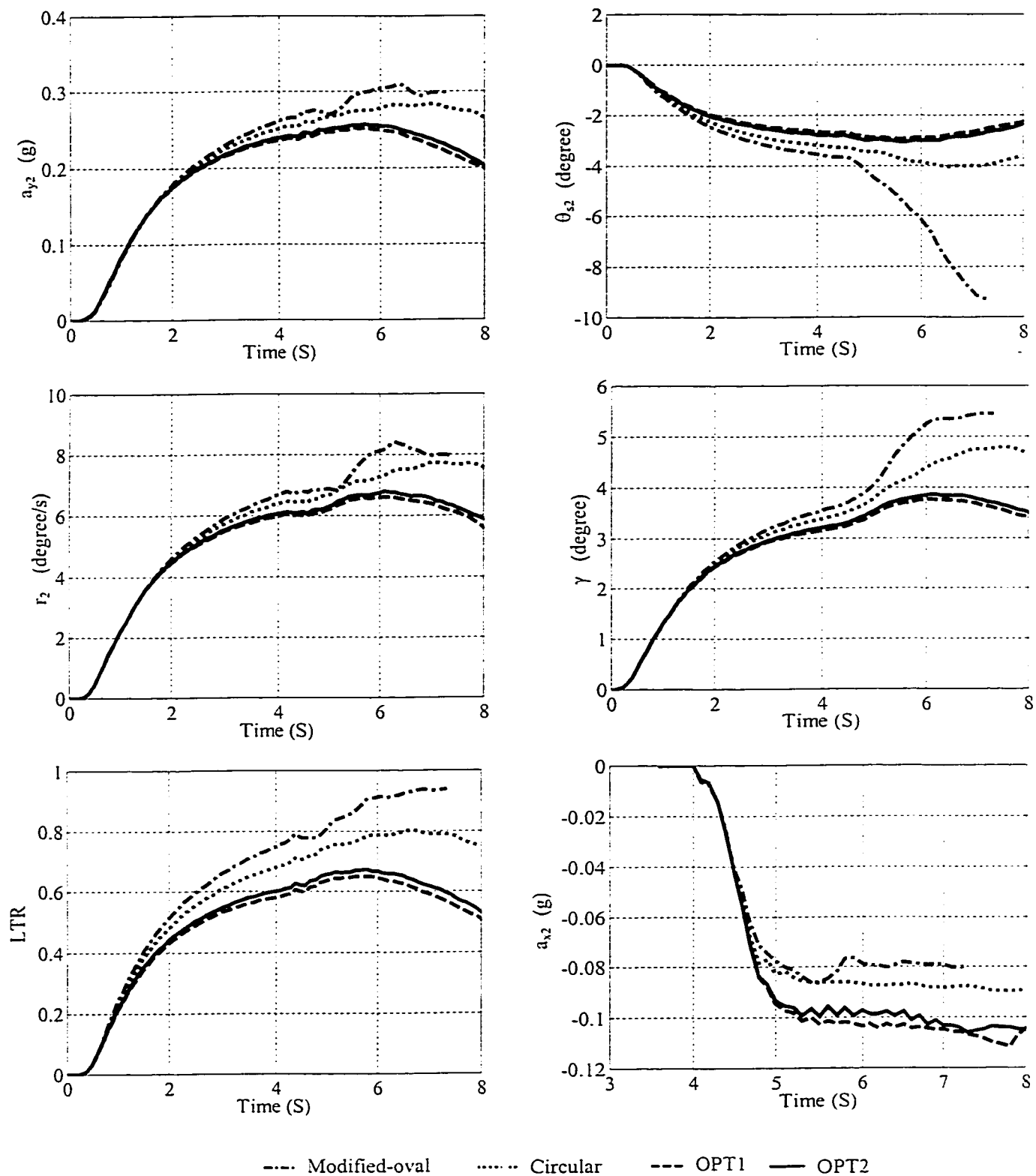


Figure 6.26: Directional and roll response of the vehicle with various tanks under steering and braking input ($\delta_r=0.8$ degree, $T_b=10$ psi, road A).

combined steering and braking operations can be clearly observed from Figures 6.25 and 6.26. When compared with the conventional tank vehicles, the combinations with the optimal tank cross-sections yield considerably lower variations in the DLF responses of tires, and lower values of LTR. These potential benefits are primarily ascribed to the relatively significant influence of lateral acceleration under low levels of longitudinal acceleration, and the generic optimal geometry, which effectively suppresses the liquid motion in the roll plane.

6.6 SUMMARY

Liquid load shift within a partly-filled tank trailer and its influence on dynamic behavior of an articulated vehicle combination subject to simultaneous applications of cornering and braking maneuvers is investigated through analysis of the three-dimensional vehicle model described in Chapter 5. The dynamic load shift properties of the tank vehicle are derived in terms of variations in c.g. coordinates and mass moments of inertia of the liquid cargo, as functions of the braking and steering input, fill volume and tank cross-section. While application of a pure lateral acceleration yields most significant variation in the lateral c.g. coordinate of the cargo, a braking input causes most significant variations in the longitudinal and vertical c.g. coordinates, which is attributed to the extensive tank length. The trajectories of the c.g. coordinates revealed that the magnitude of lateral load shift caused by lateral acceleration decreases considerably under the application of a longitudinal deceleration, due to predominant fluid movement in the pitch plane. The roll mass moment of inertia of the cargo increases considerably under longitudinal and lateral acceleration fields, while the pitch and yaw mass moments of inertia decrease considerably. The moments of inertia approach nearly

steady values when the longitudinal acceleration exceeds 0.6 g, irrespective of the lateral acceleration, fill volume and tank cross-section.

The influence of liquid load shift on the dynamic characteristics of a partly-filled five-axle tractor semitrailer tank vehicle combination under combined steering and braking maneuvers is further investigated through analyses of a comprehensive analytical vehicle model coupled with the three-dimensional quasi-static liquid cargo model. Parametric sensitivity analyses are further carried out to evaluate the influence of variations in the steering and braking input, cargo fill volume, road surface friction and tank cross-section on the directional response of the vehicle combination. From the results, it is concluded that directional dynamic performance of the combination deteriorates due to considerable magnitudes of roll, pitch and yaw moments imposed by the moving cargo. The magnitudes of such moments tend to increase with increase in both the steer input and brake treadle pressure. A comparison of the response characteristics of the vehicle with a partly-filled circular tank and an equivalent rigid cargo clearly illustrated the destabilizing effects of the moments imposed by the moving liquid cargo, which tends to be more severe for 50% fill volume conditions. On a dry road, the superimposition of braking and turning considerably increases the LTR and thus the rollover tendency of the liquid cargo vehicle. The effect on the yaw response characteristics, however, is relatively small, since the asymmetric load shift causes the lockup of the inner trailer wheels only. Although the application of braking effort during turning does not induce yaw instability problem, the braking performance tends to deteriorate considerably, as reported in earlier studies on straight-line braking of partly-filled tank trucks. The deterioration in the braking performance is further attributed to

excessive growth in the wheel-slip response of the trailer axle wheels arising from the increased load transfer due to liquid shift. On a wet or slippery road with its reduced friction potential, the significant load transfer in case of liquid cargo vehicle yields lockup of both the inside and outside wheels of the trailer, resulting in sudden drop in the lateral forces, which causes violent yaw motion of the trailer, indicative of trailer swing potential. The partly-filled tank vehicle combination thus exhibits yaw instability well before the rollover limit is reached. In all the cases considered in the study, the equivalent rigid cargo vehicle exhibits only slight variations in the DLF and considerably lower dynamic response, under identical conditions of steering and braking input, fill volume and road friction.

A comparison of liquid load shift and vehicle dynamic response characteristics attained with both conventional (circular and modified-oval) and optimal tanks reveals that the optimal cross-sections, proposed in the previous Chapters, can enhance the dynamic performance of the partly-filled tank vehicle combination under combined steering and braking maneuvers. This potential advantage is mostly attributed to the asymmetric generic optimal geometry, which effectively reduces the liquid free surface area and thus restraints the liquid motion in the roll plane, leading to considerable reduction in the lateral transfer of the normal loads.

CHAPTER 7

CONCLUSIONS AND RECOMMENDATIONS

7.1 HIGHLIGHTS OF THE INVESTIGATION

In this dissertation, the dynamic response and stability characteristics of partially-filled tank vehicles are investigated through systematic development and integration of various tank and vehicle models as well as formulation and evaluation of optimal tank designs. The study involves: road tank design through formulation and optimization of a generic tank configuration, effects of optimal tank geometry on the stability characteristics of tank vehicles through development and analyses of static roll plane and constant-speed three-dimensional directional dynamic models, evaluations of tank vehicle dynamic behavior under combined braking and steering maneuvers through development and analyses of a variable-speed three-dimensional tank vehicle model. Some of the results attained from the dissertation research have been published in [212, 226-230]. The major highlights of various aspects of the study are summarized in the following subsections.

7.1.1 Formulation of a Generic Tank Cross-section and Shape Optimization

The roll stability of partially-filled tank vehicles is substantially influenced by both the c.g. height of the tank trailer and magnitude of liquid load transfer in a complex manner. The cargo c.g. height and load shift in turn are strongly dependent upon the fill volume, tank geometry and vehicle maneuver. Circular cross-section tanks, employed in transportation of general-purpose liquid products, yield high c.g. location, but relatively

less load transfer under partial fill condition and application of a lateral acceleration field. Modified-oval tanks, used in delivery of fuel oils, on the other hand, yield relatively lower c.g. height, but considerably larger lateral load transfer under a lateral acceleration disturbance, especially under low fill volumes. Alternate tank cross-sections have been proposed in the past to achieve low c.g. height, while the influence of tank geometry on the resulting liquid load transfer under partial fill conditions has largely been neglected.

In this dissertation, a generic tank geometry is formulated to describe various commonly used tanks in transportation of fuel oils and bulk liquids in order to achieve both low c.g. height and minimal lateral load transfer for varying fill volumes. Three multivariable constrained minimization functions are formulated on the basis of overturning moment caused by moving cargo under partial fill conditions, lateral load shift with prescribed cross-section c.g. height, and weighted sum of c.g. height and shifts in the c.g. coordinates of the liquid cargo, respectively. The optimization problems are solved subject to constraints imposed on the total cross-section area, overall width and height, and perimeter to derive optimal cross-section parameters corresponding to typical fill volumes and ranges of fill volumes. The optimal solutions in all the cases invariably converge towards nearly conical shape, whose geometric parameters are dependent upon the specific reference fill volume or fill range, thus resulting in simultaneous reduction in cargo c.g. height and lateral load transfer.

7.1.2 Analysis of Load Shift and Static Roll Stability of Vehicles with Partly-Filled Optimal Tanks

The likelihood of a vehicle rollover during steady turning is strongly related to its rollover threshold. The static rollover threshold of tank vehicles is adversely influenced

by the liquid cargo shift under partial fill conditions. In this dissertation, the performance characteristics of different optimal and conventional tanks are assessed in terms of deviations of the c.g. coordinates caused by a steady lateral acceleration field, and rollover threshold of partially-filled tank vehicles subject to steady turning maneuvers and various partial fill conditions. A static roll plane model of an articulated vehicle equipped with a generic tank is developed by integrating a roll plane model of a partially-filled generic tank with that of an articulated vehicle. The coupled model is analyzed to investigate the rollover threshold acceleration limit of a tractor semitrailer tank vehicle as functions of tank geometry, fill volume and type of partial-fill condition, such as variable and constant load, and the results are compared to identify optimal tank geometry for different ranges of fill volumes.

7.1.3 Directional and Roll Dynamic Response Analysis of Partly-Filled Tank Vehicles

The directional response and dynamic roll stability characteristics of partly-filled tank vehicles are strongly dependent upon vehicle response to directional maneuvers and dynamic interactions between the moving liquid cargo and the vehicle. The movement of liquid load within the tank thus affects the directional response and control characteristics of partly-filled tank vehicles in a considerable manner. Dynamic roll stability characteristics of partly-filled tank vehicles may be enhanced by reducing the magnitude of overturning moments caused by liquid cargo load under a constant-speed directional maneuver. Although the directional dynamics and roll stability characteristics of partly-filled tank vehicles have been investigated in few studies, all the analyses have been

performed for conventional tank geometry, including circular and modified-oval cross-section tanks.

In this dissertation, a quasi-static roll plane fluid model of a partly-filled generic tank is developed and integrated with a constant-speed yaw/roll dynamic model of articulated vehicles for analyzing the influence of optimal tank geometry on the directional response and dynamic roll stability characteristics of a five-axle tractor semitrailer tank vehicle. The analyses are performed for the vehicle equipped with partly-filled tanks of various cross-sections, including conventional and optimal, under various steady and transient directional maneuvers, and different fill conditions. The dynamic response characteristics of the vehicle with different tanks, evaluated in terms of defined performance measures, including load shift and mass moments of inertia of liquid cargo as well as roll angle, lateral acceleration, yaw motion, load transfer ratio and path trajectory response of the vehicle combination, are compared to demonstrate the superior performance potentials of the proposed optimal tanks.

7.1.4 Development of a Comprehensive Dynamic Model of Partly-Filled Tank Vehicles for Braking-in-a-turn Analysis

The combined braking and steering operation is one of the most commonly encountered highway maneuvers, which has been associated with most vehicle accidents. During variable speed directional maneuvers, the load transfer in the longitudinal direction due to acceleration or deceleration, coupled with the lateral load transfer due to steering, can lead to wheel lock-up resulting in possible yaw instability and/or loss of directional control of the vehicle. The load transfers in the longitudinal and lateral directions are further exaggerated in the case of partially-filled tank vehicles due to

unrestricted liquid cargo movement in the roll and pitch planes, thus considerably influencing the stability characteristics and safety performance of the vehicles. Although a number of comprehensive variable speed directional dynamics models of heavy vehicles have been reported in the literature, they can not be directly employed for dynamic analysis of partly-filled tank vehicles under combined braking and steering maneuvers, due to lack of consideration of cargo-vehicle interactions. The reported studies on dynamics of tank vehicles, however, have considered the movement of liquid cargo in either the roll plane alone under constant-speed steering maneuvers or the pitch plane alone under straight-line braking operations. The cargo movement within a partly-filled tank and its influence on dynamic characteristics of tank vehicles under simultaneous steering and braking maneuvers have not been addressed.

In this dissertation, a three-dimensional quasi-static model of a partly-filled tank of generic cross-section is developed and integrated into a comprehensive variable-speed dynamic model of an articulated vehicle for investigating the cargo load shift and its influence on directional response, stability and braking performance of the vehicle under combined steering and braking operations. The three-dimensional model of liquid cargo within a partly-filled generic tank is developed assuming inviscid fluid and negligible contributions due to fundamental slosh frequency. The liquid load movement encountered under combined steering and braking is characterized in terms of variations in instantaneous c.g. coordinates in the roll and pitch planes, and mass moments of inertia of the liquid bulk. The longitudinal, lateral and vertical translations of the c.g. coordinates of the cargo load and its mass moments of inertia are further derived as functions of longitudinal and lateral body forces imposed on the liquid bulk, fill volume and tank

configuration. The coupled tank vehicle dynamic model incorporates dynamics of air brake systems as well as comprehensive nonlinear lateral and longitudinal force properties of tires and their interactions with the road surface, and is capable of simulating both open-loop and closed-loop steering maneuvers, stopping distance performance and directional behavior in braking.

7.1.5 Analysis of Cargo Load Shift and its Influence on Dynamic Response of Tank Vehicles under Combined Braking and Steering

The dynamic characteristics of partly-filled tank vehicles have been investigated under either constant-speed steering or straight-line braking maneuvers. These studies have clearly established that cargo movement within a partly-filled tank vehicle is a significant contributing factor leading to considerably reduced roll stability limits and braking performance of the vehicle. The cargo load shift within a partly-filled tank and its influence on the dynamic characteristics of partially-filled tank vehicles under combined steering and braking maneuvers, however, have not been reported.

In this dissertation, the directional response and stability characteristics of a partially-filled five-axle tractor-semitrailer tank vehicle are investigated under braking-in-a-turn maneuvers. The liquid cargo shifts are derived in terms of variations in the c.g. coordinates in the roll and pitch planes, and mass moments of inertia of the liquid bulk, as functions of the lateral and longitudinal body forces, fill volume and tank cross-section. The directional performance characteristics of the tank vehicle are expressed in terms of dynamic load transfer, yaw, roll and braking deceleration response of the combination. The performance characteristics of the partly-filled tank vehicle are compared with those of an equivalent rigid cargo vehicle to demonstrate the destabilizing effects of the liquid

load shift under combined steering and braking maneuvers. Parametric sensitivity analysis is further carried out to examine the influence of steering and braking inputs, cargo fill volume, tire-road friction property, and tank cross-section on the dynamic response and stability characteristics of the tank vehicle.

7.2 CONCLUSIONS

Based upon the studies carried out in this dissertation, the following specific conclusions are drawn:

- From literature review, it can be concluded that very limited efforts have been made to derive optimal tank cross-sections to minimize the overturning moment due to cargo shift within partly-filled tanks. It is further concluded that although the directional dynamics and stability characteristics of various configurations of freight vehicles have been extensively investigated, the contributions due to cargo movement and cargo-vehicle interactions have been either neglected or considered under limited maneuvers. Liquid load transfer and its influence on dynamic response and stability characteristics of tank vehicles under combined steering and braking maneuvers has not been addressed.
- From roll plane load shift analysis of the liquid cargo within partially-filled tanks, it is concluded that the conventional tanks are far from optimum in view of the roll stability of partly-filled tank vehicles. Under partial-fill conditions, the currently used tanks exhibit extensive lateral movement of the cargo. The relative loss in roll stability limits of vehicles with wider tanks is considerably larger than the corresponding gain arising from their lower cross-sectional c.g. height, especially under low fill volumes.
- The proposed generic cross-section can be effectively used to describe the geometry of currently used tanks employed in transportation of liquid bulk

products. The generic geometry further offers considerable shape flexibility to achieve lower c.g. height and reduced load transfer.

- The multivariable constrained optimization functions formulated on the basis of overturning moment caused by cargo load, lateral load shift with prescribed cross-section c.g. height, and weighted sum of c.g. height and shifts in c.g. coordinates of liquid cargo, respectively, can be effectively employed to minimize the tank cross-section c.g. height and shift of the liquid cargo, and thus the resulting overturning moment as a function of fill volume. The optimal solutions invariably converge towards relatively narrow top and wide bottom, resulting in simultaneous reduction in liquid c.g. height and lateral load transfer.
- A comparative study of load shift and overturning moment of the liquid cargo within various partially-filled optimal tanks revealed that wide bottom tanks yield low overturning moment under high fill volumes, while tanks with approximately conical geometry result in lower overturning moment under medium fill volumes.
- The derived optimal tanks can yield substantial reduction in both the load shift and c.g. height of the liquid cargo, and thus significantly enhance the static roll stability of partially-filled tank vehicles over a large fill range. Under partial-fill conditions involving variable load, optimal cross-section with the lowest c.g. height yields considerably higher and near constant values of rollover threshold limit of a tractor-semitrailer tank vehicle for medium and high fill volumes ($\geq 55\%$). The optimal cross-section, in this case, yields an increase in rollover threshold limit in the order of 7% when compared with that attained for a currently used modified-oval tank for fill volumes above 60%. Under partial-fill conditions involving constant cargo load, optimal tanks obtained corresponding to 50%-70% and 70%-90% fill volume ranges yield considerably higher and nearly constant rollover threshold limits for fill

volumes ranging from 40% to 90%. The resulting rollover threshold is approximately 12% higher than that obtained for a circular tank under high fill volumes and approximately 13% to 25% higher than that attained for a modified-oval tank with medium (40% to 70%) fill volume range.

- From a comparison of the static roll performance of a tractor-semitrailer vehicle with various optimal tanks, it is concluded that for liquid cargo transportation involving insignificant partial fill conditions, optimal tank design obtained under 100% fill volume may be considered as optimal. For situations involving large variations in the fill volume, optimal solutions achieved under 50%-90% fill range with a perimeter constraint may be considered most suitable and cost-effective for applications in general purpose transportation of bulk liquids.
- A study of the directional and roll dynamic response characteristics of a tractor-semitrailer equipped with various conventional and optimal tanks revealed that the liquid load shift within a partially-filled tank plays a dominant role in influencing the directional behavior and roll stability of tank vehicles, especially under relatively low fill volumes. Although the c.g. height of liquid cargo yields somewhat moderate contribution to the directional response characteristics of the vehicle combination under high fill volumes, its impact becomes relatively insignificant under low fill volumes.
- A comparison of the directional and roll dynamic response characteristics of the vehicle with different tanks under constant-speed directional maneuvers demonstrates that the proposed optimal tanks can significantly enhance the directional response characteristics and roll stability of partially-filled tank vehicles for both medium and high fill volumes.
- The results of the parametric study further show superior potential benefits of the optimal tanks. The potential performance gain tends to increase with

increase in the severity of the directional maneuver. Under partial fill conditions associated with constant load and relatively low vehicle speed, the vehicle exhibits stable behavior, irrespective of the tank cross-section, when subjected to small levels of steady steer inputs. The vehicle with a modified-oval tank, however, approaches roll instability, when subjected to relatively large steer inputs and low fill volumes. An increase in forward speed causes a rapid increase in the directional response magnitudes of the partly-filled tank vehicle with conventional tanks, indicating onset of a possible rollover, especially in case of the vehicle with the modified-oval tank. The partly-filled vehicle with the optimal tanks, however, remains directionally stable and exhibits considerably lower response magnitudes.

- From the transient directional response analyses of the tank vehicles, it is concluded that the vehicle with optimal as well as currently used tanks exhibit stable behavior under mild path-change and evasive maneuvers at typical highway speeds. The magnitudes of the directional response measures of the vehicle with the conventional tanks, however, are considerably larger than those of the vehicle with the optimal tanks.
- Under variable load partial fill conditions and relatively high steer inputs, the vehicle with both circular and modified-oval tanks exhibits stable behavior under 50% fill volume, while it reveals unstable response under 80% fill volume. The vehicle with the optimal tanks, however, yields stable and considerably lower response under both fill volumes.
- The load shift of the liquid cargo within a partly-filled tank subjected to combined longitudinal and lateral acceleration excitations can be approximately characterized by variations in both the coordinates of the c.g. and the mass moments of inertia of the cargo. These variations can be effectively estimated from a three-dimensional quasi-static model of a partially-filled generic tank based upon the liquid free surface gradients. The

dynamic load shift within a partly-filled tank trailer can be further expressed as functions of longitudinal and lateral accelerations imposed on the liquid bulk, fill volume and tank cross-section.

- A variable-speed yaw/roll dynamic model of a partly-filled tank vehicle incorporating lateral and longitudinal liquid motions, and braking dynamics can be effectively applied to study the directional response and braking performance of the vehicle under combined steering and braking maneuvers. This model can be effectively developed by integrating a three-dimensional quasi-static model of a partly-filled tank of generic cross-section to a comprehensive dynamic model of the rigid cargo vehicle.
- The coordinates of the c.g. and mass moments of inertia of the liquid cargo within a partly-filled tank vary considerably in both the roll and pitch planes under applications of lateral and longitudinal accelerations. While application of a pure lateral acceleration yields most significant variation in the lateral c.g. coordinate of the cargo, a braking input causes most significant variations in the longitudinal and vertical c.g. coordinates. The trajectories of the c.g. coordinates further reveal that the magnitude of lateral load shift caused by lateral acceleration decreases considerably under the application of a longitudinal deceleration.
- The roll mass moment of inertia of liquid cargo within a partially-filled tank increases considerably under a longitudinal acceleration field, while the pitch and yaw mass moments of inertia decrease significantly. The moments of inertia approach nearly steady values when the longitudinal acceleration exceeds 0.6 g, irrespective of the lateral acceleration, fill volume and tank cross-section.
- The variations in c.g. coordinates and mass moments of inertia of liquid cargo significantly affect the dynamic behavior of partly-filled tank vehicles under

braking-in-a-turn maneuvers. The dynamic performance of such vehicles deteriorates due to considerable magnitudes of roll, pitch and yaw moments imposed by the moving cargo. A comparison of the response characteristics of a partly-filled tractor semitrailer tank vehicle with that of an equivalent rigid cargo vehicle clearly illustrates the considerable destabilizing impact of the moving liquid cargo, which tends to be more severe for relatively large steering and braking inputs.

- On a dry road, the application of combined braking and turning inputs yields considerably higher load transfer ratio and thus the rollover tendency of the liquid cargo vehicle, while its influence on the yaw response characteristics is relatively insignificant. The results suggest that application of braking effort during turning is not expected to induce a yaw instability. The braking performance of the tank vehicle, however, tends to deteriorate considerably.
- On a wet or slippery road with its reduced friction potential, the significant load transfer in case of the liquid cargo vehicle yields lockup of both the inside and outside wheels of the trailer, resulting in trailer swing. The partly-filled tank vehicle combination thus exhibits yaw instability well before the rollover limit is reached.
- A comparison of the dynamic response characteristics of the vehicle with both conventional and optimal tanks reveals that the proposed optimal cross-sections also yield considerably enhanced dynamic performance of partly-filled tank vehicles under combined steering and braking maneuvers.

7.3 RECOMMENDATIONS FOR FUTURE WORK

The dissertation research presents fundamental investigations related to tank vehicle safety performance involving identification of optimal tank geometry, and directional and stability analyses of partially-filled tank vehicles under various steering

and braking inputs. It is recommended to undertake the following future studies to further explore and enhance the capabilities of the proposed design concept and methodologies.

- The proposed methodology may be further extended for investigating and enhancing the static roll stability, constant-speed directional behavior and variable-speed dynamic response characteristics of various other configurations of tank vehicles, such as compartmented tank vehicles, six-axle tractor-semitrailer tank vehicles, various double and triple (A-, B- and C-trains) tank vehicle combinations, etc.
- The proposed concept of optimal tank design offers significant potentials to minimize the highway safety risks posed by partially-filled tank vehicles. The tank design should therefore be further explored to examine its feasibility in terms of structural integrity (comprehensive stress analysis including the welding) and manufacturability.
- The proposed three-dimensional quasi-static fluid model and the corresponding coupled comprehensive tank vehicle model incorporating lateral and longitudinal liquid motion and braking dynamics need to be further validated through fluid-slosh-dynamics based tank vehicle models and field tests under various braking-in-a-turn operating conditions.
- Studies also need to be undertaken to investigate slosh frequencies of liquid cargoes within partially-filled tanks of various cross-sections during typical steering and braking-in-a-turn maneuvers and under various fill volumes, in order to examine the validity of the proposed two- and three-dimensional quasi-static models of liquid cargo with partially-filled tanks for such maneuvers.
- Studies need to be carried out to explore pitch plane optimal tank cross-section geometry in order to minimize the pitch plane transfer of liquid cargo,

thus enhancing the braking performance and stability characteristics of partially-filled tank vehicles under combined braking and steering maneuvers.

- Studies may also be carried out to explore anti-slosh devices, such as pressurized bladders to minimize the liquid free movement.
- Further studies on enhancing the safety performance of partially-filled tank vehicles may also be attempted to explore possible closed-loop directional response and stability control systems, and/or open-loop early warning safety devices to avert the driver of an impending instability.

REFERENCES

1. Heglund, R. E., *Truck Safety - An Agenda for the Future*, SAE Publication No. P-181, pp. 154-159, 1986
2. Mayenburg, M., Rossow, G. and Patterson, C., *Truck Safety Technology for the 21st Century*, SAE Paper No. 952260, 1995
3. Kurtz, E. F. and Anderson, R. J., *Handling Characteristics of Car-Trailer Systems: a State of the Art Survey*, Vehicle System Dynamics, Vol. 6, pp. 217-243, 1977
4. Troger, H. and Zeman, K., *A Nonlinear Analysis of the Generic Types of Loss of Stability of the Steady State Motion of A Tractor-Semitrailer*, Vehicle System Dynamics, Vol. 13, pp. 161-172, 1984
5. Nalcez, A. G. and Genin, J., *Dynamic Stability of Heavy Articulated Vehicles*, Int. J. of Vehicle Design, Vol. 5, no. 4, pp. 417-426, 1984
6. U.S. Department of Transportation (DOT), *Cargo Tank Incident Report*, Hazardous Material Incident Report, 1983
7. Campbell, K. L., *National Estimates of the Number of Trucks, Travel and Accident Experience of Tractor Semi-Trailers Used to Transport Hazardous Materials*, University of Michigan, Transportation Research Institute Report No. UMTRI-89-1, Jan. 1989
8. Strandberg, L., *Lateral Stability of Road Containers*, VTI (The Swedish National Road and Traffic Research Institute) Report No. 138A, Sweden, 1978
9. Bauer, H. F., *Dynamic Behavior of an Elastic Separating Wall in Vehicle Containers: Part 1*, Int. J. Vehicle Design, Vol.2, No. 1, pp. 45-77, 1981
10. Bauer, H. F., *Dynamic Behavior of an Elastic Separating Wall in Vehicle Containers: Part 2*, Int. J. Vehicle Design, Vol.3, No. 3, pp. 307-333, 1982
11. Ranganathan, R., *Stability and Directional Response Characteristics of Heavy Vehicles Carrying Liquid Cargo*, Ph.D. Thesis, Concordia University, 1990
12. Transport Dangerous Goods, *Dangerous Occurrences Reports 1981-1983. Summary of Reports on File, Evaluation and Analysis*, Report TP 5695E, Aug. 1984
13. Rakheja, S. and Sankar, S., *Tank Vehicle Accidents: A Survey of Reports on File*, CONCAVE Report No. 14-87, Concordia University, Oct. 1987

14. Ervin, R. D., Mallikarjunarao, C. and Gillespie, T. D., *Future Configuration of Tank Vehicles Hauling Flammable Liquids in Michigan*, UM-HSRI-80-73-1, 1980
15. Mumane, T. J., *Vehicle Accident Statistics Producing Rollover and Spills involving Tank Semi-Trailers*, SAE Truck and Bus Meet., Charlotte, NC, 1989
16. Park, S., *Simulation and Experiment of Nonlinear Dynamics of Liquid-Filled Shell Structure Subjected to Low Speed Impulsive Loading*, Ph.D. Dissertation, The Pennsylvania State University, 1996
17. Tyndall, L. H., Augspurger, Q., Johnson, N. B., *Integrity of MC 307/312 Cargo Tanks*, Final Report, Dynamic Science, Inc., Oct., 1984
18. National Transportation Safety Board, *Hazardous Materials Accident Report - Overturn of a Tractor-Semitrailer (Cargo Tank) with the Release of Automotive Gasoline and Fire*, Carmichael, California, PB91-917004, Sept. 1991
19. National Transportation Safety Board, *Hazardous Materials Special Investigation Report - Cargo Tank Rollover Protection*, PB92-917002, Feb. 1992
20. National Transportation Safety Board, *Highway/Hazardous Materials Accident Summary Report -Collision of Tractor/Cargo Tank Semitrailer and Passenger Vehicle and Subsequent Fire*, Yonkers, New York, PB98-916202, May 1998
21. Jindra, F., *Off-tracking of Tractor-trailer Combinations*, Automobile Engineer, Vol. 53, No. 3, pp. 96-101, 1963
22. Bidwell, J. B., *State of the-Art- Vehicle Control and Road Holding*, SAE Paper No. 700366, 1970
23. Dugoff, H. and Murphy, R. W., *The Dynamic Performance of Articulated Highway Vehicles -A Review of the State-of-the-art*, SAE Paper No. 710223, 1971
24. Eshleman, R. L. and Desai, S. D., *Articulated Vehicle Handling, Summary Final Report*, Report No. DOT/HS-800 673, IIT Research Institute, Apr. 1972
25. Hazemoto, T., *Analysis of Lateral Stability for Doubles*, SAE paper No. 730688, 1973
26. Dunbar, L. K., *Articulated Vehicles: Stability and Analysis*, Ph.D. Thesis, University of Notre Dame, 1979
27. Crolla, D. A. and Hales, F. D., *The Lateral Stability of Tractor and Trailer Combinations*, Journal of Terra-mechanics, Vol. 16, No. 1, pp. 1-22, 1979
28. Segel, L. and Ervin, R. D., *The Influence of Tire Factors on the Stability of Trucks and Tractor Trailers*, Vehicle System Dynamics, Vol. 10, pp. 39-59, 1981

29. Vlk, F., *Lateral Dynamics of Commercial Vehicle Combinations – a Literature Survey*, Vehicle Systems Dynamics, Vol. 11, No. 6, pp. 305-324, 1982
30. Bechtold, J. C., *Vehicle Stability and 102*, Modern Bulk Transporter, pp. 65-69, Sept. 1983
31. Vlk, F., *Handling Performance of Truck-Trailer Vehicles: A State-of-the-art Survey*, Int. J of Vehicle Design, Vol.6, No. 3, pp. 323-361, 1985
32. Vanderploeg, M. J. and Bernard, J. E., *Dynamics of Double Bottom Commercial Vehicles*, Int. J. of Vehicle Design, Vol. 6, No. 2, pp. 139-148, 1985
33. Fancher, P. S., *The Static Stability of Articulated Commercial Vehicles*, Vehicle System Dynamics, Vol. 14, pp. 201-227, 1985
34. Vlk, F., *Handling Performance of Truck-Trailer Vehicles: A State of the Art Survey*, Int. J. of Vehicle Design, Vol. 6, No., 3, pp. 323-361, 1985
35. Pflug, H. C., *Lateral Dynamic Behavior of Truck-Trailer Combinations due to the Influence of the Load*, Vehicle System Dynamics, Vol. 15, pp. 155-175, 1986
36. Fancher, P. and Matew, A., *A Vehicle Dynamics Handbook for Single-Unit and Articulated Heavy Trucks*, DOT HS 807 185, Final Report, US Department of Transportation, May 1987
37. Bakker, E., Nyborg, L. and Pacejka, H. B., *Tire Modeling for Use in Vehicle Dynamics Studies*, SAE Paper No. 870421, 1987
38. Segel, L., *The Mechanics of Heavy Duty Trucks and Truck Combinations*, The International Association for Vehicle Design, Aston Clinto, UK, 1987
39. Vlk, F., *Lateral Stability of Articulated Buses*, Int. J. of Vehicle Design, Vol. 9, No. 1, pp. 35-51, 1988
40. Bakker, E., Pacejka, H. B. and Lidner, L., *A New Tire Model with an Application in Vehicle Dynamics Studies*, SAE Paper No. 890087, 1989
41. Aurell, J., and Edlund, S., *The Influence of Steered Axles on the Dynamic Stability of Heavy Vehicles*, SAE Paper No. 892498, 1989
42. Sankar, S., Rakheja, S. and Piche, A., *Directional Dynamics of a Tractor-Semitrailer with Self- and Forced-Steering Axles*, SAE Paper No. 912686, 1991
43. Nordstrom, O., *Stability, Steerability and Braking Performance of Heavy Duty Vehicles: A Review of Experimental and Theoretical Research and Regulation Proposal by VTI in Sweden*, Heavy Vehicle System, Int. J. of Vehicle Design, Vol. 1, No.1, 1993

44. El-Gindy, M., Tong, L. and Tabarrok, B., *Frequency Response Analysis of Canadian Logging Trucks*, *Vehicle System Dynamics*, Vol. 23, pp. 325-349, 1994
45. Elwell, M. F., *The Modeling and Control of N-trailer Multi-articulated Systems*, Ph.D. Thesis, The University of Utah, 1995
46. Hichael, W., Sayers M. W. and Dongsuk H., *A Generic Multibody Vehicle Model for Simulating Handling and Braking*, *Vehicle System Dynamics Supplement 25*, pp. 599-613, 1996
47. Palkovics, L. and El-Gindy, M., *Examination of Different Control Strategies of Heavy-Vehicle Performance*, *Journal of Dynamic Systems, Measurement, and Control*, Vol. 118, pp. 489-498, 1996
48. Kack, B. and Richard, M. J., *Effect of Load-Distributing Devices on the Stability of Heavy Vehicles*, *Heavy Vehicle Systems, Int. J of Vehicle Design*, Vol. 4, No. 1, pp.29-48, 1997
49. Karmiadji, D. W., *Interaction Between the Tractor and Trailer as A Multi-body System*, Ph.D. Thesis, The University of Alabama, 1997
50. Jindra, F., *Tractor and Semi-Trailer Handling*, *Automobile Engineer*, Vol. 53, pp. 438-446, 1963
51. Jindra, F., *Tractor and Trailer Handling*, *Automobile Engineer*, Vol. 55, pp. 60-69, 1965
52. Jindra, F., *Handling Characteristics of Tractor-Trailer Combinations*, SAE Paper No. 650720, 1965
53. Ellis, J. R., *The Ride and Handling of Semi-trailer Articulated Vehicles*, *Automobile Engineer*, Vol. 56, pp. 523-529, 1966
54. Schmid, I., *Engineering Approach to Truck and Tractor Train Stability*, SAE Paper No. 670006, 1967
55. Pacejka, H. B., *Simplified Analysis of Steady-state Turning Behavior of Motor Vehicles*, *Vehicle System Dynamics*, Vol. 2, pp. 161-172, 1973
56. Vlk, F., *A Linear Study of the Transient and Steady Turning Behavior of Articulated Buses*, *Int. J. of Vehicle Design*, Vol. 5, No. 1-2, pp. 171-196, 1984
57. Mikulcik, E. C., *The Dynamics of Tractor-Semitrailer Vehicles: the Jackknifing Problem*, SAE Paper No. 710045, 1971
58. Tobler, W. E. and Krauter, A. I., *Tractor Semitrailer Dynamics: Design of the Fifth Wheel*, *Vehicle System Dynamics*, Vol. 1, pp. 123-160, 1972

59. Krauter, A. I. and Wilson, R. K., *Simulation of Tractor-semitrailer Handling*, SAE Paper No. 720922, 1972
60. Susemihl, E. A. and Krauter, A. I., *Jackknifing of Tractor Semitrailer Trucks-Detection and Corrective Action*, J. of Dynamic Systems, Measurement, and Control, Transactions ASME, pp. 244-252, 1974
61. Tobler, W. E., *General Rigid-Body Dynamics and Application to Vehicle Behavior*, Ph.D. Thesis, Cornell University, 1974
62. Mikulcik, E. C., *Stability Criteria for Automobile-Trailer Combinations*, Vehicle System Dynamics, Vol. 9, pp. 281-289, 1980
63. Mallikarjunarao, C. and Fancher, P., *Analysis of the Directional Response Characteristics of Double Tankers*, SAE Paper No. 781064, 1978
64. Fancher, P. S., *The Transient Directional Response of Full Trailers*, SAE Paper No. 821259, 1982
65. Ervin, R. D. and Mallikarjunarao, C., *A Study of the Yaw Stability of Tractor-Semitrailer Combinations*, Pro. 7th IAVSD Symposium on Dynamics of Vehicle on Roads and Tracks, Swets and Zeitlinger, 1982
66. El-Gindy, M. and Wong, J. Y., *Steering Response of Articulated Vehicles in Steady State Turns*, SAE Paper No. 852235, 1985
67. MacAdam, C. C. and Fancher, P. S., *A Study of the Closed-Loop Directional Stability of Various Commercial Vehicle Configurations*, Proceedings of 9th IAVSD Symposium held in Linköping University, Linköping, Sweden, June 24-28, pp. 367-382, 1985
68. Fancher, P. S., *Directional Dynamics Considerations for Multi-Articulated, Multi-Axled Heavy Vehicles*, SAE Paper No. 892499, 1989
69. El-Gindy, M., *Directional Response of a Tractor Towing a Semitrailer*, Int. J. of Vehicle Design, Vol. 10, No. 2, pp. 210-226, 1989
70. Vallurupalli, R. K., *Directional Dynamic Analysis of an Articulated Vehicle with Articulation Dampers and Forced-Steering*, Master Thesis, Concordia University, Canada, 1993
71. Rakheja, S., Vallurupalli, R. K. and Woodrooffe, J., *Influence of Articulation Damping on the Yaw and Lateral Dynamic Response of the Vehicle*, Heavy Vehicle Systems, Int. J. of Vehicle Design, Vol.2, No. 2, 1995
72. Ervin, R. D., *The Influence of Size and Weight Variables on the Roll Stability of Heavy Duty Trucks*, SAE Paper No. 831163, 1983

73. Ervin, R. D., *The Dependence of Truck Roll Stability on Size and Weight Variables*, Int. J. of Vehicle Design, Special Issue on Vehicle Safety, pp. 192-208, 1986
74. Jones, I. S. and Penny, M. B., *Engineering Parameters Related to Rollover Frequency*, SAE Paper No. 900104, 1990
75. Hinch, J., Shadle, S. and Klein, T. M., *NHTSA's Rollover Rulemaking Program-Results of Testing and Analysis*, SAE Paper No. 920581, 1992
76. Klein, T. M., *A Statistical Analysis of Vehicle Rollover Propensity and Vehicle Stability*, SAE Paper No. 920584, 1992
77. Tamny, S., *Operating Vehicle Roll Stability*, SAE Paper No. 932945, 1993
78. Mallikarjunarao, C., Ervin, R. D. and Segal, L., *Roll Response of Articulated Motor Trucks during Steady-Turning Maneuvers*, Computational Method in Ground Transportation Vehicles, ASME Winter Annual Meeting, pp. 133-152, Nov. 1982
79. Shapley, C. G., *The Rolling Motions of Road Vehicles*, Vehicle System Dynamics, Vol. 4, No.1, 1975
80. Isermann, H., *Overtuning Limits of Articulated Vehicle with Solid and Liquid Loads*, Motor Industry Research Assoc., Translation No. 22/76, 1976
81. Miller, D. W. G. and Barter, N. F., *Rollover of Articulated Vehicles. Vehicle Safety Legislation - Its Engineering and Social Implications*, The Institution of Mechanical Engineers, Great Britain, 1975
82. El-Gindy, M. and Hosamel-deen, Y. H., *Sensitivity Parametric Analysis of UMTRI Static Roll Model*, Int. J. of Vehicle Design, Vol. 10, No. 2, pp. 187-189, 1989
83. Preston-Thomos, J. and El-Gindy, M., *Static Rollover Thresholds of Heavy Vehicles*, Proceedings of CSME Forum, Montreal, pp. 946-951, 1992
84. Ruhl, R. L. and Ruhl, R. A., *Prediction of Steady State Roll Threshold for Loaded Flat Bed Trailers-Theory and Calculation*, SAE Paper No. 973261, 1997
85. Rakheja, S. and Piche, A., *Development of Directional Stability Criteria for an Early Warning Safety Device*, SAE Paper No. 902265, SP-843, pp. 1-13, 1990
86. Billing, A. M., *Rollover Tests of Double Trailer Combinations*, Ontario Ministry of Transportation and Communications Report No. TVS-CV-82-1 14, 1982
87. Nalecz, A. G., *Influence of Vehicle and Roadway Factors on the Dynamics of Tripped Rollover*, Int. J. of Vehicle Design, Vol. 10, No. 3, pp. 321-345, 1989

88. Nalecz, A. G., Lu, Z. and d'Entremont, K. L., *Investigation into Dynamic Measures of Vehicle Rollover Propensity*, SAE Paper No. 930831, 1993
89. Preston-Thomas, J. and Woodrooffe, J. H. F., *A Feasibility Study of a Rollover Warning Device for Heavy Trucks*, Technical Report, TP 10610E, National Research Council Canada, Sept. 1990
90. Gillespie, T. D. and Verma, M. K., *Analysis of the Rollover Dynamics of Double-Bottom Tankers*, SAE Paper No. 781065, 1978
91. Verma, M. K. and Gillespie, T. D., *Roll Dynamics of Commercial Vehicles*, Vehicle System Dynamics, Vol. 9, pp. 1-17, 1980
92. Das, N. S., *Estimation of Dynamic Rollover Threshold of Commercial Vehicles Using Low Speed Experimental Data*, SAE Paper No. 932949, 1993
93. Liu, P.J., Rakheja, S. and Ahmed, A.K.W., *Dynamic Rollover Threshold of Articulated Freight Vehicles*, Heavy Vehicle System, Int. J. of Vehicle Design, Vol. 5, Nos. 3/4, pp. 300-322 1998
94. Liu, P. J., *Analysis, Detection and Early Warning Control of Dynamic Rollover of Heavy Freight Vehicles*, Ph.D. Thesis, Concave, Concordia University, Jan. 1999
95. Strandberg, L., Nordström, O. and Nordmand, S., *Safety Problems in Commercial Vehicle Handling*, Symposium on Commercial Vehicle Braking and Handling, Ann Arbor, Michigan, USA, May 1975
96. Nordstrom, O., Magnusson, G. and Strandberg, L., *The Dynamic Stability of Heavy Vehicle Combinations*, Proceedings of the Third International Conference on Vehicle System Dynamics, edited by Sachs, H. K., 1975
97. Ellis, J. R., *A Model of the Semi-Trailer Vehicle Including Roll Modes*, SAS Report, Cranfield Institute of Technology, 1976, Pro. of the 5th VSD-2nd IUTAM Symposium, Wien, 1977
98. Gillespie, T. D. and MacAdam, C. C., *Constant Velocity Yaw/Roll Program, User's Manual, Technical Report*, The University of Michigan Transportation Research Institute, UMTRI-82-39, Oct. 1982
99. MacAdam, C. C., *A Computer-Based Study of the Yaw/Roll Stability of Heavy Trucks Characterized by High Centers of Gravity*, SAE Paper No. 821260, 1982
100. Wong, J. Y. and El-Gindy, M., *Computer Simulation of Heavy Vehicle Dynamic Behavior, User's Guide to the UMTRI Models*, Technical Report 3, Vehicle Weights and Dimensions Study, Road and Transportation Association of Canada, June 1985

101. Ervin, R. D, *Influence of Weights and Dimensions on the Stability and Control of Heavy-duty Trucks in Canada*, UMTRI Report, No. 86-35, 1986
102. Tabarrok, B. and Tong, X., *Directional Stability Analysis of Logging Trucks by a Yaw Roll Model*, SAE Paper No. 932946, 1993
103. Tabarrok, B. and Tong, X., *A Computer Simulation Analysis of Road Dynamics of Log Hauling Trucks*, SAE Paper No. 942305, 1994
104. Tong, X., Tabarrok, B. and El-Gindy, M., *Computer-Based Analysis of the Dynamics Performance of Log Hauling Trucks*, SAE Paper No. 952637, 1995
105. Nelson, R. E. and Fitch, J. W., *Optimum Braking, Stability and Structural Integrity for Longer Truck Combinations*, SAE Paper No. 680547, 1968
106. Limpert, R., *An Investigation of the Brake Force Distribution on Tractor-semitrailer Combinations*, SAE Paper No. 710044, 1971
107. Limpert, R. and Warner, C. Y., *Proportional Braking of Solid-Frame Vehicles*, SAE Paper No. 710047, 1971
108. Sankar, S., Guntur, R. and Sankar, T. S, *Effect of Wheel Slip on the Stability and Stopping Ability of a Road Vehicle*, Int. J. of Vehicle Design, Vol. 3, No. 1, pp. 77-89, 1982
109. Shadle, S. G., Emery L. H. and Brewer, H. K., *Vehicle Braking, Stability and Control*, SAE Paper No. 830562, 1983
110. Radlinski, R. W., *Braking Performance of Heavy U.S. Vehicles*, SAE Paper No. 870492, 1987
111. Dorion, S. L. and Pickard, J. G., *Feasibility of Anti-Jackknifing Systems for Tractor Semitrailers*, SAE Paper No. 891631, 1989
112. Stribersky, A. and Fancher, P. S., *The Nonlinear Behavior of Heavy-Duty Truck Combinations with Respect to Straight-line Stability*, J. of Dynamic Systems, Measurement, and Control, Transactions of ASME, Vol. 111, pp. 577-582, 1989
113. Leucht, P. M., *The Direction Dynamics of the Commercial Tractor-Semitrailer Vehicle during Braking*, SAE Paper No. 700371, 1970
114. Murphy, R. W., Limpert, R. and Segel, L., *Development of Braking Performance Requirements for Buses, Trucks, and Tractor-trailers*, SAE Paper No. 710046, 1971
115. Singh, M., *Stability Bounds of a Tractor Semi-trailer*, Vehicle System Dynamics, Vol. 9, pp. 69-86, 1980

116. Uffelman, F., *Automotive Stability and Handling Dynamics in Cornering and Braking Maneuvers*, Vehicle System Dynamics, Vol. 12, pp. 203-223, 1983
117. Essers, U. and Glasner, E. C., *The Braking Performance of Commercial Vehicle while Cornering with and without an Anti-Lock System*, SAE Paper No. 881823, 1988
118. Gohring, E. and von Glasner, E. C., *The Impact of Different ABS-philosophies on the Directional Behavior of Commercial Vehicles*, SAE Paper No. 892500, 1989
119. MacAdam, C. C., Fancher, P. S. and Hu, G. T. *et al.*, *A Computerized Model for Simulating the Braking and Steering Dynamics of Trucks, Tractor-Semitrailers, Doubles, and Triples Combinations*, User's Manual, Phase 4, MVMA Project 1197, UM-HSRI-80-58, Sept. 1980
120. Verma, V. S., Guntur, R. R. and Wong, J. Y., *The Directional Behavior during Braking of a Tractor/semi-trailer Fitted with Anti-locking Devices*, Int. J. of Vehicle Design, Vol. 1, No. 3, pp. 195-220, 1980
121. Day, T. D., *An Overview of the HVE Developer's Toolkit*, SAE Paper No. 940923, 1994
122. Day, T. D., *Difference Between EDVDS and Phase 4*, SAE Paper No. 1999-01-0103, 1999
123. Zhang, D. J. and Tabarrok, B., *On Nonlinear Yaw-Roll-Pitch Model of the Dynamics of Log Hauling Trucks*, Heavy Vehicle Systems, Int. J. of Vehicle Design, Vol. 5, Nos. 3/4, pp.181-207, 1998
124. Lieh, J., *A Multibody Dynamics Program for Truck Simulation*, SAE Paper No. 942303, 1994
125. Sayers, M. W. and Riley, S. M., *Modeling Assumptions for Realistic Multibody Simulations of Yaw and Roll Behavior of Heavy Trucks*, SAE Paper No. 960173, 1996
126. Gillespie, T. D. and Sayers, M. W., *A Multibody Approach with Graphical User Interface for Simulating Truck Dynamics*, SAE Paper No. 1999-01-3705, 1999
127. Clark, B. A., Ruhl, R. L. and Strauss M. G., *Dynamics and Roll Stability of a Loaded Class 8 Tractor-Livestock Semi-Trailer*, SAE Paper No. 1999-01-3732, 1999
128. Yang, X., *A Close-loop Driver/Vehicle Directional Dynamics Predictor*, Ph.D. Thesis, Concordia University, Apr. 1999

129. El-Gindy, M. and Wong, J. Y., *A Comparison of Various Computer Simulation Models for Predicting the Directional Responses of Articulated Vehicles*, Vehicle System Dynamics, Vol. 16, pp. 249-268, 1987
130. Wong, J. Y., *Theory of Ground Vehicles*, John Wiley & Sons, Inc., 2nd Edition, 1993
131. Winkler, C. B. and Bogard, S. E., *Simple Predictors of the Performance of A-Trains*, SAE Paper No. 932995, 1993
132. El-Gindy, M. and Woodrooffe J. H., *The Effects of Tractor Parameter Variations on the Dynamic Performance of B-Train Double*, Transportation Systems, AMD-Vol. 108, ASME, Nov. 1990
133. Allen, R. W. and Rosenthal, T. J., *A Computer Simulation Analysis of Safety Critical Maneuvers for Assessing Ground Vehicle Dynamic Stability*, SAE Paper No. 930760, 1993
134. Winkler, C. B., Fancher, P. S. and Bareket, Z. *et al.*, *Heavy Vehicle Size and Weight: Test Procedures for Minimum Safety Performance Standards*, Final Technical Report, Michigan University Transportation Research Institute, Report No. UMTRI-92-13/ DOT/HS 807 855, Apr. 1992
135. Aurell, J. and Winker, C. B., *Standard Test Procedures for the Lateral Stability of Heavy Vehicle Combinations*, Proceedings of the 4th international Symposium on Heavy Vehicle Weights and Dimensions, June, 1995
136. El-Gindy, M., *An Overview of Performance Measures for Heavy Commercial Vehicles in North America*, Int. J. of Vehicle Design, Vol. 16, Nos. 4/5, pp. 441-463, 1995
137. McFarlane, S., Sweatman, P. and Docile P. *et al.*, *The Correlation of Heavy Vehicle Performance Measures*, SAE Paper No. 973190, 1997
138. Bauer H. F., *On the Destabilizing Effect of Liquids in Various Vehicles*, Vehicle System Dynamics, Vol. 1, pp. 227, 1972
139. Cooper, R. M., *Dynamics of Liquids in Moving Containers*, J. of American Rocket Society, Vol. 30, pp. 725-729, Aug. 1960
140. Abramson, H. N., *The Dynamic Behavior of Liquids in Moving Containers*. NASA SP-106, 1966
141. Roberts, J. R., Basurto, E. R. and Chen, P. Y., *Slosh Design Handbook I*, NASA Technical Reports, NASA-CR-406, May 1966
142. Budiansky, B., *Sloshing of Liquids in Circular Canals and Spherical Tanks*, J. of Aerospace Science, Vol. 27, No. 3, 1960

143. Demirbilek, Z., *A Linear Theory of Viscous Liquid Sloshing*, Ph.D. Thesis, Texas A&M University, 1982
144. Moiseev, N. N., *On the Theory of Nonlinear Vibrations of a Liquid of Finite Volume*, J. of Applied Mathematics and Mechanics, Vol. 22, No. 5, pp. 860-870, 1958
145. Hutton, R. E., *An Investigation of Resonant, Nonlinear, Nonplanar Free Surface Oscillations of a Liquid*, NASA-TND-1870, May 1963
146. Faltinsen., O. M., *A Nonlinear Theory of Sloshing in Rectangular Tanks*, J. Ship Research, Vol. 18, No.4, pp. 224-241, 1974
147. Welch, J. E., *The MAC Method: a Computing Technique for Solving Viscous, Incompressible, Transient Fluid-Flow Problems Involving Free Surfaces*, Report No. LA-3425, Los Alamos Scientific Laboratory, New Mexico, 1966
148. Hirt, C. W., Nichols, B. D. and Romero, N. C., *SOLA - a Numerical Solution Algorithm for Transient Fluid Flow*, Report No. LA-5852, Los Alamos Scientific Laboratory, New Mexico, 1975
149. Su, T. C., Lou, J. K., Flipse, J. E. and Bridges, T. J., *A Numerical Analysis of Large Amplitude Liquid Sloshing in Baffled Containers*, Report MA-RD-940-82046, 1982, The Texas A & M University, College Station
150. Komatsu, K., *Non-linear Sloshing Analysis of Liquid in Tanks with Arbitrary Geometry*, Int. Journal of Non-Linear Mechanics, Vol.22, pp. 193-207, 1987
151. Liu, W. K., *Variational Approach to Fluid-Structure Interaction with Sloshing*, Nuclear Engineering and Design, Vol. 106, pp. 69-85, 1988
152. Mciver, P., *Sloshing Frequencies for Cylindrical and Spherical Containers Filled to an Arbitrary Depth*, J. of Fluid Mechanics, Vol. 204, pp. 243-257, 1989
153. Kassinos, A. C. and Krusa, J. M., *A Numerical Model for 3-D Viscous Sloshing in Moving Containers*, Proceedings of ASME Winter Annual Meeting, Symposium on Recent Advances and Application in CFD, edited by O. Baysal, Vol. B, pp. 75-86, 1990
154. Chen, K. H. and Pletcher, R. H., *Simulation of 3-D Liquid Sloshing Flows Using a Strongly Implicit Calculation Procedure*, AIAA Journal, Vol.31, No. 5, pp. 901-910, 1993
155. Armenio, V. and Rocca, M. L., *On the Analysis of Sloshing of Water in Rectangular Containers: Numerical Study and Experimental Validation*, Ocean Engineering, Vol. 23, No. 8, pp. 705-739, 1996

156. Solaas, F. and Faltinsen., O. M, *Combined Numerical and Analytical Solution for Sloshing in Two-dimensional Tanks of General Shape*, J. of Ship Research, Vol. 41, No. 2, pp. 118-129, 1997
157. Nakayama, T. and Washizu, K, *Non-Linear Analysis of Liquid Motion in a Container subjected to Forced Pitching Oscillation*, Int. J. Num. Meth. Eng., Vol. 15, pp. 1207-1219, 1980
158. Lewin, L., Burger, M. and Souli, M, *Simulation of Dynamic Fuel Slosh Using an Explicit Finite Element Approach*, ASME Press. Vess. Piping Conf., Orlando, FL, USA, pp. 101-110, 1997
159. Wu, G. X., Ma, Q. W. and Taylor, R. E., *Numerical Simulation of Sloshing Waves in a 3D Tank Based on a Finite Element Method*, Applied Ocean Research, Vol. 20, pp. 337-355, 1998
160. Faltinsen., O. M., *A Numerical Nonlinear Method of Sloshing in Tanks with Two-Dimensional Flow*, J. Ship Research, Vol. 22, No. 3, pp. 193-202, 1978
161. Nakayama, T. and Washizu, K., *The Boundary Element Method Applied to the Analysis of Two-Dimensional Nonlinear Sloshing Problems*, Int. J. Num. Meth. Eng., Vol. 17, pp. 1631-1646, 1981
162. Nakayama, T. and Washizu, K., *Boundary Element Analysis of Non-Linear Sloshing Problems*, Development in Boundary Element Methods, edited by P.K. Banerjee and S. Murkerjee, Vol. 3, Applied Science, London, pp. 191-211, 1984
163. Nakayama, T., *Boundary Element Method Applied to the Analysis of Shallow Liquid Sloshing in Moving Tanks*, JSME International Journal, Series C, Vol. 39, No. 4, pp. 800-807, 1996
164. Hwang, J. H., Kim, I. S. and Seol, Y. S. *et al.*, *Numerical Simulation of Liquid Sloshing in Three-Dimensional Tanks*, Computers and Structures, Vol. 44, Nos. 1-2, pp. 339-342, 1992
165. Ortiz, J. L., *Modeling Flexible Multibody Systems-Fluid Interaction*, Ph.D. Thesis, Mechanical Engineering Dept., Texas Tech. University, Lubbock, TX, 1996
166. Ortiz, J. L. and Barhorst, A. A., *Closed-Form Modeling of Fluid-Structure Interaction with Nonlinear Sloshing: Potential Flow*, AIAA Journal, Vol. 35, No. 9, 1997
167. Solaas, F., *Analytical and Numerical Studies of Sloshing in Tanks*, Ph.D. Thesis, The Norwegian Institute of Technology, Trondheim, 1995
168. Sumner, I. E., *Experimentally Determined Pendulum Analogy of Liquid Slashing in Spherical and Oblate-Spherical Tanks*, NASA-TN-2637, 1965

169. Dodge, F. T., *Analytical Representations of Lateral Sloshing by Equivalent Mechanical Models*, The Dynamic Behavior of Liquids in Moving Containers, edited by Abramson, H. N., NASA-SP-106, pp. 199-224, 1966
170. NASA Space Vehicle Design Criteria (Structure), *Propellant Slosh Load*, NASA SP-8009, Aug. 1968
171. Abzug, M. J., *Fuel Slosh in Skewed Tanks*, J. of Guidance, Control, and Dynamics, Vol. 19, No. 5, pp. 1172-1177, 1996
172. Rakheja, S., Sankar, S. and Ranganathan, R., *Roll Plane Analysis of Articulated Tank Vehicles during Steady Turning*, Vehicle System Dynamics, Vol. 17, No. 1, pp. 81-104, 1988
173. Ranganathan, R., Rakheja, S. and Sankar, S., *Influence of Liquid Load Shift on the Dynamic Response of Articulated Tank Vehicles*, Vehicle System Dynamics, Vol. 19, No. 4, pp. 177-200, 1990
174. Popov, G., *Dynamics of Liquid Sloshing in Road Containers*, Ph.D. Thesis, Concordia University, 1991
175. Popov, G., Sankar, S. and Sankar, T. S. et al., *Liquid Sloshing in Rectangular Road Containers*, Computer and Fluids, Vol. 21, pp. 551-569, 1992
176. Popov, G., Sankar, S. and Sankar, T. S. et al., *Dynamics of Liquid Sloshing in Horizontal Cylindrical Road Containers*, Pro. Inst. of Mechanical Engineers, Vol. 207, Part C: J. of Mechanical Engineering Science, pp. 399-406, 1993
177. Popov, G., Sankar, S. and Sankar, T. S., *Dynamics of Liquid Sloshing in Baffled and Compartmented Road Containers*, J. of Fluids and Structures, Vol. 7, pp. 803-821, 1993
178. Slibar, A. and Troger, H., *The Steady State Behavior of a Tank Trailer System Carrying Rigid or Liquid Load*, VSD-IUTAM Symposium on Dynamics of Vehicles on Roads and Tracks, Vienna, 1977
179. Ervin, R. D., Fancher, P. S. and Gillespie, T. D. et al., *Ad Hoc Study of Certain Safety-Related Aspects of Double-Bottom Tankers*, Highway Safety Research Institute, University of Michigan, Report No. UM-HSRI-78-18, May 1978
180. Winkler, C. B., Nisonger, R. L. and Ervin, R. D., *Testing of Michigan Double-Bottom Tanker*, SAE Paper No. 781066, 1978
181. Culley, C., Anderson, R. L. and Wesson, L. E., *Effect of Cargo Shifting on Vehicle Handling*, Dynamic Science, Inc., Report No. FHWA-RD-78-76, Mar. 1978

182. Bohn, P. F., Butler, M. C. and Dunkle, H. D. *et al.*, *Computer Simulation of the Effect of Cargo Shifting on Articulated Vehicles Performing Braking and Cornering Maneuvers*, Vol. 1, Executive Summary, The John Hopkins University, May 1981
183. Khandelwal, R. S. and Nigam, N. C., *Digital Simulation of the Dynamics of a Vehicle Carrying Liquid Cargo on a Random Uneven Surface*, Vehicle System Dynamics, Vol. 11, No. 4, pp. 195-214, 1982
184. Mallikarjunarao, C., *Road Tanker Design: Its Influence on the Risk and Economic Aspects of Transporting Gasoline in Michigan*, Ph.D. Thesis, University of Michigan, 1982
185. Larocque, G. R., Croce, P. A. and Cece, J., *Feasibility Study of a System Safety Monitor for Hazardous Material Trucking*, SAE Paper No. 852357, 1985
186. Croce, P. A., Larocque, G. R. and Long, M. H., *et al.*, *A Feasibility Study of a Sealed Safety Monitor for Trucks Carrying LNG and other Hazardous Materials*, Arthur D. Little, Inc., U. S. Dept. of Energy Report DOE/EV/10502-1, Dec. 1982
187. Sankar, S., Ranganathan, R. and Rakheja, S., *Impact of Dynamic Fluid Slosh Loads on the Directional Response of Tank Vehicles*, Vehicle System Dynamics, Vol. 21, No. 6, pp. 385-404, 1992
188. Sankar, S. and Rakheja, S., *Liquid Tanker Stability*, Final Report, Transport Canada, Transportation Development Center Report No. Tp 10690 E, Nov. 1990
189. Rakheja, S., Sankar, S. and Ranganathan, R., *Influence of Tank Design Factors on the Rollover Threshold of Partially Filled Tank Vehicles*, SAE Paper No. 892480, 1989
190. Ranganathan, R., Rakheja, S. and Sankar, S., *Effects of Vehicle Configurations and Tank Design Factors on Directional Dynamics of Tank Vehicles*, Transactions of the Canadian Society of Mechanical Engineering, Vol. 17, No. 4, pp. 923-942, 1993
191. Ranganathan, R., Rakheja, S. and Sankar, S., *Directional Response of a B-train Vehicle Combination Carrying Liquid Cargo*, J. of Dynamic Systems, Measurement and Control, Transactions of the ASME, Vol. 115, No. 1, pp. 133-139, 1993
192. Rakheja, S. and Sankar, S., *Field Testing of a Tank Truck and Study of Fluid Slosh*, SAE Paper No. 912679, 1991
193. Rakheja, S., Ranganathan, R. and Sankar, S., *Field Testing and Validation of Directional Dynamics Model of a Tank Truck*, Int. J. of Vehicle Design, Vol. 13, No. 3, pp. 251-275, 1992

194. Rakheja, S., *Estimation of Rollover Threshold of Partially Filled Tank Trucks*, Pro. Inst. Mech. Engrs, Vol. 205, Part D: Journal of Automobile Engineering, pp. 69-71, 1991
195. Rakheja, S. and Ranganathan, R., *Estimation of the Rollover Threshold of Heavy Vehicles Carrying Liquid Cargo: a Simplified Approach*, Heavy Vehicle Systems, Int. J. of Vehicle Design, Vol. 1, No. 1 pp. 79-98, 1993
196. Ranganathan, R., Ying, Y. and Miles J. B., *Analysis of Fluid Slosh in Partially Filled Tanks and Their Impact on the Directional Response of Tank Vehicles*, SAE Paper No. 932942, 1993
197. Rakheja, S. and Wang, Z., *Analysis of Braking Process of a Partially-Filled Tractor Tank Semitrailer*, Advances in Transportation Systems, CSME Forum SCGM, pp. 326-333, 1996
198. Ranganathan, R. and Ying, Y. S., *Impact of Liquid Load Shift on the Braking Characteristics of Partially Filled Tank Vehicles*, Vehicle System Dynamics, Vol. 26. pp. 223-240, 1996
199. Ranganathan, R., Ying, Y. and Miles, J. B., *Development of a Mechanical Analogy Model to Predict the Dynamic Behavior of Liquids in Partially Filled Tank Vehicles*, SAE Paper No. 942307, 1994
200. Ibrahim, I. M., El-Nashar, M. A. and Younes, Y. K., *Ride Behavior of Trucks Transporting Liquids*, Heavy Vehicle Systems, Int. J. of Vehicle Design, Vol. 5, Nos. 3/4, 1998, pp. 261-276, 1998
201. Bogomaz, G. I., Markova, O. M. and Chernomashentseva, Y. G., *Mathematical Modeling of Vibrations and Loading of Railway Tanks Taking into Account the Liquid Cargo Mobility*, Vehicle System Dynamics, Vol. 30, pp. 285-294, 1998
202. Aquaro, M., Mucino, V. H. and Gautam, M. *et al.*, *A Finite Modeling Approach for Stability Analysis of Partially Filled Tanker Trucks*, SAE Paper No. 1999-01-3708, 1999
203. Salem, M. I., Mucino, V. H. and Gautam, M. *et al.*, *Review of Parameters Affecting Stability of Partially Filled Heavy-duty Tankers*, SAE Paper No. 1999-01-3709, 1999
204. Canadian Standards Association, *Highway Tanks and Portable Tanks for the Transportation of Dangerous Goods*, CSA Preliminary Standard B338-1982, Mar. 1982
205. Code of Federal Regulations, *Title 49-Transportation, Part 178*, 10-1-98 Version, Department of Transportation, USA, 1998

206. Wang, Z., Rakheja, S. and Sun, C., *Influence of Partition Location on the Braking Performance of Partially-Filled Tank Truck*, SAE Paper No. 952639, 1995
207. Ibrahim, I. M., *Anti-Slosh Damper Design for Improving the Roll Dynamic Behavior of Cylindrical Tank Trucks*, SAE Paper No. 1999-01-3729, 1999
208. Richardson, W. G., *New Equipment Design Necessary to Improve Safety of MC306 Tank*, Modern Bulk Transporter, pp. 53-55, Sept. 1982
209. Klingenberg, B., Rossow, G. and Jacobsen, R., *FACT-The Freightliner/Heil Advanced Concept Truck*, SAE Paper No. 892462, 1989
210. Popov, G., Sankar, S. and Sankar, T. S., *Optimal Shape of a Rectangular Road Container*, J. of Fluids and Structures, Vol.7, pp. 75-86, 1993
211. Popov, G., Sankar, S. and Sankar, T. S., *Shape Optimization of Elliptical Road Containers due to Liquid Load in Steady-State Turning*, Vehicle System Dynamics, Vol. 25, pp. 203-221, 1996
212. Kang, X., Rakheja, S. and Stiharu, I., *Optimal Tank Geometry to Enhance Static Roll Stability of Partially-filled Tank Vehicles*, SAE Paper No. 1999-01-3730, SAE Transactions J. of Commercial Vehicles, 2000
213. Roy, D. N., *Applied Fluid Mechanics*, Ellis Horwood Limited, England, 1988
214. Bakker, E., Pacejka, H. B. and Lidner, L., *A New Tire Model with an Application in Vehicle Dynamics Studies*, SAE Paper No. 890087, 1989
215. Schuring, D. J., Pelz, W. and Pottinger, M. G., *The BNPS Model—an Automated Implementation of the “Magic Formula” Concept*, SAE Paper No. 931909, 1993
216. Fancher, P. S., Ervin, R. D., Winkler, C. B. and Gillespie, T. D., *A Factbook of the Mechanical Properties of the Components for Single-Unit and Articulated Heavy Trucks*, The University of Michigan Transportation Research Institute, Ann Arbor, MI, UMTRI-86-12, DOT HS 807 125, Dec. 1986
217. Bernard, J. E., Winkler, C. B. and Fancher, P. S., *A Computer-Based Mathematical Method for Predicting the Directional Response of Trucks and Tractor-Trailers, Phase II Technical Report*, Motor Truck Braking and Handling Performance Study, Highway Safety Research Institute, The University of Michigan, Ann Arbor, PB-221-630, June 1973
218. Winkler, C. B., Bernard, J. E. and Fancher, P. S., *et al.*, *Predicting the Braking Performance of Trucks and Tractor-Trailers. Phase III Technical Report*, Motor Truck Braking and Handling Performance Study, Highway Safety Research Institute, The University of Michigan, Ann Arbor, PB-263-216, June 1976

219. Gilleppe, T. D., MacAdam, C. C. and Hu, G. T., *Truck and Tractor-Trailer Dynamic Response Simulation-T3DRS, Final Report*, Contract No. DOT-FH-11-9330, Highway Safety Research Institute, The University of Michigan, Ann Arbor, Report No. UM-HSRI-79-38, Mar. 1979
220. Gupta, V., *A Submodel Component Reanalysis Technique for Liquid Tanker Body Design using the Finite Element Method*, Master Thesis, Concordia University, 1988
221. *ANSYS User's Manual*, Release 5.5, SAS IP, Inc., 1998
222. Cook, R. D. and Young, W. C., *Advanced Mechanics of Materials*, 2nd Edition, Prentice Hall, 1999
223. Moaveni, S., *Finite Element Analysis: Theory and Application with ANSYS*, Upper Saddle River, NJ: Prentice Hall, 1999
224. Davis, S., Masser, P., Culley, C. and Edwards, J., *Analysis of Cargo Tank Integrity in Rolllovers, Final Report*, Dynamic Science, Inc., U.S. Department of Transportation, Federal Highway Administration, USA, PB-279-506, Oct. 1977
225. Tyndall, L. H., Augspurger, Q. and Johnson, N. B., *Integrity of MC 330/331 Cargo Tanks*, Dynamic Science, Inc., Bureau of Motor Carrier Safety, Federal Highway Administration, U.S. Department of Transportation, USA, Jan. 1984
226. Kang, X., Rakheja, S. and Stiharu, I., *Tank Shape Optimization for Enhancement of Roll Stability of Partially-filled Tank Vehicles in Steady Turning*, presented at ASME IMECE-2000, Orlando, Florida, Nov. 2000
227. Kang, X., Rakheja, S. and Stiharu, I., *Directional Dynamics of a Partly-Filled Tank Vehicle under Braking and Steering*, presented at SAE 2000 Bus & Truck Meeting, Portland, Oregon, Dec. 2000
228. Kang, X., Rakheja, S. and Stiharu, I., *Cargo Load Shift and its Influence on Tank Vehicle Dynamics under Braking and Turning*, accepted for Heavy Vehicle Systems, Int. J. of Vehicle Design, 2000
229. Kang, X., Rakheja, S. and Stiharu, I., *Effects of Tank Shape on the Directional & Roll Dynamic Response of a Partly-Filled Tank Vehicle*, accepted for Vehicle System Dynamics, Int. J. of Vehicle Mechanics and Mobility, 2000
230. Kang, X., Rakheja, S. and Stiharu, I., *Dynamic Response and Stability Characteristics of Partly-filled Articulated Liquid Cargo Vehicles under Braking-in-a-turn*, to be submitted to Automobile Engineering, Proc. of the Institute of Mechanical Engineers, Part D, U.K.

APPENDIX A

INFLUENCE OF TANK CROSS-SECTION ON TANK STRUCTURAL INTEGRITY

In this section, the three optimal cross-sections proposed in Chapter 3, Opt.5 for relatively insignificant partial fill conditions, and OPT1 and OPT2 for 50%-70% and 70%-90% fill volume ranges, respectively, are further evaluated from tank structural integrity point of view.

Due to the high complexity of the shape of the optimal tanks, it is virtually impossible to conduct a complete stress analysis of the tank structure by classical analytical methods. A simplified finite element model for a cleanbore tank of generic cross-section with its mount is thus developed. The stress distributions of various optimal (OPT1, OPT2 and Opt.5) and conventional (circular and modified-oval) tanks are then evaluated based on the FE model and compared to investigate the influence of tank cross-section. The modeling consideration, analysis procedure and preliminary results are briefly summarized in this section.

A.1 Finite Element Model of a Generic Tank and its Supports

Tank description

A cleanbore tank of generic cross-section and length $L=12.19$ m (480 in) with two end caps (heads) is considered for the modeling and analysis. As indicated in Chapter 2, the generic tank cross-section can effectively describe the currently used circular and modified-oval tanks. The tank body is assumed to be mounted on the trailer chassis through four identical supports, which are located symmetrically about both the vertical axis and the length of the tank. Each support is composed of a saddle, a pad, and a

channel, with the channel representing the interface between the support and the trailer frame. The tank body rests on the saddles and is welded to them. Details of the tank body and its supports are shown in Figure A1. In the figure, L_s is the support length, L_d represents the longitudinal distance between two supports, and d_s denotes the lateral distance between two adjacent supports; s_{a1} and s_{a2} represent the saddle arc lengths on the right- and left-side of the pad, respectively, h_p is pad height, while d_{c1} and d_{c2} are channel widths on the left- and right-side of the pad, respectively, as shown in Figure A1 (b).

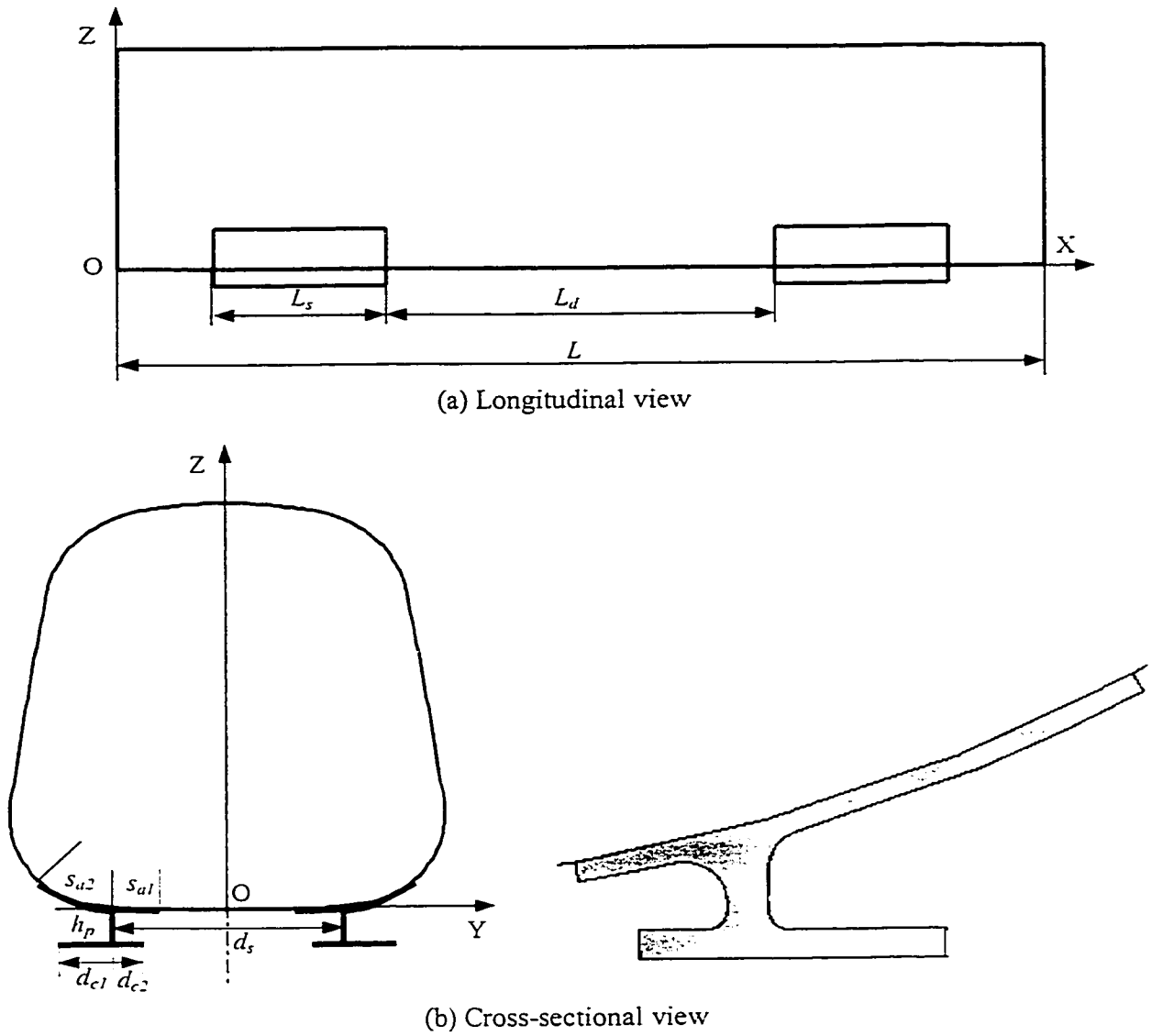


Figure A1: Schematic diagram of a generic tank and its supports.

The geometry of the supports is selected according to reference [220]. The saddle, pad and channel may assume different thickness. The tank and its supports are assumed to be made of aluminum 5454, with yield strength of 414 Mpa. The following material properties are used for the analysis of the tank structure [220]:

- Modulus of elasticity: 68.9 GPa
- Density: 2712.67 kg/m³
- Poisson's ratio: 0.33

Modeling assumptions

With an aim to evaluate the cross-section geometry effect and to simplify the modeling and analysis, the following assumptions are made in building the model:

- Preliminary stress analysis under static loading condition;
- The tank exterior accessories, such as liquid inlet and outlet holes, manhole cover, welds are not modeled as these areas are not of great concern and would not significantly affect the analysis results;
- Cleanbore cylindrical tank with no internal structures, such as baffles, compartments, and enforcement rings;
- Relatively larger material thickness for the tank shell and supports, and lighter liquid cargo are considered to avoid large structural deformation due to the absence of tank internal structures.

Model generation using ANSYS

The ANSYS system, which is a large-scale general-purpose finite element package [221], is used for creating the tank and support geometry, meshing the model, applying material properties, boundary conditions and loads, solving the finite element

problem, and presenting the results. Three steps are involved in a typical ANSYS analysis: (i) pre-processing phase, including geometry creation, material property definition, selection of the element type, and mesh generation; (ii) solution phase, including constraint and load applications, element matrix formulation, overall matrix triangularization (wave-front), and calculations of displacements, strains and stresses, etc.; and (iii) post-processing phase, including result (displacements, strains, stresses, etc.) operations, visualization and output. The pre-processing is carried out using the PREP7 module, while the post-processing may be performed by a number of post-processors available within ANSYS for processing and presentations of the resulting data. Stress contour plots as well as stress distributions along pre-defined paths on the tank body can be generated within the General Postprocessor (POST1). User interaction with the modeling and analysis process is achieved by using either the Graphic User Interface Menu (GUI) or ANSYS commands specific to each phase.

The geometry model of the tank and its supports is generated utilizing the basic drawing tools within PREP7 with bottom-up modeling. The cross-section geometry of the tank is firstly generated to exact dimensions, which are described in Chapter 2, by creating respective arcs and gluing them together. The tank shell is then created by extending the cross-section geometry along the longitudinal axis X using the 'Extrude' command. The supports are created similarly using geometry modeling commands. The tank and supports are then assembled to generate the full model of the tank and its supports. To facilitate the modeling and design modifications, the ANSYS parametric design language (PDL), which makes it possible to build a geometry model in terms of design parameters (variables), is used in developing the model. For example, changing

the geometric parameters of the generic cross-section in the program can conveniently yield the different tank configurations. Figure A2 illustrates the geometric model of the tank body and its supports.

The generated tank and support geometry model may be meshed with either solid or shell elements. Due to the significant dimension variations of the tank and support geometry, as shown in Figure A2, if a solid element is used, the total number of DOF would considerably exceed the maximum capacity of the available ANSYS version used. In addition, the high ratio between the arc radii of the tank cross-section and shell thickness as well as high aspect ratio of the support also justifies the selection of a shell element. The 8-node structural shell element, SHELL93 in the ANSYS Element Library, is selected, as it is particularly well suited to model curved shells. This element has 6-DOF at each node: translations in the nodal x, y and z directions and rotations about the nodal x, y and z axes [221].

Two element shapes including triangular and quadrilateral type elements can be generated automatically by setting element shape control command 'MSHAPE' to 1 and 0, respectively. Figure A3 illustrates a quarter finite element model of the tank and its support meshed using the triangular shape. The meshed model provides the basis for further analyses.

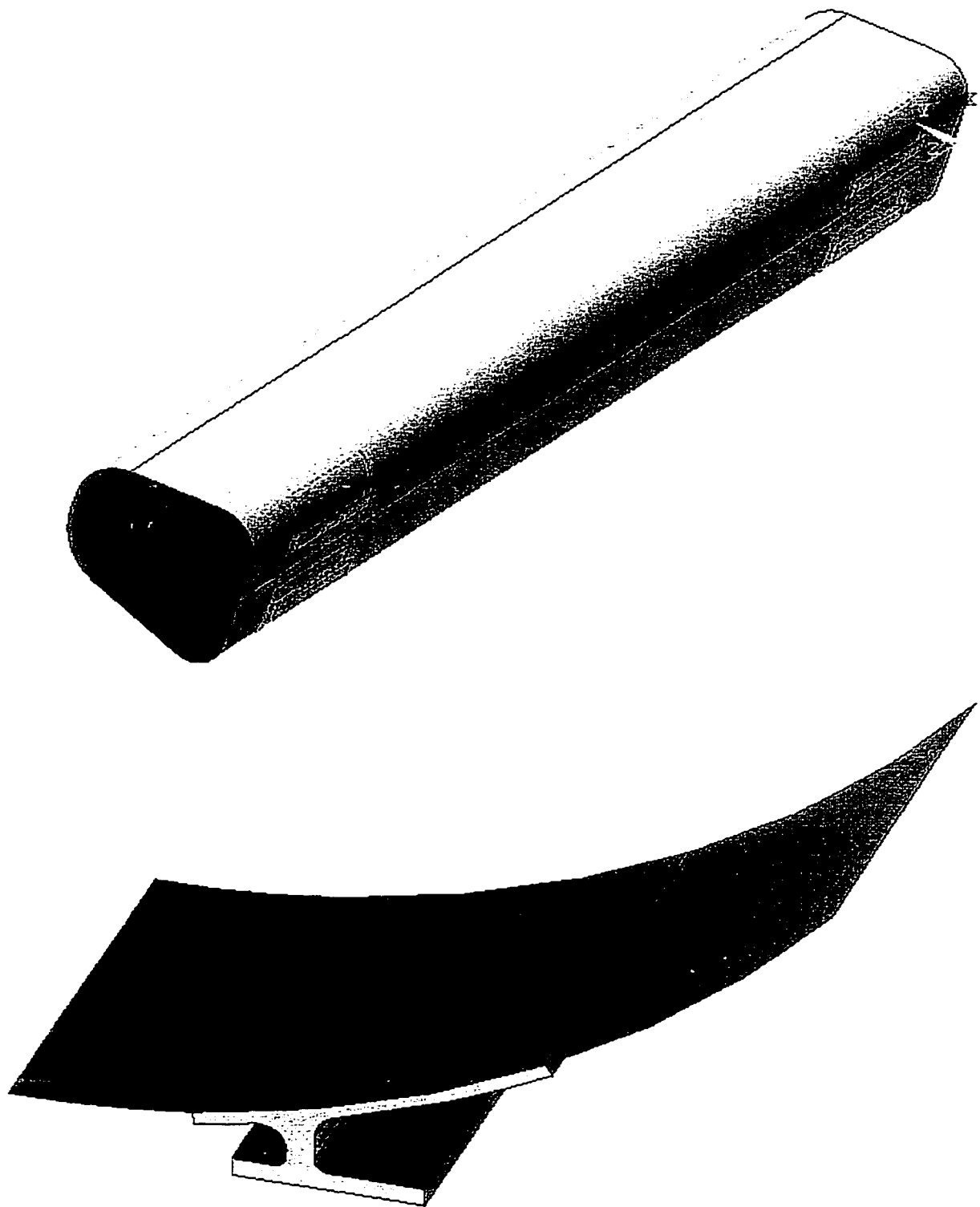


Figure A2: Geometric model of a generic tank and its supports.

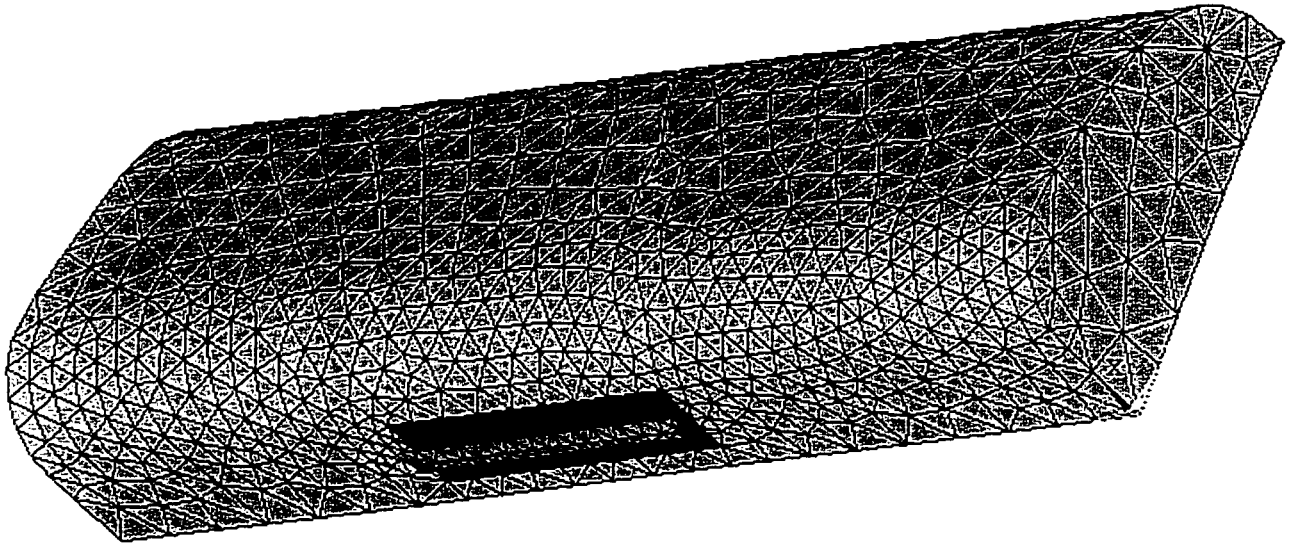


Figure A3: Quarter finite element model of the tank and its supports.

Load and boundary conditions

Two static load cases are considered in this preliminary stress analysis: (i) weight of the liquid cargo; and (ii) weight of the tank structure. The load due to structural weight is calculated directly by the software system based upon dimensions of the tank geometry and density of the materials used. The weight of the liquid cargo is simulated as hydrostatic pressure acting on the inner wetted wall of the tank. The hydrostatic pressure due to the liquid cargo is expressed as a function of vertical coordinate z in the tank body-fixed coordinate system as:

$$P = \rho g(h-z) \quad (A1)$$

where h represents static liquid height, P represents liquid pressure, ρ is mass density of the liquid cargo, and g is the gravity acceleration.

The boundary conditions (displacement constraints) are applied directly on the channel bases, which represent the interfaces between the tank supports and the trailer frame, assuming negligible influence of trailer frame flexibility. The connections between

the quarter tank and other part of the tank body are represented by symmetric boundary conditions [221].

A.2 Stress Distribution of Various Conventional and Optimal Tanks

The developed finite element model is solved using the static structural analysis option of ANSYS to calculate the stress distribution of different tanks under various liquid fill conditions. The General Postprocessor is utilized to visualize and present analysis results in the forms of stress contours, and stress distributions along designated paths on the tank body. In all the analyses, the von Mises or equivalent stress, which is based upon the distortion-energy theory or the von Mises-Hencky theory [222], is evaluated.

The validity of the model is firstly examined using static equilibrium conditions: the sum of the computed reaction forces on the support is exactly balanced by the liquid and structural weights. The finite element model is further validated based on a lot of testing runs, involving different element types and sizes, meshing shapes, and liquid fill volumes. The results show that variations in meshing shape and density yield insignificant deviation in the results. Furthermore, the resulting stress response based on both the nodal and element solutions of an analysis shows good agreement (the difference between the two solutions is within 5%). This convergence is further confirmed by the error-estimation in ANSYS, which measures the error in each element due to mesh discretization, based on the difference between averaged and unaveraged nodal stress values.

The dimensional parameters of the support used for the final analysis are selected as: $L_s=1.500$ m, $L_d=5.000$ m, $d_s=0.750$ m, $h_p=0.065$ m, $d_{c1}=0.100$ m and $d_{c2}=0.050$ m. The thicknesses for the shell and saddles are selected to be 0.008 m and 0.010 m, respectively, while those for the support pads and channels are selected to be 0.020 m [220].

It should be pointed out that, due to variations in the radii of arcs 1 and 2 with different tanks, as described in Chapter 3, the radii of the saddles, which fit and support the tank body through arcs 1 and 2, also vary, depending on the particular tank cross-section. It is thus impossible to maintain identical saddle geometry in the analysis. The saddle arc lengths, s_{a1} and s_{a2} , however, are hold constant (0.210 m and 0.220 m, respectively) to ensure identical saddle length for different tanks. The variation in the saddle geometry curvature, however, may influence the comparative study considerably.

Figures A4 through A13 present the stress (in Pa) distributions of one-fourth of circular, modified-oval, OPT1, OPT2, and Opt.5 tanks, respectively, under liquid (mass density: 750 kg/m³) fill volume of 80%. The figures illustrate the tank stress distributions in terms of equivalent stress contour of the tank body and stress patterns along two longitudinal paths on the tank body, one on the top line (s_{top}) and another on connecting line between arcs 2 and 3 of the cross-section (s_{yz3}). To facilitate the analysis, the stress components in the global Cartesian system, s_x (in tank-body lateral axis direction), s_y (in tank vertical axis direction) and s_z (axial stress, in tank longitudinal axis direction), are also presented, as shown in Figures 5, 7, 9, 11, 13, where the vertical axis denotes stresses (in Pa), while the horizontal axis (s) represents the longitudinal distance (in m) from the origin of the tank body system. The symbols in the legend column on the right hand of the stress contour figures, Figures 4, 6, 8, 10, 12, represent the ANSYS version

number, date and time of display, type of plot (NODAL SOLUTION), load step number (STEP), substep number (SUB), time value (TIME), label of plotted item (SEQV: equivalent stress), maximum deformation (DMX, in m), maximum stress value (SMX) and contour legend, etc., while MX and MN on the contour plots denote locations of maximum and minimum stress values, respectively.

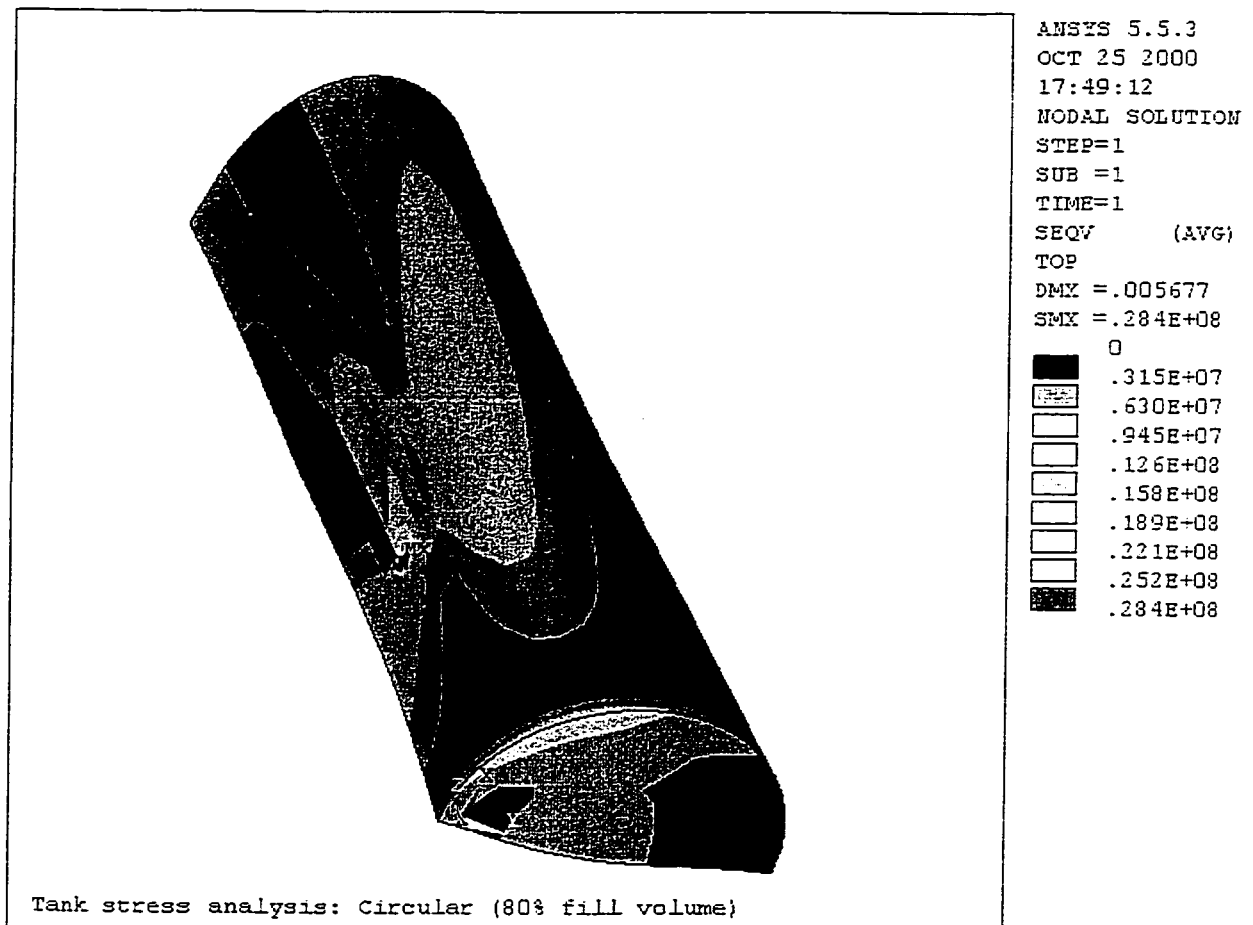


Figure A4: Stress contour of the quarter circular tank.

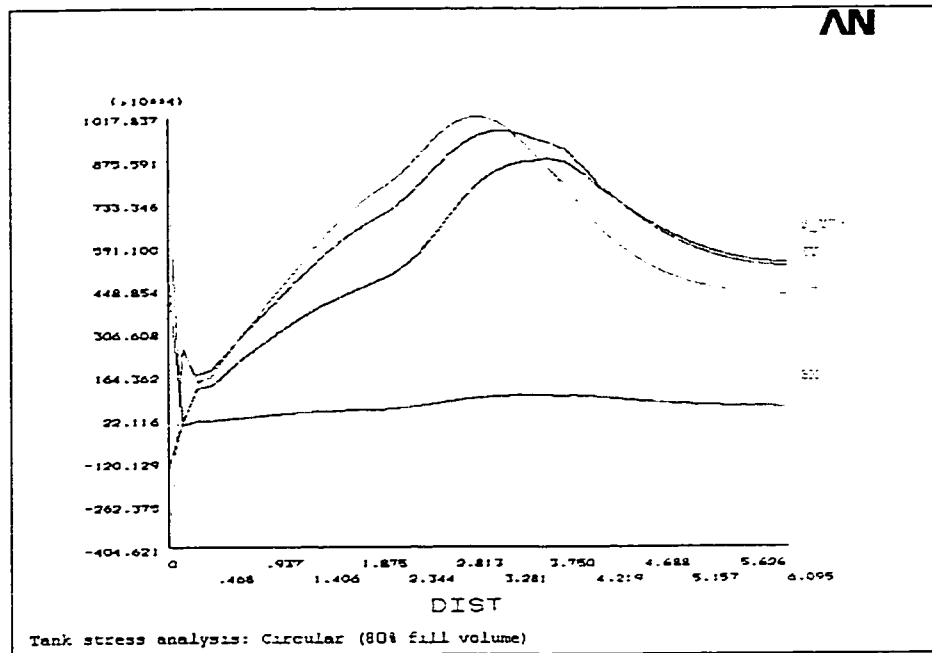
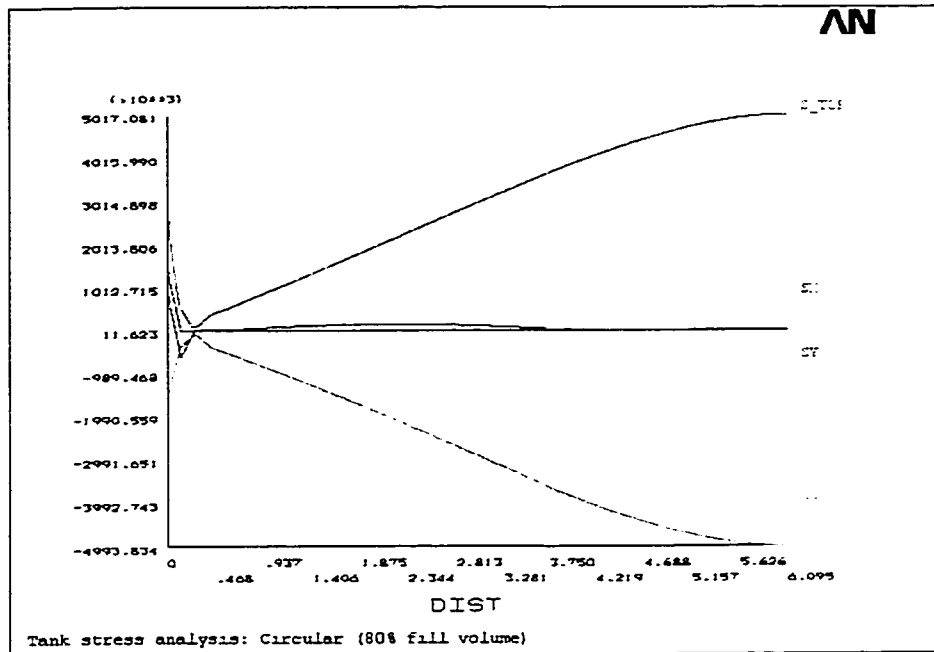


Figure A5: Stress distribution along longitudinal direction of the quarter circular tank.

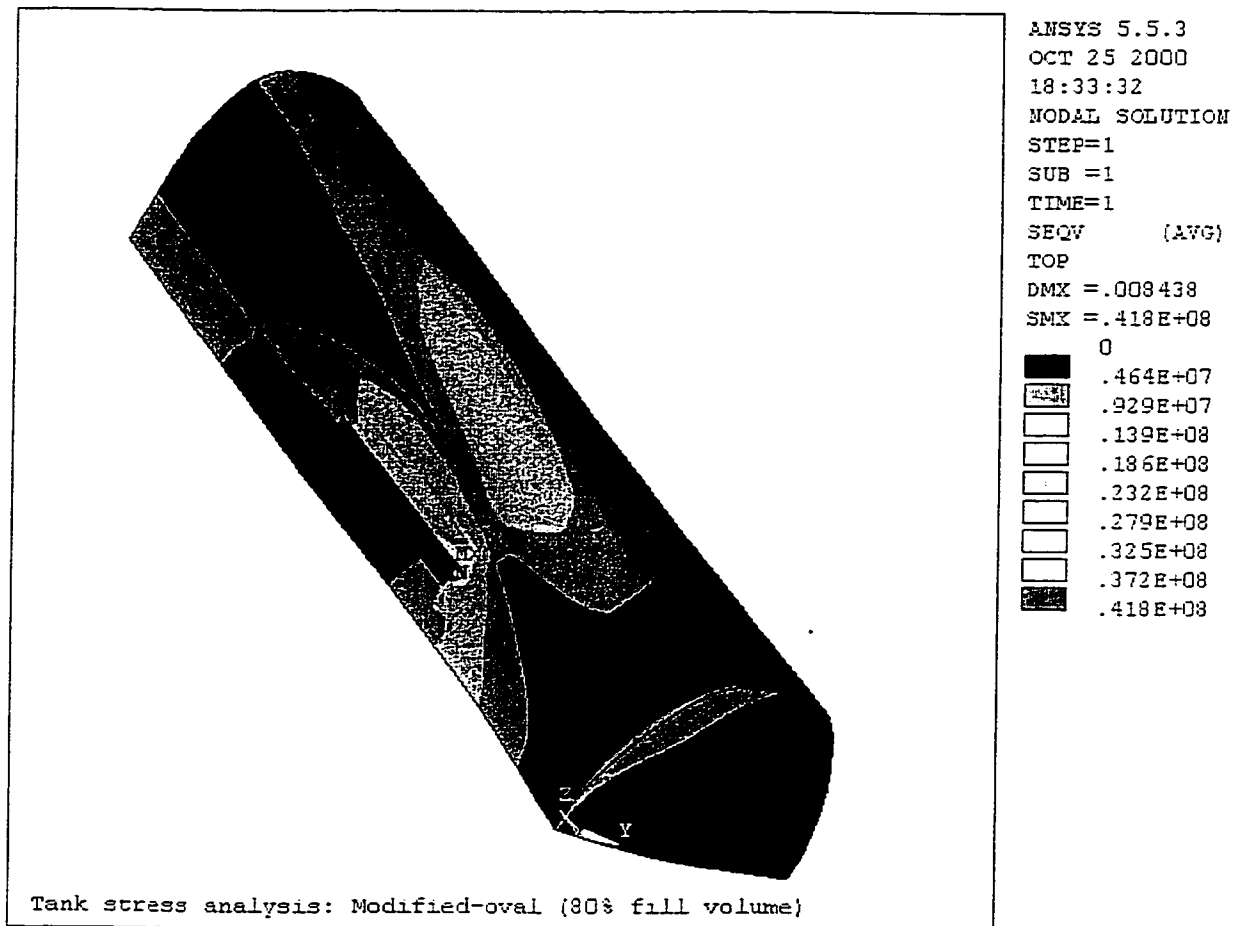


Figure A6: Stress contour of the quarter modified-oval tank.

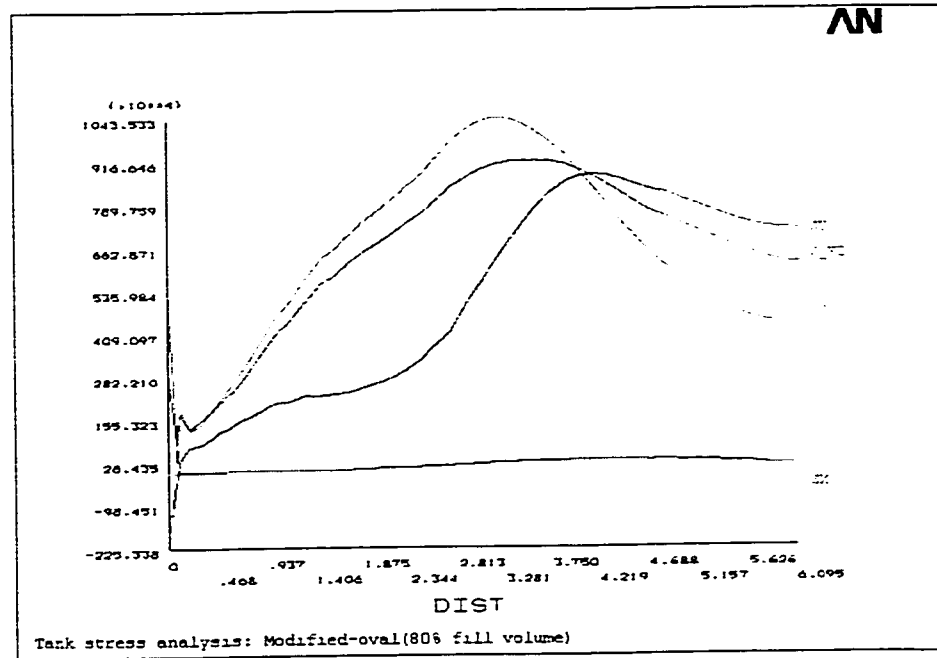
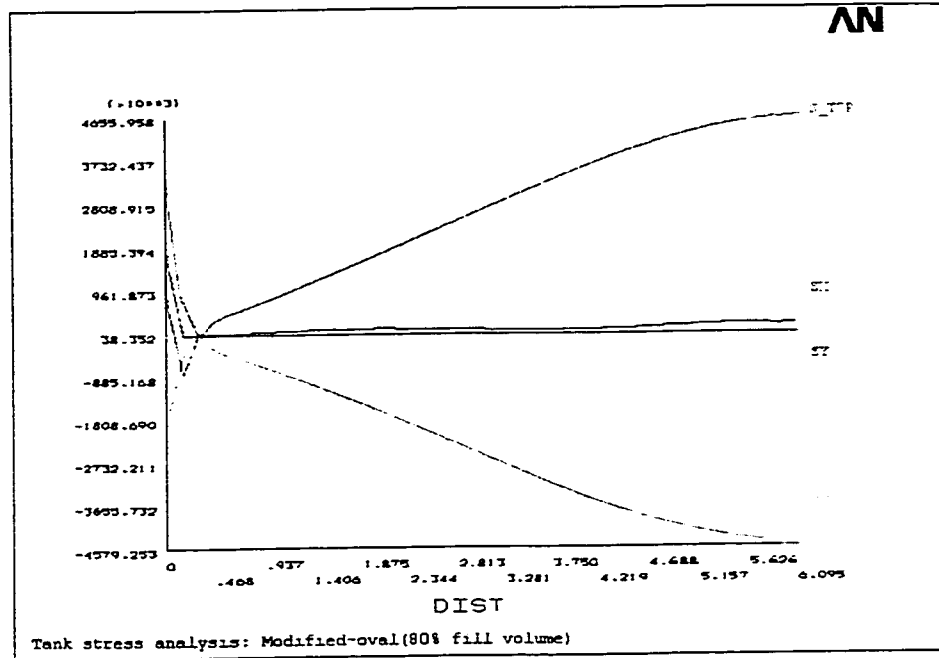


Figure A7: Stress distribution along longitudinal direction of the quarter modified-oval tank.

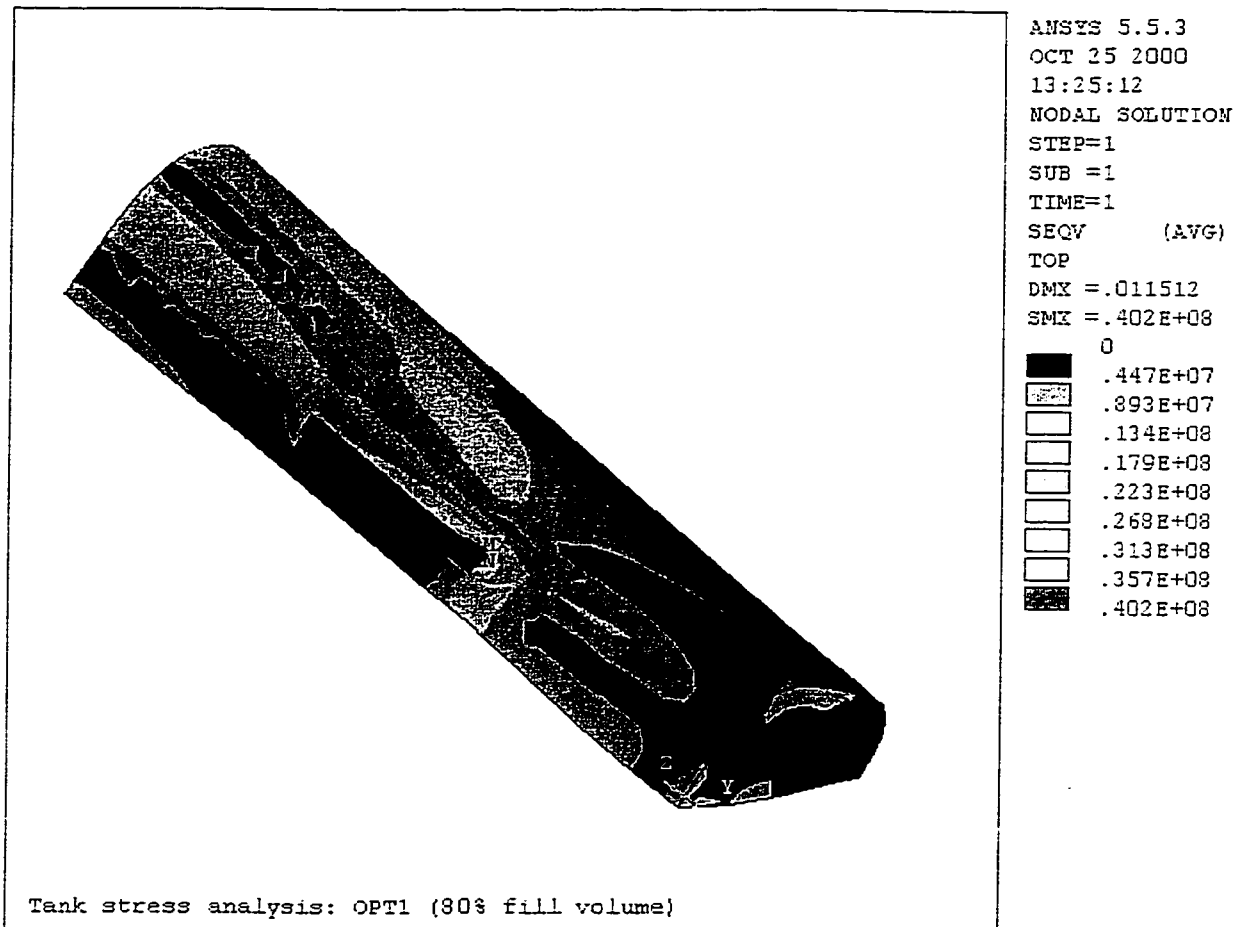


Figure A8: Stress contour of the quarter OPT1 tank.

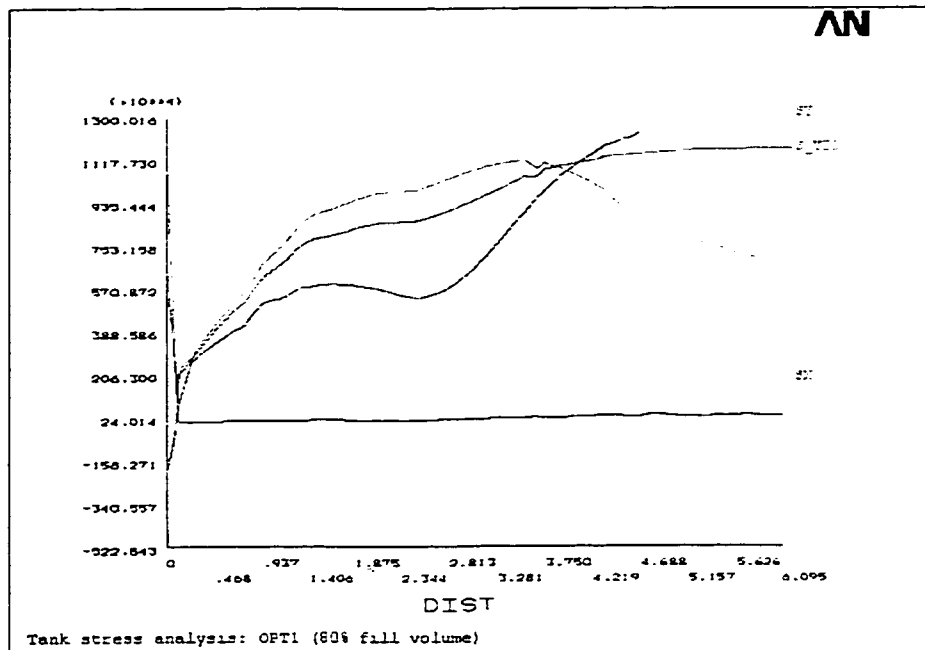
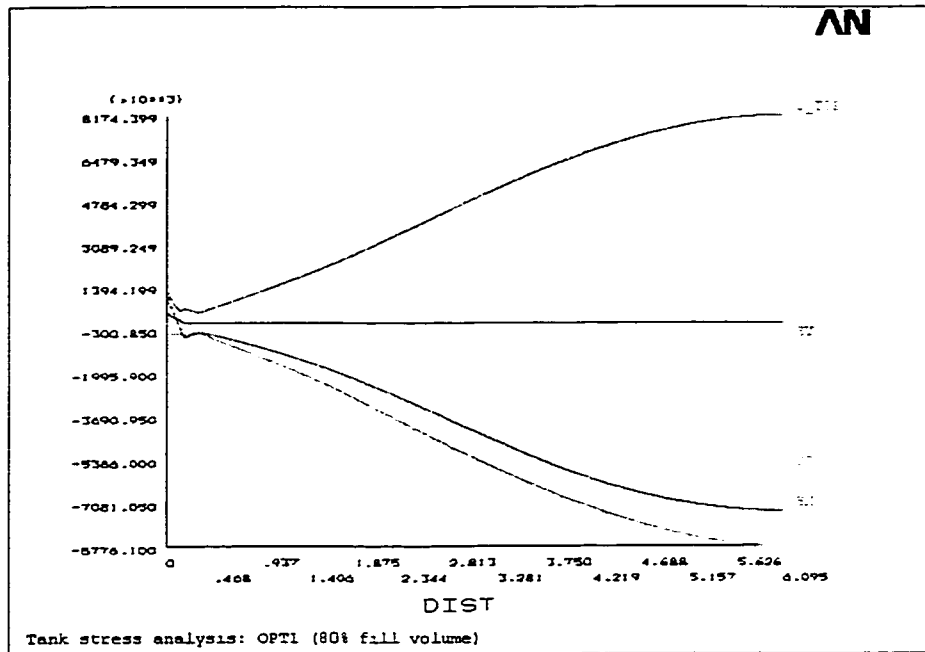


Figure A9: Stress distribution along longitudinal direction of the quarter OPT1 tank.

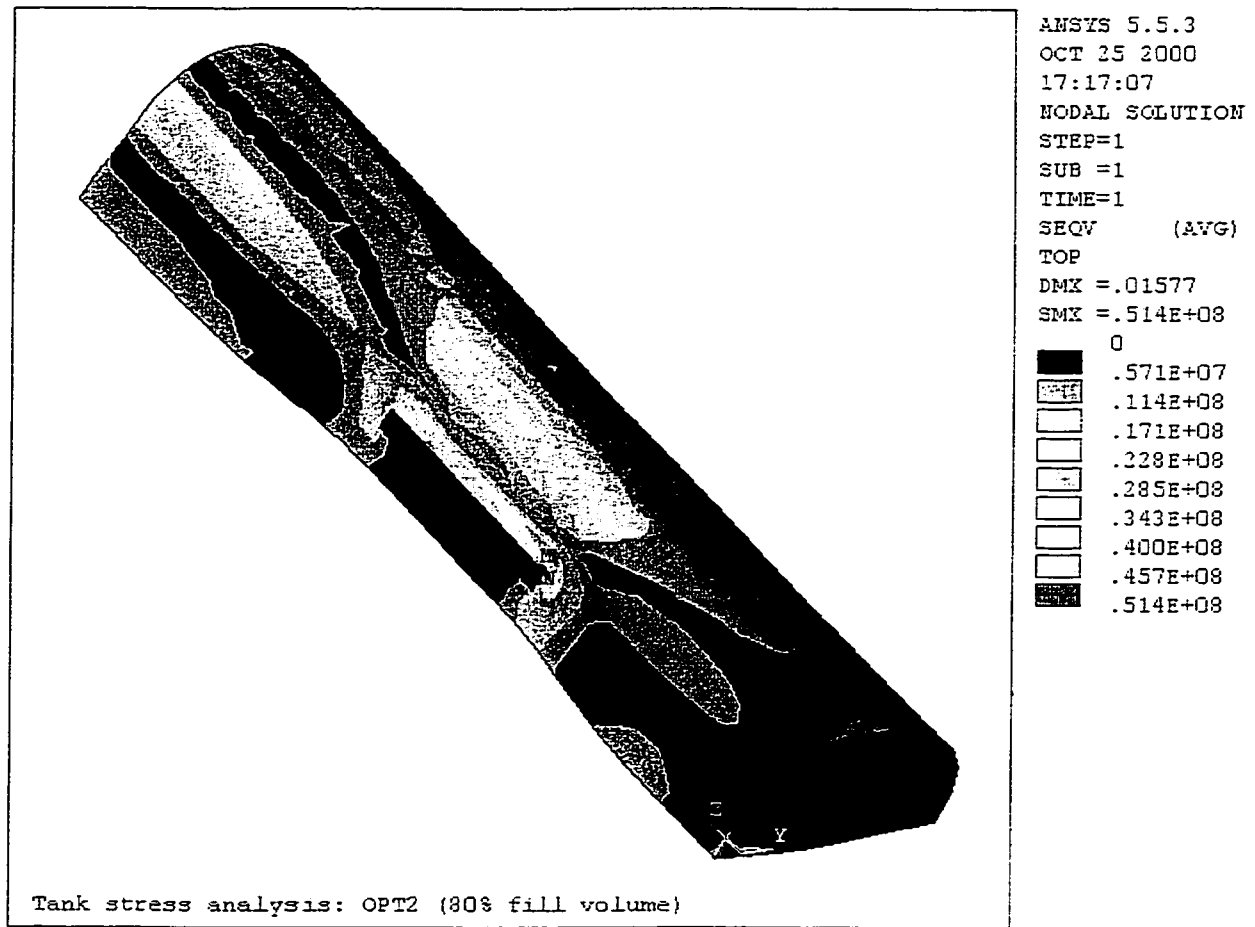


Figure A10: Stress contour of the quarter OPT2 tank.

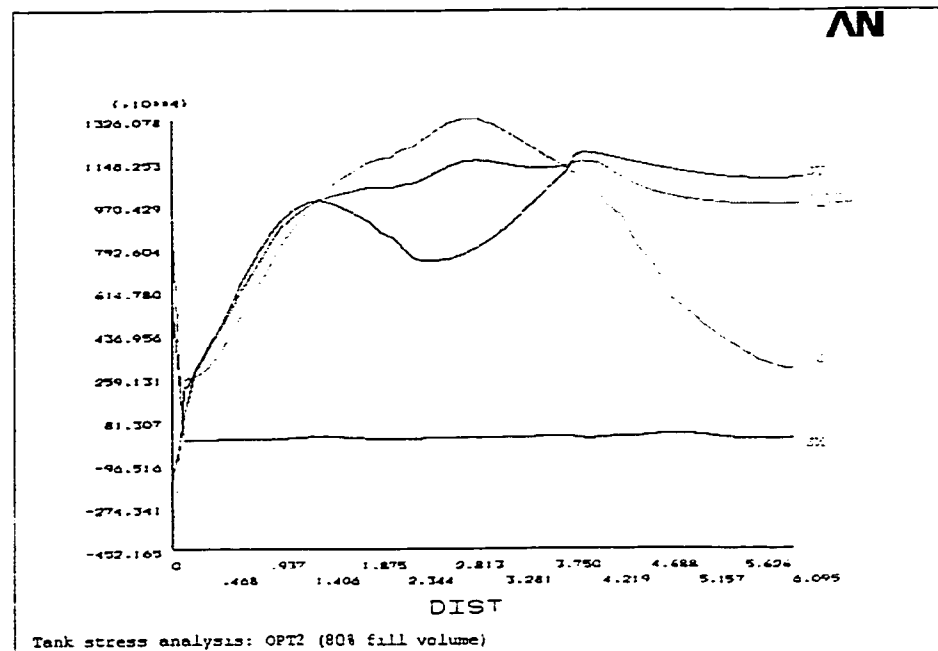
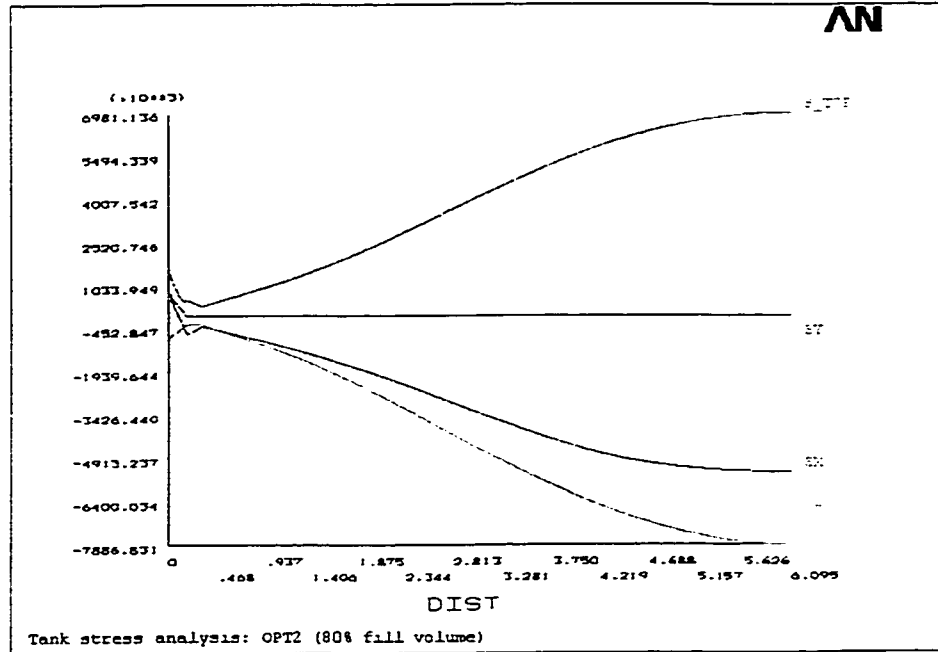


Figure A11: Stress distribution along longitudinal direction of the quarter OPT2 tank.

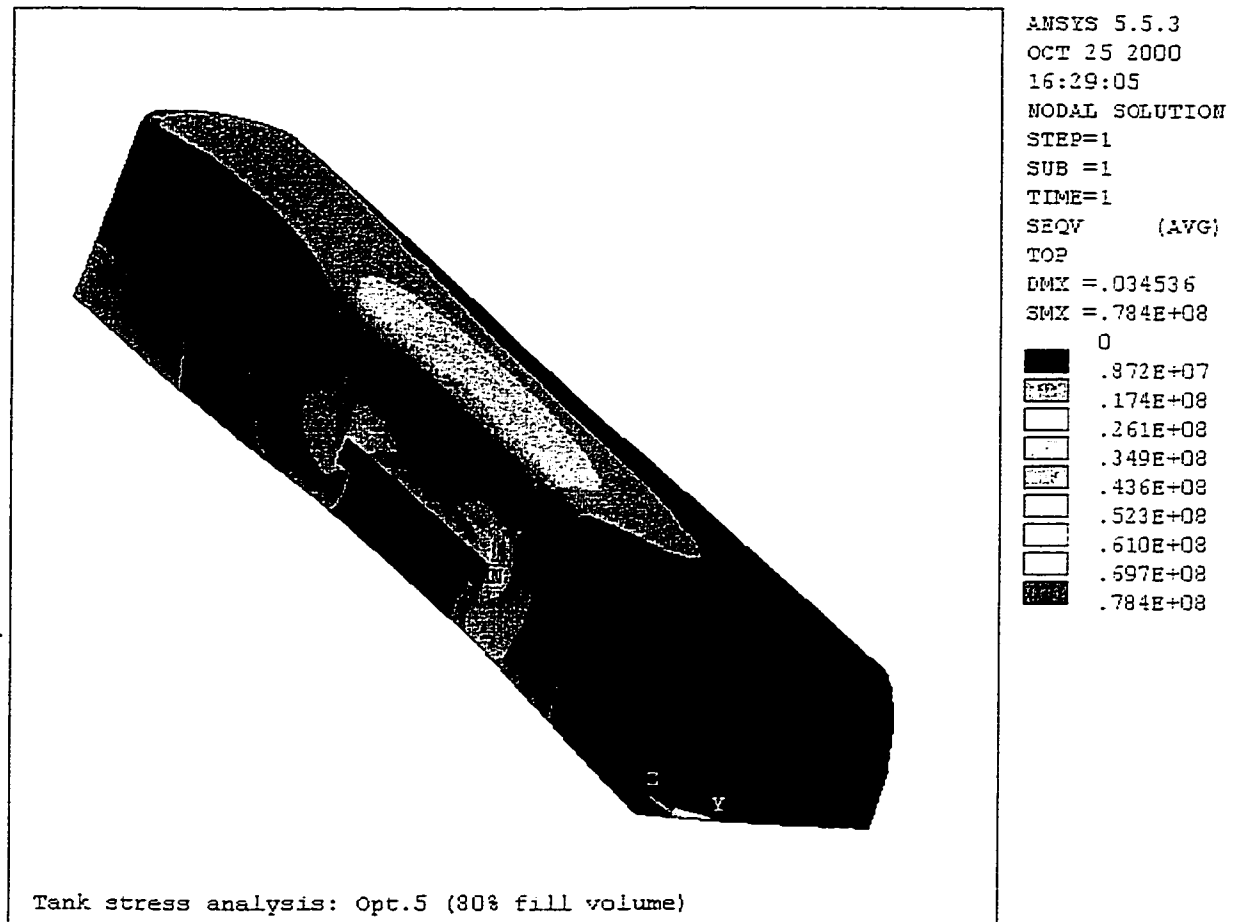


Figure A12: Stress contour of the quarter Opt.5 tank.

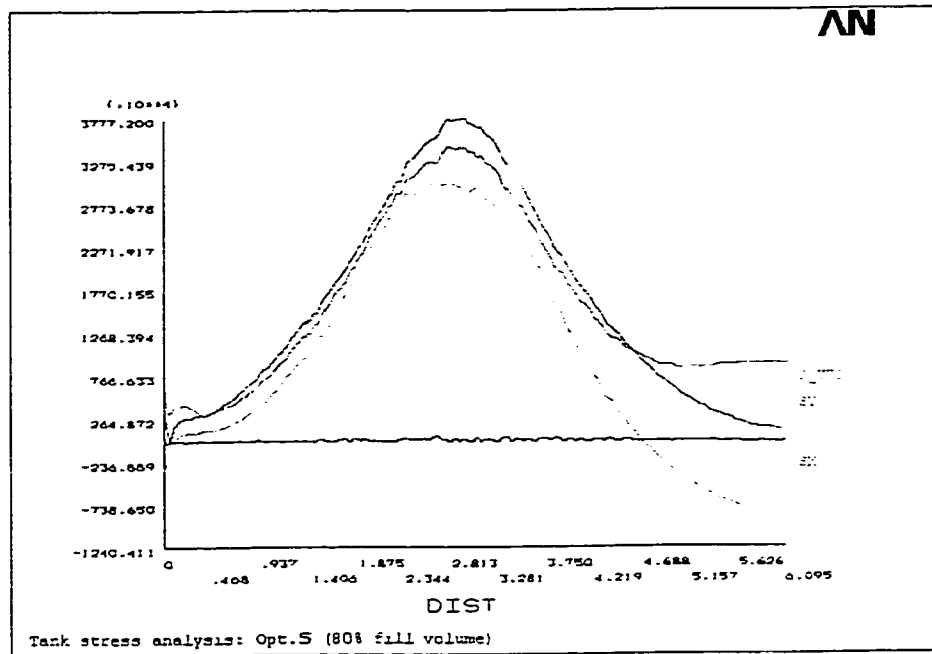
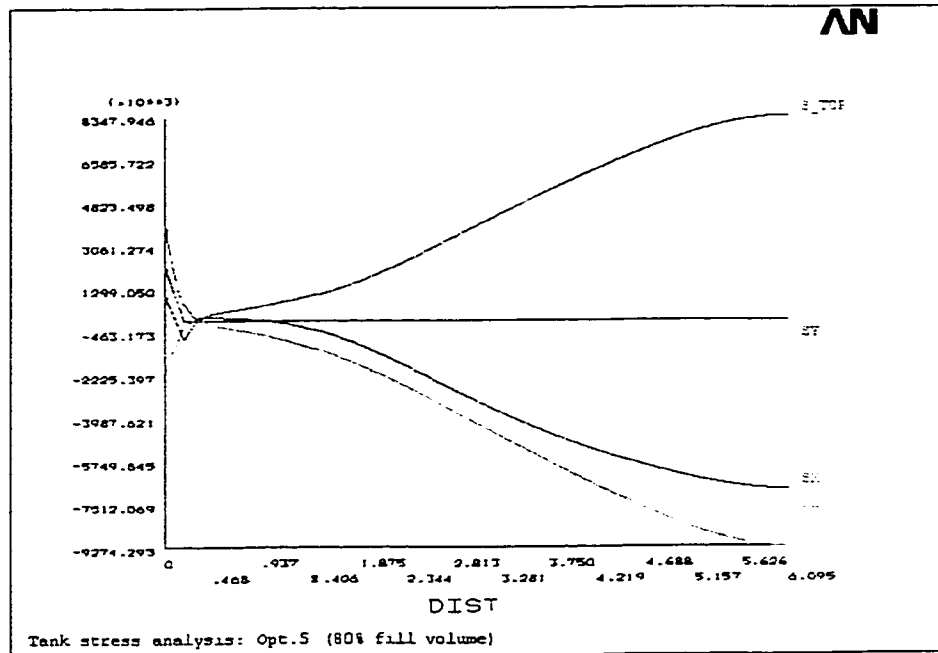


Figure A13: Stress distribution along longitudinal direction of the quarter Opt.5 tank.

The stress contours reveal significant stress concentration around the supports, regardless of tank cross-section, with the highest stress occurring at the interface of the tank body and its supports, due to the significant geometry variation and thus abrupt transition of structural rigidity between the tank shell and supports. All the tanks also experience considerable stress concentration near the connection between the cap (head) and shell (especially lower portion of the cap), and on arc 2 of the tank cross-section (especially the near support areas), attributed mostly to sharp geometry change around the periphery of tank heads and relatively large curvature of arc 2, respectively. The stress concentration on the heads of Opt.5 tank is relatively invisible, due to the most significant stress concentration around the supports and on arc 2 of the shell, as shown in Figure A12. In terms of maximum stress, the Opt.5 tank yields the highest value, owing to the most significant geometry variation and thus considerable curvature of its cross-section and saddles, the OPT2 yields the second largest and the modified-oval yields the third largest, while the circular tank reveals the smallest magnitude, attributed mostly to its round cross-section and thus less geometry variation of the saddles. The contour results thus suggest that round tanks yield relatively less stress concentration around support interface than wide tanks under nearly identical support condition. In terms of maximum structural deformation, the conventional tanks reveal the least values, and the OPT1 and OPT2 yield moderate values, while the Opt.5 results in the largest magnitude, which is considerably higher than those of the conventional tanks. This indicates that a cylindrical tank of asymmetric cross-section may be more flexible than the conventional symmetric design, without considering the influence of different support geometry.

The equivalent stress distribution along the tank top line (s_{top}) reveals similar trend for different tanks, with considerable stress variation near the cap due to high stress concentration, and then increasing monotonously with increase in distance from the cap. It is interesting to note that in the cases of the conventional tanks, the tank top line is virtually under pure compression (axial stress s_z) in the longitudinal direction due to bending caused by liquid load, while the lateral stress (tangential stress s_x) is negligible, as shown in Figures 5 and 7. The tank body thus can be considered as a bending beam. In the cases of optimal tanks, however, the lateral compression stress (s_x) is considerable, with magnitudes comparable to those of the longitudinal stress (s_z), as shown in Figures 9, 11, 13, attributed mostly to the asymmetric cross-section of the optimal geometry. The highest value of the equivalent stress occurs at the middle of the tank shell, as shown in Figures 5, 7, 9, 11, 13, with the optimal tanks yielding moderately higher values (6.98 MPa to 8.34 MPa) than the conventional tanks (5.02 MPa and 4.66 MPa, respectively), owing to considerable lateral stress on the top of the optimal tanks.

The equivalent stress distribution along the connection line between arcs 2 and 3 of the tank shell (s_{yz3}) exhibits considerable variations due to the significant influence of the supports, irrespective of the cross-section. The equivalent stress response of all the tanks, with the exception of OPT1, reaches a peak point around the middle of the support, and then decreases with increase in the distance from the cap and finally approaches a stable level at the middle of the tank length. In the case of OPT1, the equivalent stress response reaches a maximum at the middle of the tank length, attributed possibly to combined influence of its relatively less geometry transition at lower portion of the cross-section and the corresponding support saddles. The magnitudes of the stress components

(extension) in the longitudinal and vertical directions (s_z and s_y) are considerable, while that in the lateral direction (s_x) is negligible. This slight lateral stress (s_x) is attributed to the fact that the slope at the connection point between arcs 2 and 3 is nearly normal to the lateral axis of the tank body-fixed system, especially in the cases of the optimal tanks, as illustrated in Chapter 2. In terms of peak equivalent stress value, the circular tank yields the minimum stress (8.80 MPa) and the modified-oval yields the second minimum (9.17 MPa). OPT1 and OPT2 yield moderately high values of 11.75 MPa and 11.90 MPa, respectively, due to combined influence of their asymmetric geometry and the associated supports, while Opt. 5 results in a considerably high stress value of 34.45 MPa, which is nearly 4 times that of the conventional tanks, owing to the most significant geometry curvature of its cross-section and the corresponding saddles.

A.3 Summary

A simplified finite element model for a cleanbore cylindrical tank of generic cross-section and its supports is developed using the ANSYS software. The model allows static stress analysis of cylindrical tank of different cross-sections under various cargo fill conditions, and thus forms the basis for further investigations such as tank support design modification and optimization, modal analysis of the tank structure, etc.

The stress distributions of various optimal and conventional tanks in terms of equivalent stress contour and stress patterns along defined paths on the tank longitudinal direction are preliminarily analyzed and compared to investigate the influence of tank cross-section. The preliminary analysis results reveal that tank supports yield the most significant influence on the stress distribution of the tank structure, regardless of tank cross-section, and that the optimal tanks proposed for typical fill ranges, OPT1 and

OPT2, yield moderately higher stress on both the lower and upper portions of the tank shell than the conventional tanks, under identical cargo load and nearly identical supports, due to the asymmetric feature of the optimal geometry and its complex interaction with the supports. The low c.g. tank proposed for relatively insignificant partial fill conditions, Opt.5, however, exhibits considerably higher stress concentration around the supports than the other tanks, attributed to the most significant geometry variation and considerably high curvature of its cross-section and support saddles.

Due to the idealized simplifications in developing the finite element model and the difficulty in achieving identical support geometry for different tank cross-sections, this comparative study should only be considered as qualitative and inconclusive. Further work is definitely needed to model and analyze more realistic tanks with relatively detailed internal and external structures, such as ring stiffeners, overturn protections, structural fillets for the caps and supports, to improve the present model. In addition, the high stress concentration around the supports may be reasonably reduced by improved geometry and structural design of the supports. Support parametric study and design optimization is thus also needed to reduce the stress concentration. Furthermore, stress analysis of the tank structure considering the flexibility of the trailer body and relatively realistic loading conditions with liquid sloshing effect, and tank containment analysis under rollover situations of the tank vehicle are also needed.